UNIVERSITÀ DEGLI STUDI DI PAVIA

DOTTORATO IN SCIENZE CHIMICHE E FARMACEUTICHE

XXX CICLO

Coordinatore: Chiar.mo Prof. Mauro Freccero

Recognition processes based on molecular cages and tripodal receptors

Tutore

Chiar.ma Prof.ssa Valeria Amendola

Tesi di Dottorato di

Ana Miljković

a.a. 2016- 2017

Index

1. Introduction

1.1 Molecular recognition

Molecular recognition consists in the molecules' capability of interacting with each other through noncovalent bonds such as van der Waals forces, electrostatic interactions[1], hydrophobic forces,[2] hydrogen bonding, coordinative interactions[3], π-π interactions and halogen bonding.

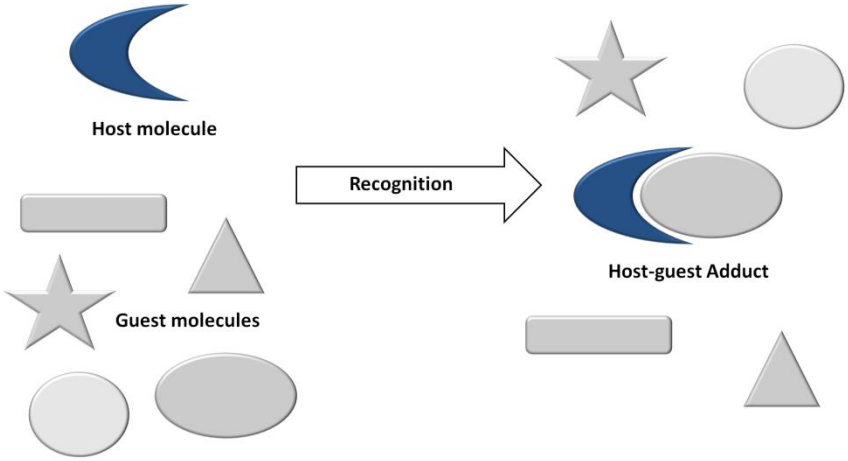

Figure 1. Recognition process

The process of molecular recognition follows the principles of **molecular complementarity,** between the receptor (host) and the substrate (guest), and of receptor preorganisation.[4-5] The solvent as well plays an indirect role in driving the molecular recognition in solution.[6-7]

Molecular recognition is defined by the energy and the information involved in the bonding, and in the ability of a receptor to select a particular substrate (selectivity). The first formulation of the principle of molecular complementarity dates back to the work of Emil Fischer on enzymatic catalysis in 1894 and is generally known as the key-lock principle. The receptor (or host) is characterised by having an active site (e.g. the electron pair of an amino nitrogen, the vacant coordinative position of a metal ion or the charge of an ion), which is capable of establishing reversible interactions with the substrate (guest). The selectivity of molecular recognition is ensured by the receptor's preorganisation and by the complementarity with the substrate, in a relationship similar to that between a key and its lock.

Currently, the principle of complementarity assumes a wider form and it refers to (i) steric complementarity, which takes into account the size and shape of host and guest, and to (ii) interaction sites complementarity, e.g. between H-bond donors and acceptors.

The preorganisation principle was described by Cram and Artz[8] as follows: "the higher is the organization of receptor and substrate, and the less is their solvation prior to the complexation, the more stable will be the resulting complex." In other words, to optimize molecular recognition, the interaction sites should be pre-arranged in a sufficiently rigid structure to avoid the costs of conformational reorganization during the complex formation process. Moreover, the smaller the number of solvent molecules inside the receptor cavity, the lower will be the energy cost for desolvation.

When the fundamental requirements listed above are met, the stability of the adduct and the selectivity of the recognition will be high.

1.2 Azacryptands as Molecular Cages

Molecular cages are defined as hollow structures that form a three-dimensional cavity capable of encapsulating some particular species or class of analytes. These systems attracted considerable attention in modern supramolecular chemistry because of their possible applications in molecular recognition, catalysis, drug delivery, biosensing, separation and storage.[9] A classic example is provided by octamine cages (called azacryptand), where two *tren* subunits (*tren* = tris(2-aminoethyl)amine) are linked by either aliphatic (-CH_2CH_2-) or aromatic (1,3-xylyl) spacers.[10] The terms “cryptand” and “cryptate” were introduced by Lehn, in the 1960s, to define bicyclic molecular systems, containing either oxygen or nitrogen donor atoms, capable of binding charged species.

Small size azacryptands, as the free bases, can bind a single metal ion inside their cavities. In addition, these receptors, when they are fully protonated, can also act as hosts for anions, through the formation of both H-bonding and electrostatic interactions within their cavity. Bistren azacryptands, with their large cavities, can accommodate two metal ions and a bridging anion, forming the so called "cascade" complexes. This type of process has been applied since the 1980s for the selective recognition of anions of different size and bite length. Molecular cages, containing fluorescent spacers between the *tren* subunits or exploiting the indicator displacement paradigm, have been employed in the detection of anionic species in water at μM concentrations.[11-12] In addition, the immobilization of molecular cages on solid matrices[13] or surfaces has led to the

development of (i) new materials for solid phase extraction of anionic pollutants, (ii) selective electrodes for the detection of analytes in aqueous solution.

1.2.1 Protonated Cryptands as Receptors for Anions

The first protonated receptors reported in literature by Lehn and co-workers can accommodate halide anions within their cavity, due to the formation of strong electrostatic and H-bonding interactions (Figure 2a,b)[14]. In its tetraprotonated form, receptor 2a can bind Cl^- thanks to the formation of four hydrogen bonds, supported by electrostatic interactions. The X-ray structure of the adduct shows that the chloride anion is encapsulated inside the receptor cavity.[15] Larger anions such as I^-, NO_3^-, ClO_4^- don't give any interaction. The selectivity for Cl^- can be explained through the geometrical complementarity existing between the anion and the receptor cavity.

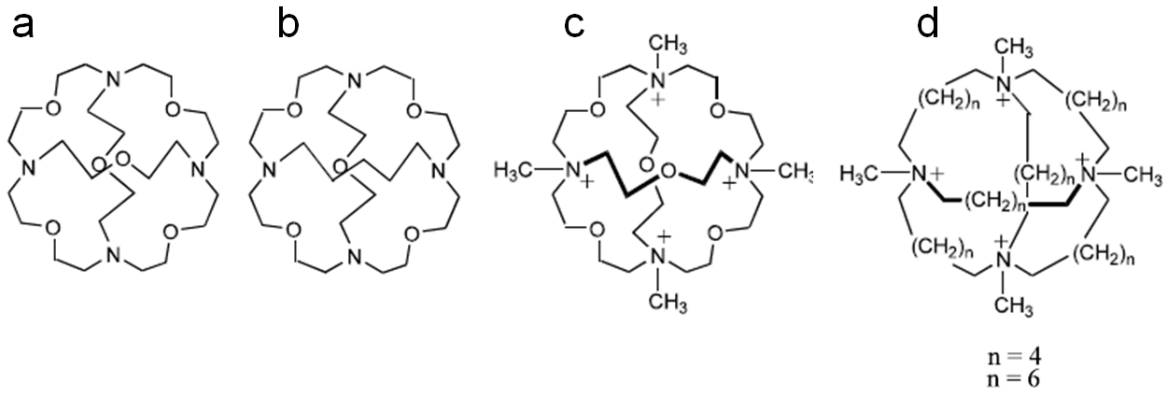

Figure 2. Lehn[14] (a,b) and Schmidtchen[16] (c,d) receptors.

Receptor 2a is an excellent example of a preorganized receptor for chloride, thanks to the multiple H-bonding interactions that it can establish. The addition of methyl groups causes the receptor to adopt a different conformation. In fact, Schmidtchen at al.[16] reported the synthesis of a quaternized host analogue to Lehn's receptors (Figure 2c and 2d). These new cages, having an expanded cavity, show selectivity for larger anions. For instance, NMR experiments on 2d in aqueous solution (Figure 2d, n = 6) showed the formation of a stable complex with iodide. The X-ray structure of the adduct revealed that the anion is contained in the receptor cavity, stabilized by electrostatic interactions.[17]

The search for novel preorganized structures, to obtain powerful and selective anion receptors, induced supramolecolar chemists to synthesize even more complex molecules. Indeed, when the host is preorganized and has the optimal binding conformation, no additional energetic costs arise, resulting in favourable binding. Polyamine cryptands in their positively charged forms are efficient receptors for anions due to their preorganization.[18]

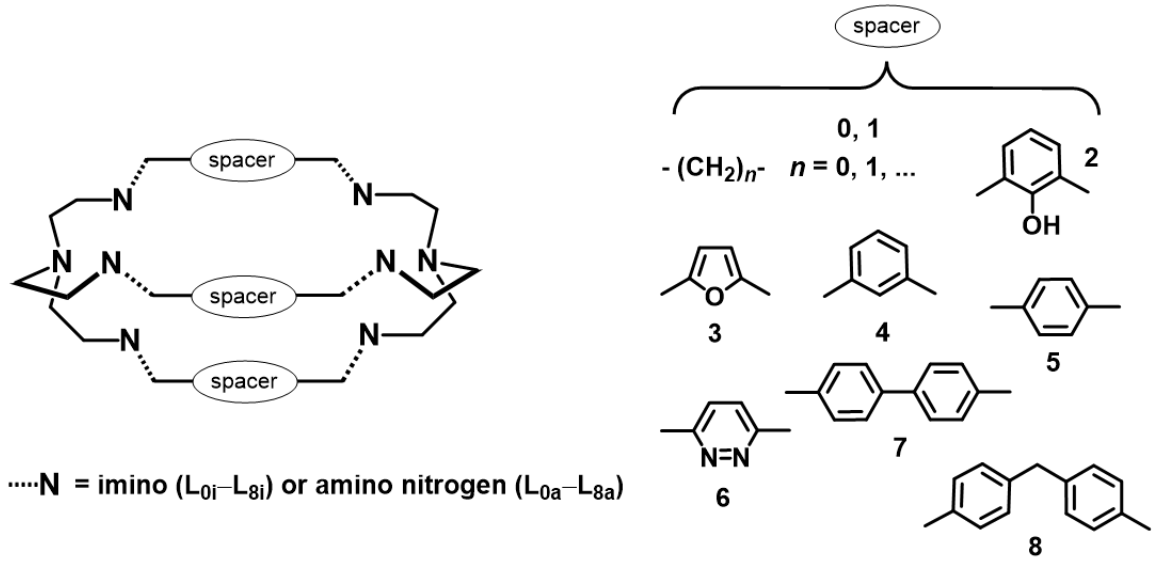

Figure 3. Hexaimino (**L_{0i}–L_{8i}**) and octaamino (**L_{0a}–L_{8a}**) bistren cryptands (with spacers **0**–**8**).

The bistren azacryptands generated great interest for both their versatility and for the easy synthesis,[19] consisting in the [2+3] condensation of *tren* (tris(2-aminoethyl)amine) with a dialdehyde, generally without a metal template. The reduction of imine bonds in the obtained Schiff-base cryptands (**L_{0i}-L_{8i}**) leads to saturated cages with different potentialities (**L_{0a}-L_{8a}**).

As a matter of fact, protonated polyamines are widely used as receptors for anions in aqueous solution. In fact, polyamine systems are more stable in aqueous solution than their polyimine precursors, especially in acidic conditions.

Since her studies on hexaprotonated azacryptands as receptors for anions, Jane Nelson understood that the selectivity was mostly driven by the "good complementary of fit between the host and anionic guests".[20] The spacers between the tren subunits have a crucial role in the binding of analytes within the cavity, because they determine the distance between the protonated sites of the cage and define the shape of the cavity, thus controlling the selectivity. Also the cavity size can be modulated choosing spacers of proper length. Selectivity is due to the geometrical complementarity between the anion and the receptor's cavity and it depends on the protonation state of the receptors.[21] The amino group can act either as an hydrogen bond donor, in the protonated form, or

as an acceptor, as the free base, being useful to bind protonated anions such as phosphates. In the hexaprotonated form of the cage, ammonium groups may point inside the cavity to bind the included anion.[22] Of course, depending on the species to be included, suitable dialdehydes will be chosen, giving the desired size of the host.

Taking advantage of this "rule", Kristin Bowman-James, Jane Nelson and other authors have proposed a series of polyprotonated azacryptands as selective receptors for perfluoro- and oxo-anionic species in water.[23] In particular, the selective recognition of dicarboxylate anions has been considered an intriguing field, due to the biological and environmental interest of this class of substrates.[24]

For example, in 2002, J. Nelson and co-workers have shown that the oxalate anion has a high affinity for the esaprotonated cavity of m-xylyl and furanyl azacryptands (i.e., $\mathbf{L_{4a}}H_6^{6+}$ and $\mathbf{L_{3a}}H_6^{6+}$ respectively). In this case, they observed the formation of stable 1:1 inclusion complexes with both receptors. In their crystals, these complexes exhibit multiple H-bonding interactions between each carboxylate group and the NH^+ donors of the host; π-stacking is also observed between the C=O groups and aromatic spacers.[25]

Another example is given by the hexaprotonated *m*-xylyl azacryptand, $\mathbf{L_{4a}}H_6^{6+}$, that can capture anions of smaller size, such as fluoride. K. Bowman-James et al. obtained crystals of the 1:1 inclusion complex, in which the anion occupies one protonated *tren* subunit, while the other binding site is occupied by a water molecule, which forms multiple H-bonds with the ammonium groups.[26]

Another interesting example is given by the same authors, which used *p*-xylyl spacers (**5** in Figure 3), to obtained a molecular cage ($\mathbf{L_{5a}}H_6^{6+}$) with a larger cavity, able to encapsulate two fluoride ions and a bridging water molecule.[27] The inclusion of two anions has been also observed with tosylated azacryptands, capable of capturing two halides simultaneously.[28]

One of the main applications of these systems is the extraction of anionic pollutants, such as the radioactive anion $^{99}TcO_4^-$ and its model ReO_4^-. In fact, J. Nelson and others demonstrated that using this type of receptors, for the extraction of pertechnetate from a water phase to a chloroform one, is strongly influenced by the protonation of the cage.[29]

Ten years later, our group demonstrated the affinity of the hexaprotonated *p*-xylyl azacryptand (Figure 4) for the pertechnetate anion by NMR and ITC studies in aqueous solution and by X-ray diffraction studies on a single crystal of the 1:1 inclusion complex.[30]

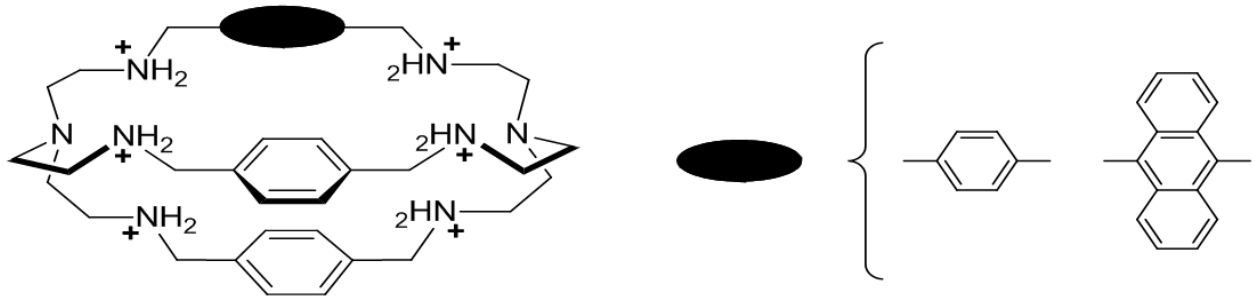

Figure 4. The $\mathbf{L_{5a}}H_6^{6+}$ azacryptand in its hexaprotonated form, selective molecular receptor for the $^{99}TcO_4^-$ anion in water. By substitution of one *p*-xylyl spacer with a 9,10-anthracenyl fragment, a fluorescent chemosensor for the $^{99}TcO_4^-$ anion was obtained.

Another interesting example is the asymmetric cage in which one of the p-xylyl spacers has been replaced by a 9,10-anthracenyl fragment, which allowed us to obtain an ON-OFF fluorescent chemosensor for pertechnetate in water (see Figure 4). At pH 2, the hexaprotonated azacryptand showed its maximum fluorescence. Under these conditions, the addition of $Na^{99}TcO_4$ to a solution of the receptor led to a decrease of the emission due to the formation of a 1:1 inclusion complex . This allowed the detection of the radioactive anionic pollutant at micromolar concentrations in aqueous solution. [31]

1.2.2 Schiff-base and Polyamine Cryptands

Schiff-base , as well as the corresponding polyamine systems, have been studied by J. Nelson and other Authors as both mono- [32] and dinucleating ligands [33] for metal ions. In the presence of divalent transition metal ions, receptors with imino groups are subject to hydrolysis, therefore amino-cryptands are preferable for complexation of species like Cu(II) in aqueous solution.[34]

In the case of dimetallic complexes, solvent molecules and anionic guests can be involved in the binding of metal ions within the cavity. Also in this case spacers play an active role. This was observed by J. Nelson et al. with the hexaimino cryptand $\mathbf{L_{2i}}$ in which methylphenol units act as spacers (see **2** in Figure 3). This ligand forms mononuclear complexes with different metal ions. For example, with lanthanide ions kinetically stable cryptates were obtained;[35] while, with Cd(II) and Pb(II), mononuclear or binuclear complexes were formed, depending on pH.

Under neutral conditions, a mononuclear complex was obtained, with the Cd(II) ion located in one of the *tren* subunits, while the other site was occupied by the protons transferred from the phenol spacers to the imine nitrogens. The deprotonated phenols could participate in the binding of the metal substrate, leading to a stable mononuclear complex. On the other hand, under basic

conditions, the receptor acted as a dinuclear ligand, binding two Cd(II) ions, one for each *tren* subunit.[36]

Using pyridazine groups (**6** in Figure 3) as the spacers, Brooker et al. tried to isolate a series of dinuclear copper azacryptates, with the metal ions in a different redox states, i.e. [(I,I), (I,II) and (II,II)] (Figure 5). However, hard N_{sp3} amino donors favor the +2 redox state of copper, resulting in the oxidation of the dinuclear Cu(I) cryptates by the air. Indeed only the dicopper(II) complex, $[Cu_2\mathbf{L_{6a}}]^{4+}$, was obtained. On the other hand, with the hexaimine cryptand $\mathbf{L_{6i}}$, both (I,I) and the mixed-valence (I,II) complexes were synthesized.[37]

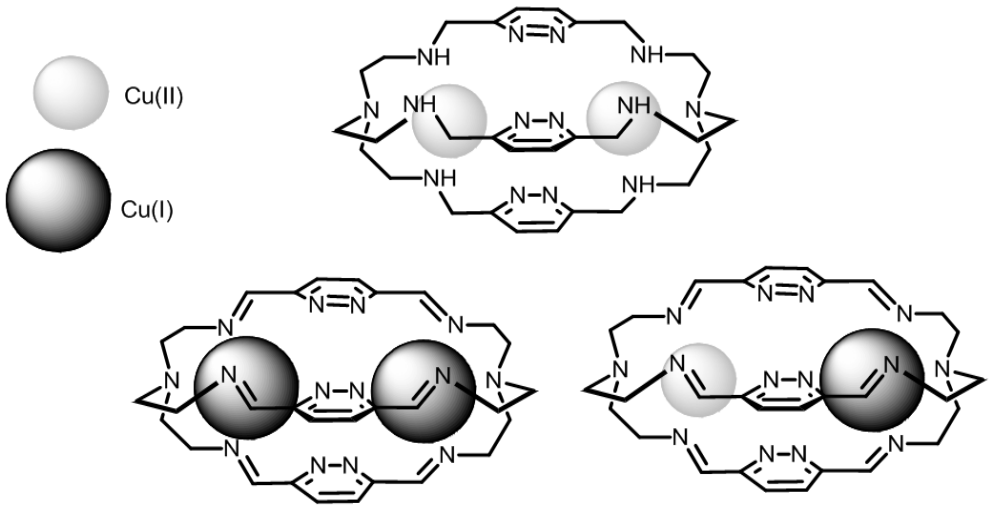

Figure 5. Dinuclear azacryptates reported by Brooker et al. With azacryptand $\mathbf{L_{6a}}$, only the (II,II) complex was obtained, $[Cu_2\mathbf{L_{6a}}]^{4+}$.The (I,I) and the (I,II) species could be obtained using the hexaimino analogue cryptand $\mathbf{L_{6i}}$.

1.2.3 Metal-ligand receptor

Receptors can be positively charged, not only for the presence of ammonium/tetraalkylammonium fragments, but also because of the incorporated metal ions.[38] In fact, azacryptands can form the so-called "cascade complexes".[39] The term "cascade", proposed by J.-M. Lehn and coworkers, refers to the azacryptand complexes, in which two metal ions are encapsulated within the cavity, and are linked through a bridging anion. However, the term can be also used in the case of the tritopic complexes of azacryptands with halides, containing two halide anions bridged by a water molecule.[40] There are many examples of "cascade complexes", based on bistren azacryptands with divalent transition metal ions [e.g. Cu(II), Ni(II), Zn(II)] and bridging anions [e.g. halides, pseudo-

halides, cyanide, etc.].[41] Dinuclear cryptates are usually flexible enough to permit the inclusion of anionic species. However, this conformational rearrangement can be expensive in terms of energy and can lead to a loss of selectivity.

Dinuclear cryptates were also used as catalytic nano-reactors. As shown by J. Nelson et al., dimetallic [e.g. Cu(II), Ni(II), Zn(II)] complexes of the *m*-xylyl bistren cryptand **L$_{4a}$** catalyse CO_2 uptake-reactions within their cavities, through the development of methylcarbonate-bridged complexes in methanol solution, via CO_2 insertion into the OMe^- bond.[42]

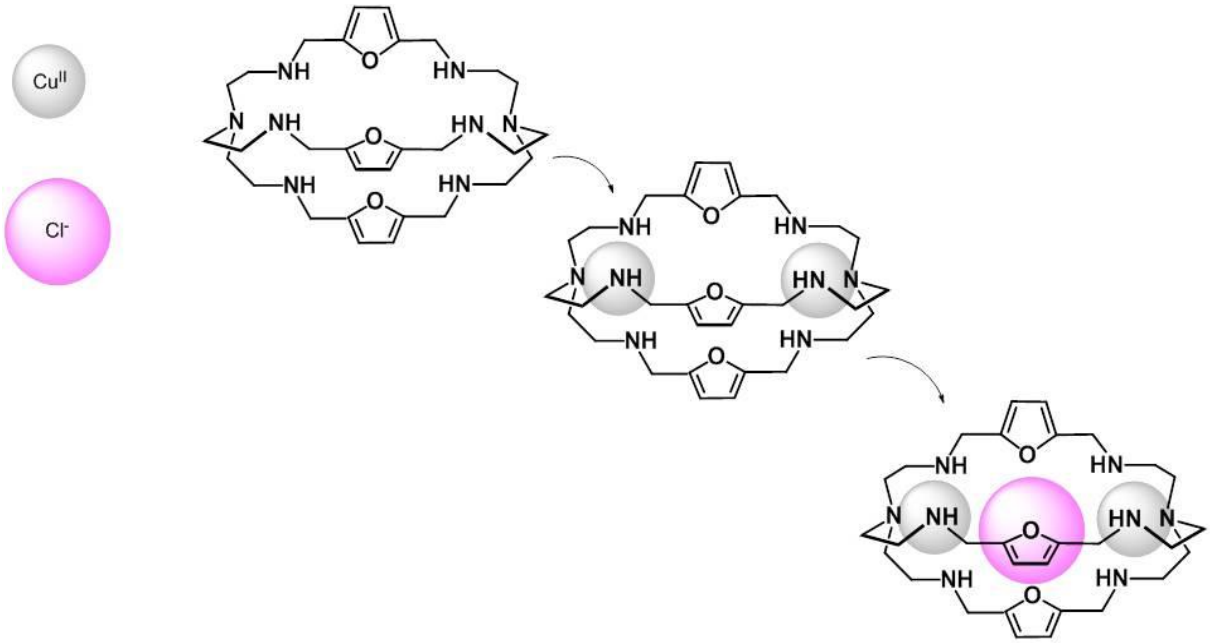

Figure 6. The formation of the "cascade"complex, $[Cu_2\mathbf{L}_{3a}(Cl)]^{3+}$, obtained by mixing azacryptand **L$_{3a}$** with 2 eqv. of Cu(II) and 1 eqv. of chloride, in aqueous solution at pH 5.

The selective recognition of halides by the dicopper(II) furanyl azacryptate, $[Cu_2\mathbf{L}_{3a}]^{4+}$, is highlighted by the development of intense CT bands in the UV-vis. spectrum.[43]

For example, when chloride interacts with the host, the solution changes colour to yellow, due to the development of an absorption band at about 412 nm in the visible spectrum. Anyway, the cage's affinity for anionic guests (in terms of binding constants) is strongly affected by cavity distortions, due to the progressive replacement of the furanyl spacers with *p*-xylyl fragments (**3** and **5**, respectively, in Figure 3). So the selectivity order changes, as well as the optical response of the ligand to the anion, for example with the disappearance of the CT bands observed for the dicopper(II) furanyl azacryptate with halides.[44]

The methylation of amine can also modify the binding tendencies of azareceptors, due to the distortion effects caused by sterically bulky groups. This effect was observed by Nelson et al. in the case of N-methylated azacryptands, for which the coordination of metal ions and anions outside the cavity replaced the formation of "cascade" complexes.[45]

Another field well investigated by supramolecular chemists is the selective recognition of dicarboxylate anions; in this context, azareceptos play a very important role too. An interesting example is reported by Rita Delgado, in her studies on the dicopper(II) *p*-xylyl azacryptate, $[Cu_2\mathbf{L_{5a}}]^{4+}$, with dicarboxylate anions. In fact, in this case, the typical cascade complex was obtained only with the succinate anion while, with oxalate and malonate, the formation of unusual tricopper(II) cryptates was observed.[46]

In the case of molecular cages, selectivity can be improved by choosing more rigid spacers. For example, the dimetallic cryptand (**7** in Figure 3) can recognize L-glutamate even in the presence of other neurotrasmettitors such as L-aspartate and GABA.[47] Using the rhodamine indicator in a "chemosensing ensemble assay"[48], anion recognition could be highlighted by the revival of the indicator's fluorescent emission.

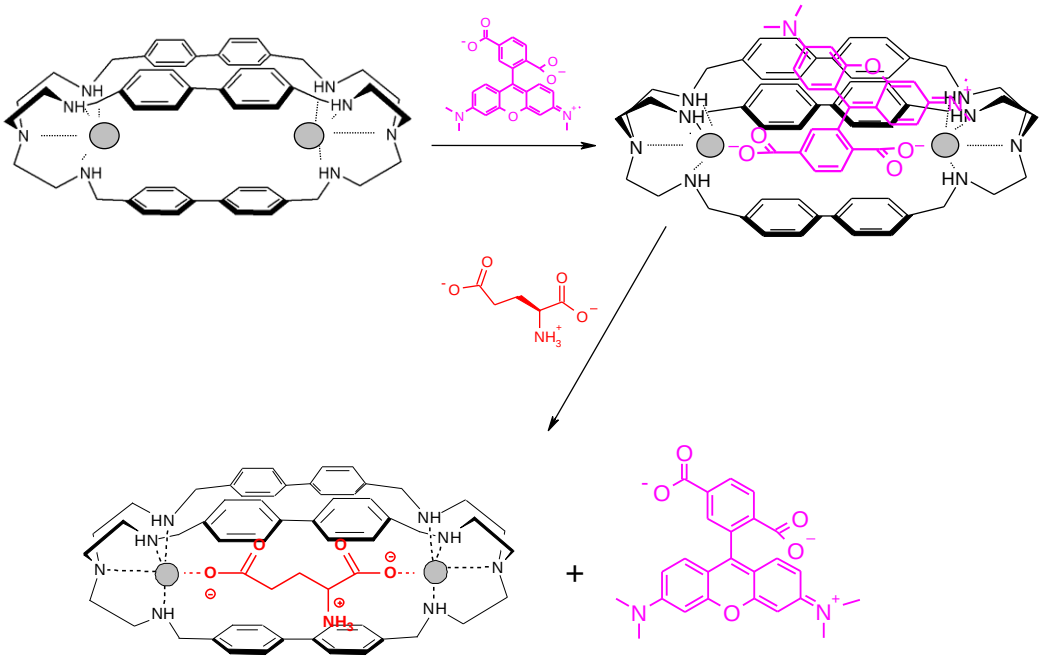

Figure 7. Bistren cryptand selective for L-glutamate.

Another example is given by the dicopper azacryptate containing biphenylmethane spacers (**8** in Figure 3). Recently, Mateus et al. demonstrated that the dicopper complex $[Cu_2\mathbf{L_{8a}}]^{4+}$ is capable of binding dicarboxylate substrates with association constants ranging from 7.34 to 10.01 log units, in MeOH/H_2O 1:1 (pH ~ 7).

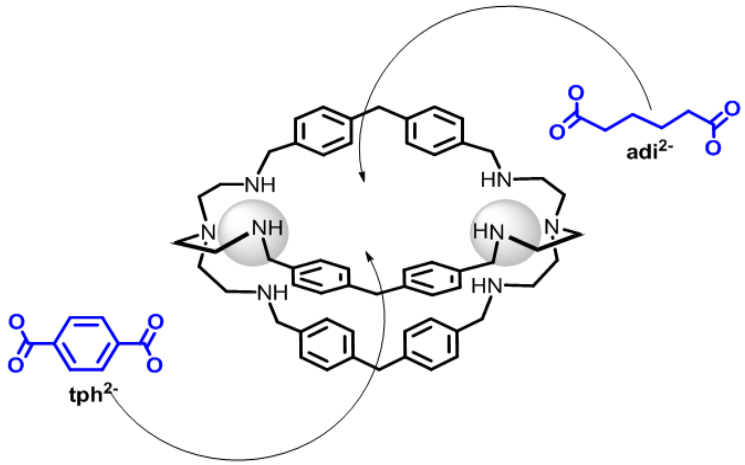

Figure 8. "Cascade" complex, obtained by mixing azacryptand $\mathbf{L_{8a}}$ with 2 eqv. of Cu(II) and 1 eqv. of dicarboxylate anion (either tph^{2-} or adi^{2-}) in , in MeOH/H_2O 1:1 (pH ~ 7).

In particular, adipate and terephthalate anions (see Figure 8) are recognized with great selectivity. This behaviour comes from the best fit of the anion's bite length with the distance between the copper ions within the cavity. Anion inclusion was accompanied by a distortion of the coordination geometry around the Cu(II) centres, from trigonal-bipyramidal to square-pyramidal, as observed through X-ray diffraction studies. Obviously, the inclusion complex is stabilized by multiple interactions [i.e. Van der Waals and C–H···π] between the carboxylate anion and the cavity. The anion binding could be monitored through the changes in the d-d bands between 600 and 850 nm, due to the geometry distortion around the copper ions.[49]

1.2.4 Cages on solid supports

The immobilization on solid supports or nanomaterials is crucial for the application of azacryptands as supramolecular sensors, heterogeneous catalysts or solid-phases for the extraction of anionic pollutants. However, the immobilization of the receptor must not interfere with its binding properties.

Some years ago, our group proposed a new solid phase for the extraction of ReO_4^- and TcO_4^- from water, by immobilization of azacryptand $\mathbf{L_{5a}}$ on mesoporous silica MCM-41 and Amberlite CG50.

The silica matrix, showing the best performance, could be prepared through a very simple procedure: MCM-41 was first modified using a triethoxysilane derivative and then with azacyptand **L$_{5a}$**. Each cage was bound to silica, through a chain attached to one of the secondary amines and the total amount of **L$_{5a}$** bound to the solid phase ranged between 0.2 and 0.3 mmol g^{-1}, as demonstrated by the physico-chemical characterisation of the final solids [by elemental analysis (CHN), FT-IR, micro-Raman, ^{29}Si MAS NMR, sorption isotherms, etc.]. The tertiarization of one secondary amine of the receptor did not lead to a loss of affinity for the target anions, which was similar to that in solution.

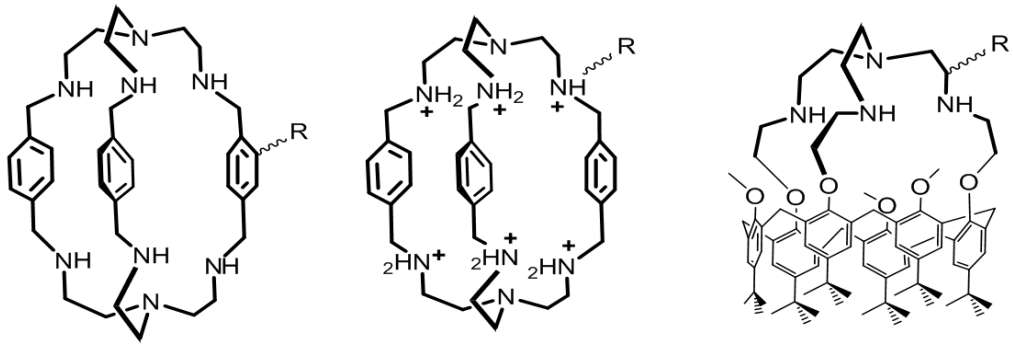

Figure 9. Properly modified azacryptands suitable for functionalization of solid supports.

Choosing the functionalisation of the ligand backbone, it is possible to attach the cage to a solid support without involving the secondary amino groups. This is very important when the tertiarization of the amines may affect the coordination capabilities of the ligand, e.g. in the complexation of transition metal ions. An example is given by receptor **L$_{5a}$** containing a thioether moiety attached to one of the spacers. The thioether group allowed us to append the dicopper cryptate on the surface of a self-assembled monolayer of gold nanostars (GNS). Studies on the release of Cu(II) from GNS monolayers pointed out an increased kinetic inertness of the complex compared to [Cu$_2$**L$_{5a}$**]$^{4+}$ in solution, while the general coordination capabilities of the cage remained the same.[50]

Another way to attach a molecular cage on a surface involves the functionalisation of the *tren* moiety. For instance, Olivia Renaud et al. synthesised a new calix[6]azacryptand, containing a terminal azide group on the *tren* subunit. This molecule was then immobilized on gold-modified electrodes, using CuAAC electroclick reactions. The immobilized copper complex showed a quasi-reversible cyclic voltammetry trace, due to the Cu(II)/Cu(I) redox couple. The modified electrodes

were successfully applied in the selective detection of primary alkylamines through cavitary binding in water.[51]

1.3 Tripods or pseudo-cage receptors

Tripodal receptors consist of multi-armed ligands, in which each arm carries a functional group that can interact with the target species. These receptors can be considered as intermediate between cyclic and acyclic ligands with regards to preorganization and they are able to bind an ion more effectively than analogous acyclic systems. Tripodal ligands have several advantages over monodentate and even bidentate receptors due to the enhanced chelating effects, and the presence of multiple interaction sites toward given guests. This type of receptor topology has a profound effect on the selectivity, because it provides the cavity size and flexibility required to fit the guest. [52] In fact, the selectivity of a tripodal receptor relates greatly to the rigidity of its arms and its cavity size.[53] Tripodal ligands have been reported as efficient recognition components in ion-selective electrode membranes[54] and optical sensors.[55]

An example of tripodal receptors is represented by the family of molecules shown in Figure 10.[56] Sato et al. demonstrated that the tripod **L$_{9a}$** interacts more strongly with chloride than with bromide and iodide in acetonitrile. Kim et al. showed that anion recognition was based on the H-bonding interactions between the anion and the positively charged imidazolium units. Selectivity could be improved by adding nitro groups (see tripod **L$_{9b}$** in Figure 10) on the receptor framework. [57]

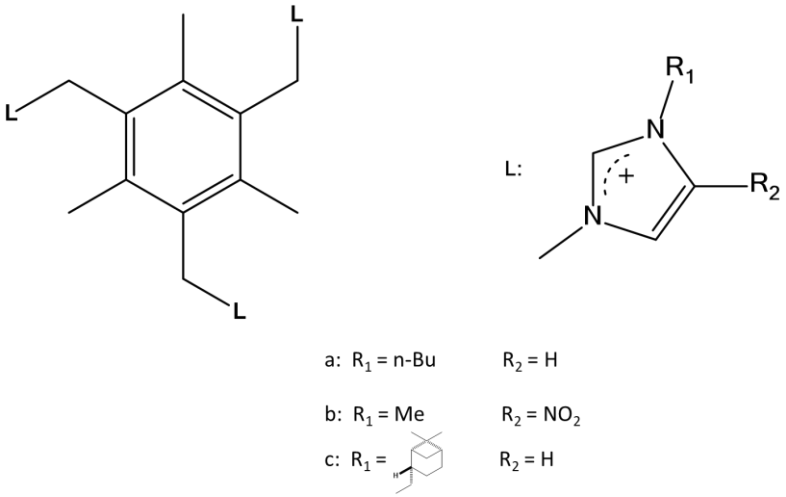

Figure 10. Family of tripodal receptors (**L$_9$**). The different substituents modulate the affinity of the receptor for the anions.

Another interesting system, able of discriminating asymmetric anions, is receptor **L$_{9}$c** (see Figure 10), synthesized by Howarth et al. This system is selective for (R)-2-aminopropionate while it scarcely interacts with the S enantiomer.[58] A similar tripodal system containing benzimidazoles as the binding units was synthesized by Duan et al. (Figure 11). [59]

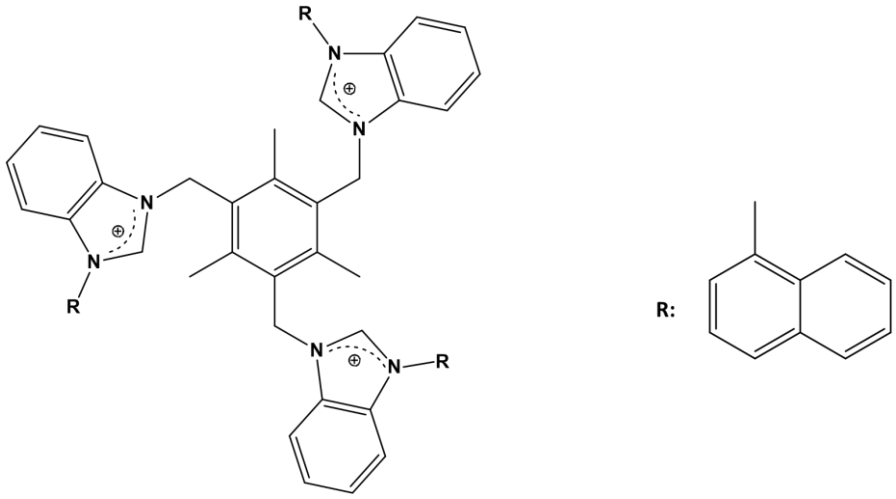

Figure 11. Tripod containing benzimidazoles and naphthyl groups (**L$_{10}$**). Due to the presence of naphthyl groups, the system acts as a chloride-regulated fluorescence switch.

The presence of naphthalene groups on the receptor **L$_{10}$** allowed the Authors to follow the anion binding process through emission studies. In fact, while the free ligand showed the typical fluorescence of naphthalene, the binding of chloride promoted the development of a new band, which could be attributed to the excimer emission.

In 2012 Hossain and coworkers reported an urea-based tripodal receptor, containing p-cyanophenyl groups (**L$_{11}$**, Figure 12), suitable for the recognition of spherical anions.

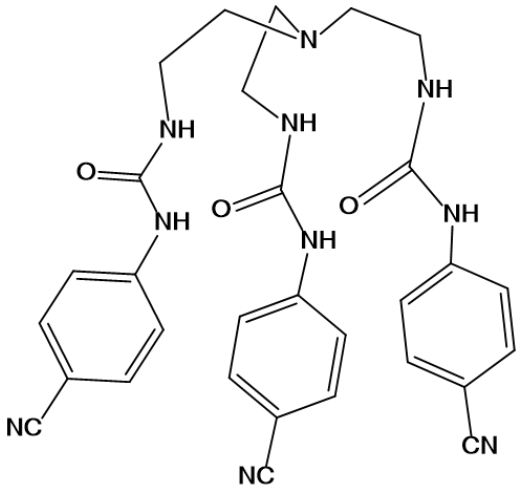

Figure 12. Urea-Based tripodal receptor (**L_{11}**).

The experimental and theoretical studies confirmed the affinity of this receptor for halides. In particular, the ^{1}H-NMR titrations suggested that the molecule formed a 1:1 complex with all the investigated anions in solution, with a binding trend in the order of fluoride > chloride > bromide > iodide. The experimental observations are correlated with DFT calculations, indicating the formation of an encapsulated complex with hydrogen bond donors from urea's NH groups. The affinity trend suggested that the binding was primarily dominated by the relative basicity of halides. Structural characterization of the chloride and bromide complexes, formed in acidic conditions, suggested that the halide ion was externally bonded to two receptors with four NH bonds, while the protonated tertiary nitrogen pointed toward the cavity. The difference in solution and solid-state could be due to the proton on the tertiary nitrogen, that probably prevented the encapsulation of the anion in the cavity. Interestingly, the protonated receptors were assembled with water molecules, forming a perfect cage to encapsulate a silicon hexafluoride anion. [60]

In 2016 Talukdar et al. reported another class of tripodal trisamide- and tris-urea-based receptors (see Figure 13), which could mediate Cl^{-} transport across liposomal membranes. These receptors presented a benzoxazine core, and were synthesized in one-pot with Mannich aminomethylation, followed by a sequential ring closure condensation to connect each arm.

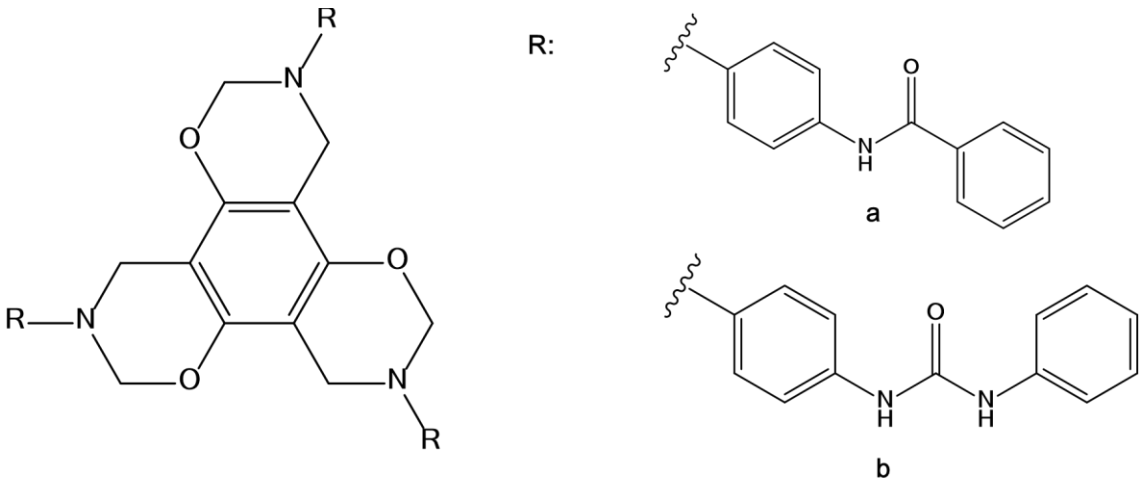

Figure 13. Structures of tripodal receptors **L12a** and **L12b**.

^{1}H-NMR titrations in d_6-DMSO revealed that the tris-urea compound is better as a chloride receptor in comparison to the tris-amide ligand, forming a 1:1 complex with the anion. The tris-urea receptor is also effective as anion carrier, with a selectivity sequence of $Cl^- > NO_3^- > Br^- > I^- > SCN^- > ClO_4^-$. Molecular dynamics simulation suggested that the anion binding was assisted by water molecules. [61]

Another interesting example is represented by the tripodal tris(urea) cationic receptors **L13a** and **L13b**, containing p-tolyl and octyl substituents (Figure 14), respectively. Their association behavior with anionic guests was studied by Steed et al. through a variety of methods. Interestingly, the crystal structures of the host-anion complexes showed that the receptor assumed different geometries, thus confirming its conformational flexibility. In solution, this flexible nature leads to the complexation of a variety of inorganic anions.

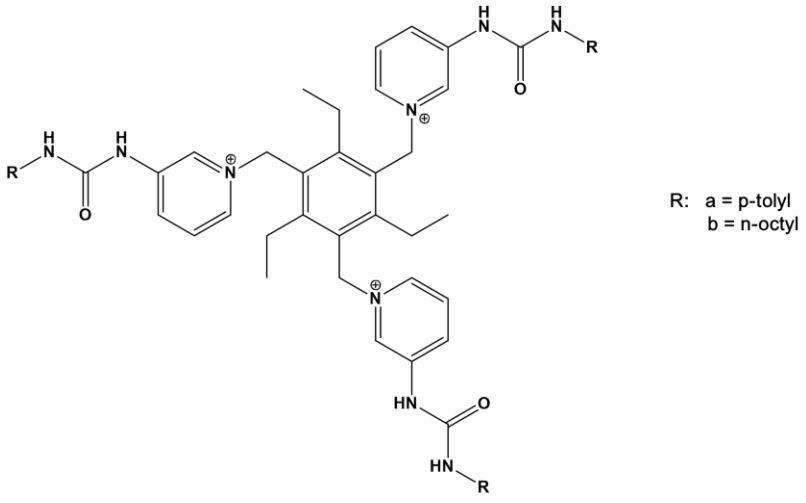

Figure 14. Tripodal Anion Receptors **L13a** and **L13b**.

In fact, ^{1}H-NMR titrations demonstrated that both **L$_{13}$a** and **L$_{13}$b** displayed a significant affinity for halides and hydrogen sulfate. These studies also suggested the persistence of CH···X^{-} interactions, involving the pyridinium units, despite the presence of the N-H donors belonging to the urea moieties. [62]

In 2008, Fabbrizzi and coworkers reported the synthesis and study of a new redox responsive receptor for anions (Figure 15). The tripodal system **L$_{14}$**$^{3+}$ forms a 1:1 complex with Co^{II} in which the metal is octahedrally coordinated by three bpy fragments. The [Co^{II}(**L$_{14}$**)]$^{5+}$ complex provides a cavity suitable for solvent or anion inclusion. X-ray diffraction studies on [Co^{II}(**L$_{14}$**)···H$_2$O]Cl(PF$_6$)$_4$ · 2MeCN showed that a water molecule is included in the cavity. In the crystals, the water oxygen atom receives six H-bonds from the C-H fragments of the three imidazolium subunits and of the three proximate pyridine rings, achieving a distorted trigonal prismatic geometry.

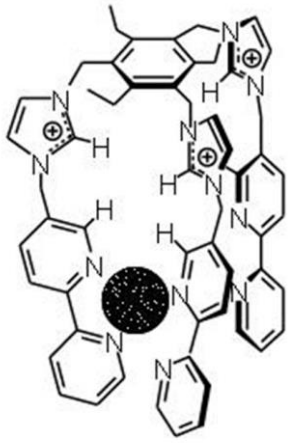

Figure 15. Metal Complex of Anion tripodal receptor (**L$_{14}$**).

Anion inclusion in an aqueous MeCN solution induced a distinct cathodic shift of the potential of the Co^{III}/Co^{II} couple, whose magnitude decreased along the series: Cl^{-} > Br^{-} ~ NCO^{-} > I^{-} ~ NCS^{-}, reflecting the anion tendencies to receive H-bonds from the receptor. [63]

Figure 16 shows the tris(2-aminoethyl)amine(tren) based pentafluorophenyl-substituted tripod **L$_{15}$,** in its triprotonated form. This receptor was studied by potentiometric titrations and X-ray diffraction analysis. Potentiometric titration experiments in methanol/water (1:1 v/v) mixture pointed out a high affinity of the receptor toward fluoride and acetate anions, and a lesser affinity for other anionic guests (e.g., chloride, bromide, nitrate, sulfate, dihydrogenphosphate, and p-toluenesulphonate).

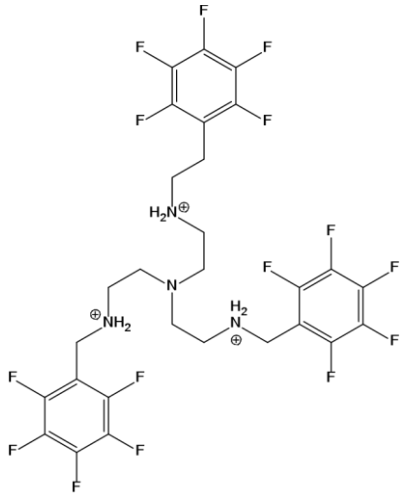

Figure 16. Pentafluorobenzyl tripod $[H_3(\mathbf{L_{15}})]^{3+}$, suitable for anions encapsulation into the cavity.

Crystallographic results showed that the fluoride anion is bound inside the C_{3v}-symmetric cavity of $[H_3(\mathbf{L_{15}})]^{3+}$, forming H-bonding interactions with the protonated amino groups. Interestingly, two molecules of the triprotonated amine can encapsulate the octahedral hexafluorosilicate anion, forming a 2:1 receptor:anion complex in the solid state. [64]

Tripodal systems suitable for the recognition of the phosphate anion was reported by Ansyl et al. Ligands **L$_{16}$a** and **L$_{16}$b** contain a tris(2-ethylamino)amine unit with appended benzylamine and guanidinium groups, respectively. A stoichiometric amount of copper(II) chloride organizes the ligands to yield the desired anion receptors, characterised by high affinity and selectivity for phosphate in aqueous media at neutral pH.

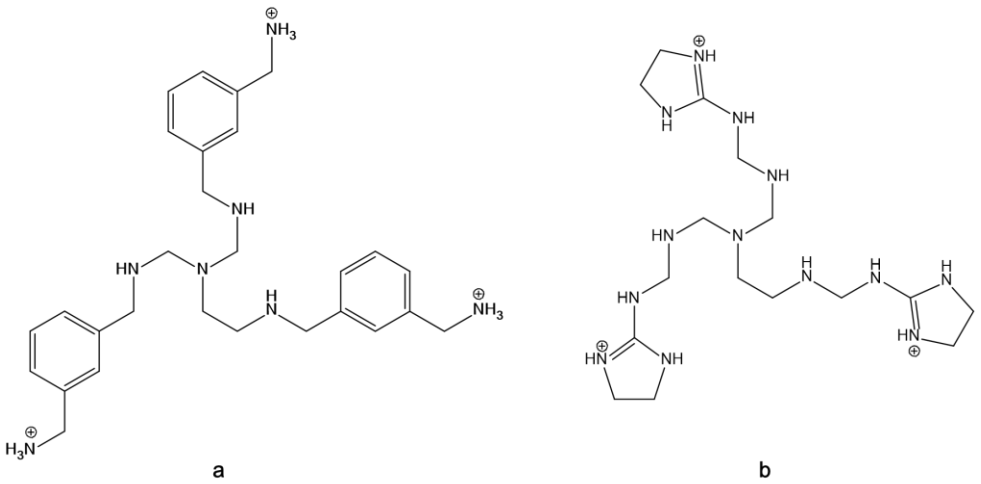

Figure 17. Tripodal receptors suitable for phosphate recognition (**L$_{16}$a** and **L$_{16}$b**).

Selectivity, in particular, is due to the design of the cavity, which provides excellent shape, size, and charge complimentarity to the anion. On the other hand, the high affinity depends on the combination of different type of interactions within the cavity, due to the presence of ammonium/guanidinium groups and the Cu(II) centre. Notably, the flexibility of **L_{16}a** compared to that of **L_{16}b** decreases its selectivity for phosphate. In contrast, the rigidity of **L_{16}b** leads to a decrease in affinity for the anion while increasing selectivity. [65]

A tripodal hexaurea receptor (**L_{17}**) suitable for the selective binding and extraction of sulfate is reported in the Figure 18. The molecule is capable of completely encapsulating the anion in a complementary cavity that is covered by aromatic rings. Recognition takes advantage of a combination of complementarity, chelate and hydrophobic effects.

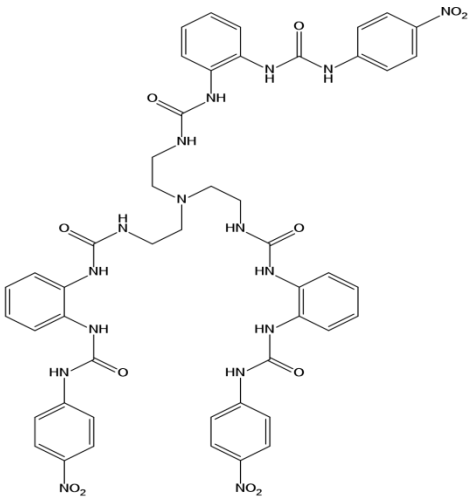

Figure 18. Schematic view of tripodal hexaurea sulfate receptor (**L_{17}**), reported to extract sulfate quantitatively into chloroform in competition with nitrate.

With this receptor as a liquid-liquid extractant, almost quantitative extraction of sulfate ions from an aqueous to an organic phase in a recyclable manner has been achieved, and may be promising in the remediation of nuclear waste. [66]

A series of fluorinated tripodal anion transporters containing urea and thiourea groups have been prepared and their anion transport properties studied by Gale et al.. Anion transport assays using ion-selective electrodes demonstrated that this class of compounds is capable of transporting chloride through a lipid bilayer via a variety of mechanisms.

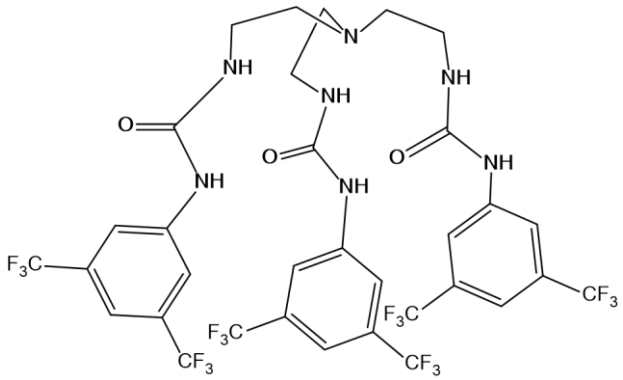

Figure 19. Structure of tripodal receptor containing 3,5-bis(trifluoromethyl)phenyl group (**L_{18}**).

Calculations indicated that increasing the degree of fluorination of the tripodal transporters increases the lipophilicity of the transporter and this is demonstrated to be the major contributing factor in the superior transport activity of the fluorinated compounds. The most active transporter contained a urea functionality appended with a 3,5-bis(trifluoromethyl)phenyl group (Figure 19) was able to mediate transmembrane chloride transport at receptor to lipid ratios as low as 1:250000. ^{1}H-NMR titration and single crystal X-ray diffraction studies revealed the ability of the tripodal receptors to bind different anions with 1:1 or 2:1 stoichiometry in solution and in the solid state. It was also provided that the active fluorinated anion transporters can function as anticancer agents in vitro. [67]

Roelens et al. showed that a suitably functionalised tripodal system can be applied in the selective recognition of specific glycoside guests. In fact, acetalic substituents located in a pyrrolic tripodal structure provided a new artificial receptor, **L_{19}**, that showed affinity for mannosides. Binding properties were determined by NMR, ITC, and ESI-MS techniques.

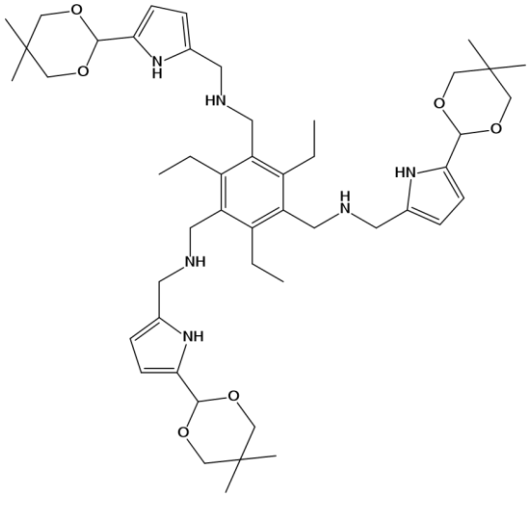

Figure 20. Pirrolic tripodal receptor (**L_{19}**).

This pyrrolic tripodal receptor exhibited the best recognition properties toward mannosides ever reported for a H-bonding synthetic receptor. The Authors demonstrated that implementing additional H-bonding substituents, strategically located into the architecture of the pyrrolic tripodal receptor, could enhance both the affinity for a specific glycoside and selectivity with respect to other monosaccharides. [68]

References

[1] Cosic, I.; *IEEE Trans. Biomed. Eng.*, **1994**, 41 (12), 1101-1114.

[2] Lockett, M. R.; Lange, H.; Breiten, B.; Heroux, A.; Sherman, W.; Rappoport, D.; Yau, P.O.; Snyder, P. W. and Whitesides, G.M.; *Angew. Chem. Int. Ed.*, **2003**, 52 (30), 7714-7717.

[3] Breiten, B.; Lockett, M. R.; Sherman, W.; Fujita, Shuji.; Al-Sayah, M.; Lange, H.; Bowers, C.M.; Heroux, A.; Krilov, G. and Whitesides, G. M.; *J. Am. Chem. Soc.,* **2013**, 135 (41), 15579–15584.

[4] Lehn, J. M.; *Supramolecular Chemistry*; **1995**; Weinheim: Wiley-VCH. ISBN 978-3-527-29312-4. OCLC 315928178.

[5] Gellman, S. H.; *Chem. Rev*., **1997**, 97 (5), 1231-1232.

[6] Baron, R.; Setny, P.; McCammon, J. A.; *J. Am. Chem. Soc*., **2010**, 132 (34), 12091-12097.

[7] Baron, R.; McCammon, J. A.; *Annu. Rev. Phys. Chem.*, **2013**, 64, 151-175.

[8] Artz, S.P.; Cram, D.J. *J. Am. Chem. Soc*. **1984**, *106*, 2160-2170.

[9] Amendola, V.; Bergamaschi, G.; and Miljkovic, A.; *Supramolecular Chemistry*, **2017**. DOI: 10.1080/10610278.2017.1339885.

[10] Boiocchi, M.; Bonizzoni, M.; Fabbrizzi, L.; Piovani, G.; and Taglietti, A.; *Angew. Chem. Int. Ed.*, **2004**, 43, 3847-3852.

[11] Amendola, V.; Bergamaschi, G.; Boiocchi, M.; Alberto, R.; Braband, H.; *Chem. Sci*., **2014**, 5, 1820-1823.

[12] Bergamaschi, G.; Miljkovic, A.; Marcheggiani, S.; and Poggi, A.; Hindawi Publishing Corporation, *International Journal of Inorganic Chemistry*, **2016**, Article ID 3415690.

[13] Amendola, V.; Alberti, G.; Bergamaschi, G.; Biesuz, R.; Boiocchi, M.; Ferrito, S. and Schmidtchen, F.P.; *Eur. J. Inorg. Chem*. **2012**, 21, 3410-3414.

[14] Graf, E.; Lehn, J. M.; *J. Am. Chem. Soc.*, **1976**, 98, 6403–6405.

[15] Metz, B.; Rosalky, J.M.; Weiss, R.; *J. Chem. Soc., Chem. Commun.,* **1976**, 533–534.

[16] (a) Schmidtchen, F. P.; *Angew. Chem. Int. Ed. Engl.,* 16, **1977**, 720–721. (b) Schmidtchen, F. P.; *Chem. Ber.*, **1980**, 113, 864–874; (c) Schmidtchen, F. P.; *Chem. Ber*., **1981**, 114, 597–607; (d) Schmidtchen, F. P.; *Angew. Chem. Int. Ed. Engl*., **1981**, 20, 466–468; (e) Schmidtchen, F. P.; *J. Mol.Catal*., **1986**, 37, 141–149; (f) Schmidtchen, F. P.; *Chem. Ber*., **1984**, 117, 725–732. (g) Schmidtchen, F.P.; *J. Org. Chem*., **1986,** 51, 5161-5168; (h) Schmidtchen, F. P.; *J. Am. Chem. Soc.*,

1986, 108, 8249–8255; (i) Schmidtchen, F. P.; *Tetrahedron Lett*., **1986**, 27,1987–1990; l) Worm, K.; Schmidtchen, F. P.; *Angew. Chem. Int. Ed. Engl.*, **1995**, 34, 65-66.

[17] Schmidtchen, F. P.; Müller, G.; *J. Chem. Soc., Chem. Commun.*, **1984**, 1115-1116.

[18] (a) Kang, S. O.; Llinares, J. M.; Day, V. W.; Bowman-James, K.; *Chem. Soc. Rev.*, **2010**, *39*, 3980-4003; (b) Ghosh, S.; Roehm, B.; Begum, R. A.; Kut, J.; Hossain, Md. A.; Day, V. W.; Bowman-James, K.; *Inorg. Chem.*, **2007**, *46*, 23, 9519-9521; (c) Amendola, V.; Bonizzoni, M.; Esteban-Gomez, D.; Fabbrizzi, L.; Licchelli, M.; Sancenon, F.; Taglietti, A.; *Coord. Chem. Rev*., **2006**, *250*, 1451–1470; (d) Bianchi, A.; Micheloni, M.; Paoletti, P.; *Coord. Chem. Rev.*, **1991**, *110*, 17; (e) Dietrich, B.; *Pure Appl. Chem.*, **1993**, *65*, 1457; (f) Ilioudis, C.A.; Steed, J.W.; *J. Supramol. Chem.*, **2001**, *1*, 165; (g) McKee, V.; Nelson, J.; Town, R.M.; *Chem. Soc. Rev.*, **2003**, *32*, 309; (h) Bowman-James, K.; *Acc. Chem. Res.*, **2005**, *38*, 671.

[19] (a) Dietrich, B.; Guilhem, J.; Lehn, J. M.; Pascard C.; Souveaux, E. *Helv. Chim. Acta* **1984**, *67*, 91-104; (b) McDowell, D.; Nelson, J. *Tetrahedron Lett.;* **1988**, *29*, 385-386; (c) Marrs, D.; McKee, V.; Nelson, J.; Luand Q.; Harding, C. J. *Inorg. Chim. Acta,* **1993**, *211*, 195-202; (d) Lu, Q.; McKee, V.; Nelson, J.; *J. Chem. Soc., Chem. Commun*., **1994**, 649-651; (e) Latour, J. M.; Lu, Q.; Harding, C. J.; Martin, N.; Marrs, D.; McKee, V.; Nelson, J. *J. Chem. Soc., Dalton Trans*., **1994**, 1471-1478; (f) McKee, V.; Nelson, J.; Town, R. M. *Chem. Soc. Rev*., **2003**, *32*, 309-325; (g) Alibrandi, G.; Amendola, V.; Bergamaschi, G.; Fabbrizzi, L.; Licchelli, M. *Org. Biomol. Chem*. **2015**, *13*, 3510-3524.

[20] (a) Morgan, G. G.; McKee, V.; Nelson, J.; *Prog. Inorg. Chem*., **1998**, *47*, 163; (b) Morgan, G. G.; McKee, V.; Nelson, J. *J. Chem. Soc., Chem. Commun*., **1995**, 1649-1652.

[21] (a) Mateus, P.; Bernier, N.; Delgado, R.; *Coord. Chem. Rev*., **2010**, 254, 1726-1747; (b) Yang, L.-Z.; Li, Y.; Jiang, L.; Fenga, X.-L.; Lu, T.-B.; *Cryst.Eng.Comm*., **2009**, 11, 2375-2380.

[22] McKee, V.; Nelson, J.; Town, R. M.; *Chem. Soc. Rev*, **2003**, *32*, 309-325.

[23] (a) Mason, S.; Clifford, T.; Seib, L.; Kuczera, K.; Bowman-James, K. *J. Am. Chem. Soc.* **1998**, *120*, 8899–8900; (b) Clifford, T.; Danby, A.; Llinares, J. M.; Mason, S.; Alcock, N. V.; Powell, D.; Aguilar, J. A.; Garcia-España, E.; Bowman-James, K. *Inorg. Chem*., **2001**, *40*, 4710-4720; (c) Hynes, M. J.; Maubert, B.; McKee, V.; Town R. M.; Nelson, J. *J. Chem. Soc., Dalton Trans*., **2000**, 2853-2859.

[24] Lehn, J. M. ; Méric, R. ; Vigneron, J. P. ; Bkouche-Waksman, I. ; Pascard, C. ; J. *Chem. Soc., Chem. Commun.*, **1991**, 62-64.

[25] Nelson, J.; Nieuwenhuyzen, M.; Pál, I.; Town, R. M.; *Chem. Commun*. **2002**, 2266-2267.

[26] (a) Clifford, T.; Mason, S.; Llinares, J. M.; Bowman-James, K, *J. Am. Chem. Soc.* **2000**, *122*, 1814-1815; (b) Aguilar, J. A.; Clifford, T.; Danby, A.; Llinares, J. M.; Mason, S.; Garcia- España, E.; Bowman-James, K. *Supramol. Chem*. **2001**, *13*, 405-417.

[27] Hossain, M. A.; Llinares, J. M.; Mason, S.; Morehouse, P.; Powell, D.; Bowman-James, K. *Angew. Chem. Int. Ed*. **2002,** *41*, 13, 2335-2338.

[28] Morehouse, P.; Hossain, M. A.; Llinares, J. M.; Powell, D.; Bowman-James, K.; *Inorg. Chem*. **2003**, *42*, 8131-8133.

[29] (a) Farrell, D.; Gloe, K.; Gloe, K.; Goretzki, G.; McKee, V.; Nelson, J.; Nieuwenhuyzen, M.; Pál, I.; Stephan, H.; Town R. M.; Wichmann, K.; *Dalton Trans.,* **2003** , 1961-1968; (b) Stephan, H.; Gloe, K.; Kraus, W.; Spies, H.; Johannsen, B.; Wichmann, K.; Reck, G.; Chand, D. K.; Bharadwaj, P. K.; Müller, U.; Müller, W. M.; Vögtle F.; *Fundamentals and Applications of Anion Separations* (Eds.: B. A. Moyer, R. P. Singh), Kluwer, New York, **2004**, 151-168.

[30] (a) Amendola, V.; Alberto, R.; Bergamaschi, G.; Braband, H.; Fox, T.; *Angew. Chem. Int. Ed.* **2012**, *51*, 9772-9776; (b) Amendola, V.; Alberti, G.; Bergamaschi, G.;. Biesuz, R.; Boiocchi, M.; Ferrito, S.; Schmidtchen, F. P. *Eur. J. Inorg. Chem.* **2012**, 3410-3417.

[31] Amendola, V.; Bergamaschi, G.; Boiocchi, M.; Alberto R.; Braband, H.; *Chem. Sci.* **2014**, *5*, 1820-1826.

[32] (a) Hunter, J.; Nelson, J.; Harding, C.; McCann, M.; McKee, V.; *Journal of the Chemical Society, Chemi. Comm.,* **1990**, *17*, 1148-1151; (b) Coyle, J.; Drew, M. G. B.; Harding, C. H.; Nelson, J.; Town, R. M.; *J. Chem. Soc., Dalton Trans*., **1997**, 1123-1125; (c) Deeney, F. A.; Harding, C. H.; Morgan, G. G.; McKee, V.; Nelson, J.; Teat, S. J.; Clegg, W.; *J. Chem. Soc., Dalton Trans*., **1998**, 1837-1843.

[33] (a) Drew, M. G. B.; Harding, C. J.; Howarth, O. W.; Lu, Q.; Marrs, D. J.; Morgan, G. G.; McKee, V. and Nelson, J.; *J. Chern. Soc. Dalton Trans.,* **1996**, 3021-3030; (b) McKee, V.; Nelson, J.; Speed, D. J. and Town, R. M.; *J. Chem. Soc., Dalton Trans.,* **2001**, 3641-3646.

[34] (a) Arnaud-Neu, F.; Fuangswasdi, S.; Maubert, B.; Nelson, J.; McKee, V. *Inorg. Chem.* **2000**, *39*, 573-579; (b) Harding, C. J.; Lu, Q.; Malone, J. F.; Marrs, D. J.; Martin, N.; McKee, V.; Nelson, J. *J. Chem. Soc., Dalton Trans*., **1995**, 1739-1747.

[35] Drew, M. G. B.; Howarth, O. W.; Harding, C. J.; Martin, N.; Nelson, J. *J. Chem. Soc., Chem. Commun.*, **1995**, 903-905.

[36] Drew, M. G. B.; Howarth, O. W.; Morgan G. G.; Nelson, J. *J. Chem. Soc., Dalton Trans. Inorg. Chem.*, **1994**, *21*, 3149-3158.

[37] Brooker, S.; Ewing, J. D.; Ronson, T. K.; Harding, C. J.; Nelson, J.; Speed, D. J. *Inorg. Chem*. **2003**, *42*, 2764-2773.

[38] (a) Beer, P.D.; Hayes, E.J.; *Coord. Chem. Rev.*, **2003**, *240*, 167; (b) De Silva, A. P.; McCaughan, B.; McFinney, B. O. F.; Querol, M.; *Dalton Trans*, **2003**,1902; (c) Bowman-James, K.; *Acc. Chem. Res.* **2005**, *38*, 671-678; (d) O'Neil, E.J.; Smith, B.D.; *Coord. Chem. Rev.* **2006**, *250*, 3068-3080; (e) Amendola, V.; Bonizzoni, M.; Esteban-Gòmez, D.; Fabbrizzi, L.; Licchelli, M.; Sancenòn, F.; Taglietti, A.; *Coord. Chem. Rev.* **2006**, *250*, 1451-1470.

[39] (a) Lehn, J. M.; Pine, S. H.; Watanabe, E. I.; Willard, A. K.; *J. Am. Chem. Soc.* **1977**, *99*, 6766-6768; (b) Lehn, J. M.; *Pure Appl. Chem.* **1980**, 52, 2441-2459; (c) Lehn, J. M.; *Science*, **1985**, 227, 849-856; (d) Jazwinski, J.; Lehn, J. M.; Lilienbaum, D.; Ziessel, R.; Guilheim, J.; Pascard, C.; *J. Chem. Soc. Chem. Commun*., **1987**, 1691-1692; (e) Taylor, R. W.; Begum, R. A.; Day, V. W.; Bowman-James, K.; *Cooperativity and the Chelate, Macrocyclic and Cryptate Effects*, Edited by Philip A. Gale, Jonathan W.Steed, From Supramolecular Chemistry: From Molecules to Nanomaterials, **2012**, 1, 67-93.

[40] Hossain, M. A.; P. Morehouse,; Powell, D.; Bowman-James, K.; *Inorg. Chem*. **2005**, 44, 2143-2149.

[41] (a) Lu, Q.; Latour, J. M.; Harding, C. J.; Martin, N.; Debbie J. Marrs, McKee, V. Nelson, J.; *J. Chem. Soc. Dalton Trans*. **1994**, 1471-1478; (b) Harding, C. J.;. Mabbs, F. E.; MacInnes, E. J. L.; McKee, V.; Nelson, J.; *J. Chem. Soc., Dalton Trans*., **1996**, 3227-3230; (c) Escuer, A.; Harding, C. J.; Dussart, Y.; Nelson, J.; McKee, V.; Vicente, R.; *J. Chem. Soc., Dalton Trans*., **1999**, 223-227; (d) Amendola, V.; Fabbrizzi, L.; Mangano, C.; Pallavicini, P.; Poggi, A.; Taglietti, A.; *Coord. Chem. Rev*. **2001**, 219-221, 821-837; (e) Bond, A. D.; Derossi, S.; Harding, C. H.; McInnes, E. J. L.; McKee, V.; McKenzie, C. J.; Nelson, J.; Wolowska, J.; *Dalton Trans*., **2005**, 2403-2409; (f) Bond, A. D.; Derossi, S.; Jensen, F.; Larsen, F. B.; McKenzie, C. J.; Nelson, J.; *Inorg. Chem*. **2005**, 44, 5987-5989; (g) Amendola, V.; Bonizzoni, M.; Esteban-Gómez, D.; Fabbrizzi, L.; Licchelli, M.; Sancenón, F.; Taglietti, A.; *Coord. Chem. Rev*., **2006**, 250, 1451-1470.

[42] Dussart, Y.; Harding C. H.; Dalgaard, P.; McKenzie, C.; Kadirvelraj, R.; McKee, V.; Nelson, J.; *J. Chem. Soc., Dalton Trans*., **2002**, 1704-1713.

[43] (a) Amendola, V.; Bastianello, E.; Fabbrizzi, L.; Mangano, C.; Pallavicini, P.; Perotti, A.; Lanfredi, A. M.; Ugozzoli, F.; *Angew. Chem., Int. Ed*. **2000**, 39, 2917-2920; (b) Amendola, V.; Bergamaschi, G.; Boiocchi, M.; Fabbrizzi, L.; Poggi, A.; Zema, M.; *Inorg. Chim. Acta*, **2008**, 361(14-15), 4038-4046.

[44] Bergamaschi, G.; Boiocchi, M.; Perrone, M. L.; Poggi, A.; Viviani, I.; Amendola, V.; *Dalton Trans*., **2014**, 43, 11352-11360.

[45] Derossi, S.; Farrell, D. T.; Harding, C. H.; McKee, V.; Nelson, J.; *Dalton Trans.*, **2007**, 1762-1772.

[46] Esteves, C. V.; Mateus, P.; André, V.; Bandeira, N. A. G.; Calhorda, M. J.; Ferreira, L. P.; Delgado, R.; *Inorg. Chem*. **2016**, 55, 7051-7060.

[47] Boiocchi, M.; Bonizzoni, M.; Fabbrizzi, L.; Piovani, G.; Taglietti, A.; *J. Am. Chem. Soc.*, **2004**, 43, 3847-3852.

[48] (a) Wiskur, S.L.; Ait-Haddou, H.; Lavigne, J.L.; Anslyn, E.V.; *Acc. Chem. Res.*, **2001**, 34, 963; (b) Martinez-Manez, R.; Sancenon, F.; *Chem. Rev.*, **2003**, 103, 4419; (c) Fabbrizzi, L.; Marcotte, N.; Stomeo, F.; Taglietti, A.; *Angew. Chem. Int.Ed.*, **2002**, 41, 3811; (d) Wiskur, S.L.; Ait-Haddou, H.; Lavigne, J.L.; Anslyn, E.V.; *Acc. Chem. Res*., **2001**, 34, 963; (e) Martinez-Manez, R.; Sancenon, F.; *Chem. Rev.*, **2003**, 103, 4419; (f) Marcotte, N.; Taglietti, A.; *Supramol. Chem*., **2003**, 15, 617.

[49] Mateus, P.; Delgado, R.; André, V.; Duarte, M. T.; *Inorg. Chem*. **2015**, 54, 229-240.

[50] Amendola, V.; Bergamaschi, G.; Cabrini, E.; Dacarro, G.; Rossi, N.; Pallavicini, P.; Taglietti, A.; *New J. Chem*, **2016**, 40, 5722-5730.

[51] De Leener, G.; Evoung-Evoung, F.; Lascaux, A.; Mertens, J.;Porras-Gutierrez, A. G.; Le Poul, N.; Lagrost, C.; Over, D.; Leroux, Y. R.; Reniers, F.; Hapiot, P.; Le Mest, Y.; Jabin, I.; Reinaud, O.; *J. Am. Chem. Soc.* **2016**, 138, 12841-12853.

[52] (a) Berrocal, M. J.; Cruz, A.; Badr, I. H. A.; and Bachas, L. G.; *Anal. Chem.* **2000**, 72, 5295-5299. (b) Kuswandi, B.; Nuriman; Verboom, W.; and Reinhoudt, D. N.; *Sensors* **2006**, *6*, 978-1017

[53] (a) Sato, K.; Arail, S.; Yamagishi, T.; *Tetrahedron Lett.*, **1999**, 40, 5219-5222. (b) Ballester, P.; Costa, A.; Deyii, P. M.; Vega, M; Morey, J.; *Tetrahedron Lett.*, **1999**, 40, 171-174. (c) Fan, A. L.; Hong, H. K.; Valiyaveettil, S.; Vittal, J. J.; *J. Supramol. Chem*., **2002**, 2, 247-254.

[54] (a) Reinoso-Garcia, M. M.; Dijkman, A.; Verboom, W.; Reinhoudt, D. N.; Malinoswka, E.; Wojciechowska, D.; Pietrzak, M.; Selucky, P.; *Eur. J. Org. Chem*. **2005**, 2131-2138. (b) Kim, S.-G.; Kim, K.-H.; Jung, J.; Shin, S. K.; Ahn, K. H.; *J. Am. Chem. Soc*. **2002**, 124, 591-597. (c) Kim, Y.-K.; Ha, J.; Cha, G. S.; Ahn, K. H.; *Bull. Korean Chem. Soc.* **2002**, 23, 1420-1424. (d) Sasaki, S.; Ozawa, S.; Citterio, D.; Iwasawa, N.; Suzuki, K.; *Anal. Sci*., **2001**, 17, 1659-1661. (e) Reinoso-Garcia, M. M.; Janczewski, D.; Reinhoudt, D. N.; Verboom, W.; Malinoswka, E.; Pietrzak, M.; Hill, D.; Baca, J.; Gruner, B.; Selucky; P; Gruttner, C.; *New J. Chem.*, **2006**, 30, 1480-1492.

[55] (a) Schmuck, C.; Schwegmann, M.; *Org. Biomol. Chem.*, **2006**, 4, 836-838. (b) Wei, L. H.; He, Y. B.; Wu, J. L.; Qin, H. J.; Xu, K. X.; Meng, L. Z.; *Chin. J. Chem.*, **2005**, 23, 608-612. (c) Niikura, K.; Bisson, A. P.; Anslyn, E. V.; *J. Chem. Soc., Perkin Trans. 2*, **1999**, 1111-1114. (d) Wiskur, S. L.; Ait-Haddou, H.; Lavigne, J. J.; Anslyn, E. V.; *Acc. Chem. Res.*, **2001**, 34, 963-972.

[56] Sato, K.; Arai, S.; Yamagishi, T. ; *Tetrahedron Lett.*, **1999**, 40, 5219-5222.

[57] Ihm, H.; Yun, S.; Kim, H. G.; Kim, J. K. and Kim, K. S.; *Org. Lett.*, **2002**, 4, 2897-2900.

[58] Howarth, J.; Al-Hashimy, N. A.; *Tetrahedron Lett*., **2001**, 42, 5777-5779.

[59] Bai, Y.; Zhang, B. G.; Xu, J.; Duan, C. Y.; Dang, D. B.; Liu, D.J.; Meng, Q. J.; *New J. Chem*., **2005**, 29, 777–779.

[60] Pramanik, A.; Powell, D. R.; Wong, B. M. and Hossain, Md. A.; *Inorg. Chem*., **2012**, 51, 4274-4284.

[61] Roy, A.; Saha, D.; Mukherjee, A. and Talukdar, P.; *Org. Lett.;* **2016**, 18, 5864−5867.

[62] Turner, D. R.; Paterson, M. J. and Steed, J. W.; *J. Org. Chem.* **2006**, 71, 1598-1608.

[63] Amendola, V.; Boiocchi, M.; Colasson, B.; Fabbrizzi, L.; Monzani, E.; Jesús Douton-Rodriguez, M. and Spadini, C.; *Inorg. Chem.* **2008**, 47, 4808-4816.

[64] Bose, P.; Ravikumar, I. and Ghosh, P.; *Inorg. Chem.* **2011**, 50, 10693-10702.

[65] Tobey, S. L.; Jones, B. D. and Anslyn, E. V.; *J. Am. Chem. Soc.* **2003**, 125, 4026-4027.

[66] Jia, C. D.; Wu, B. A.; Li, S. G.; Huang, X. J.; Zhao, Q. L.; Li, Q.S.; Yang, X. J.; *Angew. Chem., Int. Ed.*, **2011**, 50, 486.

[67] Busschaert, N.; Wenzel, M.; Light, M. E.; Iglesias-Hernandez, P.; Perez-Tomas, R. and Gale, P. A.; *J. Am. Chem. Soc.,* **2011**, 133, 14136-14148.

[68] Nativi, C.; Cacciarini, M. Francesconi, O.; Moneti, G. and Roelens, S.; *Org. Lett.*, **2007**, Vol. 9, No. 23.

2. Tripodal hydrogen- and halogen-bonding anion receptors based on 3-iodopyridinium units

2.1 Introduction

Anion recognition is a relevant issue in supramolecular chemistry due to the importance of anionic species in the chemical and biochemical fields. In particular, the synthesis of new selective receptors for anions has involved many research groups in last years.[1] In the receptor design, several types of non-covalent interactions have been considered, including electrostatic forces and hydrogen bonding (HB). [2-3] The latter, in particular, is very important in this context, because it can be effective in polar solvents, and it can lead to the selective recognition of anionic species even in water. In last years, halogen bonding (XB) has also become popular among supramolecular chemists.[4] This type of interaction has been applied in the construction of sophisticated supramolecular architectures and functional materials, and to obtain selective anion recognition in competing media, as shown by Beer[5] and others.[6-8]

Halogen bonding and HB have significant similarities. Both interactions are characterised by high directionality; they can lead to shorter contact distances than the sum of the Van der Waals radii of the involved atoms. They both involve electrophilic species [i.e., H and X atoms for HB and XB, respectively] and a nucleophilic atom [i.e., N, O, S, etc.], therefore binding has a dominant electrostatic contribution. However, theoretical and experimental studies have shown that polarization, charge transfer, and dispersion forces also play an important role.[9] Notably, the balance between HB and XB is fundamental in determining the structure of the compounds in the solid state.[10]

The similar features of HB and XB have encouraged chemists to synthesize new molecular systems based on one or other type of interaction, especially in the field of anion recognition.[11] The synthesis of selective anion receptors, containing positively charged and/or HB-donor fragments is rather common in this context.[12] Stronger anion binding is actually obtained when several HB-donor groups converge towards the anionic guest, better if within a well-defined cavity,[13-15] as observed by Steed et al. in a series of 3-aminopyridinium-based receptors.[16]

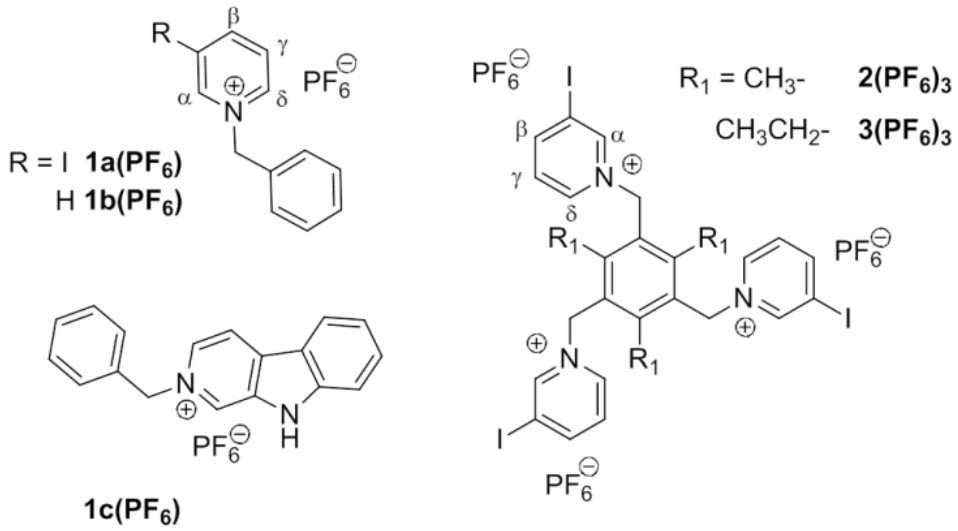

Figure 1. Pyridinium-based anion receptors

In this work, we evaluated the behaviour of receptors containing different interaction sites suitable for the recognition of anionic species. In particular, we aimed to combine XB and HB donor groups around the bowl-shaped cavity of a tripodal system. To achieve this goal, we synthesized new receptors, containing three 3-iodopyridinium units appended to trialkylbenzene platforms, and we investigated their anion binding capabilities through NMR and UV-vis spectroscopies. We also compared our results to those obtained for the simple N-benzyl-3-iodopyridinium molecule, and to those already available for analogous tripodal receptors barely based on electrostatic or HB interactions. A computational study was carried out to evaluate the contribution of HB and XB to the stability of the complexes. X-ray diffraction studies were also performed.

2.2 Experimental

2.2.1. Materials and methods

All reagents for syntheses were purchased from Sigma-Aldrich and used without further purification. All reactions were performed under dinitrogen. Mass spectra were acquired on a Thermo Finnigan ion trap LCQ Advantage Max instrument equipped with an ESI source. ^{1}H- and ^{13}C-NMR spectra were recorded on a Bruker ADVANCE 400 spectrometer (operating at 9.37 T, 400 MHz). UV-vis. spectra were run on a Varian Cary 50 SCAN spectrophotometer, with quartz cuvettes of the appropriate path length (1 or 0.1 cm) at 25.0 ± 0.1°C under inert conditions. Solvents were dried by common methods. **1b**(PF_6) was prepared according to a known procedure.[17] The

experimental procedures of NMR and UV-vis. titrations have been described elsewhere.[18] Titration data were processed with the Hyperquad package[19] to determine the equilibrium constants.

2.2.2. Computational details

All calculations were carried out with the Gaussian 09 package.[20] Conformation analysis and geometry optimizations were carried out at the MP2 level for complex **1a**$^{+}$/X^{-}, **1b**$^{+}$/X^{-}and **1c**$^{+}$/X^{-}. For the complex **2**$^{3+}$/X^{-}, structural optimizations were carried out using the B3LYP functional due to the larger species size.[21] MP2 single point energies were subsequently obtained employing the B3LYP geometries. A polarized/augmented double zeta basis set (6-31+G(d,p) for light atoms and he LANL2DZ basis set augmented with the diffuse function from the aug-cc-pVDZ set for the halogen atoms) was used in all the calculations; effective-core potentials (LANL) were also used for Cl, Br, and I to reduce computational costs. Solvent effects were evaluated using the PCM model and different solvents were selected in order to reproduce the experimental conditions.[22] Basis set superposition errors were estimated via the Counterpoise approach at the MP2 level in all cases. The calculation of chemical shifts for the hydrogen atoms was carried out employing the GIAO procedure as implemented in Gaussian 09.[23]

2.2.3. Crystal structure analysis

Diffraction data for **1a**(PF_6) (colourless, 0.43 x 0.28 x 0.07 mm3) and **1a**(I) (pale yellow, 0.45 x 0.14 x 0.08 mm3) crystals were collected by means of an Enraf-Nonius CAD4 four circle diffractometer, whereas diffraction data for **2**$(NO_3)_2(PF_6)$ (colourless, 0.23 x 0.07 x 0.05 mm3) and **2**$(Br)(PF_6)_2$ (colourless, 0.17 x 0.10 x 0.08 mm3) crystals were collected on a Bruker-AXS diffractometer equipped with the SMART-APEX CCD detector. Both instruments work at room temperature with MoKα X-radiation (λ = 0.71073 Å). Crystal data were reported on Table S1.

Data reductions (including intensity integration, background, Lorentz and polarization corrections) for intensities collected with the conventional diffractometer were performed with the WinGX package;[24] absorption effects were evaluated with the psi-scan method[25] and absorption correction was applied to the data. Frames collected by the CCD-based system were processed with the SAINT software[26] and intensities were corrected for Lorentz and polarization effects; absorption effects were empirically evaluated by the SADABS software[27] and absorption correction was applied to the data.

All crystal structures were solved by direct methods (SIR 97)[28] and refined by full-matrix least-squares procedures on F^2 using all reflections (SHELXL-2014).[29] Anisotropic displacement

parameters were used for all non-hydrogen atoms. Hydrogens have been placed at calculated positions and their positions refined according to a riding model.

Positional disorder affected a nitrate counter ion in the **2**$(NO_3)_2(PF_6)$ crystal and the NO_3^- anion resulted placed over two alternative positions half populated. The X-ray diffraction quality of the **2**$(NO_3)_2(PF_6)$ crystal did not allow a full unconstrained structure refinement and the geometries of the disordered nitrate counter ions, as well as those of the hexafluorophosphate ion, were restrained to the expected ones using soft DFIX and DANG restraints.

2.2.4. Synthesis

2.2.4.1. Synthesis of 1a(PF_6)

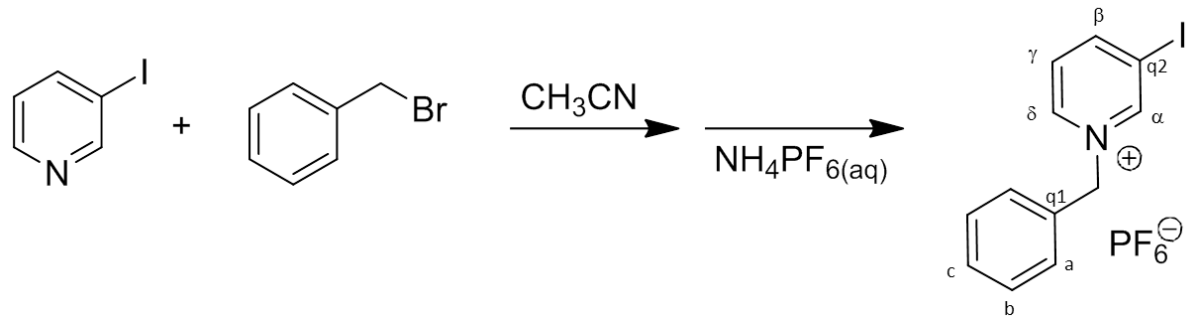

1a

To a solution of 3-iodopyridine (0.10 g, 0.49 mmol) in acetonitrile (10 mL), an acetonitrile solution of benzyl bromide (0.10 g, 0.58 mmol, in 10 mL) was added under stirring. The mixture was refluxed for 72 hrs. The solvent was then evaporated to dryness, and the solid residue was washed with dichloromethane and filtered. The final product was then isolated as an hexafluorophosphate salt by dissolving the solid in warm water, and treating it with a saturated solution of NH_4PF_6(aq). The white solid was collected and dried. Yield: 71%

$C_{12}H_{11}NIPF_6$: found: C, 32.62; H, 2.56; N, 3.16%, calculated: C, 32.68; H, 2.51; N, 3.18%

ESI–MS, MeOH (m/z): 296.15 [**1a**]$^+$.

^{1}H–NMR (400 MHz), d_6–DMSO (ppm): 9.65 (s, H-α, 1H), 9.15 (d, H-β, 1H), 8.97 (d, H-δ, 1H), 7.93 (t, H-γ, 1H), 7.51 (d, H-b, 2H), 7.49 (m, H-c and H-d, 3H), 5.44 (s, CH_2, 2H).

^{13}C–NMR (400 MHz), d_6–DMSO (ppm): 155.94 (C-β), 151.67 (C-α), 145.09 (C-δ), 134.01 (q1), 131.69 (C-c), 131.14 (Ca), 130.97 (C-b), 130.66 (C-γ), 95.71 (q2), 66.23 (CH_2).

2.2.4.2. Synthesis of 2(PF$_6$)$_3$

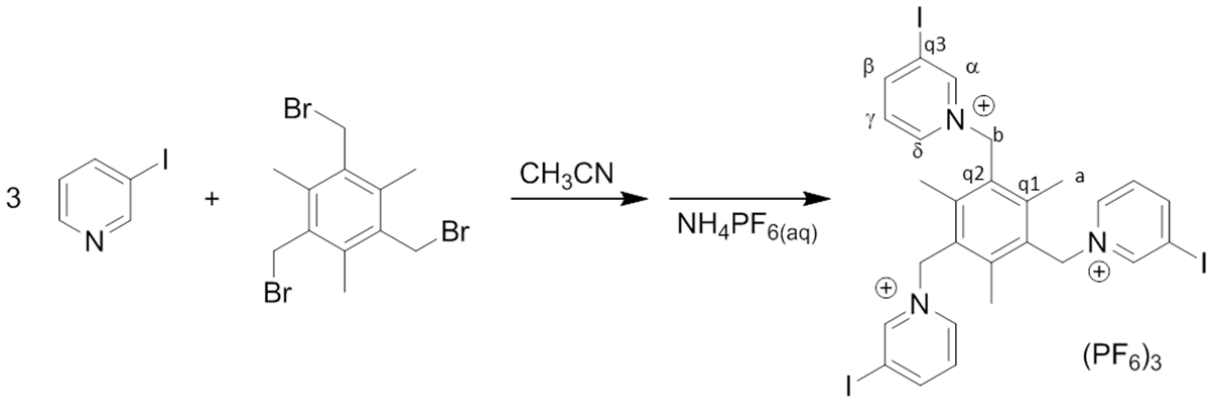

2

To a solution of 3-iodopyridine (0.19 g, 0.93 mmol) in acetonitrile (5 mL), an acetonitrile solution of 1,3,5-tribromomethyl mesitylene (0.10 g, 0.25 mmol, in 7 mL) was added under stirring. The mixture was refluxed for 72 hrs. The solvent was then evaporated to dryness, and the solid residue was washed with dichloromethane and filtered. The final product was then isolated as an hexafluorophosphate salt by dissolving the solid in warm water, and treating it with a saturated solution of NH_4PF_6(aq). The white solid was collected and dried. Yield: 62%

$C_{27}H_{27}N_3I_3P_3F_{18}$: found: C, 26.65; H, 2.32; N, 3.40%, calculated: C, 26.82; H, 2.25; N, 3.48%

ESI–MS, MeOH (m/z): 258.50 [**2**]$^{3+}$, 459.94 [**2** +PF_6^-]$^{2+}$.

^{1}H–NMR (400 MHz), d_6–DMSO (ppm): 9.42 (s, H-α, 3H), 8.99 (d, H-β, 3H), 8.52 (d, H-δ, 3H), 7.83 (t, H-γ, 3H), 5.99 (s, H-b, 6H), 2.24 (s, H-a, 9H).

^{13}C–NMR (400 MHz), d_6–DMSO (ppm): 154.97 (C-β), 151.12 (Cα), 145.49 (q1), 143.34 (C-δ), 131.37 (C-γ), 129.57 (q2), 97.30 (q3), 59.84 (C-b), 18.23 (C-a).

2.2.4.3. Synthesis of 3(PF$_6$)$_3$

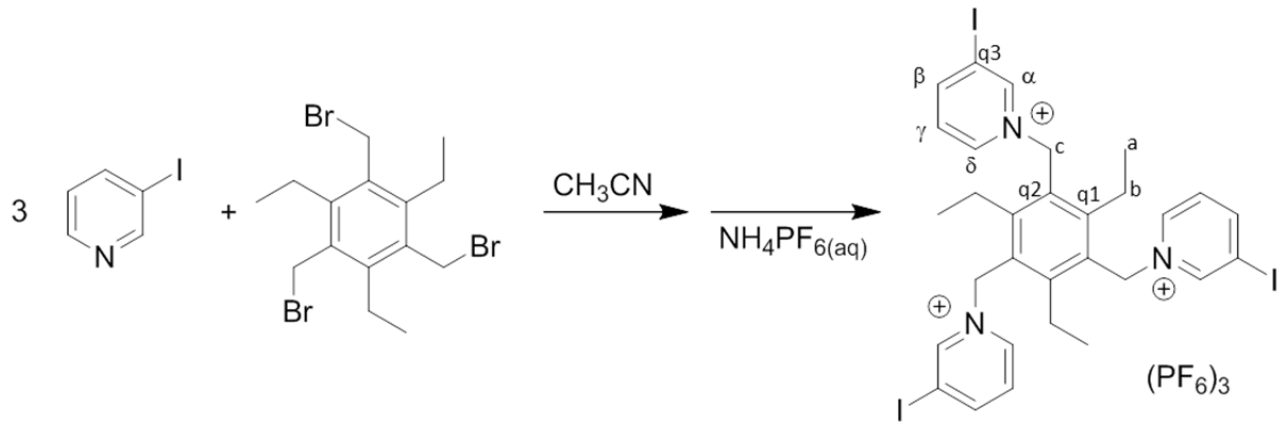

3

To a solution of 3-iodopyridine (0.19 g, 0.93 mmol) in acetonitrile (5 mL), an acetonitrile solution of 1,3,5–tribromomethyl–2,4,6–triethylbenzene (0.10 g, 0.23 mmol, in 7 mL) was added under stirring. The mixture was refluxed for 72 hrs. The solvent was then evaporated to dryness, and the solid residue was washed with dichloromethane and filtered. The final product was then isolated as an hexafluorophosphate salt by dissolving the solid in warm water, and treating it with a saturated solution of NH_4PF_6(aq). The white solid was collected and dried. Yield: 56%

$C_{30}H_{33}N_3I_3P_3F_{18}$: found: C, 28.67; H, 2.72; N, 3.24%, calculated: C, 28.80; H, 2.66; N, 3.36%

ESI–MS, MeOH (m/z): 272.33 [**3**]$^{3+}$, 480.50 [**3** + PF_6^-]$^{2+}$.

^{1}H–NMR (400 MHz), d_6–DMSO (ppm): 9.54 (s, H-α, 3H), 9.00 (d, H-β, 3H), 8.53 (d, H-δ, 3H), 7.84(t, H-γ, 3H), 5.96 (s, H-c, 6H), 2.60 (m, H-b, 6H), 0.77 (t, H-a, 9H).

^{13}C–NMR (400 MHz), d_6–DMSO (ppm): 154.98 (C-β), 151.62 (C-α), 151.52 (q1), 142.96 (C-δ), 130.17 (C-γ), 128.75 (q2), 97.05 (q3), 58.35 (C-c), 24.77 (C-b), 16.28 (C-a).

2.3. Results and discussion

The iodopyridinium-based receptors, reported in Figure 1, were synthesized modifying a procedure, used in the preparation of polypyridinium systems.[14-15] The interaction with anionic guests of all receptors was investigated by NMR and UV-vis titrations in organic solvents (acetonitrile, DMSO). Due to the low solubility of receptors **2**$(PF_6)_3$ and **3**$(PF_6)_3$ in acetonitrile, NMR titrations on these two receptors were done in d_6-DMSO/CD_3CN mixture.

2.3.1. ^{1}H-NMR titrations on the mono-branched pyridinium-based receptors

The anion binding studies on receptor **1a**$^+$ (1.85 mM) were performed by ^{1}H-NMR titrations with TBACl, TBABr and TBAI in CD_3CN. The formation of 1:1 complexes with chloride, bromide, and iodide was observed, and the binding constants were calculated from the fitting of the ^{1}H-NMR titration data (see Table 1). Spectra and profiles are shown in the Figures below.

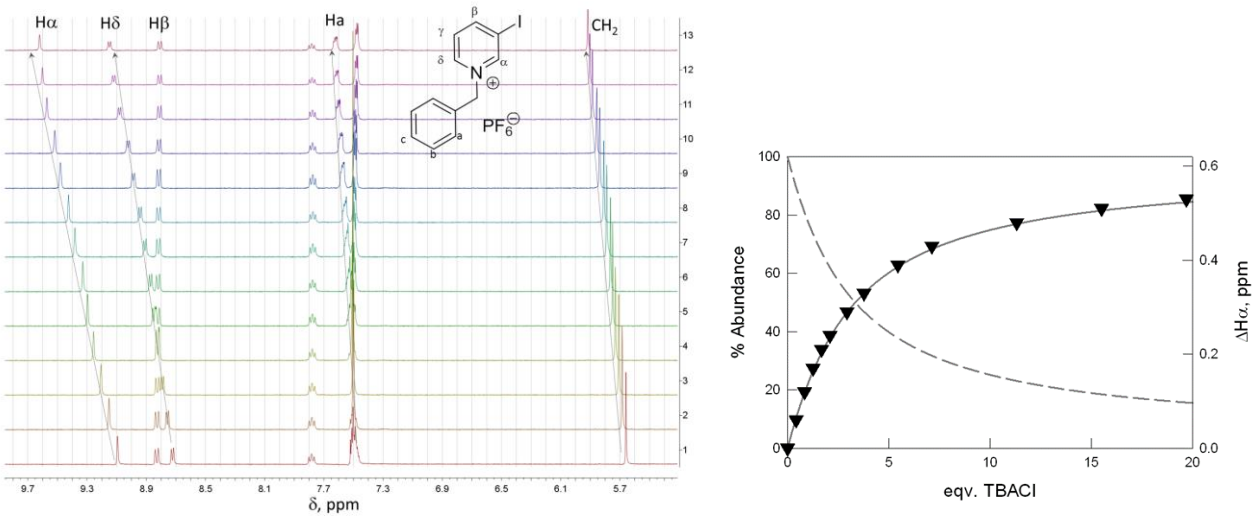

Figure 2. Family of ^{1}H-NMR spectra and profile for the titration of **1a**$^+$ (1.85 mM) with TBACl in CD_3CN, superimposed to the distribution diagram obtained for the formation of a 1:1 complex characterized by LogK_{11} = 2.30(3). The black triangles show the shift of proton Hα vs. equivalents of chloride.

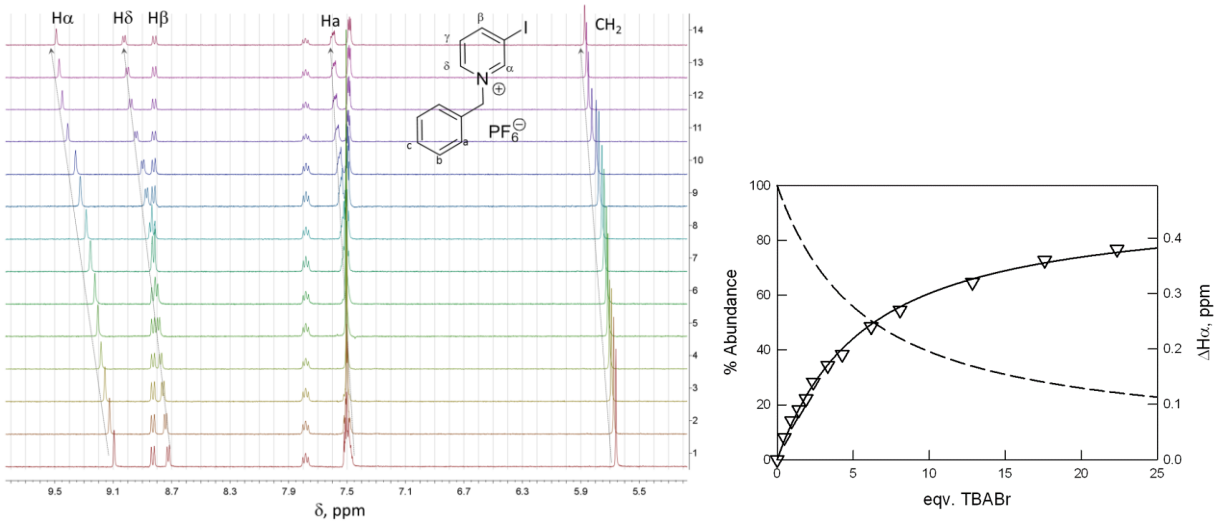

Figure 3. Family of ^{1}H-NMR spectra and profile for the titration of **1a**$^+$ (1.85 mM) with TBABr in CD_3CN. The profile (white triangles) shows the shift of protons Hα vs. equivalents of anion. The profile is superimposed to the distribution diagram built for the formation of a 1:1 complex characterized by LogK_{11} = 1.98(4).

In the case of receptor **1a**$^+$, anion addition influenced especially protons Hα and Hδ, in the ortho positions to the nitrogen. The corresponding signals underwent a significant downfield shift (Δδ= +0.53 ppm and +0.43 ppm for Hα and Hδ, respectively).

^{1}H-NMR titrations evidenced the preference of **1a**$^+$ for the chloride anion, followed by bromide and iodide (see Figure 4). This is not unusual, as it is the common trend observed in pyridinium systems. On the other hand, upon addition of TBAF to a solution of **1a**(PF_6) in CD_3CN, the disappearance of signals of most aromatic protons was observed, suggesting either a fluoride-induced deprotonation or decomposition processes.[20]

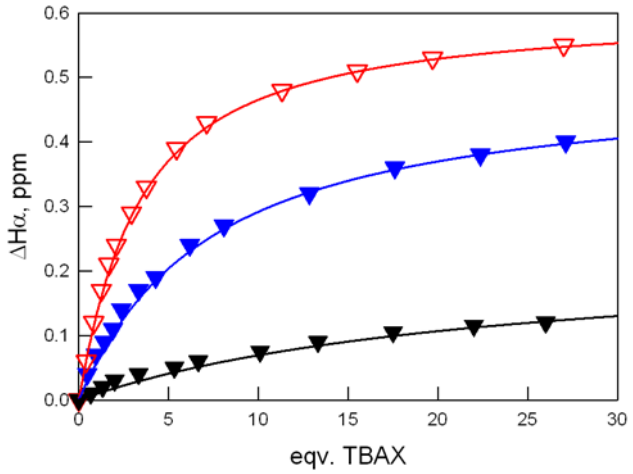

Figure 4. ^{1}H-NMR titrations of **1a**$^+$ with halides in CD_3CN. Variation of the chemical shift of Hα upon anion (as TBA salt) addition (symbols: red, chloride; blue, bromide; black, iodide). The experimental profiles are superimposed to the formation curves of the 1:1 adducts with the anions, calculated according to the constants reported in Table 1.

In the case of receptor **1b**$^+$, protons Hα were de-shielded but to a lower extent (+0.40 ppm up to 20 eqv. of chloride, see Figure 6). As a matter of fact, the iodopyridinium receptor **1a**$^+$ is able to binding halide anions through different modes (i.e. HB and XB). Anion···π interactions may also participate.[30] The observed downfield shifts are due to the HB rather than to XB, for which up-field shifts would have been expected.[31]

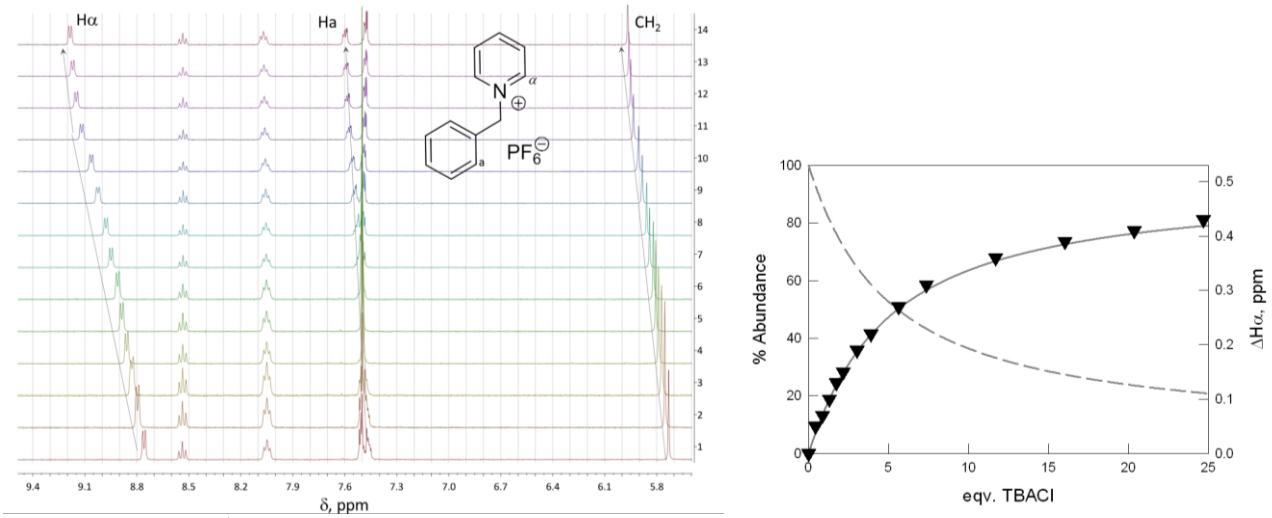

Figure 6. Family of ^{1}H-NMR spectra and profile for the titration of **1b**$^+$ (1.85 mM) with TBACl in CD_3CN. The profile (black triangles) shows the shift of protons Hα vs. equivalents of chloride. The profile is superimposed to the distribution diagram built for the formation of a 1:1 complex characterized by LogK_{11} = 2.06(1).

However, clarifying the different contributions in solution is difficult, as different binding modes may occur simultaneously. The binding constants, shown in Table 1, point out that anion affinity is higher for **1a**$^+$ than for the simple N-benzyl pyridinium analogue, **1b**$^+$. We could thus conclude that the iodine-substituent had a positive effect on the anion binding capabilities of our pyridinium receptors, as a likely consequence of its electron-withdrawing effect on the pyridine hydrogen atoms.

Anion	**LogK$_{11}$/1a$^+$**	**LogK$_{11}$/1b$^+$**	**LogK$_{11}$/1c$^+$[14]**
Cl^-	2.30(3) [2.27(1)][a]	2.06(1)	[3.20(1)][a]
Br^-	1.98(4) [2.08(1)][a]	n.d.	[2.48(1)][a]
I^-	1.70(6)	n.d.	n.d.

Table 1. Affinity constants determined by ^{1}H-NMR titrations with halides as TBA salts (in CD_3CN, T = 25°C). [a]Constants obtained through UV-vis titrations in CH_3CN (25°C). In parenthesis, the uncertainties on the last figures are reported.

2.3.2. UV-vis titrations on the mono-branched pyridinium-based receptors in CH_3CN

The interaction of **1a**$^+$ with chloride and bromide was also investigated by UV-vis titrations in acetonitrile. The receptor displays a band at 290 nm (2.1×10^3 $M^{-1}cm^{-1}$), corresponding to a charge transfer that involves the iodine substituent. During anion addition, this band broadens. From the fitting of the profiles, the affinity constants for both chloride and bromide were determined [2.27(1) and 2.08(1) Log units, respectively], confirming NMR titration results. Both UV-vis spectra and distribution diagrams are shown in Figures 7-8.

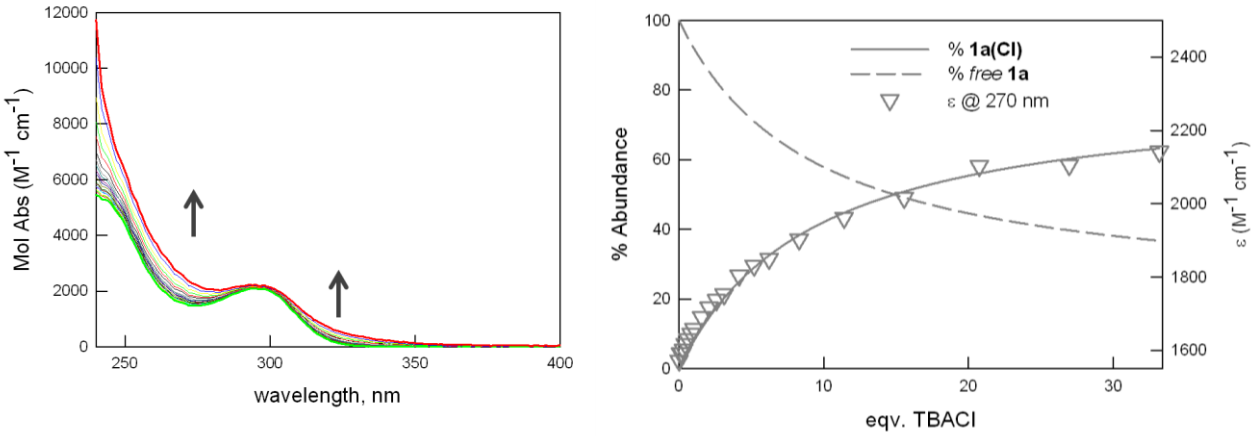

Figure 7. UV-vis spectra recorded during the titration of **1a**$^+$ (0.5 mM) with TBACl in acetonitrile (left) and titration profile (right) superimposed to the distribution diagram built for the formation of a 1:1 complex characterized by LogK_{11} = 2.27(1). The triangles show the profile of the Mol Abs at 270 nm vs. equivalents of chloride.

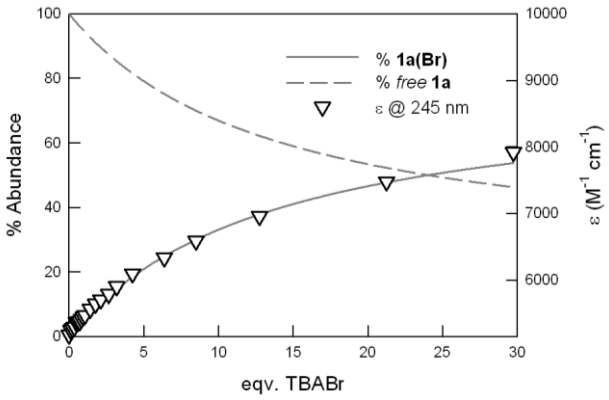

Figure 8. UV-vis titration profile of **1a(PF$_6$)** (0.5 mM) with TBABr in acetonitrile, superimposed to the distribution diagram built for the formation of a 1:1 complex characterized by LogK_{11} = 2.08(1). The triangles show the profile of the Mol Abs at 245 nm vs. equivalents of bromide.

The affinity constants obtained for receptor **1a**$^{+}$ are lower than those determined in the same conditions for the 9H-β-carbolin-2-ium system[14] (see **1c**$^{+}$ in Table 1). This suggests that the NH group in 9H-β-carbolin-2-ium has a stronger effect on anion affinity than the iodine atom in the studied receptors.

2.3.3. Computational studies

To evaluate the higher anion affinity of **1a**$^{+}$ compared to **1b**$^{+}$, we performed computational studies on both receptors in presence of Cl^{-} and Br^{-}. Several low-lying solution conformers were optimized.

Notably, the computational studies supported the experimental results as far as the relative stability of the complexes, even if this may be due to entropic effects due to the lower population of low lying isomers as in the iodide case. The theoretical results suggested that the halogen-bonded species (d) shown in Figure 9 lies at least 0.9 kcal/mol above the other stable conformers found for **1a**$^{+}$/Cl^{-} and **1a**$^{+}$/Br^{-} [i.e. Figure 9, (a) and (c), respectively], and has a lower IPDE (see Table 2), which indicates that it is not the most relevant species in solution.

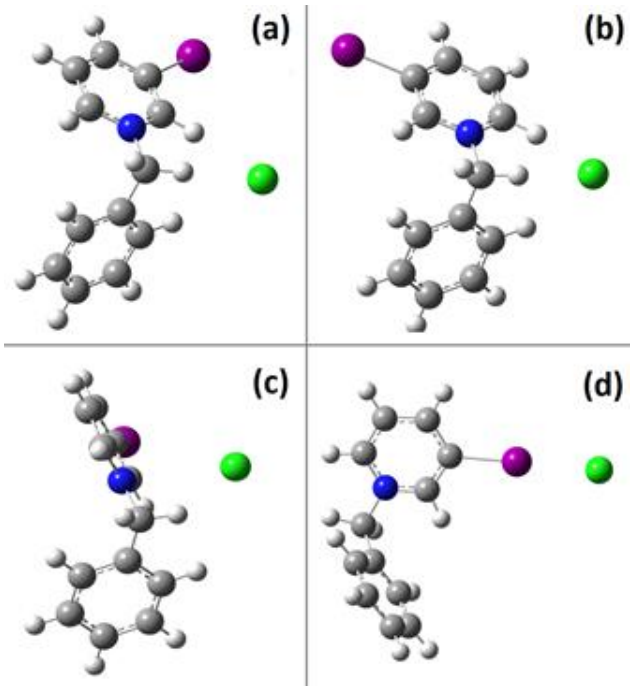

Figure 9. Geometries of four possible conformers for the binding of Cl^{-} by **1a**.

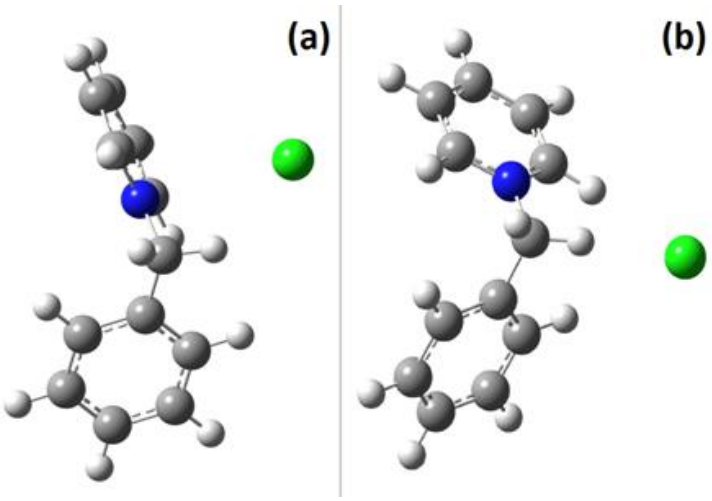

Figure 10. Geometries of two possible conformers for **1b**$^{+}$/Cl^{-}.

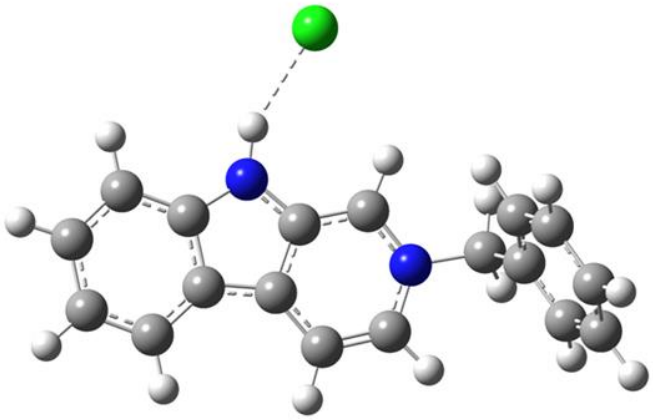

Figure 11. Optimized structure of the **1c**$^{+}$/Cl^{-} complex, from which it is evidenced the strong HB with Cl^{-}.

Comp.	**IPDE** (kcal/mol) **X=Cl**$^{-}$	**IPDE** (kcal/mol) **X=Br**$^{-}$	**IPDE** (kcal/mol) **X=I**$^{-}$
1a^{+}	7.06$^{(a)}$; 6.67$^{(b)}$; 6.64$^{(c)}$; 5.86$^{(d)}$	6.48$^{(a)}$; 6.13$^{(b)}$; 6.84$^{(c)}$; 5.58$^{(d)}$	6.04$^{(a)}$; 5.68$^{(b)}$; 7.14$^{(c)}$; 5.34$^{(d)}$
1b^{+}	6.50$^{(a)}$; 5.62 $^{(b)}$	6.00$^{(a)}$; 5.78$^{(b)}$	n.d.
1c^{+}	9.83	8.75	n.d.

Table 2. Ion pair dissociation energies, IPDE=E(S^{+}/X^{-})-E(S^{+})-(X^{-}), where S^{+} is the pyridinium cation and X^{-} is the anion. Solvent effects are introduced via the PCM model. The letters refer to the isomers shown in Figure 9 for **1a**$^{+}$, and in Figure 10 for **1b**$^{+}$.

Counterpoise corrected energies are given below:

Comp.	**IPDE** (kcal/mol) **X=Cl**$^-$	**IPDE** (kcal/mol) **X=Br**$^-$	**IPDE** (kcal/mol) **X=I**$^-$
1a	5.65; 5.39 4.93; 4.12	4.84; 4.95 5.07; 3.91	4.58; 4.34 5.12; 4.24
1b	5.22; 4.14	4.15; 4.72	
1c	8.40	7.28	

Table 3. Counterpoise corrected IPDE for the species in Table 2; the order of the isomers is maintained.

Interestingly, the structures shown in Figures 9 and 10 fully support the NMR assignments, justifying the incremental shifts of the hydrogen atoms involved in the interaction with the anions. Chemical shifts computed at the B3LYP/6-31+G(d,p)/GIAO level, in fact, suggested that Hα, Hδ and the methylene protons should all be substantially shifted downfield (Δδ=1.0-3.3 ppm) for the species shown in Figure 9, (a) and (b). On the other hand, Hβ and Hγ should remain mostly unchanged. Only minor shifts are instead predicted for the X-bonding species [i.e., Figure 9(d)]. As for the size of the computed chemical shifts, these appear larger than the experimental data. Such apparent discrepancy can be readily rationalized, considering that the measured shifts represent the average of all possible structures accessible within the time scale of the NMR measurement. In this respect, the small energy differences reported in Table 2 suggest that the ion pairs are highly fluxional, so that the structures in Figures 9 and 10 represent only limiting cases. This is confirmed by the energy profiles shown in Figure 12. The fluxionality also explains the presence in the NMR spectrum of a singlet for CH_2, instead of the double doublet expected on symmetry considerations (i.e., the symmetry-breaking induced by the interaction with the anion). Counterpoise corrected IPDE (see Table 3) also support our considerations.

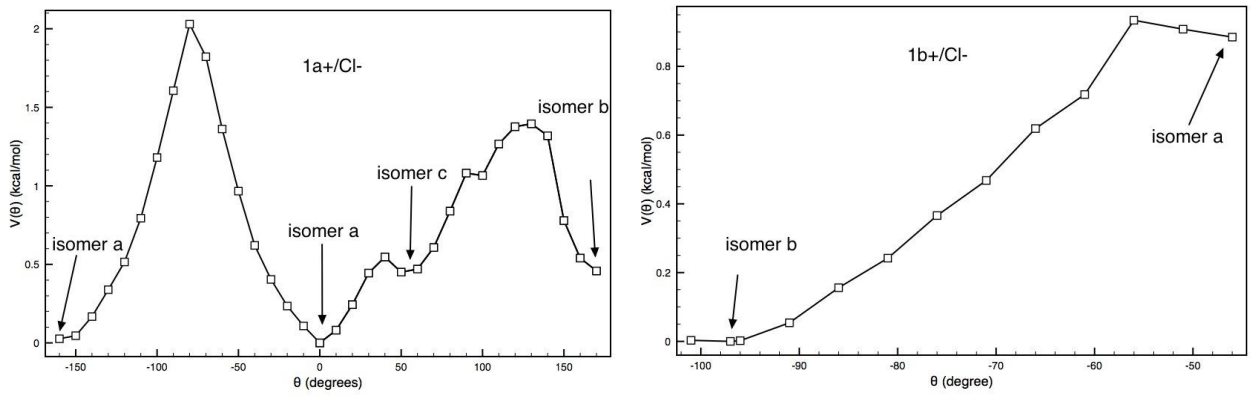

Figure 12. Relaxed torsional scan around the CH_2-N bond in the **1a**$^+$/Cl$^-$ and **1b**$^+$/Cl$^-$ complexes; the position of the lowest isomers in Figures 9 and 10 are also indicated for the sake of clarity.

2.3.4. X-Ray diffraction studies on 1a(I) and 1a(PF_6)

By slow diffusion of diethyl ether into acetonitrile solutions of **1a**(PF_6), in both the absence and presence of TBAI, single crystals suitable for X-Ray diffraction studies were obtained. In the solid state, the presence of HB and XB interactions was observed in both **1a**(PF_6) and **1a**(I).

In the case of **1a**(PF_6), the interactions between the molecular cation $\mathbf{1a}^+$ and the PF_6^- anion are weak (see Tables 4-5, and the SI for details). On the other hand, significant XB interactions could be detected in **1a**(I), where two similar but not symmetrically equivalent $\mathbf{1a}^+$ molecular cations interact with the same I^- ion through two C-I···I^- halogen bonds. In particular, the I···I^- distances [i.e., 3.541(1) and 3.575(2) Å, see Table 5] were much shorter than the value of 4.18 Å, obtained by summing the van der Waals radius of iodine (1.98 Å)[32] and the ionic radius of iodide (2.20 Å)[33].

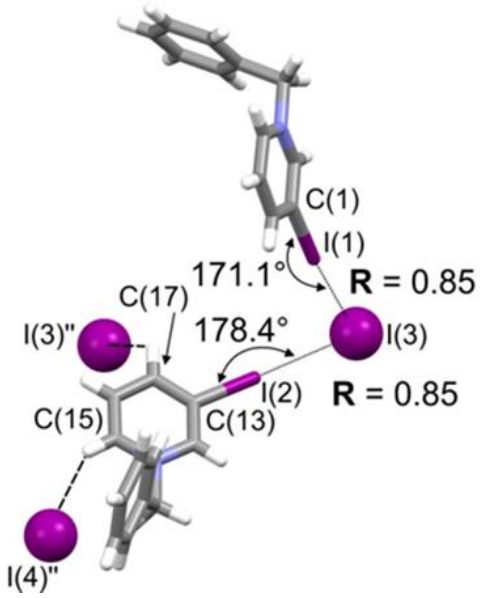

Figure 13. A simplified sketch of the crystal structure of **1a**(I). Atom names are shown only for atoms involved in C-I···Y halogen bonds (drawn with dotted lines) and weak C-H···A hydrogen bonds (drawn with dashed lines). The normalized R values = $d_{I\cdots Y}/(r_I + r_Y)$ and the C-I···Y bond angles are reported. Simmetry code: (') = - 1 + x, ½ - y, -1/2 + z; (") =1 + x, y, z.

The normalized R parameters [defined as the ratio between the observed I···I^- separation and the sum of the proper radii of the involved species] are 0.85 for both interactions, thus confirming the strength of the two halogen bonds. As a further proof, the two C-I···I^- angles are almost linear [178.4(3) and 171.1(3)°, respectively], the closest to 180° corresponding to a well-established XB interaction (Table 5). Notably, similar features were found by Rissanen,[10] in the crystal structure of an ethanol-clathrate hydrate crystal, containing two independent $\mathbf{1a}^+$ molecular cations interacting

with a chloride anion. In that case, two short halogen bonds were observed, involving the C-I XB-donor groups of two **1a**$^+$ molecular cations and two independent Cl^- anions. The calculated R values, 0.83 and 0.85, as well as the observed C-I···Cl^- angles, 174.1(1) and 174.6(1)°, are similar to those measured in our system.

In the **1a**(I) crystal, weak HB interactions were also observed. The shortest C-H···I^- distances involve two C-H bonds of the iodopyridinium moiety and two I^- anions [i.e. 3.72(1) and 3.77(1) Å, see Table 4]. These separations are shorter than 3.90 Å, obtained by summing the Van der Waals radius of C (1.70 Å)[32] and the ionic radius of I^- (2.20 Å).[33]

In the crystal structure of **1a**(PF_6) (see Figure 14), only a weak HB interaction is present, with the shortest D···A separation of 3.13(1) Å. This distance, involving a C-H bond of the iodopyridinium moiety and a F atom of the counter ion, is only slightly shorter than the sum of Van der Waals radii of C and F atoms: 3.17 Å.[32] Geometrical features for the HB interaction are reported in the Table 4.

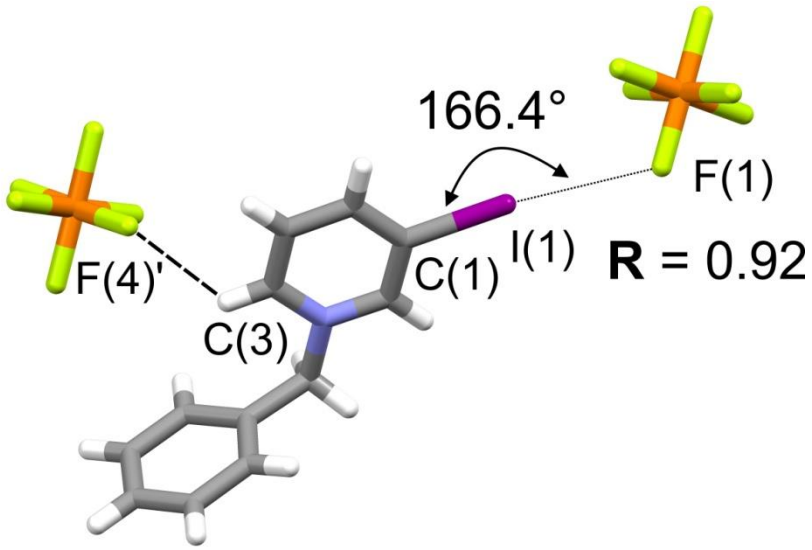

Figure 14. A simplified sketch of the crystal structure of **1a**(PF_6). Atom names are shown only for atom involved in C-I···Y halogen bonds (drawn with dotted lines) and weak C-H···A hydrogen bonds (drawn with dashed lines). The normalized **R** values = $d_{I\cdots Y}/(r_I + r_Y)$ and the C-I···Y bond angle are reported. Symmetry code: (') = - 1 + x, ½ - y, -1/2 + z; (") =1 +x, y, z.

A weak XB interaction was also found, between the C-I group of the iodopyridinium (XB-donor) and a F atom of PF_6^- (XB-acceptor). Also in this case, the I···F distance [i.e. 3.18(1)Å] is shorter than the sum of the Van der Waals radii for I and F atoms: 3.45 Å;[32] (see Table 5). However, the normalized R value [defined as the ratio between the observed I···F separation and the sum of their Van der Waals radii] is only 0.92, and the C-I···F angle is 166.4(3)°, i.e. far from the linear values

expected for a typical R-X···Y halogen bond.[34] In conclusion, the crystal structure of **1a**(PF_6) suggested that only weak HB and XB interactions occurred between the **1a**$^+$ molecular cation and the PF_6^- anion.

Comp.	D donor group	H···A (Å)	D···A (Å)	D-H···A	A acceptor atom
1a(PF_6)	C(3)-H(3)	2.526(5)	3.133(9)	123.2(5)	F(4)'$_{PF6}$-
1a(I)	C(15)-H(15)	3.326(13)	3.773(13)	112.0(9)	I(4)"$_I$-
1a(I)	C(17)-H(17)	3.221(12)	3.719(12)	115.7(9)	I(3)"$_I$-

Table 4. Geometrical features for the C-H···A hydrogen-bond interactions in the crystal structures of receptor **1a**. The reported contacts have D···A separations shorter than the sum of the Van der Waals radii of the involved atom. Symmetry code: (') = - 1 + x, ½ - y, - 1/2 + z; (") =1 + x, y, z; ("') – 1 + x, y, z.

	XB donor group	C-I (Å)	I···Y (Å)	R	C-I···Y	XB acceptor atom
1a(PF_6)	C(1)-I(1)	2.089(7)	3.181(6)	0.92	166.4(3)	F(1)$_{PF6}$-
1a(I)	C(1)-I(1)	2.093(10)	3.575(2)	0.85	171.1(3)	I(3)$_I$-
1a(I)	C(13)-I(2)	2.100(10)	3.541(1)	0.85	178.4(3)	I(3)$_I$-

Table 5. Geometrical features for the C-I···Y halogen bonds in the crystal structures of receptor **1a**. The normalized R value is defined as: $d_{I\cdots Y}/(r_I + r_Y)$, with r_I = 1.98 Å and r_Y = 1.47 Å for $F_{[PF6]-}$, 1.52 Å for $O_{[NO3]-}$, 2.20 Å for I_{I-}.

2.3.5. Tripodal 3-iodopyridinium-based receptors

Bowl-shaped positively charged systems, obtained by appending three pyridinium groups to a tris(alkyl)benzene scaffold, are known to form stable complexes with anions in acetonitrile solution. Different studies demonstrated that anion affinity is influenced by the receptor pre-organisation imparted by the alkyl chains on the platform, and depends on the presence of HB donor groups on the pyridinium arms.[14-15]

In order to understand how the presence of XB-donor groups could affect the anion binding properties of pyridinium-based tripodal receptors, we synthesised **2**$(PF_6)_3$ and **3**$(PF_6)_3$. These molecules were obtained by reacting an excess of 3-iodopyridine with 1,3,5-tribromomethyl mesitylene and 1,3,5–tribromomethyl–2,4,6–triethylbenzene, respectively. The two platforms exert a different degree of pre-organisation on the tripodal receptors, and this could affect anion affinity.

2.3.5.1. Anion binding studies on the tripodal receptors

Anion affinity was investigated by UV-vis and NMR titrations in pure acetonitrile and in acetonitrile/10% DMSO mixture. Due to the low solubility of the receptors in pure acetonitrile, UV-vis titrations were performed at 2.0 x 10^{-5} M concentration. Both $\mathbf{2}^{3+}$ and $\mathbf{3}^{3+}$ have an absorption band at about 295 nm. Upon anion addition (as the TBA salt), an hyper-chromic effect was observed (see Figure 16).

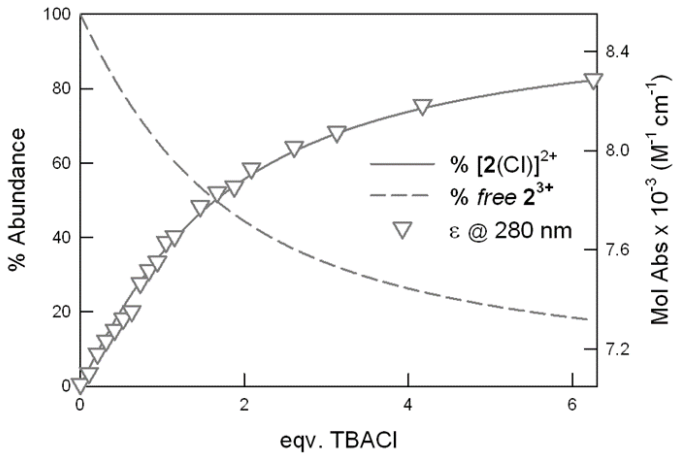

Figure 15. UV-vis titration profile of $\mathbf{2}(PF_6)_3$ (0.02 mM) with TBACl (20°C) in pure acetonitrile, superimposed to the distribution diagram built for the formation of a 1:1 complex characterized by $LogK_{11}$ = 4.65(1). The triangles show the profile of the Mol Abs at 280 nm vs. equivalents of added chloride.

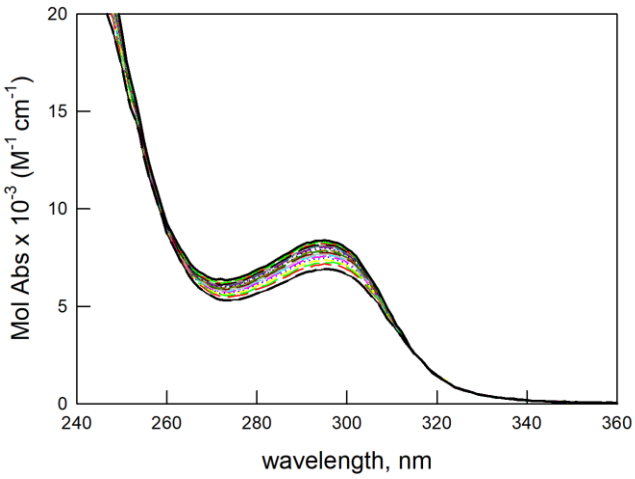

Figure 16. UV-vis spectra recorded during the titration of $\mathbf{3}(PF_6)_3$ (0.02 mM) with TBACl (20°C) in pure acetonitrile.

The titration profiles suggested the presence of a single equilibrium and the formation of a 1:1 complex with all anions. The binding constants are shown in Table 6. The affinity trend is similar in the two receptors (i.e., Cl^- >> Br^- > CH_3COO^- > HSO_4^-, NO_3^- > I^-). However, a stronger binding was observed for $\mathbf{3}^{3+}$ with spherical anions, Cl^- and Br^- in particular. This might be due to a higher pre-organisation imparted by triethyl arms to the bowl-shaped receptor, compared to the methyl groups of $\mathbf{2}^{3+}$.

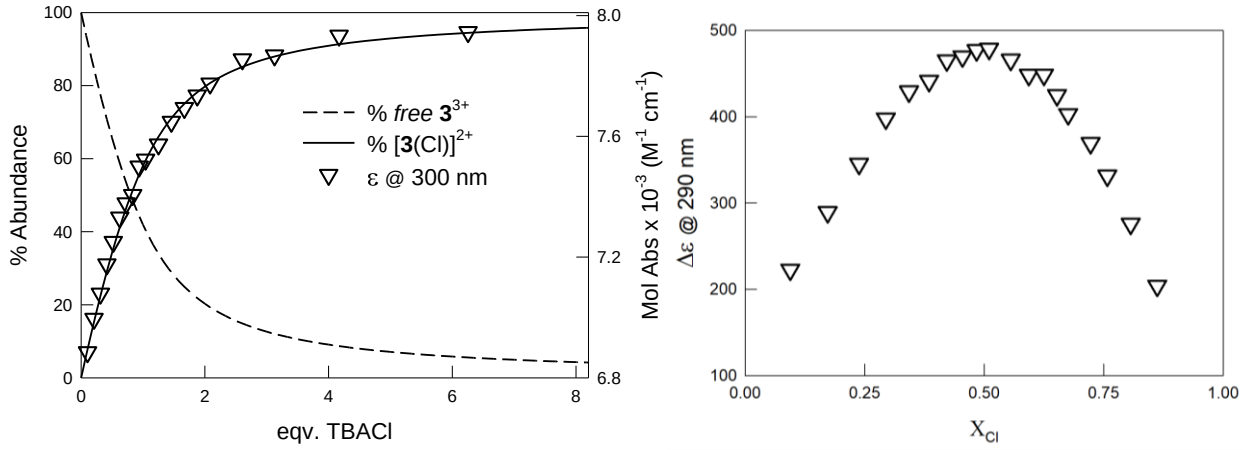

Figure 17. Titration profile (left) of $\mathbf{3}(PF_6)_3$ (0.02 mM) with TBACl (20°C) in pure acetonitrile.at 300 nm, superimposed to the distribution diagram built for the formation of a 1:1 complex, $LogK_{11}$ = 5.16(1) and Job plot at 290 nm (right).

For chloride, UV-vis titrations were also done in CH_3CN/DMSO (10% DMSO) mixture. The increased solubility allowed us to work at higher concentrations ($2.0x10^{-4}$ M) than in pure acetonitrile. A lower affinity was observed in this mixture due to the competing effect of DMSO on anion binding. Anyhow, these studies confirmed the formation of 1:1 complexes, with stronger binding capabilities for $\mathbf{3}^{3+}$ (see Table 6) compared to $\mathbf{2}^{3+}$.

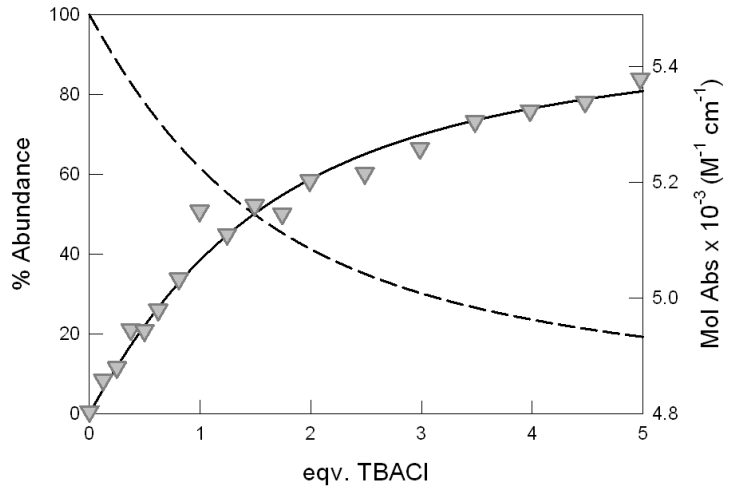

Figure 18. UV-vis titration profile of **2(PF$_6$)$_3$** (0.2 mM) with TBACl in acetonitrile/DMSO mixture (10% DMSO), superimposed to the distribution diagram built for the formation of a 1:1 complex characterized by LogK_{11} = 3.70(2). The triangles show the profile of the Mol Abs at 311 nm vs. equivalents of added chloride.

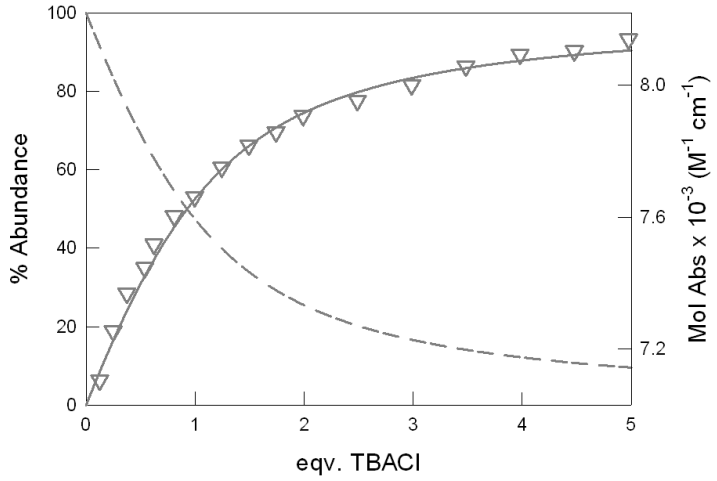

Figure 19. UV-vis titration profile of **3(PF$_6$)$_3$** (0.2 mM) with TBACl in acetonitrile/DMSO mixture (10% DMSO), superimposed to the distribution diagram built for the formation of a 1:1 complex characterized by LogK_{11} = 4.07(2). The triangles show the profile of the Mol Abs at 300 nm vs. equivalents of added chloride.

Anion	**Log K$_{11}$/2^{3+}**	**Log K$_{11}$/3^{3+}**
Cl^-	4.65(1) [3.70(2)][a]	5.16(1) [4.07(2)[a]; 4.04(3)[b]]
Br^-	4.46(1)	4.91(2)
I^-	3.59(1)	3.71(1)
CH_3COO^-	4.45(1)	4.40(2)
HSO_4^-	4.13(1)	4.08(2)

Table 6. Affinity constants determined through UV-vis. titrations of **2**$^{3+}$ and **3**$^{3+}$ with anions (as the TBA salts) in 100% CH_3CN. [a]In the presence of 10% DMSO (25°C). [b]Constants obtained through ^{1}H-NMR titrations in CD_3CN/d_6-DMSO mixture (10% d_6-DMSO). The uncertainties are reported in parentheses.

2.3.5.2. ^{1}H-NMR titration of tripod 3^{3+} in CD_3CN/d_6-DMSO mixture

To gain more information about the interaction of receptor $\mathbf{3}^{3+}$ with anions, ^{1}H-NMR titration studies were performed with chloride in CD_3CN/d_6-DMSO mixture (10% d_6-DMSO).

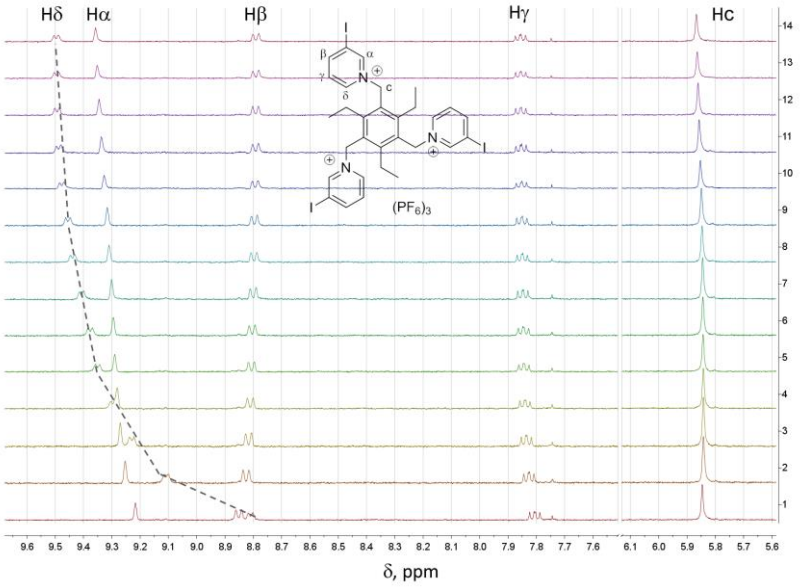

Figure 20. ^{1}H-NMR spectra taken during the titration of $\mathbf{3}(PF_6)_3$ with TBACl in CD_3CN/d_6-DMSO mixture (10% d_6-DMSO).

Notably, protons Hδ, in the para positions to iodine, seemed to be directly involved in the binding, undergoing a down-field shift [$\Delta\delta$ = +0.70 ppm] upon chloride addition [vs. +0.43 ppm for $\mathbf{1a}^+$]. Protons Hα were also affected, even if to a significantly lower extent [$\Delta\delta$ = +0.14 ppm for $\mathbf{3}^{3+}$ vs. + 0.54 ppm for $\mathbf{1a}^+$]. The slight shielding of protons Hβ was attributed to an increase of the electron density on the receptor upon anion binding.

These results indicated that the interaction with the chloride anion mainly involves the ortho protons of pyridinium groups. Notably, in most examples in the literature including the mono-branched receptor $\mathbf{1a}^+$, the ortho- protons are the most affected by anion binding, due to the direct participation of the C-H bonds in the interaction (as HB-donor groups).[14-15] By treating the experimental data, obtained through ^{1}H-NMR titrations, the affinity constant was determined (see Table 6 and Fig. 21). The distribution diagram of the species, with the superimposed titration profile, is shown in Figure 21.

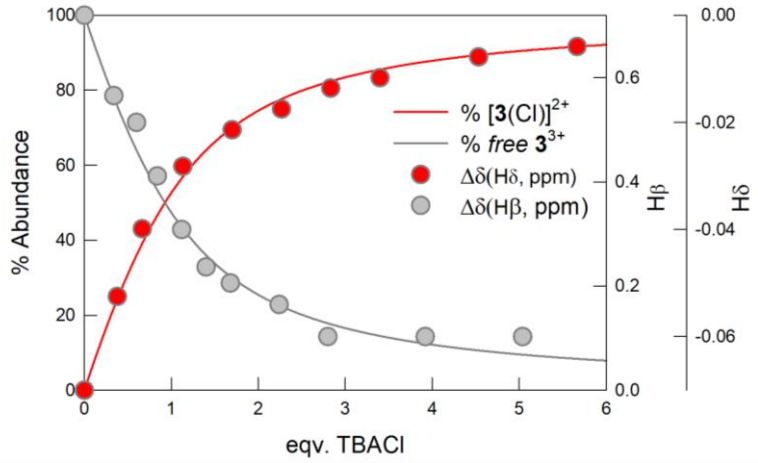

Figure 21. ^{1}H-NMR profiles for the titration of $\mathbf{3}^{3+}$ with TBACl in acetonitrile/DMSO mixture. The distribution diagram was obtained, by considering a 1:1 binding constant of 4.04 Log units.

2.3.5.3. Computational studies on tripodal receptors

The experimental data are confirmed by the theoretical studies on the $\mathbf{2}^{3+}/Cl^{-}$ or $\mathbf{2}^{3+}/Br^{-}$ complexes (Table 7). Also in these cases, various conformers were obtained, their structures differing in the relative position of the pyridinium groups with respect to the plane of the phenyl ring ("3-up" or "2-up, 1-down"). Differences were observed in the position of the Hα and Hδ atoms pointing towards the anion. The four lowest lying species with Cl^{-} are shown in Figure 22; these low energy conformers are all within 3.7 kcal/mol, a little wider interval than the one observed in the case of $\mathbf{1a}^{+}$. In particular, the substitution of Hδ with Hα (of the same pyridinium ring) in the interaction with Cl^{-} raised the energy by 0.8 kcal/mol for the "3-up" isomer, its two conformers (a and b in Figure 22) being the most stable species in solution.

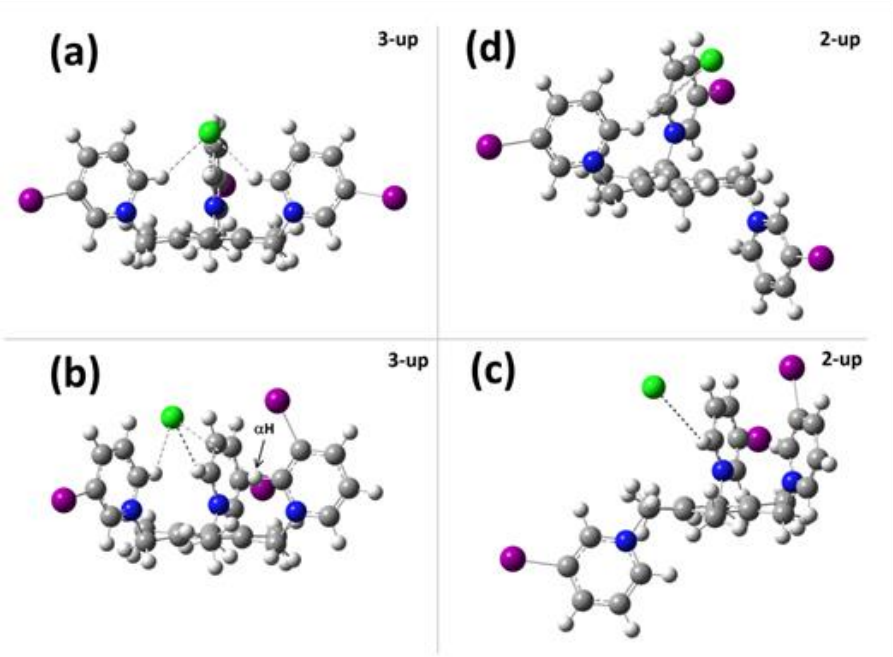

Figure 22. Lowest conformers for $\mathbf{2^{3+}/Cl^-}$**.** Top and bottom conformers differ due to the rotation of an iodo-pyridinium group in the up position around the CH_2-N bond. Such rotation substitutes Hα to Hδ in the contact with the anion.

Since the population of the remaining two species (c and d, Figure 22) is lower, the energy data explained the smaller change in the chemical shift of Hα, observed upon NMR titration with chloride (see Figure 20).

Also the ionic pair dissociation energies (IPDE) and counterpoise corrected energies for the complexes were calculated and reported in the tables below.

Comp.	**IPDE** (kcal/mol) **X=Cl**$^-$	**IPDE** (kcal/mol) **X=Br**$^-$
$\mathbf{2^{3+}}$	8.34[(a)]; 7.55[(b)]; 6.05[(c)]; 5.67[(d)]	9.05[(a)]; 8.97[(d)]

Table 7. Ionic pair dissociation energies. IDPE=E(S^+/X^-)-E(S^+)-(X^-), where S^+ is the ligand molecule and X^- is the anion. All the energies take into account the effect of appropriate solvent via SCRF models. Letters refer to the conformer labels in Figure 22.

Comp.	**IPDE** (kcal/mol) **X=Cl**$^-$	**IPDE** (kcal/mol) **X=Br**$^-$
2	6.43; 4.88, 6.04; 5.21	7.26; 7.46

Table 8. Counterpoise corrected IPDE for the species in Table 7; the order of the isomers is maintained.

2.3.5.4. Crystal structures of 2(NO$_3$)$_2$(PF$_6$) and 2(Br)$_2$(PF$_6$)$_2$

By slow diffusion of diethyl ether into acetonitrile solutions of **2**(PF$_6$)$_3$ in the presence of nitrate and bromide (as the TBA salts), crystals of **2**(NO$_3$)$_2$(PF$_6$) and **2**(Br)(PF$_6$)$_2$ salts suitable for X-ray diffraction studies were isolated.

The conformation of the **2**$^{3+}$, as well as the arrangement of HB and XB interactions, are very similar in the nitrate and bromide salts (compare Figures 23 and 24). In both crystals, one of the three iodopyridinium arms is oriented out of the receptor's cavity, and it is placed on the other side of the trimethylbenzene's plane (i.e., "anti" conformation). Such a "2-up, 1-down" conformation has already been reported by Steed for other tripodal pyridinium-based systems.[16] This conformation also corresponds to one of the low energy conformers obtained for this receptor by theoretical calculations.

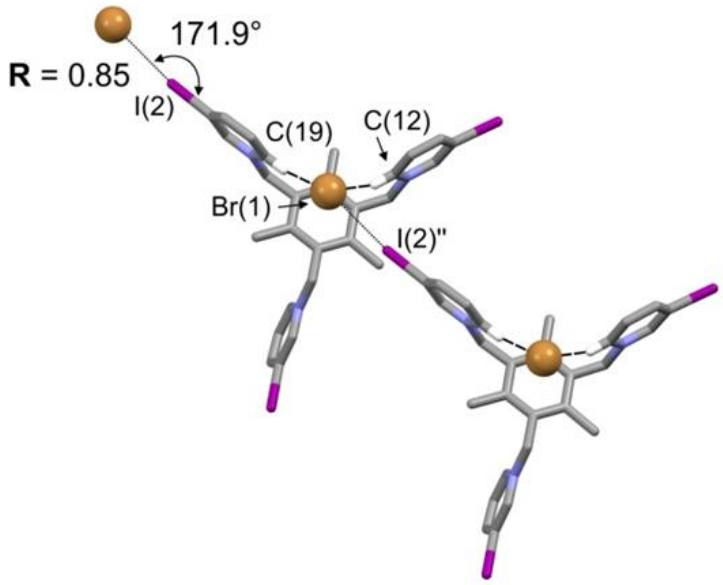

Figure 23. A simplified sketch of the crystal structure of **2**(Br)(PF$_6$)$_2$ (PF$_6^-$ counter ions are not shown for simplicity). Names are shown only for atoms involved in C-I···Y halogen bonds (drawn with dotted lines) and C-H···A hydrogen bonds (drawn with dashed lines). The normalized R values = $d_{I\cdots Y}/(r_I + r_Y)$ and the C-I···Y bond angles are reported. Symmetry code: (") x, - 1 + y, z; (''') – 1 + x, y, z.

In the crystal structure of **2**(Br)(PF$_6$)$_2$, all the iodine atoms, to comply with steric requirements, point out of the receptor's cavity. The two C-H bonds in the para position to the iodine atoms, belonging to the "2-up" arms, are instead oriented towards the centre of the cavity and interact with the bromide ion by HB interactions. The involved H atoms correspond to Hδ protons in the NMR titration.

The bromide anion is located above the centre of the trimethylbenzene ring, and profits of a XB interaction with the C-I group of a second **2**$^{3+}$ cation (see Figure 23).

In the crystal structure of **2**$(NO_3)_2(PF_6)$ the motif of HB and XB interactions is similar to that observed for bromide. Notably, two C-H groups belonging to the "2-up" iodopyridinium arms act as H-donors towards two O atoms of the nitrate ion (H-acceptors) within the cavity. This anion also interacts with the C-I(2) XB-donor group of a second $\mathbf{2}^{3+}$ cation, thus originating supramolecular chains. In the solid, other two XB interactions can be found: a strong C-I···O interaction (Table 10) between C-I(1) and O(3) of a second nitrate anion (XB-acceptor); and a weak interaction involving C-I(3) and F(3) of a PF_6^- counter ion (XB-acceptor). Notice that the positional disorder occurring in the **2**$(NO_3)_2(PF_6)$ crystal affects the nitrate counter ion, therefore this species is not always present in the molecules forming the crystal.

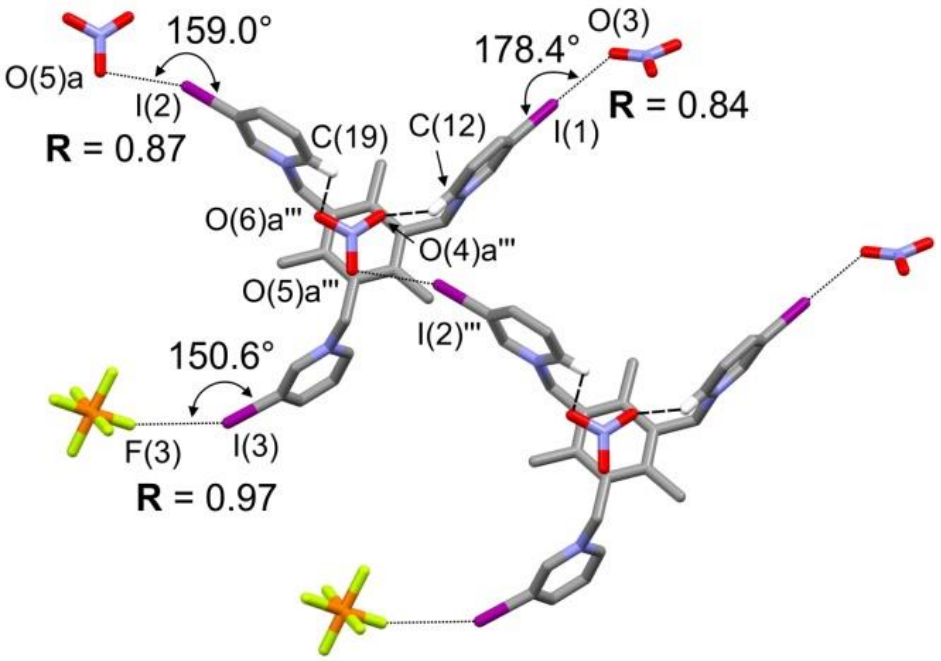

Figure 24. A simplified sketch of the crystal structure of **2**$(NO_3)_2(PF_6)$. Names are shown only for atoms involved in C-I···Y halogen bonds (drawn with dotted lines), and weak C-H···A hydrogen bonds (drawn with dashed lines). The normalized **R** values $= d_{I\cdots Y}/(r_I + r_Y)$ and the C-I···Y bond angles are reported. Symmetry code: (") x, - 1+ y, z; (''') – 1 + x, y, z.

In the case of receptor $\mathbf{3}^{3+}$, the presence of ethyl substituents on the platform should enhance the receptor's preorganization, thus forcing the pyridinium arms to point in the same direction. Unfortunately, all attempts to obtain single crystals suitable for X-ray diffraction studies were unsuccessful.

Geometrical features for both crystals are reported in Tables 9 and 10:

Comp.	D donor group	H···A (Å)	D···A (Å)	D-H···A	A acceptor atom
2$(NO_3)_2(PF_6)$	C(12)-H(12)	2.306(14)	3.104(14)	143.5(9)	O(4)a'''$_{NO3}$-
2$(NO_3)_2(PF_6)$	C(19)-H(19)	2.637(22)	2.971(22)	101.8(8)	O(6)a'''$_{NO3}$-
2$(Br)(PF_6)_2$	C(12)-H(12)	2.781(10)	3.565(10)	142.5(6)	Br(1)$_{Br}$-
2$(Br)(PF_6)_2$	C(19)-H(19)	2.707(9)	3.522(9)	146.7(6)	Br(1)$_{Br}$-

Table 9. Geometrical features for the C-H···A hydrogen-bond interactions in the crystal structures of receptor **2**. The reported contacts have D···A separations shorter than the sum of the Van der Waals radii of the involved atom. Symmetry code: (') = - 1 + x, ½ - y, - 1/2 + z; (") =1 + x, y, z; ('") – 1 + x, y, z.

	XB donor group	C-I (Å)	I···Y (Å)	R	C-I···Y	XB acceptor atom
2$(NO_3)_2(PF_6)$	C(9)-I(1)	2.091(10)	2.954(10)	0.84	178.4(4)	O(3) $_{NO3}$-
2$(NO_3)_2(PF_6)$	C(16)-I(2)	2.071(11)	3.057(20)	0.87	159.0(4)	O(5a) $_{NO3}$-
2$(NO_3)_2(PF_6)$	C(23)-I(3)	2.096(11)	3.332(10)	0.97	150.6(4)	F(3)$_{PF6}$-
2$(Br)(PF_6)_2$	C(16)-I(2)	2.110(8)	3.368(1)	0.85	171.9(3)	Br(1)$_{Br}$-

Table 10. Geometrical features for the C-I···Y halogen bonds in the crystal structures of receptor **2**. The normalized R value is defined as: $d_{I\cdots Y}/(r_I + r_Y)$, with r_I = 1.98 Å and r_Y = 1.47 Å for $F_{[PF6]-}$, 1.52 Å for $O_{[NO3]-}$, 1.96 Å for Br_{Br-}.

In the solid state, the combination of these HB and XB interactions gives origin to supramolecular chains in both **2**$(NO_3)_2(PF_6)$ and **2**$(Br)(PF_6)_2$ crystals.

2.4. Conclusions

For the first time, iodo-pyridinium units were used in tripodal systems to selectively bind anions in competing media (e.g., acetonitrile with 10% DMSO). The substituted pyridinium chromophore allowed us to follow anion binding through UV-vis titrations, in addition to the NMR technique. These studies pointed out that the iodine atom in the meta position enhances the anion binding tendencies of pyridinium. Computational studies on **1a**$^+$ suggested that this tendency depends more on the electron withdrawing effect of iodine [on the coordinating pyridyl hydrogens] rather than on the occurrence of relevant halogen bonding (XB) in solution. However, XB interactions dominate the binding of anions in the solid state.

In the case of the tripodal receptors, stable 1:1 adducts were obtained in solution for all the investigated anions. The anion was included in the bowl-shaped cavity, where it was stabilized by a combination of different interactions. In particular, X-ray diffraction studies on **2**$(NO_3)_2(PF_6)$ and **2**$(Br)(PF_6)_2$ showed that the pyridinium arms assume a "2-up, 1-down" conformation with respect

to the mesitylene platform. In both adducts, the anion was located in the receptor's cavity, forming two H-bonding interactions with the Hδ protons of the "2-up" arms, and one halogen-bonding interaction with the C-I group of a second $\mathbf{2}^{3+}$ cation. This combination of halogen- and hydrogen-bonds led to the formation of supramolecular chains in the crystals of both $\mathbf{2}(NO_3)_2(PF_6)$ and $\mathbf{2}(Br)(PF_6)_2$. In particular, in the endo-coordination of the included anion, HB interactions were preferred over XBs. This may depend on the fact that all of the iodine atoms are oriented out of the cavity, due to steric constraints.

In conclusion, the combination of different type of interactions may have a strong impact on the anion binding properties of receptors in solution, however steric constraints must be overcome first.

*The research described in this chapter was published in RSC Adv., 2016, 6, 67540.

Supplementary Section

1S. NMR spectra

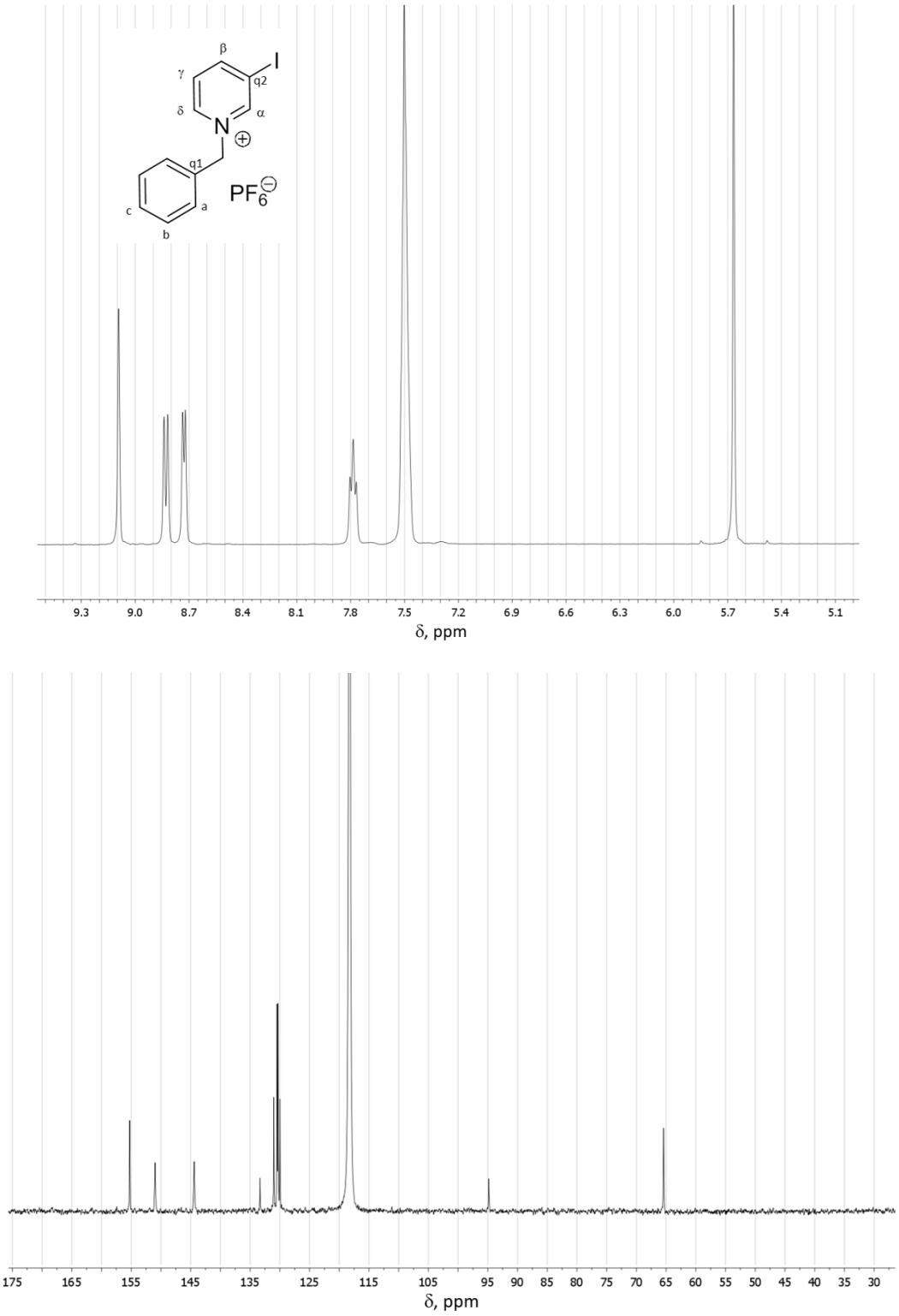

Figure S1. ^{1}H and ^{13}C-NMR spectra of **1a**(PF_6) in CD_3CN.

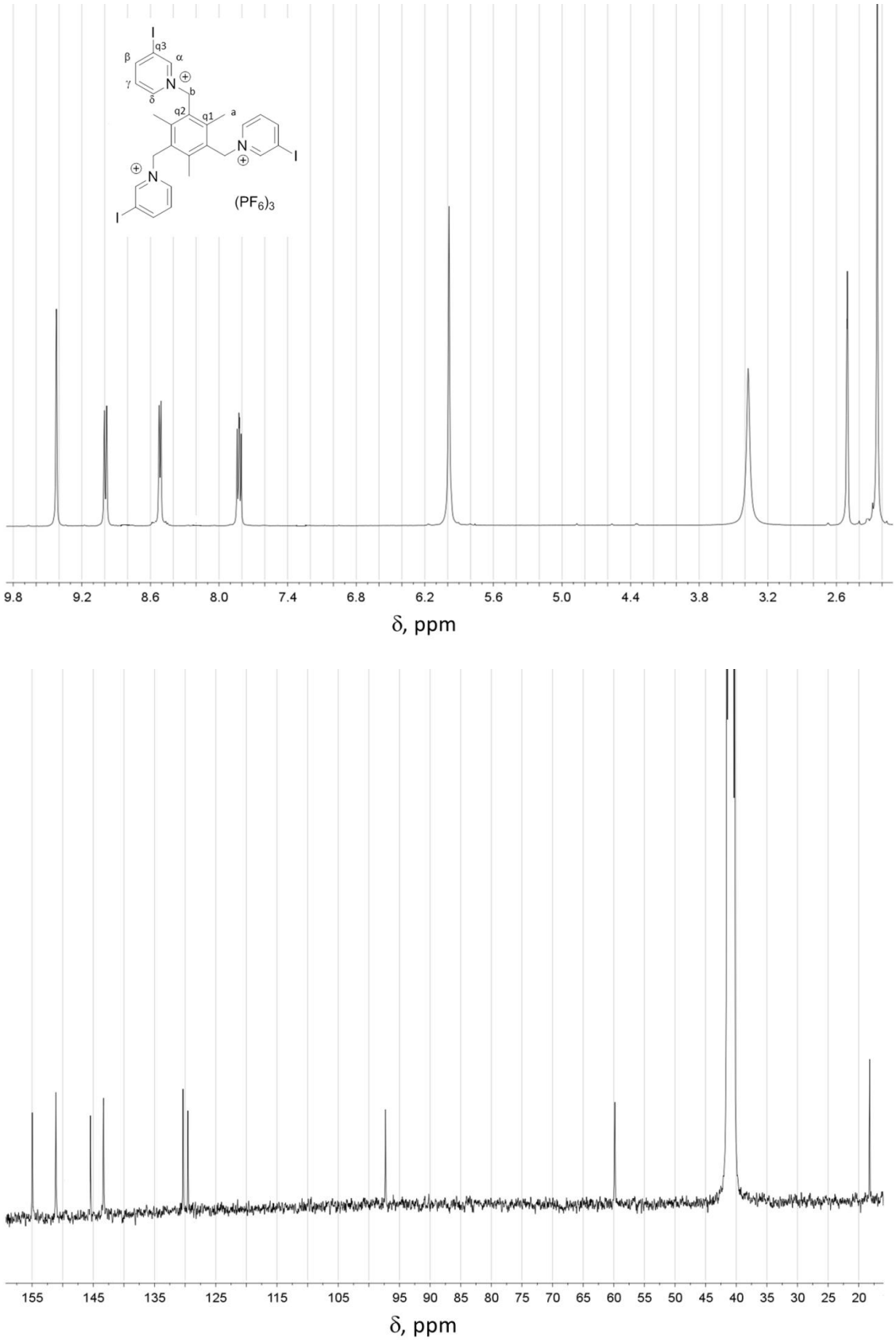

Figure S2. ^{1}H and ^{13}C-NMR spectra of **2**$(PF_6)_3$ in d_6-DMSO.

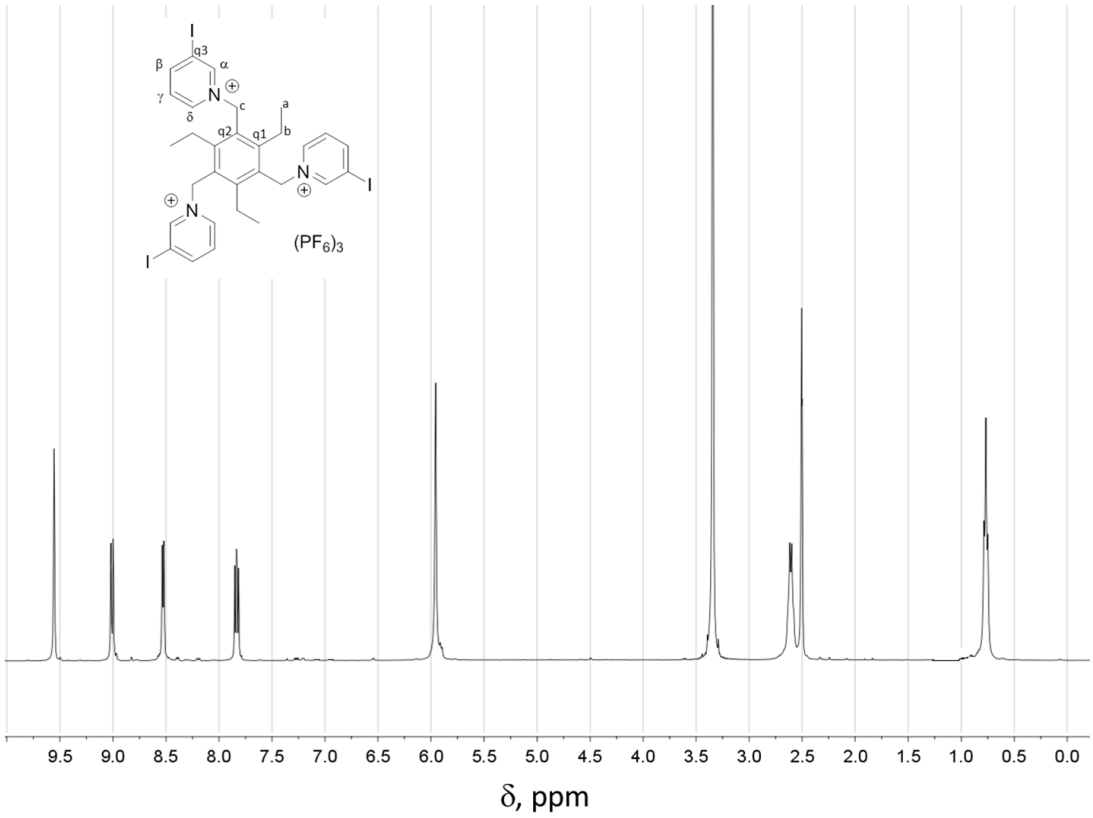

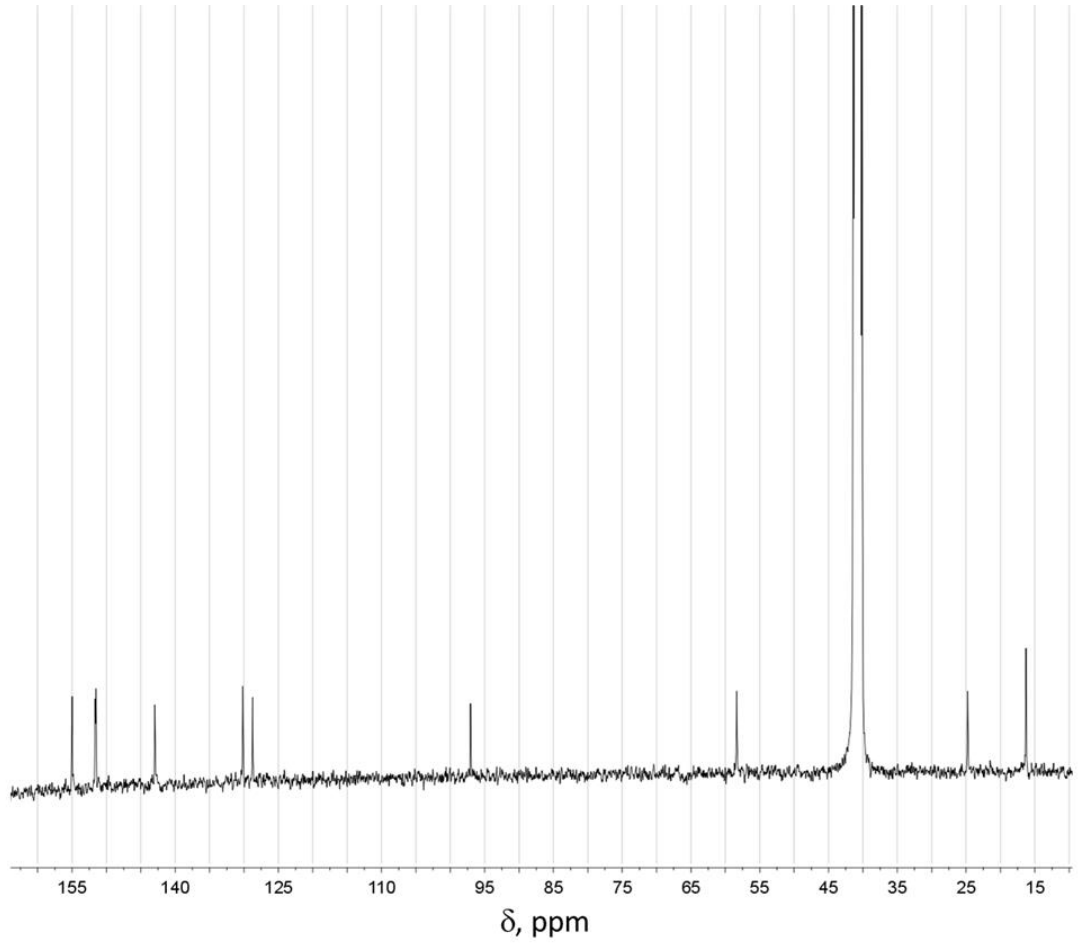

Figure S3. ^{1}H and ^{13}C-NMR spectra of **3**$(PF_6)_3$ in d_6-DMSO.

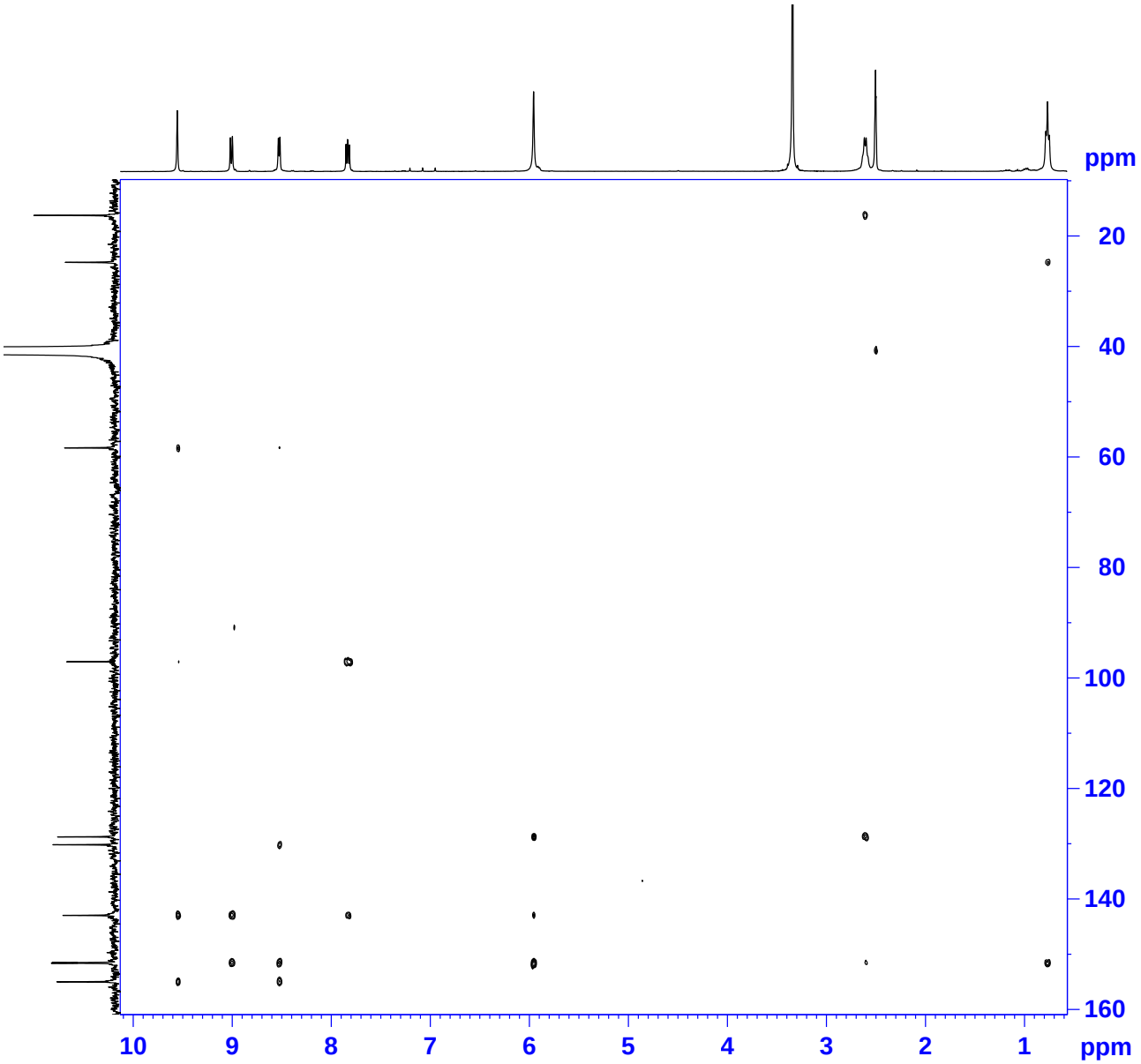

Figure S4. $^{1}H,^{13}C$-HMBC spectrum of **3**$(PF_6)_3$ in d_6-DMSO (full spectrum).

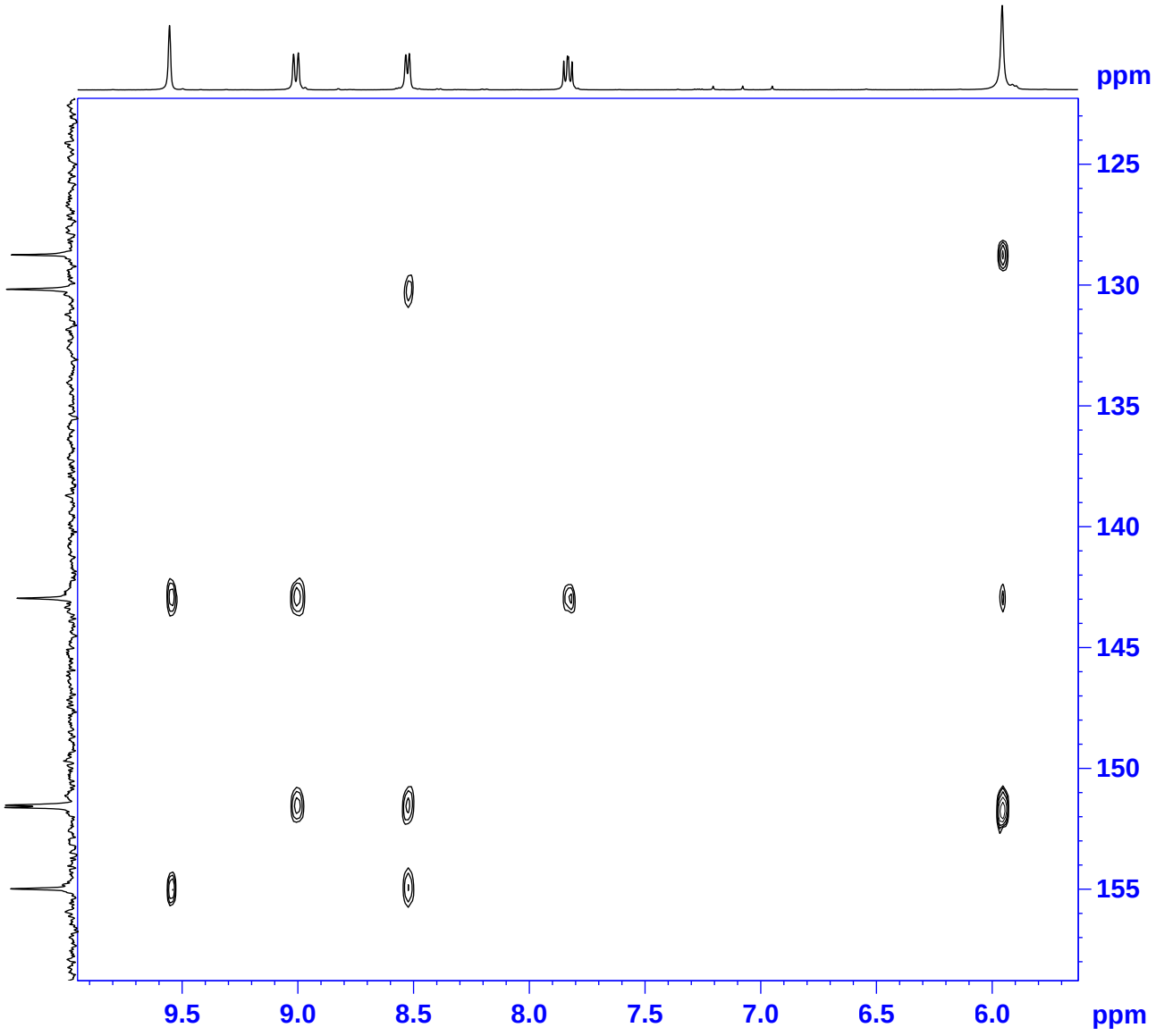

Figure S5. Detail of Figure S4 Δδ = 5.6- 9.9 ppm.

2S. ORTEP images

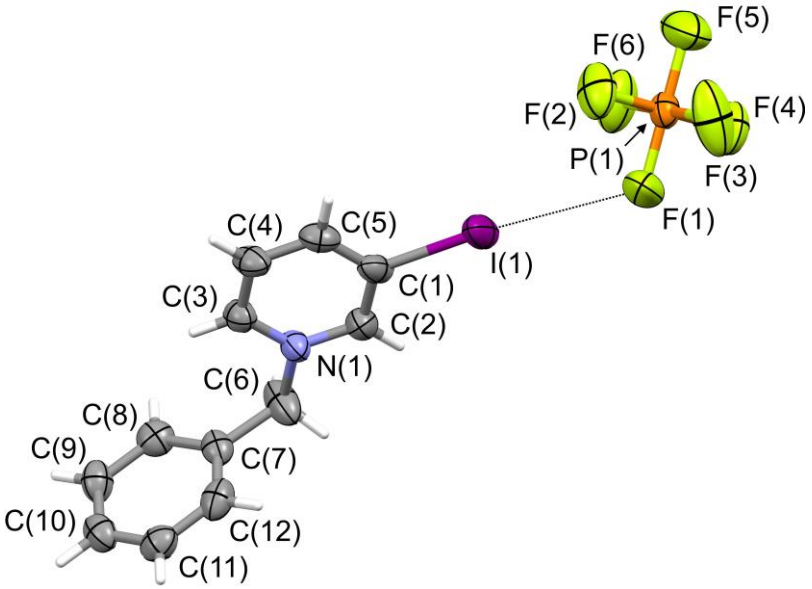

Figure S6. Plot showing thermal ellipsoids of the asymmetric unit of the **1a**(PF_6) crystal salt (ellipsoids are drawn at the 30% probability level). An XB interaction is drawn with dotted line.

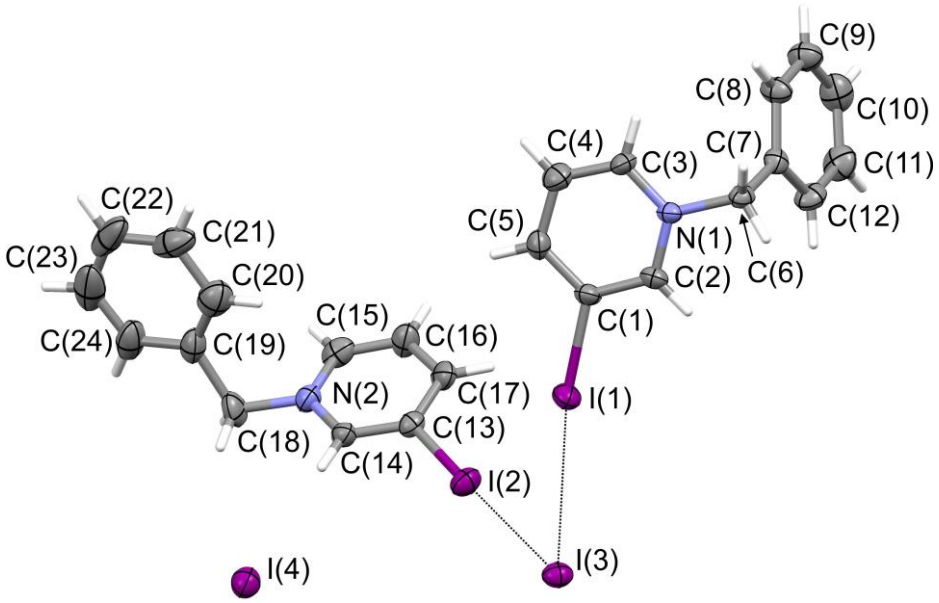

Figure S7. Plot showing thermal ellipsoids of the asymmetric unit of the **1a**(I) crystal salt (ellipsoids are drawn at the 30% probability level). Two XB interactions are drawn with dotted line.

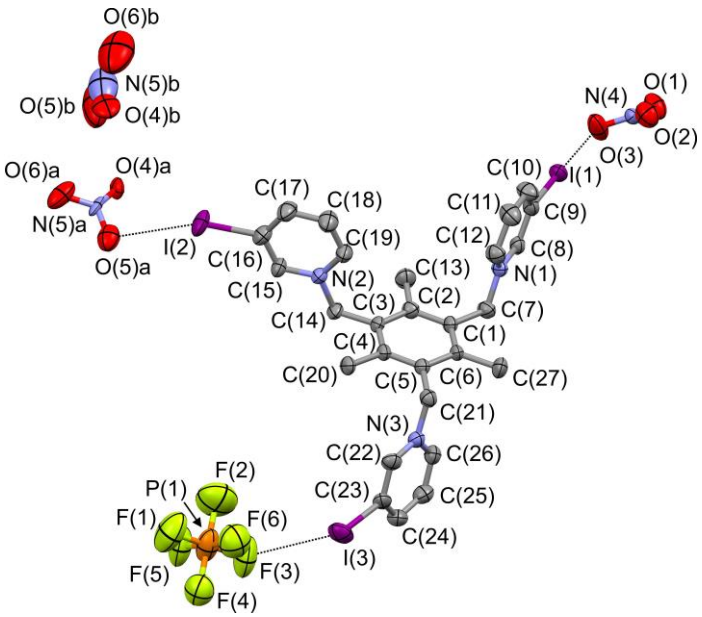

Figure S8. Plot showing thermal ellipsoids of the asymmetric unit of the **2**$(NO_3)_2(PF_6)$ crystal salt (ellipsoids are drawn at the 30% probability level, hydrogens are omitted for clarity). Three XB interactions are drawn with dotted line. Nitrate atom positions with a and b suffix are mutually exclusive and half populated.

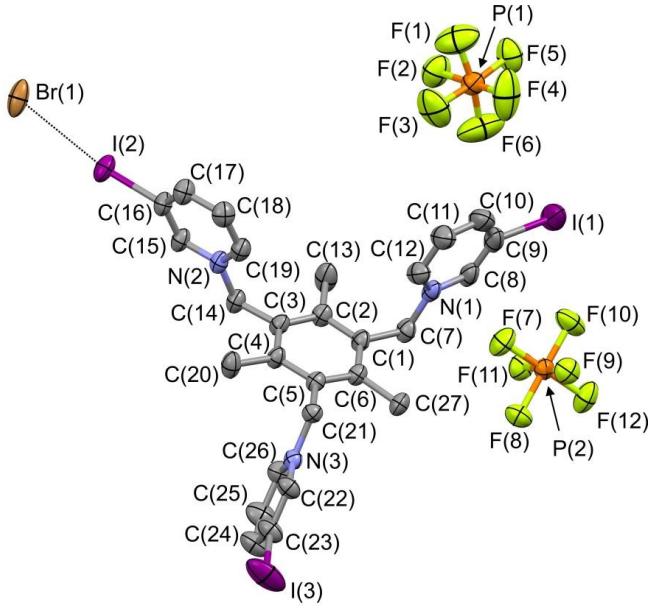

Figure S9. Plot showing thermal ellipsoids of the asymmetric unit of the **2**$(Br)(PF_6)_2$ crystal salt (ellipsoids are drawn at the 30% probability level, hydrogens are omitted for clarity). An XB interaction is drawn with dotted line.

	1a(PF_6)	**1a**(I)	**2**$(NO_3)_2(PF_6)$	**2**(Br)$(PF_6)_2$
Formula	$C_{12}H_{11}F_6INP$	$C_{24}H_{22}I_4N_2$	$C_{27}H_{27}F_6I_3N_5O_6P$	$C_{27}H_{27}BrF_{12}I_3N_3P_2$
M	441.09	846.04	1043.21	1144.06
crystal system	monoclinic	orthorhombic	triclinic	monoclinic
space group	$P2_1/c$ (no. 14)	$Pc2_1b$ (no. 29)	*P*-1 (no. 2)	*C*2/*c* (no. 15)
a [Å]	10.256(1)	7.526(3)	11.352(2)	24.163(2)
b [Å]	9.723(2)	11.789(4)	13.844(3)	11.441(1)
c [Å]	15.285(1)	30.882(6)	14.366(3)	27.559(2)
α [°]	90	90	118.339(4)	90
β [°]	96.674(9)	90	101.442(4)	97.977(1)
γ [°]	90	90	99.631(4)	90
V [Å³]	1513.8(3)	2740.1(15)	1856.0(7)	7545.1(10)
Z	4	4	2	8
ρ_{calcd} [g cm^{-3}]	1.935	2.051	1.867	2.014
μ $Mo_{K\square}$ [mm^{-1}]	2.276	4.562	2.643	3.713
Scan type	ω	ω	ω	ω
θ range [°]	2-27	2-27	2-25	2-25
measured refl.	3500	7009	19857	31513
unique refl.	3289	3899	6663	6669
R_{int}	0.0189	0.0338	0.0386	0.0447
Strong data[a]	2298	3387	4891	4435
Refined param.	190	271	469	436
R_1, wR_2[a]	0.0604, 0.1314	0.0323, 0.0630	0.0730, 0.2343	0.0651, 0.1877
R_1, wR_2[b]	0.0874, 0.1538	0.0403, 0.0677	0.0926, 0.2561	0.0920, 0.2127
GOF	1.088	1.081	1.071	1.064
residuals [e$Å^{-3}$]	0.53, -0.72	0.68, -0.51	1.60, -1.14	1.95, -1.35

Table S1. Crystal data for the studied compounds. [a] Strong data = $I_O > 2\sigma(I_O)$, [b] All data.

References

[1] (a) Busschaert, N.; Caltagirone, C.; Van Rossom W. and Gale, P.; *Chem. Rev*., **2015**, 115(15), 8038-8155; (b) Gale P. and Caltagirone, C.; *Chem. Soc Rev*., **2015**, 44(13), 4212-4227; (c) Giese, M.; Albrecht M. and Rissanen, K.; *Chem. Rev*., **2015**, 115(16), 8867-8895; (d) Blazek Bregovic, V.; Basaric N. and Mlinaric-Majerski, K.; *Coord. Chem. Rev*., **2015**, 295, 80-124; (e) Saha, I.; Lee, J. T. and Lee, C. H.; *Eur. J. Org. Chem*., **2015**, 18, 3859-3885; (f) Elmes, R. B. P. and Jolliffe, K. A.; *Chem. Commun*., **2015**, 51(24), 4951-4968; (g) Chang, K. C.; Sun, S. S.; Odago, M. O. and Lees, A. J.; *Coord. Chem. Rev*., **2015**, 284, 111-123.

[2] (a) Graf, E.; and Lehn, J. M.; *J. Am. Chem. Soc*., **1976**, 98(20), 6403-6405; (b) Lehn, J. M.; *Acc. Chem. Res*., **1978**, 11(2), 49-57.

[3] Sessler, J. L.; Gale, P. A.; Cho, W. S.; *RSC Publishing*, **2006**; Anion Coordination Chemistry, ed. Bowman-James, K.; Bianchi, A.; and García-Espana, E.; John Wiley & Sons, New York, 2012.

[4] (a) Metrangolo, P.; Neukirch, H.; Pilati T. and Resnati, G.; *Acc. Chem. Res*., **2005**, 38(5), 386-395; (b) Metrangolo, P.; Meyer, F.; Pilati, T.; Resnati, G. and Terraneo, G.; *Angew. Chem. Int. Ed*., **2008**, 47(33), 6114-6127; (c) Cavallo, G.; Metrangolo, P.; Pilati, T.; Resnati, G.; Sansotera, M. and Terraneo, G.; *Chem. Soc. Rev*., **2010**, 39(10), 3772-3783; (d) Cavallo, G.; Metrangolo, P.; Milani, R.; Pilati, T.; Priimagi, A.; Resnati, G. and Terraneo, G.; *Chem Rev*., **2016**, 116(4), 2478-2601.

[5] (a) Langton, M. J. and Beer, P. D.; *Acc. Chem. Res*., **2014**, 47(7), 1935-1949; (b) Spence, G. T. and Beer, P. D.; *Acc. Chem. Res*., **2013**, 46(2), 571-586; (c) Gilday, L. C.; Robinson, S. W.; Barendt, T.A.; Langton, M. J.; Mullaney, B. R. and Beer, P. D.; *Chem. Rev*., **2015**, 115(15), 7118-7195; (d) Langton, M. J.; Serpell, C. J. and Beer, P. D.; *Angew. Chem. Int. Ed.*, **2016**, 55(6), 1974-1987.

[6] (a) Chudzinski, M. G.; McClary, C. A. and Taylor, M. S.; *J. Am. Chem. Soc*., **2011**, 133, 10559-10567; (b) Walter, S.M.; Kniep, F.; Rout, L.; Schmidtchen, F.P.; Herdtweck, E. and Huber, S. M.; *J. Am. Chem. Soc.*, **2012**, 134(20), 8507-8512; (c) Vargas Jentzsch, A.; Hennig, A.; Mareda, J. and Matile, S.; *Acc. Chem. Res*., **2013**, 46(12), 2791-2800; (d) Schulze, B. and Schubert, U. S.; *Chem. Soc. Rev.*, **2014**, 43(8), 2522-2571; (e) Tepper, R.; Schulze, B.; Jaeger, M.; Friebe, C.; Scharf, D.; Goerls, H. and Schubert, U.S.; *J. Org. Chem*., **2015**, 80(6), 3139-3150; (f) Chakraborty, S.; Dutta, R. and Ghosh, P.; *Chem. Commun.*, **2015**, 51(79), 14793-14796; (g) Takezawa, H.; Murase, T.; Resnati, G.; Metrangolo, P. and Fujita, M.; *Angew. Chem. Int. Ed.*, **2015**, 54, 8411-8414.

[7] Jeffrey, G. A.; Saenger, W.; *Hydrogen Bonding in Biological Structures*, Springer-Verlag: Berlin, **1991**, and references cited therein.

[8] (a) Cavallo, G.; Metrangolo, P.; Pilati, T.; Resnati, G. and Terraneo, G.; *Cryst. Growth Des*., **2014**, 14 (6), 2697-2702; (b) Desiraju, G. R.; Ho, P. S.; Kloo, L.; Legon, A. C.; Marquardt, R.; Metrangolo, P.; Politzer, P.; Resnati, G. and Rissanen, K.; *Pure Appl. Chem*., **2013**, 85, 1711-1713.

[9] (a) Karpfen, A.; *Struct. Bond*., **2008**, 126, 1-15; (b) Fourmigue, M.; *Curr. Opin. Solid. State Mater. Sci.*, **2009**, 13(3/4), 36-45; (c) Nepal, B. and Scheiner, S.; *J. Phys. Chem. A*, **2015**, 119 (52), 13064-13073; (d) Wang, H.; Wang, W. and Jin, W. J.; *Chem. Rev*., **2016**, 116 (9), 5072-5104.

[10] Raatikainen, K.; Cametti, M. and Rissanen, K.; *Beilstein J. Org. Chem*., **2010**, 6, 4, 1-13.

[11] (a) Cornes, S. P.; Davies, C. H.; Blyghton, D.; Sambrook, M. R. and Beer, P. D.; *Org. Biomol. Chem*., **2015**, 13, 2582-2587; (b) Mercurio, J. M.; Caballero, A.; Cookson, J. and Beer, P. D.; *RSC Adv.*, **2015**, 5, 9298-9306.

[12] (a) Amendola, V.; Fabbrizzi, L.; Monzani, E.; *Chem. Eur. J*., **2004**, 10, 76-82; (b) Amendola, V.; Bonizzoni, M.; Esteban-Gomez, D.; Fabbrizzi, L.; Licchelli, M.; Sancenon, F.; Taglietti, A.; *Coord. Chem. Rev*., **2006**, 250, 1451-1470; (c) Amendola, V.; Esteban-Gomez, D.; Fabbrizzi, L. and Licchelli, M.; *Acc. Chem. Res*., **2006**, 39(5), 343-353; (d) Alibrandi, G.; Amendola, V.; Bergamaschi, G.; Fabbrizzi, L. and Licchelli, M.; *Org. Biomol. Chem*., **2015**, 13(12), 3510-3524.

[13] (a) Amendola, V.; Alberti, G.; Bergamaschi, G.; Biesuz, R.; Boiocchi, M.; Ferrito, S. and Schmidtchen, F. P.; Eur. *J. Inorg. Chem*., **2012**, 21, 3410-3417; (b) Alberto, R.; Bergamaschi, G.; Braband, H.; Fox, T. and Amendola, V.; *Angew. Chem. Int. Ed*., **2012**, 51(39), 9772-9776.

[14] Amendola, V.; Boiocchi, M.; Fabbrizzi, L. and Palchetti, A.; *Chem. Eur. J*., **2005**, 11, 120-127.

[15] Amendola, V.; Boiocchi, M.; Fabbrizzi, L. and Palchetti, A.; *Chem. Eur. J*., **2005**, 11, 5648-5660.

[16] Wallace, K.J.; Belcher, W.J.; Turner, D.R.; Syed, K.F. and Steed, J.W.; *Chem. Eur. J.*, **2005**, 11, 5648-5660.

[17] Vu, V. H.; Jouanno, L. A.; Cheignon, A.; Roisnel, T.; Dorcet, V.; Sinbandhit, S. and Hurvois, J. P.; *Eur. J. Org. Chem*., **2013**, 5464-5474.

[18] Bergamaschi, G.; Boiocchi, M.; Monzani, E. and Amendola, V.; *Org. Biomol. Chem*., **2011**, 9, 8276-8283.

[19] Gans, P.; Sabatini, A. and Vacca, A.; *Talanta*, **1996**, 43, 1739-1753.

[20] Gaussian 09, Revision B.01, M. J. Frisch, G. W. Trucks, H. B. Schlegel, G. E. Scuseria, M. A. Robb, J. R. Cheeseman, G. Scalmani, V. Barone, B. Mennucci, G. A. Petersson, H. Nakatsuji, M. Caricato, X. Li, H. P. Hratchian, A. F. Izmaylov, J. Bloino, G. Zheng, J. L. Sonnenberg, M. Hada, M. Ehara, K. Toyota, R. Fukuda, J. Hasegawa, M. Ishida, T. Nakajima, Y. Honda, O. Kitao, H. Nakai, T. Vreven, J. A. Montgomery, Jr., J. E. Peralta, F. Ogliaro, M. Bearpark, J. J. Heyd, E. Brothers, K. N. Kudin, V. N. Staroverov, R. Kobayashi, J. Normand, K. Raghavachari, A. Rendell, J. C. Burant, S. S. Iyengar, J. Tomasi, M. Cossi, N. Rega, J. M. Millam, M. Klene, J. E. Knox, J. B. Cross, V. Bakken, C. Adamo, J. Jaramillo, R. Gomperts, R. E. Stratmann, O. Yazyev, A. J. Austin, R. Cammi, C. Pomelli, J. W. Ochterski, R. L. Martin, K. Morokuma, V. G. Zakrzewski, G. A. Voth, P. Salvador, J. J. Dannenberg, S. Dapprich, A. D. Daniels, Ö. Farkas, J. B. Foresman, J. V. Ortiz, J. Cioslowski, and D. J. Fox, Gaussian, Inc., Wallingford CT, 2009.

[21] (a) Becke, A. D.; *J. Chem. Phys*. **1993**, 98 (7), 5648–5652; (b) Lee, C.; Yang, W. and Parr, R. G.; *Phys. Rev. B*, **1998**, 37, 785-789; (c) Vosko, S. H.; Wilk, L. and Nusair, M.; *Can. J. Phys*., **1980**, 58, 1200-1211; (d) Stephens, P. J.; Devlin, F. J.; Chabalowski, C. F. and Frisch, M. J.; *J.Phys.Chem*., **1994**, 98, 11623-11627.

[22] [PCM] Cossi, M.; Rega, N.; Scalmani, G. and Barone, V.; *J. Comput. Chem*., **2003**, 24 (6), 669-681.

[23] (a) Ditchfield, R.; *Mol. Phys*., **1974**, 27 (4), 789-807; (b) Wolinski, K.; Hilton, J. F. and Pulay, P.; *J. Am. Chem. Soc.*, **1990**, 112 (23), 8251-8260.

[24] Farrugia, L.J.; *J. Appl. Crystallogr*., **1999**, 32, 837-838.

[25] North, A.C.T.; Phillips, D.C. and Mathews, F.S.; *Acta. Crystallogr*., **1968**, A24, 351-359.

[26] Bruker, SAINT Software Reference Manual. Version 6, Bruker AXS Inc., Madison, Wisconsin, USA, 2003.

[27] Krause, L.; Herbst-Irmer, R.; Sheldrick, G.M. and Stalkeand, D.; *J. Appl. Crystallogr*., **2015**, 48, 3-10.

[28] Altomare, A.; Burla, M. C.; Camalli, M.; Cascarano, G. L.; Giacovazzo, C.; Guagliardi, A.; Moliterni, A. G.; Polidori, G. and Spagna, R. J.; *J. Appl. Crystallogr*., **1999**, 32, 115-119.

[29] Sheldrick, G. M.; *Acta Crystallogr*., **2008**, A64, 112-122.

[30] Hay, P. and Custelcean, R.; *Cryst. Growth Des.*, **2009**, 9, 2539-2545.

[31] Cametti, M.; Raatikainen, K.; Metrangolo, P.; Pilati, T.; Terraneo, G. and Resnati, G.; *Org. Biomol. Chem.*, **2012**, 10, 1329.

[32] Bondi, A.; *J Phys. Chem*., **1964**, 68, 441-451.

[33] Shannon, R.D.; *Acta Crystallogr*., **1976**, A32, 751-767.

[34] Desiraju, G.R.; Ho, P.S.; Kloo, L.; Legon, A.C.; Marquardt, R.; Metrangolo, P.; Politzer, P.A.; Resnati, G. and Rissanen, K.; *Pure Appl. Chem*. **2013**, *85*, 1711.

3. The powerful synergy of C-H donor groups within a bowl-shaped cavity of a tripodal receptor

3.1 Introduction

Imidazolium is a frequently used unit in the design of anion receptors because of its ability as H-bond donor and to establish electrostatic interactions with the substrate. The imidazole is represented by the resonances shown in Figure 1. [1]

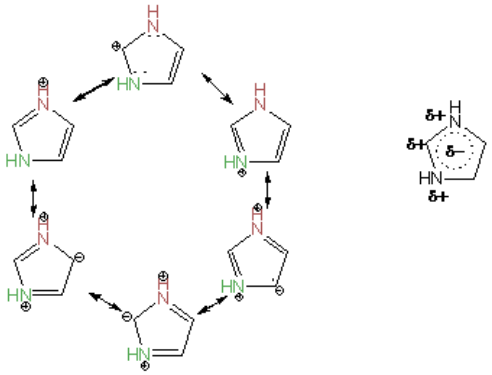

Figure 1. Imidazole resonances.

The presence of a delocalized positive charge makes the C-H group, between the two nitrogen atoms, strongly-activated for hydrogen bond donation: the imidazolium fragment is therefore able to interact strongly with the anions by both H bonds and electrostatic interactions.

The first examples of imidazolium-based receptors were reported in 1999 by Alcade [2] and Sato [3]. Since then, several examples of receptors containing this fragment, inserted in rigid cavities or linked to fluorogenic or chromogenic units, have been reported. The presence of fluorophores/chromophores on the receptor framework enabled researchers to perform anion binding studies, using UV-vis. or emission spectroscopies in addition to ^{1}H-NMR.

In Figure 2, receptor **a,** containing imidazolium fragments, is reported. This macrocycle can interact with different anions.[2] In particular, the de-shielding effect observed in the ^{1}H-NMR spectrum, for the C-H directly involved in the interaction, varies in the order $H_2PO_4^-$ > F^- > CH_3COO^-> CN^- > Cl^-.

Another interesting example of this type of receptors is compound **b**, studied by Sato and collaborators (Figure 2). The molecule forms 1:1 complexes with halides and oxoanions in d_6-DMSO, with affinity in the order HSO_4^- > Br^- > $H_2PO_4^-$ > Cl^- > I^- > ClO_4^-.[4] This trend depends on the fit of the anion with the receptor cavity.

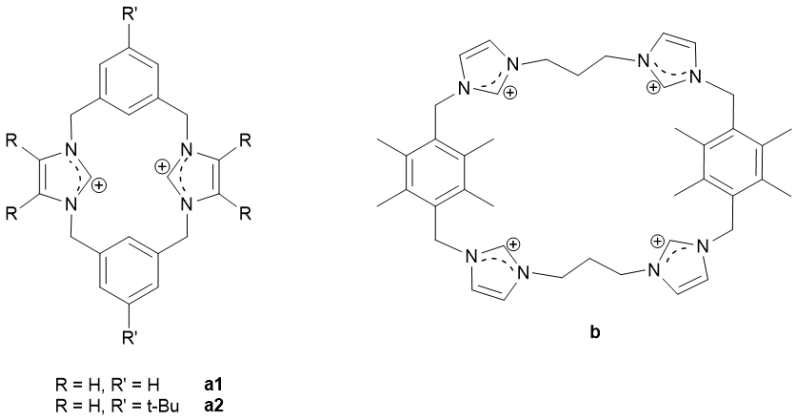

Figure 2. Receptors **a** and **b**.

In our case, we decided to use a combination of two different C-H donor units, i.e. the well- known imidazolium group in synergy with a tetrafluorobenzyl unit, within a bowl-shaped receptor (i.e. a tripod). Notably, the tetrafluorobenzyl moiety had never been explored as a C-H donor in anion recognition before; this is quite surprising, considering the pK value per hydrogen of 1,2,3,4-tetrafluorobenzene compared to benzene[5], and therefore the potentialities of the C–H group as a H-donor. In fact, H-bond donor tendencies mainly depend on the proton's acidity, which in turn relies on the substituents' capability of stabilizing the corresponding conjugated anion. Consequently, aryl protons are more acidic than the alkyl ones[6]; especially in presence of electron-withdrawing substituents, the H-bond donor tendencies of C–H groups may become comparable to those of traditional H-donors (e.g. NH and OH).[7]

3.2 Experimental section

All reagents were purchased from Alfa-Aesar and Sigma-Aldrich, and used without further purification. Mass spectra were acquired on a Thermo Finnigan ion trap LCQ Advantage Max instrument equipped with an ESI source. ^{1}H-, ^{19}F- and ^{13}C-NMR spectra were recorded on a Bruker ADVANCE 400 spectrometer (operating at 9.37 T, 400 MHz). The experimental procedures of NMR titrations are described elsewhere.[8] Titration data were processed with the Hyperquad package[9] to determine the equilibrium constants.

3.2.1. Crystal structure analysis

Diffraction data for [**1**(Cl)]$(PF_6)_2$·MeCN and [**1**(Br)]$(PF_6)_2$·MeCN isomorphous crystals were collected by means of an Enraf-Nonius CAD4 four circle diffractometer, working at room temperature with MoKα X-radiation (λ = 0.7107 Å). See Tables S1-S2 for details.

Data reductions (including intensity integration, background, Lorentz and polarization corrections) were performed with the WinGX package;[10] absorption effects were evaluated with the psi-scan method[11] and absorption correction was applied to the data.

The crystal structures were solved by direct methods (SIR 97)[12] and refined by full-matrix least-squares procedures on F^2 using all reflections (SHELXL-2014).[13] Anisotropic displacement parameters were used for all non-hydrogen atoms. Hydrogens have been placed at calculated positions and their positions refined according to a riding model.

For both isomorphous crystals, features of the acetonitrile solvent molecules were not clear, probably because of positional disorder that could not be resolved with the available diffraction data. Atoms belonging to the acetonitrile solvent molecule were refined using soft restraints for the molecular geometries and for the atom displacement parameters.

3.2.2. Synthesis and characterization of receptor 1

2,3,4,5-tetrafluorobenzylbromide was purchased from Alfa-Aesar. Other reagents (e.g. tribromomethyl mesitylene) and solvents were purchased from Sigma-Aldrich, and used without further purification. The synthesis of receptor **2**$(PF_6)_3$ is reported elsewhere.[14]

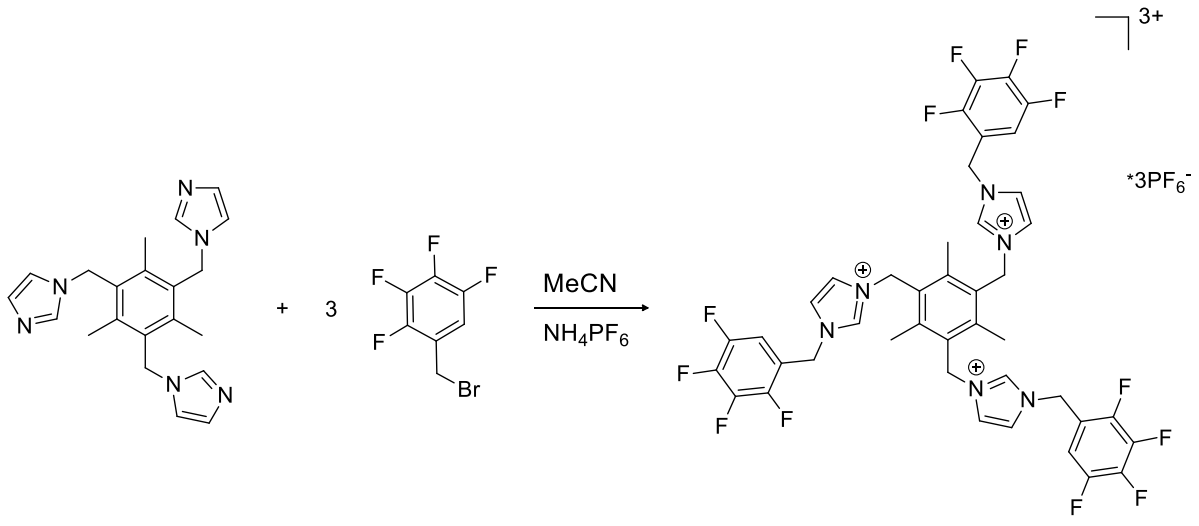

1$(PF_6)_3$

The 1,3,5-tris(N-imidazolylmethyl)-2,4,6-trimethylbenzene (0.25 g, 0.69 mmol) was dissolved in 40 ml of MeCN; under stirring, an excess of 2,3,4,5-tetrafluorobenzyl bromide (3.3 eqv) was added and the mixture was refluxed for 72 h. The course of the reaction was controlled by mass spectrometry confirming the presence of the only tri-substituted product.

MS-ESI (MeOH): m/z 467.7 [**1**+Br^-]$^{2+}$, 455.6 [**1**+NO_3^-]$^{2+}$.

The white solid obtained was washed several times with Et_2O, filtered and dried. Than was dissolved in the minimum amount of H_2O; the anion was exchanged by adding a saturated aqueous solution of NH_4PF_6. The white precipitate formed at room temperature was isolated by vacuum filtration, washed with Et_2O and dried. Yield: 65%

$C_{42}H_{33}N_6P_3F_{30}$: found: C, 39.13; H, 2.63; N, 6.49%, calculated: C, 39.27; H, 2.59; N, 6.54%

ESI-MS (MeOH): m/z 497 [**1**+PF_6^-]$^{2+}$, 447 [**1**+$HCOO^-$]$^{2+}$.

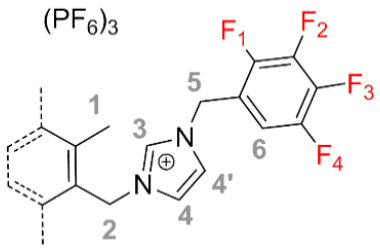

^{1}H-NMR (CD_3CN, 400 MHz), δ (ppm): 8.46 (s, 3H, H-3), 7.41 (t, 3H, H-4), 7.35 (t, 3H, H-4'), 7.29 (m, 3H, H-6), 5.45 (s, 6H, H-2), 5.36 (s, 6H, H-5), 2.24 (s, 9H, H-1).

^{13}C-NMR (CD_3CN, 400 MHz), δ (ppm): 142.17 (C-quat), 135.59 (C-H3), 129.38 (C-quat), 123.26 (C-H4', C-H4), 113.3 (C-quat), 112.69 (C-H6), 49.55(C-H2), 46.86 (C-H5), 15.25 (C-H1).

^{19}F-NMR (CD_3CN/CH_3CN 1:1, 400 MHz),), δ (ppm): – 73.2 (d, PF_6^-), – 140.4 (m, F-4), – 143.3 (t, F-1), – 155.8 (t, F-3), – 157.0 (t, F-2).

3.3. Results and discussion

Here is reported the synthesis and the study of a novel tripodal receptor, [**1**$(PF_6)_3$] containing the imidazolium group capable of interacting with anionic species through hydrogen bonds in addition to a new C-H donor group (i.e. the tetrafluorobenzyl unit).

The anion binding properties of **1** were compared with those of receptor **2,** presenting simple benzyl units appended to the mesitylene platform (Figure 3). Notably, the presence of electron-withdrawing fluorine atoms on **1** increases the acidity of the C-H bonds on the tetrafluorobenzyl units, which thus become potential hydrogen bond donors.

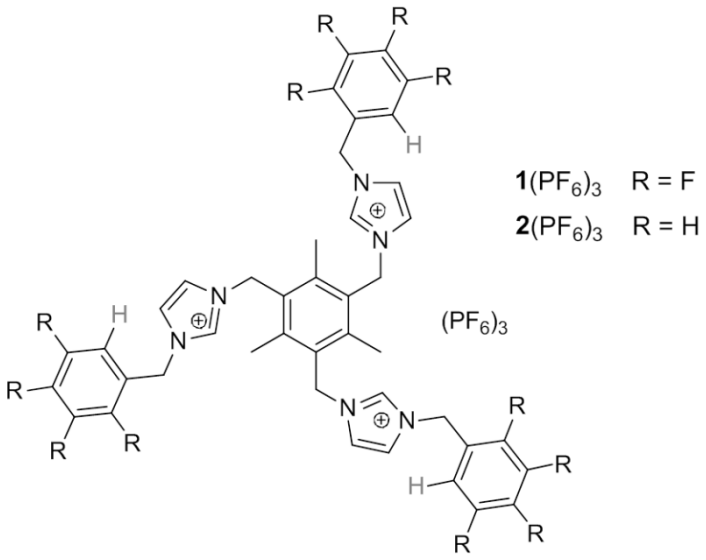

Figura 3. Tripodal imidazolium-based anion receptors.

The binding tendencies of receptors **1** and **2** toward anions have been investigated through ^{1}H-NMR titrations in pure acetonitrile, in CD_3CN/d_6-DMSO 9:1 and CD_3CN/D_2O 4:1 (v:v) mixtures. In particular, we focused our studies on the interaction with Cl^-, Br^- and I^-. In order to evaluate the affinity of our systems for these substrates, ^{19}F-NMR titrations were also performed. NMR spectroscopy allowed us to study the anion binding in solution, following the changes in the chemical shifts of receptor's atoms [either directly or indirectly involved in the binding, i.e. hydrogen and fluorine atoms, respectively]. From these variations, it was possible to obtain information on the stoichiometry of the complexes and on the nature of the receptor-anion interaction.

Also a single crystals of [**1**(Cl)]$(PF_6)_2$·MeCN and [**1**(Br)]$(PF_6)_2$·MeCN suitable for X-ray diffraction study were isolated.

3.3.1. NMR titrations of receptor 1(PF$_6$)$_3$

NMR titrations with anions were carried out at 25 °C directly in the NMR tube containing **1**(PF$_6$)$_3$ (10^{-3} M) in deuterated solvents or mixtures. In the case of ^{19}F-NMR measurements, the solutions were prepared in 1:1 CH_3CN:CD_3CN. After each addition of a sub-stoichiometric amount of the anion (as TBA salt), the NMR spectrum was recorded.

3.3.1.1. ^{1}H-NMR titration of tripod 1(PF$_6$)$_3$ with tetrabutylammonium chloride in CD_3CN

We investigated the binding tendencies of **1**$^{3+}$ towards the chloride anion by NMR titrations. Chloride was chosen as the target anionic guest as it has a spherical shape, which adapts properly to the bowl-shaped cavity[15] of our tripodal system. Moreover, among spherical anions, it is known to form stable complexes with imidazolium-based receptors in competing media.[16]

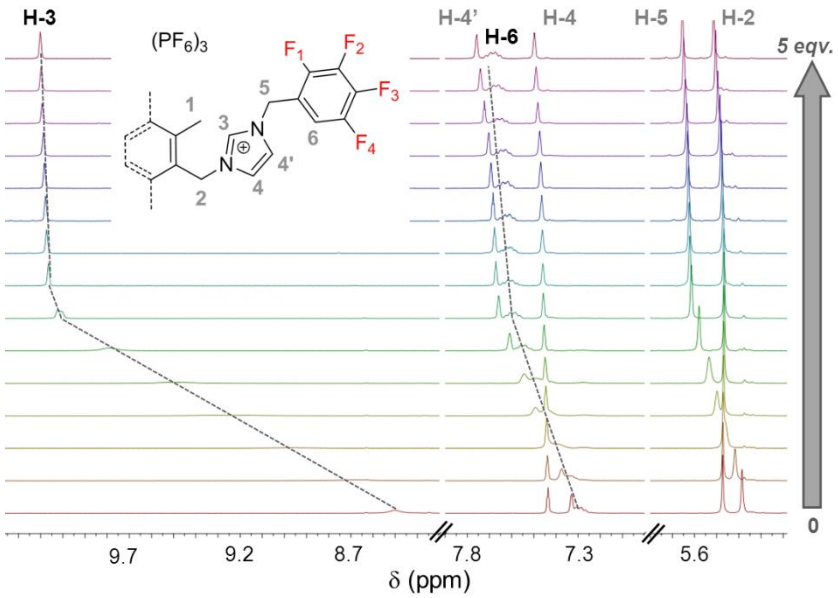

Figure 4. The family of ^{1}H-NMR spectra recorded during titration of **1** with TBAC1 in CD_3CN.

Upon chloride addition, most of the signals underwent a down-field shift. The most affected signal was that corresponding to H-3, belonging to the imidazolium unit: in fact, the chloride anion interacts with H-3 by hydrogen bond ($\Delta\delta$ = +1.6 ppm).

A significant down-field shift was also observed for the multiplet* signal of H-6 ($\Delta\delta$ = +0.38 ppm).

This result confirms that the protons of the tetrafluorobenzyl rings are involved in the coordination of the anion.

	Δδ (ppm)/**1**$(PF_6)_3$	Δδ (ppm)/**2**$(PF_6)_3$
H-3	+ 1.60[a]; + 0.89[b] ; n.a.[c]	+ 1.16[b]; n.a.[c]
H-4'	+ 0.43[a]; + 0.28[b] ; + 0.20[c]	+ 0.30[b]; + 0.11[c]
H-5	+ 0.27[a]; + 0.16[b] ; + 0.08[c]	+ 0.15[b]; + 0.03[c]
H-6, H-o	+ 0.38[a]; + 0.19[b] ; + 0.10[c]	≤ 0.01[b,c]

Table 1: ^{1}H-NMR titrations of **1**$(PF_6)_3$ and **2**$(PF_6)_3$ with TBACl in [a]pure CD_3CN, [b]CD_3CN/d_6-DMSO 9:1 and [c]CD_3CN/D_2O 4:1 (v/v) mixtures. n.a.: not available

The experimental profiles as well as the Job plots (see Figure 5) indicate the formation of a 1:1 complex between the ligand and the anion, according to the equilibrium: $\mathbf{1}^{3+} + Cl^- \rightleftarrows [\mathbf{1}^{3+} \cdots Cl^-]^{2+}$. However, the curvature was too steep to allow a reliable determination of the binding constant.

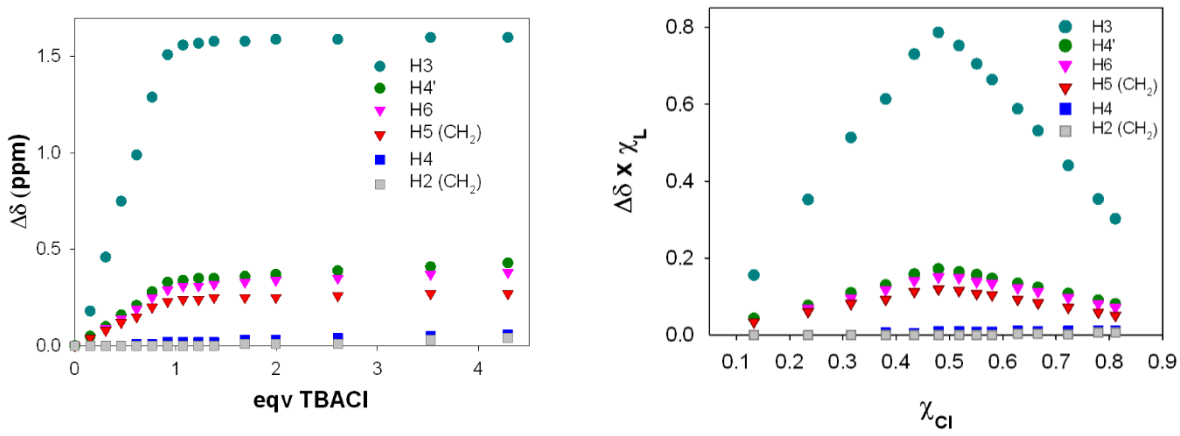

Figure 5. Profiles (left) and Job plots (right) of the ^{1}H-NMR titration of **1**$(PF_6)_3$ (1mM) with TBACl in pure CD_3CN

3.3.1.2. ^{19}F-NMR titration of the tripod 1$(PF_6)_3$ with tetrabutylammonium chloride in acetonitrile

Also ^{19}F-NMR titration of $\mathbf{1}^{3+}$ was performed with a TBAC1 solution in CH_3CN: CD_3CN 1:1 and the formation of the 1:1 $\mathbf{1}^{3+}/Cl^-$ complex was demonstrated. In the titration spectra, four different signals can be observed, due to the presence of four non equivalent F atoms in the molecular

framework (Figure 6). The assignment of the peaks to the corresponding F atoms was performed taking into account the multiplicity of the signals and the coupling constants. In particular:

$J_{F\text{-}F\ orto} \approx 20$ Hz $J_{F\text{-}F\ meta} \approx 8\text{-}10$ Hz $J_{F\text{-}F\ para} \approx 2$ Hz

$J_{F\text{-}H\ orto} \approx 8$ Hz $J_{F\text{-}H\ meta} \approx 4$ Hz $J_{F\text{-}H\ para} < 2$ Hz

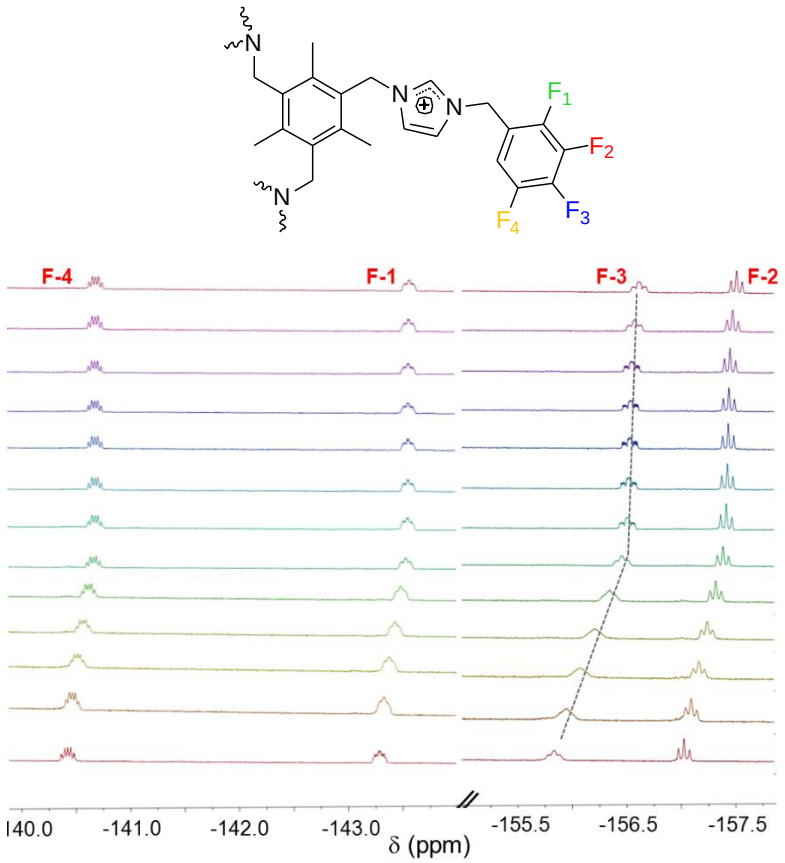

Figure 6. ^{19}F-NMR titration of 0.75 ml of a 10^{-3} M solution of $\mathbf{1}^{3+}$ with TBACI in CH_3CN:CD_3CN 1:1 solution.

Notably, upon anion addition, all the fluorine signals underwent an up-field shift, due to the shielding effect exerted by chloride. In fact, anion inclusion induced the polarization of the C–H groups involved in the binding, with a consequent increase of the electron density felt by the fluorine atoms.

Interestingly, among the aromatic fluorine atoms, the strongest up-field shifts are observed for F-3 and F-2 ($\Delta\delta$ = -0.78 and -0.49 ppm, respectively, at 4.5 eq. Cl^-), even if they are the farthest away from the bound chloride.

In fact, in the aromatic moiety, the contribution to the chemical shift of fluorine is mostly due to the mesomeric effect exerted in the ortho and para positions. It is worth noting that F-3 and F-2, in para to the residues involved in the interaction with chloride, are strongly affected by the increase in

electronic density on carbons 5 and 6, consequent to the polarisation of the C-H bonds in the adduct.

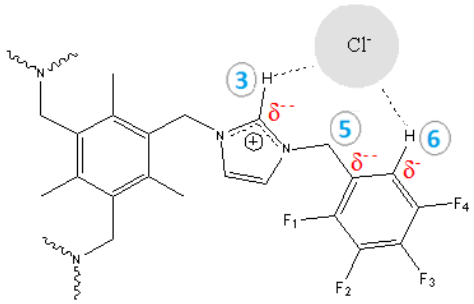

Figure 7. Schematic representation of the hydrogen bonds and the partial negative charges that form in the complex.

From the titration profiles (Δδ vs. equivalents of Cl^-) as well as from the Job plots, we observed the formation of 1:1 complex between the ligand and the anion. (Figure 8).

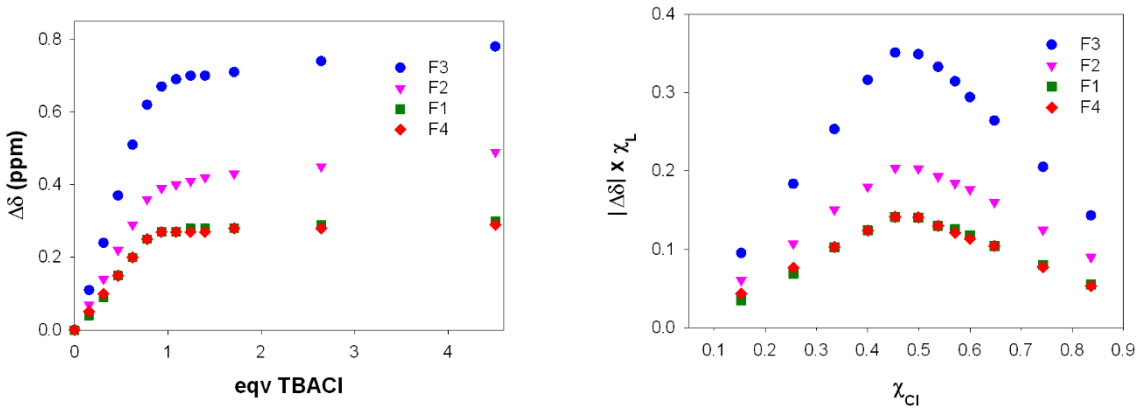

Figure 8. Profiles (left) and Job plots (right) of the ^{19}F-NMR titration of **1**$(PF_6)_3$ (1mM) with TBACl in acetonitrile.

Over the course of the titration with chloride, the signal corresponding to PF_6^- underwent a significant shift (Figure 9). This could be attributed to the displacement of one of the PF_6^- counterions from the receptor's cavity upon chloride inclusion.

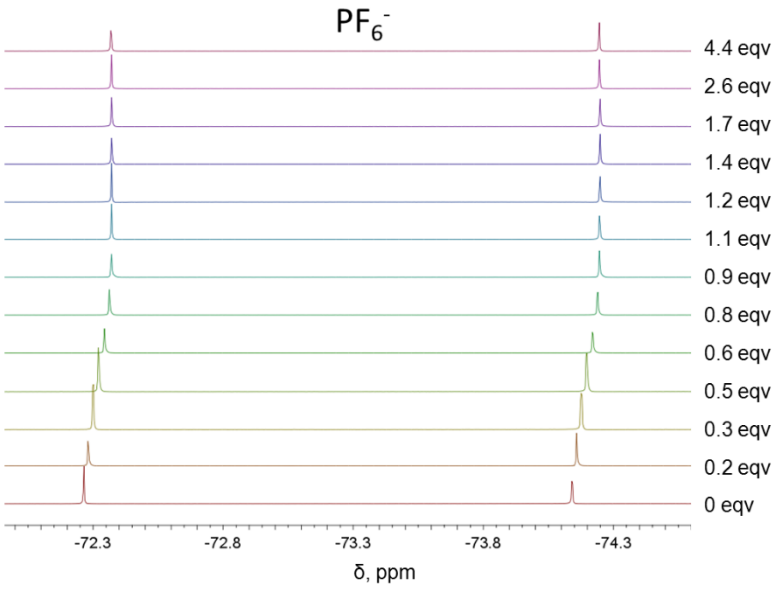

Figure 9. ^{19}F-NMR titration of 0.75 ml of a 10^{-3} M solution of $\mathbf{1}^{3+}$ with TBACl in CH_3CN: CD_3CN 1:1.

3.3.1.3. ^{1}H-NMR titration of the tripod 1 with tetrabutylammonium chloride in CH_3CN/d_6-DMSO 9:1 and CD_3CN/D_2O 4:1 mixtures

NMR titration experiments with TBACl were also performed in more competing media, i.e. in CD_3CN/d_6-DMSO 9:1 (Figure 10) and CD_3CN/D_2O 4:1 (v/v) mixtures (Figure 12).

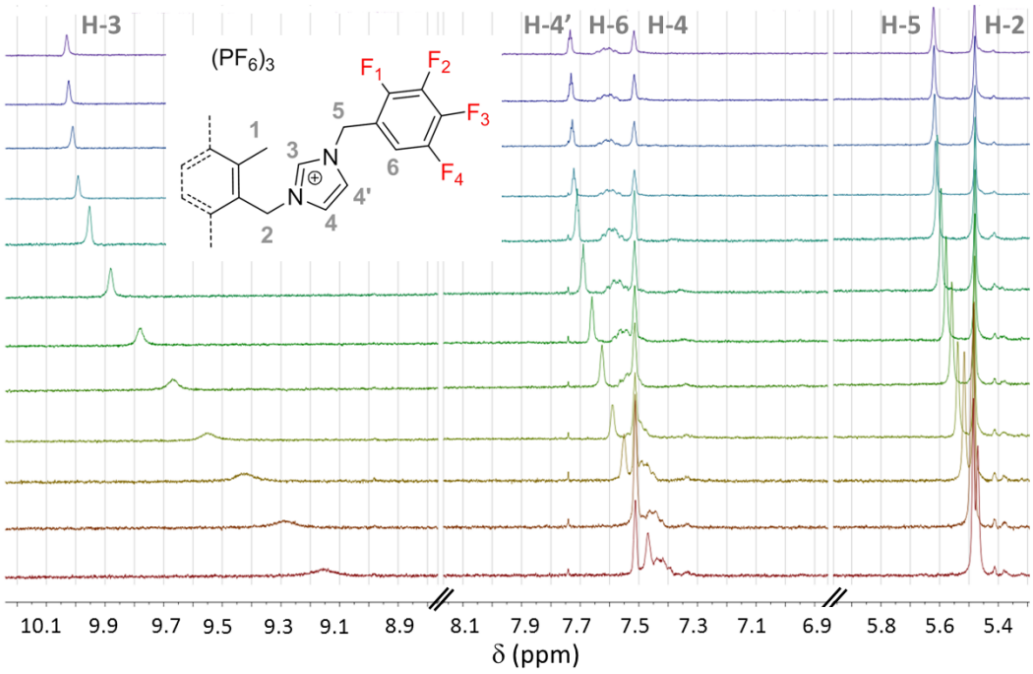

Figure 10. ^{1}H-NMR titration of $\mathbf{1}(PF_6)_3$ with TBACl in CD_3CN/d_6-DMSO 9:1 (v/v) mixture.

In CD_3CN/d_6-DMSO 9:1, the affinity of $\mathbf{1}^{3+}$ towards chloride is very high (≥ 6 log units) as shown by the steep curvature of the profile in Figure 11. As in pure acetonitrile, chloride binding mostly involves the protons of the cavity's upper-rim.

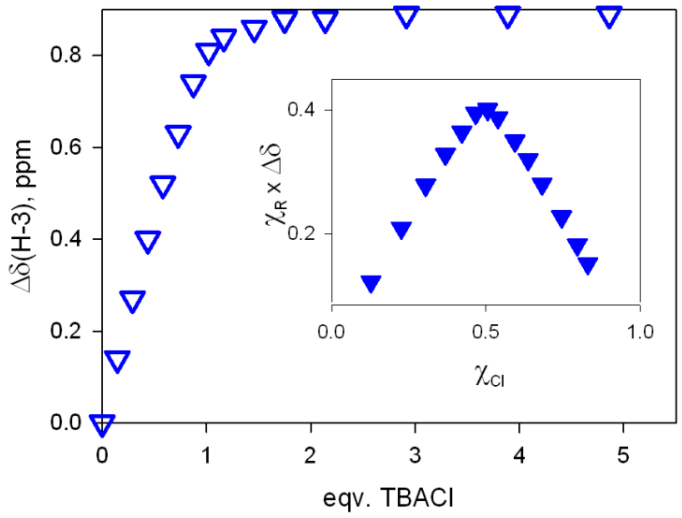

Fig. 11 ^{1}H-NMR titration of $\mathbf{1}^{3+}$ (0.2 mM) with TBACl in CD_3CN/d_6-DMSO 9:1. Inset: Job plot (χ_R, χ_{Cl} = molar fractions of $\mathbf{1}^{3+}$ and TBACl).

In CD_3CN/D_2O 4:1 (v/v) mixtures (Figure 12), the signals of the acidic protons H-3 could not be observed due to fast exchange with D_2O.[17-18] Nevertheless, thanks to the shifts of other protons, a binding constant of 3.37(7) log units was determined for the $\mathbf{1}^{3+}/Cl^-$ couple.

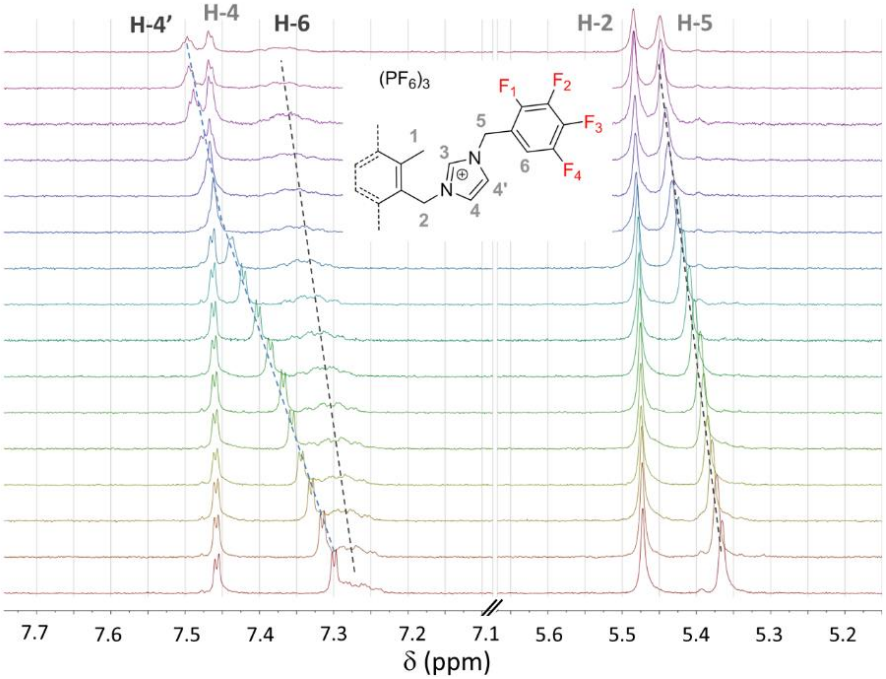

Figure 12. ^{1}H-NMR titration of $\mathbf{1}(PF_6)_3$ with TBACl in CD_3CN/D_2O 4:1 mixture.

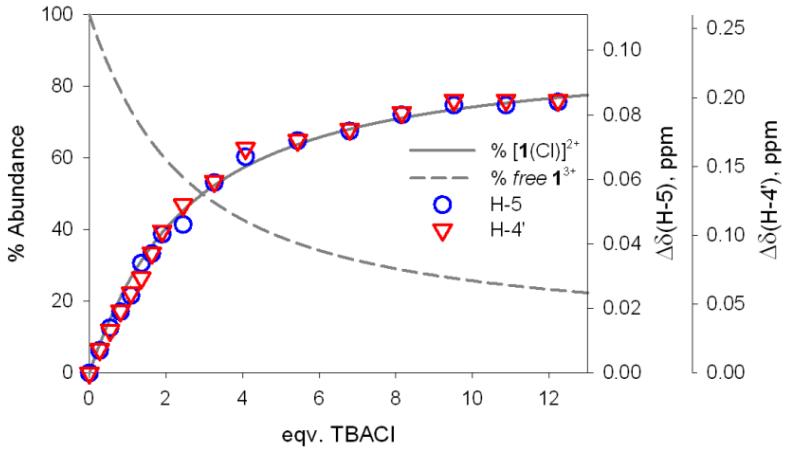

Figure 13 ^{1}H-NMR titration of **1**$(PF_6)_3$ (0.5 mM) with TBACl in CD_3CN/D_2O 4:1 mixture. Distribution diagram of the species in solution, obtained for a binding constant of 3.37(7) log units, superimposed to the experimental plot of Δδ (ppm) vs. eqv. TBACl for protons H-5 and H-4'.

3.3.1.4. ^{1}H-NMR titration of the tripod 2 with tetrabutylammonium chloride in CH_3CN/d_6-DMSO 9:1 and CD_3CN/D_2O 4:1 mixtures

In order to prove the contribution of the tetrafluorobenzyl groups to chloride binding, we performed NMR measurements on the non-fluorinated analogue receptor $\mathbf{2}^{3+}$ (see Figure 3), in CD_3CN/d_6-DMSO 9:1 (v/v) mixture and CD_3CN/D_2O 4:1 mixture (see Figures 14 and 16, respectively).

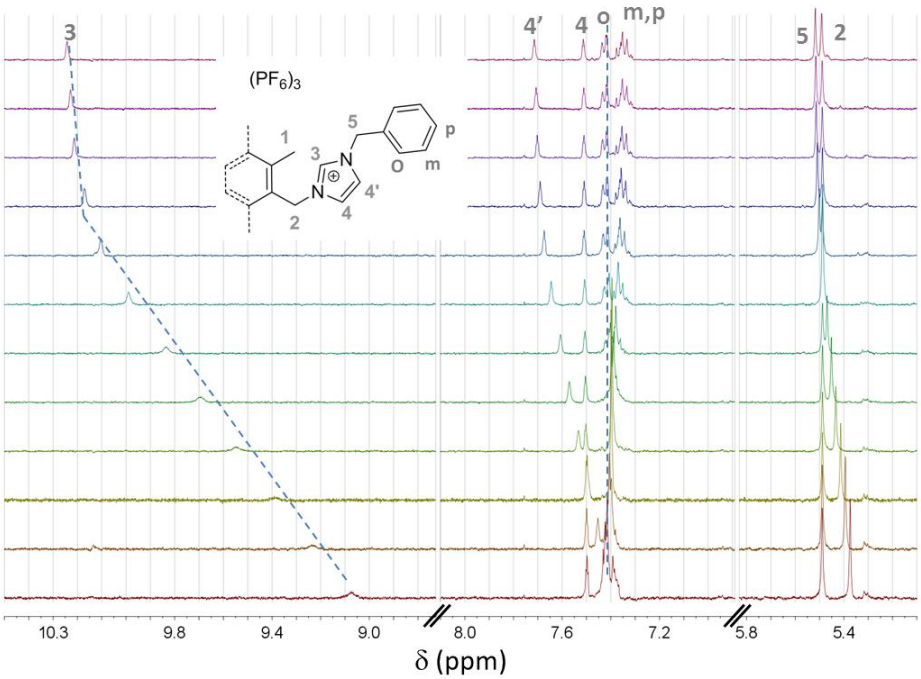

Figure 14. ^{1}H-NMR titration of **2**$(PF_6)_3$ with TBACl in CD_3CN/d_6-DMSO 9:1 (v/v) mixture.

In the case of $\mathbf{2}^{3+}$, the interaction with chloride mainly involved the imidazolium protons H-3 ($\Delta\delta$ = +1.16, see Table 1), whereas the benzyl fragment was less affected. In particular, no shifts were observed for the ortho protons, H-o (i.e. the analogues of H-6). The upfield shift observed for most aryl signals was attributed to an effect of the anionic guest. In CD_3CN/d_6-DMSO 9:1 (v/v) mixture, the ^{1}H-NMR titration of receptor $\mathbf{2}^{3+}$ with Cl^- gave a binding constant of 5.11(7) log units.

The lower chloride affinity of $\mathbf{2}^{3+}$ compared to $\mathbf{1}^{3+}$ confirms the contribution of the tetrafluorobenzyl units to the anion binding.

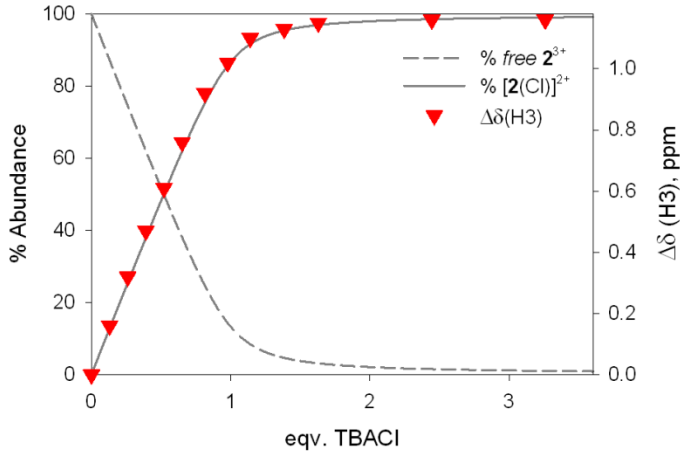

Figure 15. ^{1}H-NMR titration of $\mathbf{2}(PF_6)_3$ (0.31 mM) with TBACl in CD_3CN/d_6-DMSO mixture (10%v. d_6-DMSO). Distribution diagram of the species in solution, obtained for a binding constant of 5.11(7) log units, superimposed to the experimental plot of ($\Delta\delta$ × (ppm) vs. eqv. TBACl for protons H-3.

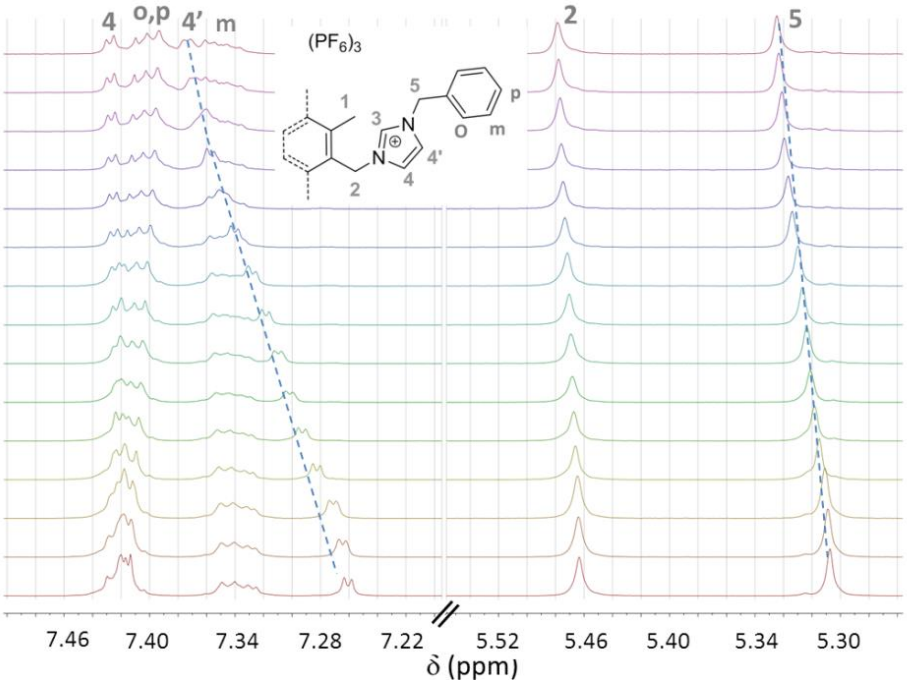

Figure 16. ^{1}H-NMR titration of $\mathbf{2}(PF_6)_3$ with TBACl in CD_3CN/D_2O 4:1 mixture.

We also performed NMR measurements on the non-fluorinated analogue receptor $\mathbf{2}^{3+}$ with chloride in CD_3CN/D_2O 4:1 mixture (see Figure 16).

Also in this case, the signals of the acidic protons H-3 could not be observed due to fast exchange with D_2O.[17-18] But, thanks to the shifts of other protons, a binding constant of 2.17(4) log units was determined for the $\mathbf{2}^{3+}/Cl^-$ couple.

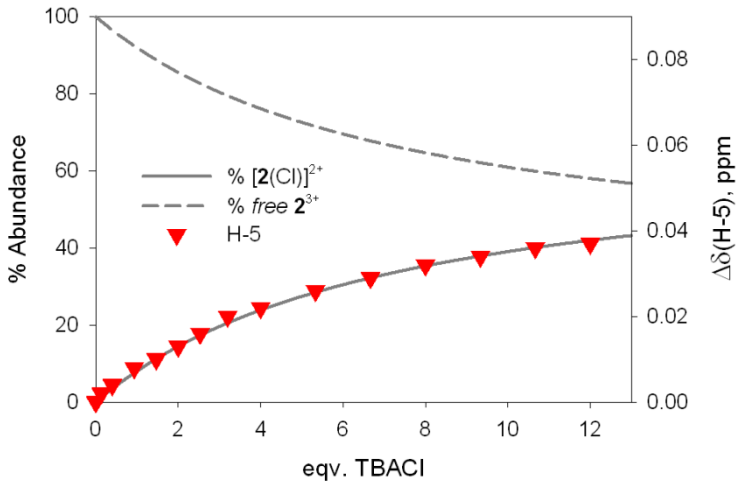

Figure 17. ^{1}H-NMR titration of $\mathbf{2}(PF_6)_3$ (1.0 mM) with TBACl in CD_3CN/D_2O 4:1 mixture. Distribution diagram of the species in solution, obtained for a binding constant of 2.17(4) log units, superimposed to the experimental plot of Δδ (ppm) vs. eqv. TBACl for protons H-5.

The higher chloride affinity of $\mathbf{1}^{3+}$ compared to $\mathbf{2}^{3+}$ was confirmed in the CD_3CN/D_2O 4:1 (v/v) mixture (Figure 18).

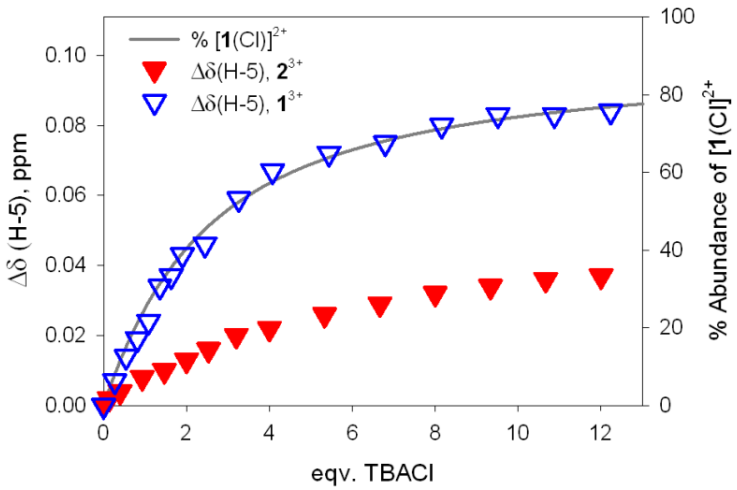

Figure 18. Experimental profiles for the ^{1}H-NMR titrations of $\mathbf{1}(PF_6)_3$ and $\mathbf{2}(PF_6)_3$ with TBACl in CD_3CN/D_2O 4:1 (v/v) mixture. The grey line corresponds to the distribution of $[\mathbf{1}(Cl)]^{2+}$ species, obtained for a $\mathbf{1}^{3+}/Cl^-$ binding constant of 3.37(7) log units.

3.3.1.5. ^{1}H-NMR titration of 1 and 2 with tetrabutylammonium bromide and iodide in CD_3CN/D_2O 4:1 mixture

^{1}H-NMR titration were also performed with other spherical anions, like Br^- and I^- (as TBA salts) in CD_3CN/D_2O 4:1 mixture.

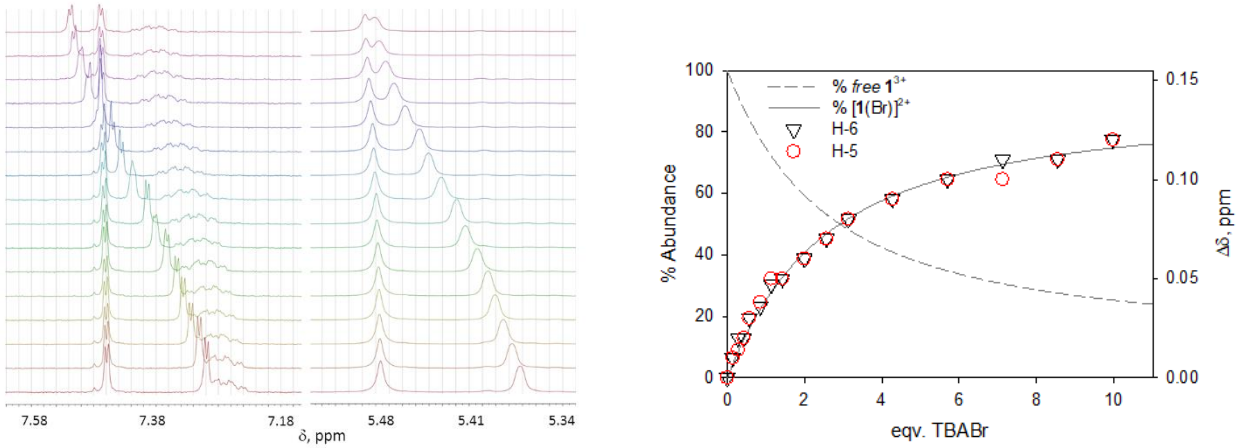

Figure 19. ^{1}H-NMR titration of **1**$(PF_6)_3$ (1.0 mM) with TBABr in CD_3CN/D_2O 4:1 mixture (left) and distribution diagram (right) of the species in solution, obtained for a binding constant of 2.66(3) log units, superimposed to the experimental plot of Δδ (ppm) vs. eqv. TBACl for protons H-6 and H-5.

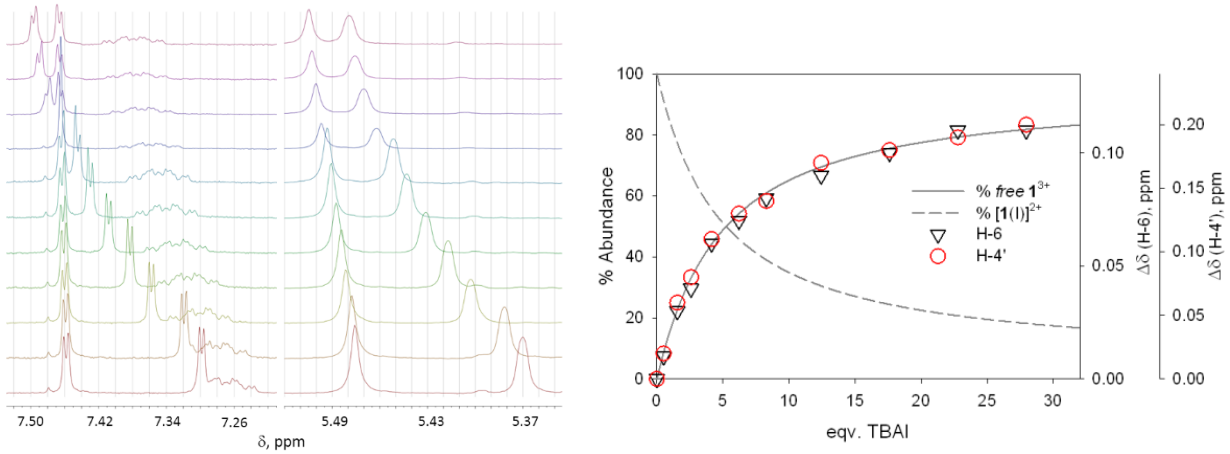

Figure 20. ^{1}H-NMR titration of **1**$(PF_6)_3$ (1.0 mM) with TBAI in CD_3CN/D_2O 4:1 mixture (left) and distribution diagram (right) of the species in solution, obtained for a binding constant of 2.34(3) log units, superimposed to the experimental plot of Δδ (ppm) vs. eqv. TBACl for protons H-6 and H-4'.

^{1}H-NMR titration studies with TBABr and TBAI allowed us to determine the constants for the $\mathbf{1}^{3+}/Br^-$ and $\mathbf{1}^{3+}/I^-$ couples, which resulted in 2.66(3) and 2.34(3) log units, respectively. Notably, the $\mathbf{1}^{3+}/Cl^-$binding constant is among the highest obtained with open-chain organic receptors in aqueous solution.[17,19-21]

In the case of receptor $\mathbf{2}^{3+}$, the precipitation occurring in solution in the presence of excess concentrations of TBABr and TBAI prevented the determination of the affinity constants for bromide and iodide anions.

3.3.2. Crystal Structures of 1^{3+} with chloride and bromide

By slow diffusion of diethyl ether into solutions containing $\mathbf{1}(PF_6)_3$ and either TBACl or TBABr, single crystals of $[\mathbf{1}(Cl)](PF_6)_2$ MeCN (Figure 21) and $[\mathbf{1}(Br)](PF_6)_2$ MeCN (Figure 22) suitable for X-ray diffraction analysis were obtained.

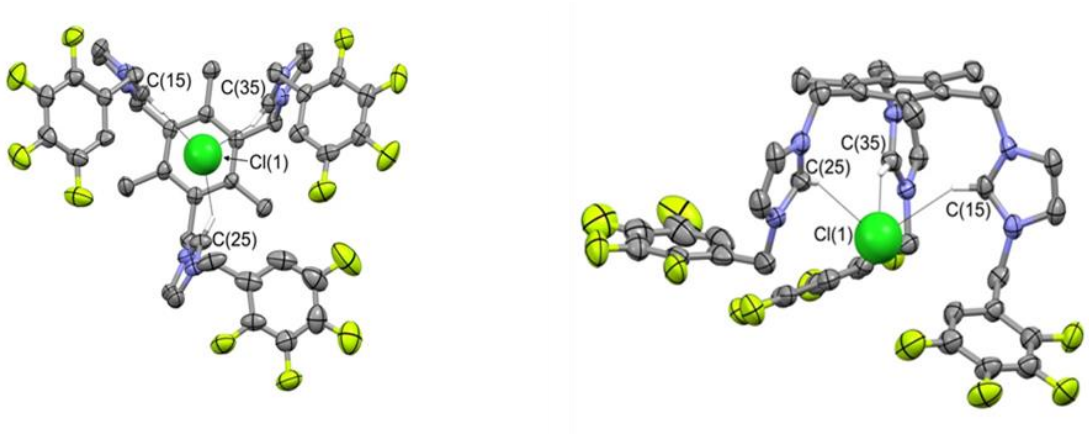

Figure 21. Crystal structure of $[\mathbf{1}(Cl)](PF_6)_2 \cdot MeCN$. Top (left) and lateral (right) views of the molecular cation $\mathbf{1}^{3+}$ interacting with chloride (PF_6^- counterions and MeCN were omitted for clarity). Atom names are only reported for atoms involved in C-H···Cl^- hydrogen bonds, drawn with black [2.56(1) < H···Cl^- < 2.66(1) Å] and grey [2.82(1) < H···Cl^- < 3.09(1) Å] dashed lines.

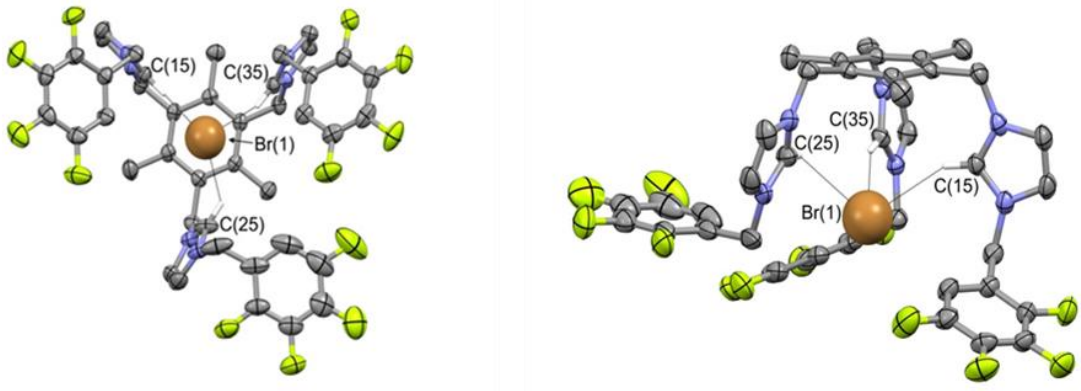

Figure 22. Crystal structure of $[\mathbf{1}(Br)](PF_6)_2 \cdot MeCN$. Top (left) and lateral (right) views of the molecular cation $\mathbf{1}^{3+}$ interacting with bromide (PF_6^- counterions and MeCN solvent molecules were omitted for clarity). Atom names are only reported for atoms involved in C-H···Br^- hydrogen bonds, drawn with black [2.68(1) < H···Br^- < 2.75(1) Å] and grey [2.94(1) < H···Br^- < 3.15(1) Å] dashed lines.

The crystals of the two compounds are isomorphous. Due to the steric constraint of the tripodal receptors, anions are placed into the open part of the cavity at a quite long distance [Cl^-, 4.063(4) Å; Br^-, 4.126(2) Å] from the best plane of the mesitylene group. The anions are only slightly displaced from the top of the mesitylene's centroid and the anion-centroid-plane angles are not significantly different for the two compounds [Cl^-, 83.1(14)°; Br^-, 82.9(8)°]. The molecular symmetries of the bowl-shaped receptors in the two crystals are the same and rather distorted from the C_3 symmetry promoted by the mesitylene scaffold. Anions are trapped within the cavity, where they form: three short C–H···X^- interactions [2.56(1) < H···Cl^- < 2.66(1) Å, 2.68(1) < H···Br^- < 2.75(1) Å] with the H-3 protons of the imidazolium groups and five long C–H···X^- interactions [2.82(1) < H···Cl^- < 3.09(1) Å, 2.94(1) < H···Br^- < 3.15(1) Å], three of which with the methylene H-5 protons and the other two involving the C–H groups of tetrafluorobenzyl rings (i.e. H-6 protons). These results confirm what was observed in solution, i.e. the cage arranges the peripheral groups in a way to point the H-5 and H-6 protons towards the anion, allowing the participation of both C_{sp3}–H and C_{sp2}–H bonds in the binding.

3.3.3. Computational Studies

All the calculations were carried out using the GAUSSIAN09 program package[22]. Both $\mathbf{1}^{3+}/Cl^-$ and $\mathbf{2}^{3+}/Cl^-$ complexes were optimized in the gas phase at the B3LYP/6-311+G(2df,p) level for the Cl atom and 6-311+G(d,p) level for the other atoms. NBO analysis was performed at the same level of calculations.[23]

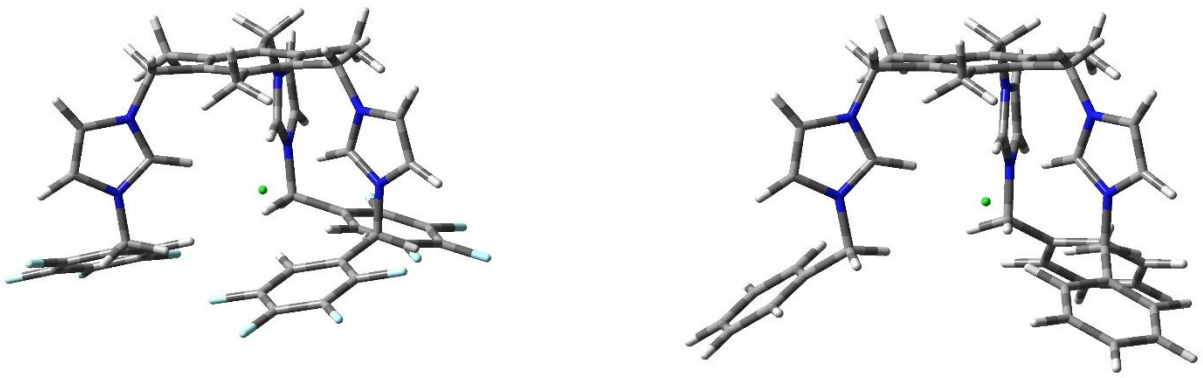

Figure 23. Three-dimensional plots of the preferred conformations of $\mathbf{[1}(Cl)]^{2+}$ (left) and $\mathbf{[2}(Cl)]^{2+}$ (right).

According to calculations, the most stable conformations of the complexes have a C_3 symmetry, with the axis passing through the mesitylene's centroid and the included anion (Figure 23). The three arms look like a three-bladed propeller with the benzyl groups, corresponding to the blades, organized either in a clockwise or in a counter-clockwise arrangement. In the case of $\mathbf{1}^{3+}/Cl^-$, the fluorine substituents strengthen the interaction between the H-6 protons and chloride. A much more closed structure is obtained compared to $\mathbf{2}^{3+}$, with the chloride anion coordinated mostly by H-3 (C3···Cl^-, 3.415 Å) and H-6 (C6···Cl^-, 3.703 Å). In the case of $\mathbf{2}^{3+}/Cl^-$, the cavity looks more accessible; the chloride anion is coordinated by H-3 (C3···Cl^-, 3.347 Å) and H-5 (C5···Cl^-, 3.946 Å), but not by H-o (Co···Cl^-, 5.230 Å).

Charge distribution and electrostatic molecular surface (MEP) were also determined. According to the NPA charges (Table 2), the highest positive charge is on H-3 atoms. The corresponding value is similar in the two complexes, suggesting that the $(C–H)^+···Cl^-$ interaction is the dominant one.

distances	[**1**(Cl)]$^{2+}$	[**2**(Cl)]$^{2+}$
C3···Cl$^-$ (Å)	3.415	3.347
C5···Cl$^-$ (Å)	4.112	3.946
C6···Cl$^-$ (Å)	3.703	5.230
NPA charges	*free* **1**$^{3+}$	*free* **2**$^{3+}$
H3	0.227	0.228
H5a	0.224	0.206
H6	0.206	0.193
ESP values		
H3	+0.367	+0.351
H5	+0.306	+0.297
H6	+0.328	+0.273

Table 2. C···Cl$^-$ distances (Å) in [**1**(Cl)]$^{2+}$ and [**2**(Cl)]$^{2+}$ complexes; corresponding NPA charges and MEP values for the H atoms in the free ligands **1**$^{3+}$ and **2**$^{3+}$.

Analogously, the MEP map showed that the highest positive values are close to H-3 (Figure 24). In the case of $\mathbf{1}^{3+}$, a high positive potential was also obtained in the proximity of H-6, in agreement with the coordination tendencies of the receptor (Table 2).

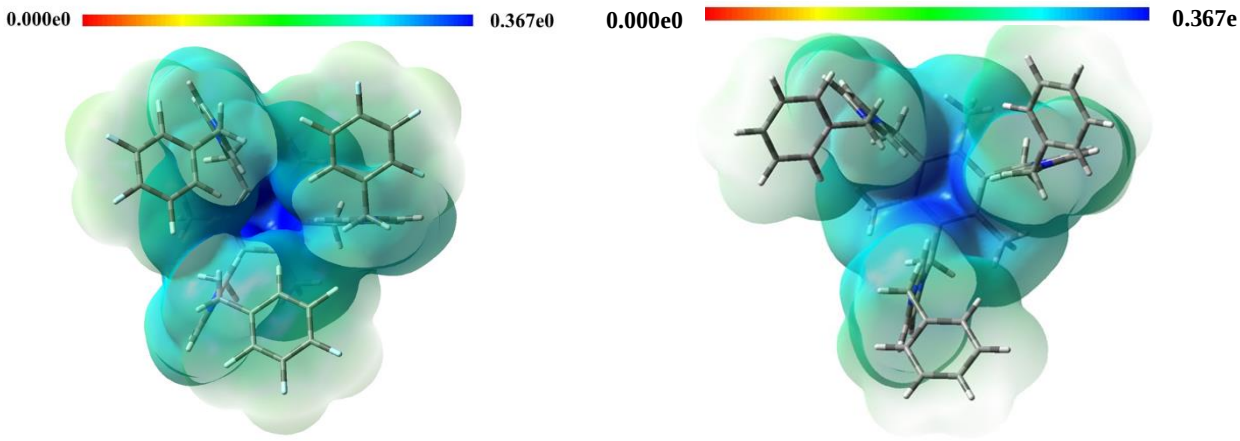

Figure 24. Molecular electrostatic potential (MEP) surface of the receptor in the complex $\mathbf{1}^{3+}/Cl^-$ (left) and of the receptor in the complex $\mathbf{2}^{3+}/Cl^-$ (right) (transparent representation, top view). The anion is omitted for clarity.

3.4. Conclusion

We synthesized a new tripodal receptor ($\mathbf{1}^{3+}$) containing three tetrafluorobenzyl units in addition to the imidazolium groups. The aim was to obtain a receptor with additional binding sites with respect to the model system $\mathbf{2}^{3+}$. ^{1}H-NMR and ^{19}F-NMR titrations were performed for both receptors ($\mathbf{1}^{3+}$ and $\mathbf{2}^{3+}$) with anions such as chloride, bromide and iodide. The results obtained in solution were confirmed in the solid state by X-ray diffraction studies on the complexes. In particular, the chloride anion binds to the upper rim of the receptor, involving the three imidazolium C-H groups, the methylene at position 5 and the C-H of the tetrafluorinated rings in the interaction. Equilibrium studies pointed out the formation of 1:1 complexes with all the investigated anions. Moreover, the binding constants were an order of magnitude higher than those obtained for the non-fluorinated receptor. The tetrafluorobenzyl moiety was thus proved to be an effective C-H bond donor. Moreover, the cooperation of neutral and cationic C-H donor groups, such as in receptor $\mathbf{1}^{3+}$, leads to a significant increase of the anion binding constants. Compared to other tripodal imidazolium-based systems reported in the literature (e.g. the nitro-system reported in 2002 by Kim et al.),[16] the binding of chloride was also achieved in aqueous solution.

The research described in this chapter was published in Chem. Commun., 2016, 52, 10910.

Supplementary Section

1S. NMR spectra

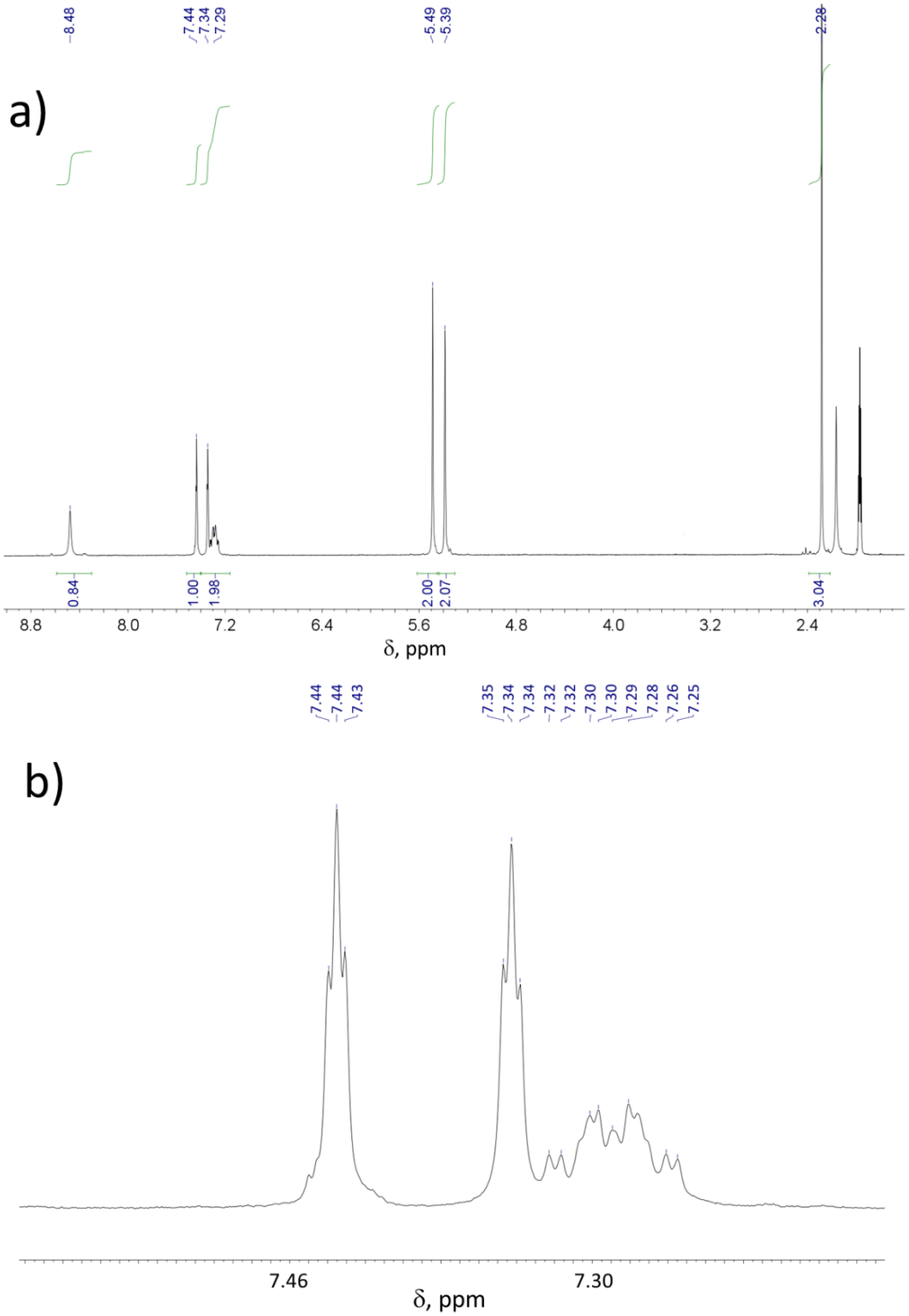

Figure S1. ^{1}H-NMR spectrum of **1**$(PF_6)_3$ in CD_3CN: a) full spectrum; b) enlargement: $\Delta\delta$ = 7.50 –7.19 ppm

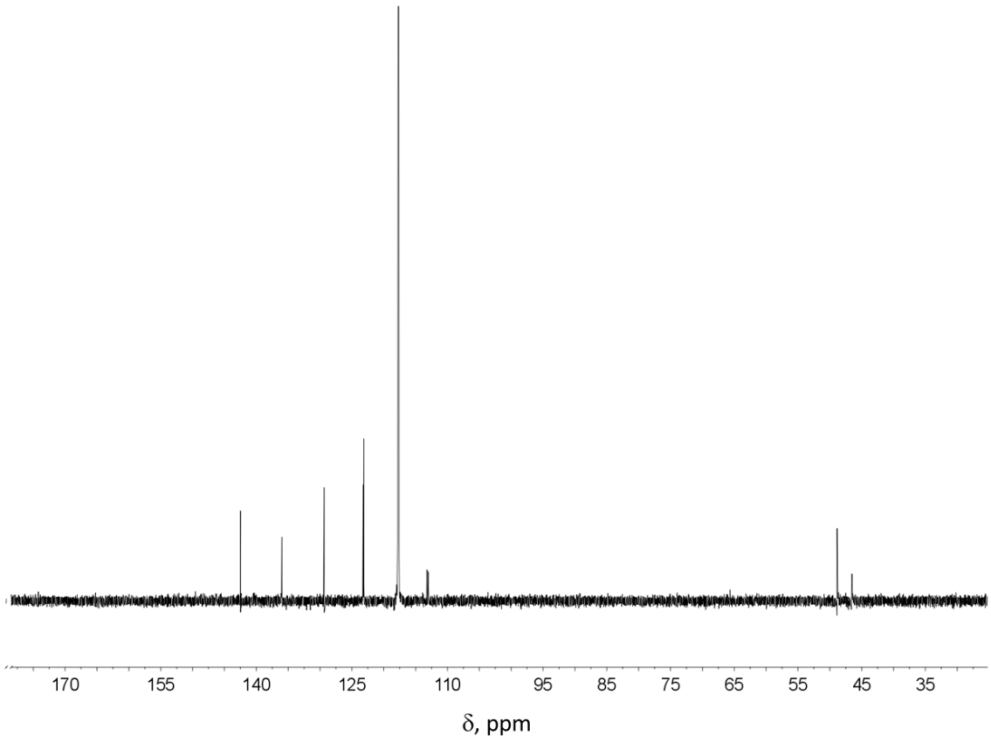

Figure S2. ^{1}H-decoupled ^{13}C-NMR spectrum of **1**$(PF_6)_3$ in CD_3CN

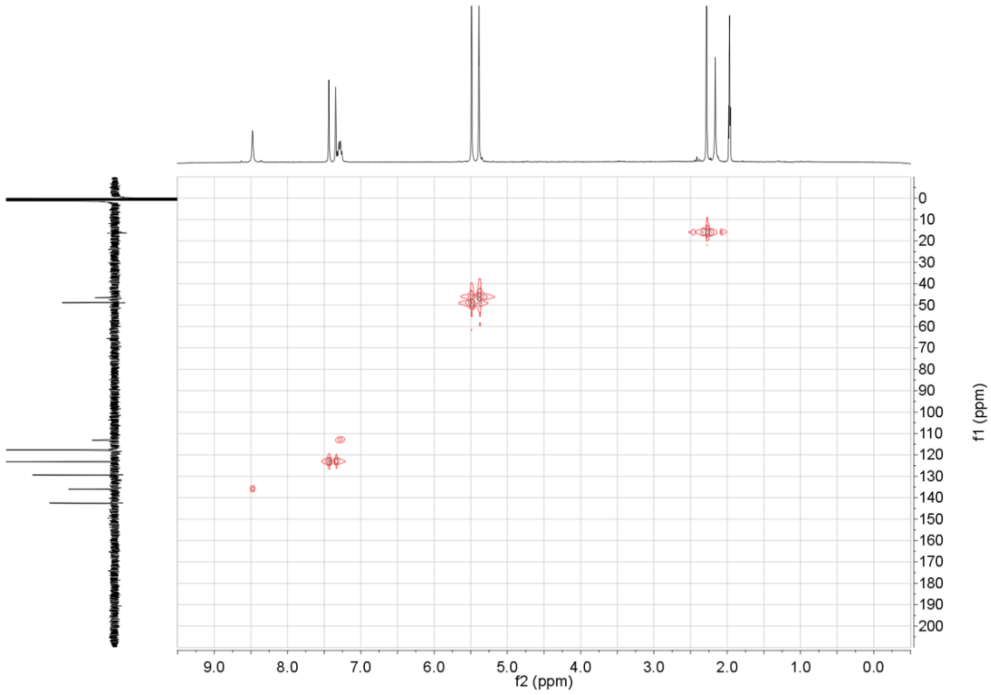

Figure S3. 2D-HSQC spectra of **1**$(PF_6)_3$ in CD_3CN

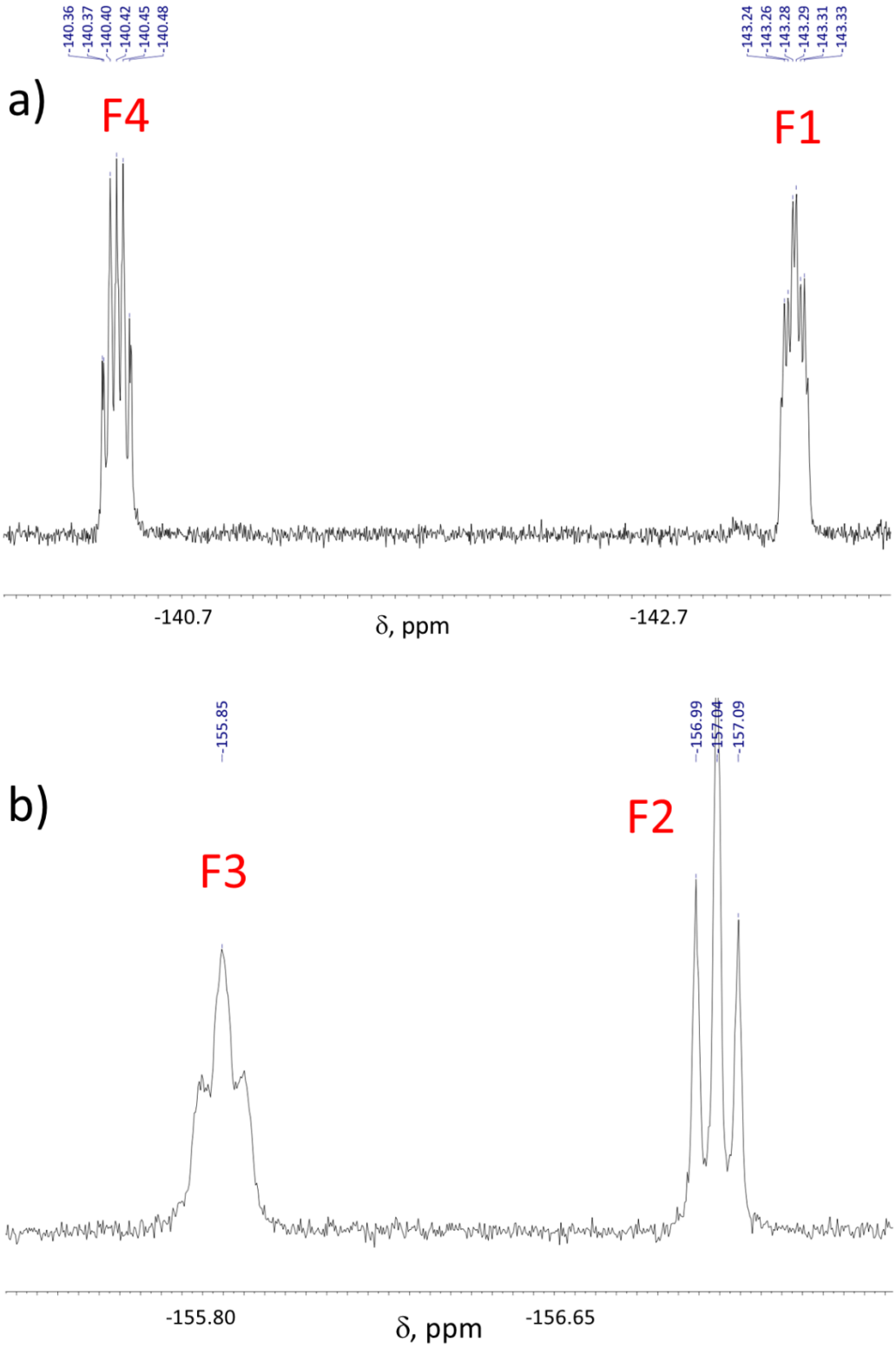

Figure S4. ^{19}F-NMR spectrum of **1**$(PF_6)_3$ in CD_3CN: details of fluorine signals

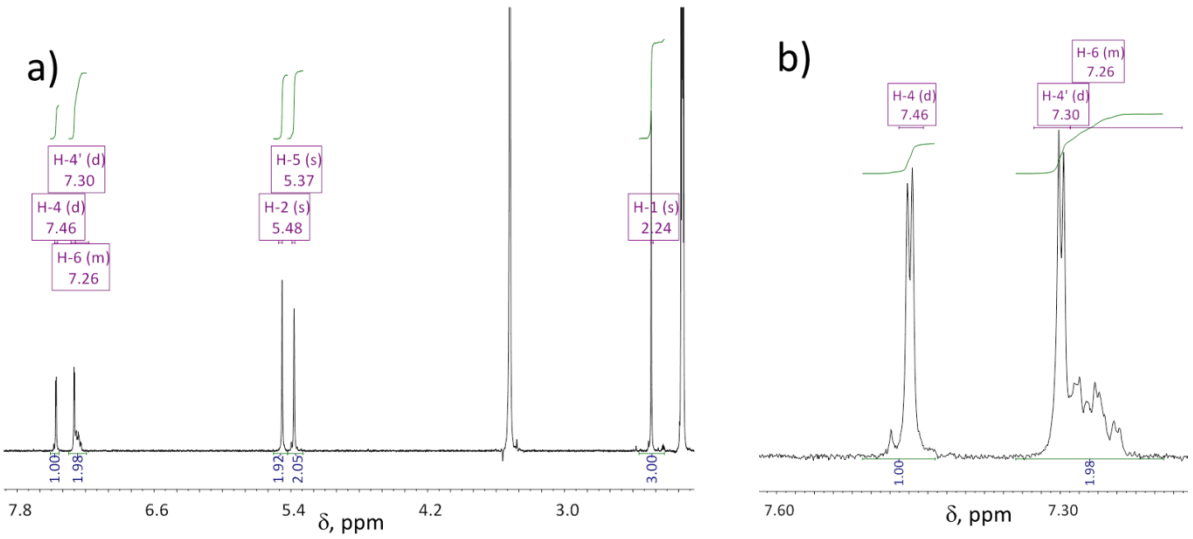

Figure S5. ^{1}H-NMR spectrum of **1**$(PF_6)_3$ in CD_3CN/D_2O 4:1: a) full spectrum, b) zoom of the aromatic region.

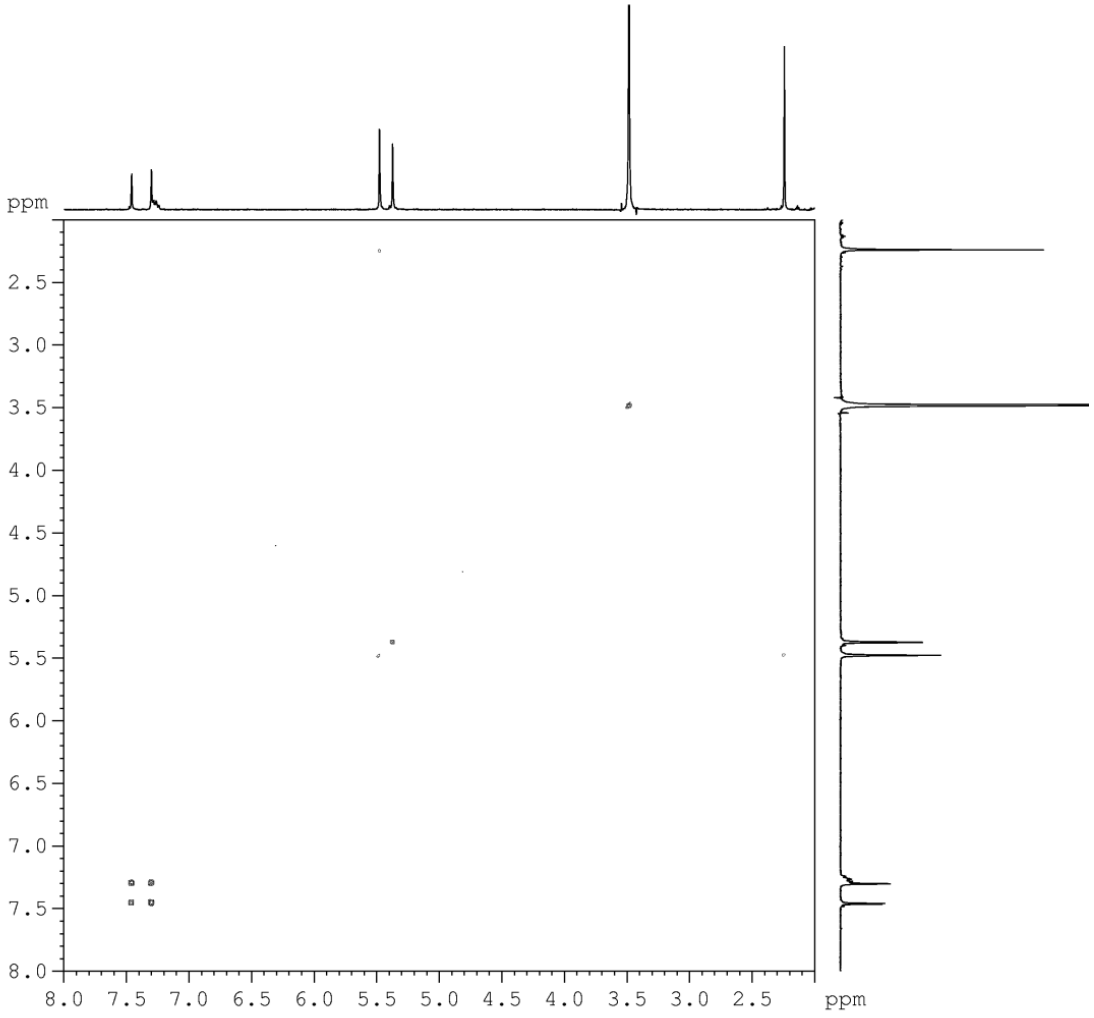

Figure S6. COSY spectrum of **1**$(PF_6)_3$ in CD_3CN/D_2O 4:1(v/v)

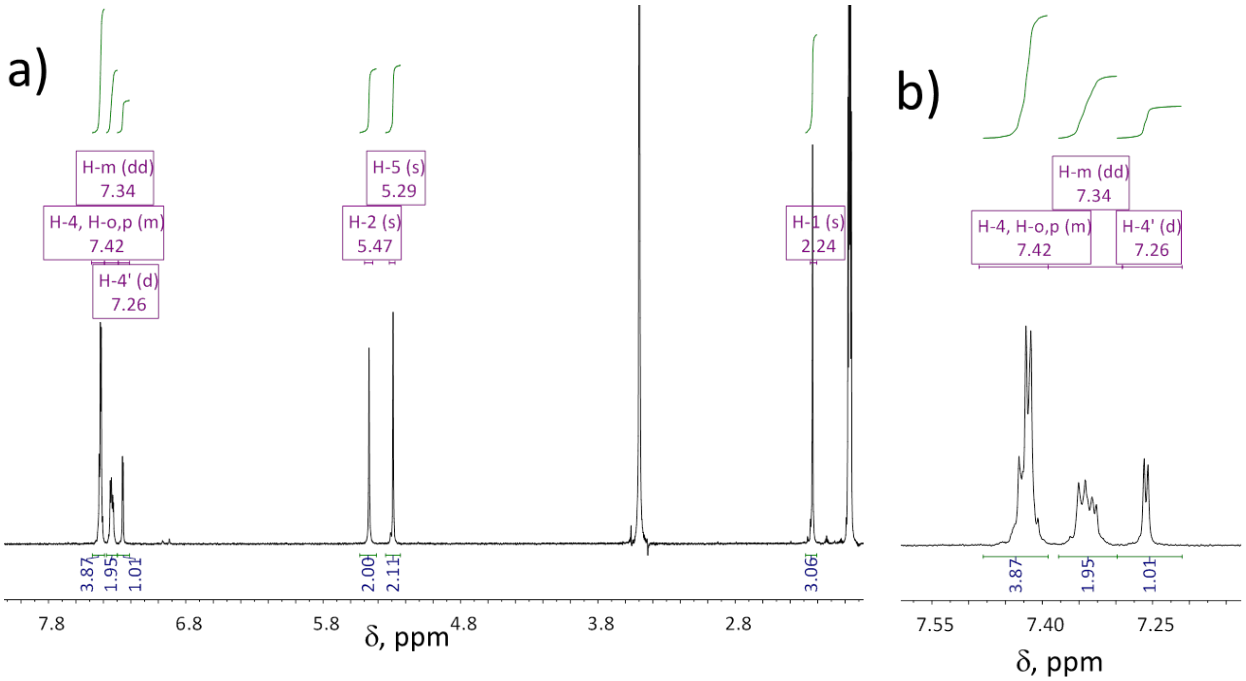

Figure S7 ^{1}H-NMR spectrum of **2**$(PF_6)_3$ in CD_3CN/D_2O 4:1: a) full spectrum, b) zoom of the aromatic region.

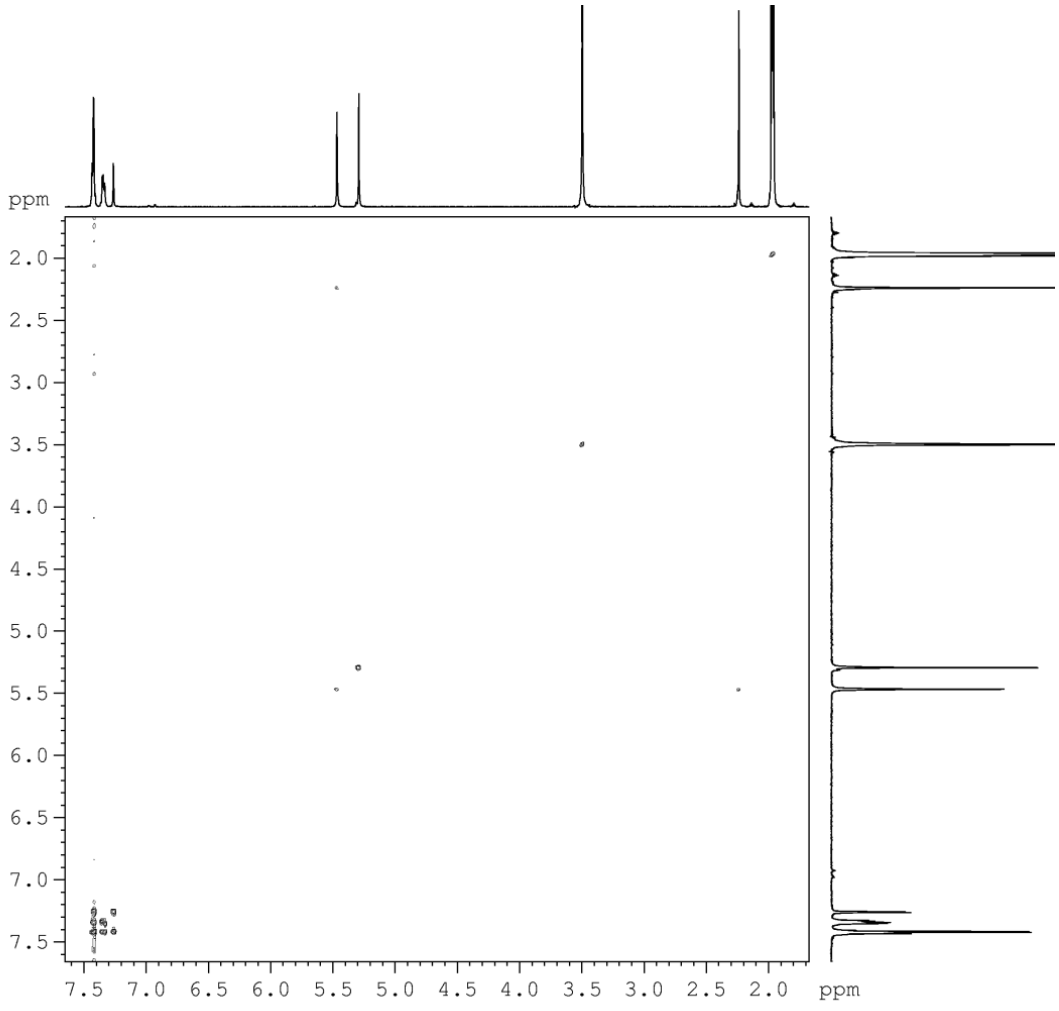

Figure S8. COSY spectrum of **2**$(PF_6)_3$ in CD_3CN/D_2O 4:1 (v/v)

2S. X-Ray diffraction studies

	[**1**(Cl)](PF$_6$)$_2$·MeCN	[**1**(Br)](PF$_6$)$_2$·MeCN
Formula	$C_{44}H_{36}ClF_{24}N_7P_2$	$C_{44}H_{36}BrF_{24}N_7P_2$
M [g/mol]	1216.19	1260.64
Dimension [mm]	0.50x0.43x0.14	0.58x0.50x0.38
colour	colourless	colourless
Crystal system	triclinic	triclinic
Space group	*P* -1 (no. 2)	*P* -1 (no. 2)
a [Å]	12.175(4)	12.226(4)
b [Å]	12.483(5)	12.514(2)
c [Å]	18.276(5)	18.219(3)
α [°]	75.34(3)	75.48(1)
β [°]	78.55(2)	78.59(1)
γ [°]	71.31(2)	71.71(2)
V [Å^3]	2524.5(15)	2540.5(11)
Z	2	2
ρ_{calcd} [g/cm^3]	1.600	1.648
μ Mo K_α [mm-^{1}]	0.269	1.002
diffractometer type	Enraf-Nonius CAD4	Enraf-Nonius CAD4
detector type	scintillation counter	scintillation counter
θ range [°]	2-25	2-25
Measured refl.	8913	8948
Unique refl.	8913	8948
R_{int}*	-	-
min/max transmission	0.88/0.96	0.65/0.70
Strong data ($I_0>2\sigma(I_0)$)	4693	7877
Refined parameters	707	707
R1, *wR2* (strong data)	0.1227, 0.2647	0.0777, 0.0850
R1, *wR2* (all data)	0.1804, 0.3054	0.2031, 0.2115
GOF	1.062	1.062
Max/min resid. [eÅ^{-3}]	0.78/-0.44	1.12/-0.57

*centrosymmetrically related reflections were not collected

Table S1: Details on the crystal structures of [**1**(Cl)](PF$_6$)$_2$·MeCN and [**1**(Br)](PF$_6$)$_2$·MeCN.

Donor group	C···A⁻ (Å)	H···A⁻ (Å)	C–H···A⁻ (°)	A acceptor atom
C(15)-H(15)	3.494(8)	2.659(8)	149.7(8)	Cl(1)
C(25)-H(25)	3.273(9)	2.555(9)	134.3(9)	Cl(1)
C(35)-H(35)	3.420(8)	2.568(8)	152.5(9)	Cl(1)
C(16)-H(16)b	3.675(9)	2.817(9)	147.9(9)	Cl(1)
C(22)-H(22)	3.854(10)	3.017(10)	150.5(11)	Cl(1)
C(26)-H(26)b	3.707(11)	2.882(11)	143.5(12)	Cl(1)
C(36)-H(36)a	3.829(9)	3.023(9)	141.4(10)	Cl(1)
C(42)-H(42)	3.935(10)	3.092(10)	151.6(11)	Cl(1)
C(15)-H(15)	3.578(5)	2.733(5)	151.4(3)	Br(1)
C(25)-H(25)	3.367(7)	2.751(7)	124.5(4)	Br(1)
C(35)-H(35)	3.540(5)	2.683(5)	153.6(3)	Br(1)
C(16)-H(16)b	3.807(6)	2.966(6)	145.7(4)	Br(1)
C(22)-H(22)	3.902(6)	3.058(6)	151.7(4)	Br(1)
C(26)-H(26)b	3.763(7)	2.940(7)	143.4(5)	Br(1)
C(36)-H(36)a	3.926(6)	3.105(6)	143.2(4)	Br(1)
C(42)-H(42)	4.005(7)	3.149(7)	154.0(5)	Br(1)

Table S2: Geometrical features for the C-H···Cl⁻ and C-H···Br⁻ hydrogen-bonds.

References

[1] López, P.; Méndez, F.; *Org. Lett.*, **2004**, 6, 1781-1783.

[2] Alcalde, E.; Alvarez-Rúa, C.; García-Granda, S.; Gracía-Rodriguez, E.; Mesquida, N.; Pérez-García, L.; *Chem. Commun.*, **1999**, 295-296.

[3] Sato, K.; Arai, S.; Yamagishi, T.; *Tetrahedron Lett.*, **1999**, 40, 5219-5222.

[4] Sato, K.; Onitake, T.; Arai, S.; Yamagishi, T.; *Heterocycles*, **2003**, 60, 779-784.

[5] (a) Streitwieser Jr., A.; Scannon, P. J. and Niemeyer, H.M.; *J. Am. Chem. Soc*., **1972**, 94, 7936; (b) Schlosser, M.; *Angew. Chem., Int. Ed.*, **1998**, 37, 1496.

[6] (a) Blair, L. K.; Baldwin, J. and Smith, W. C.; *J. Org. Chem*., **1977**, 42, 1817–1818; (b) Ionization Constants of Organic Acids in Solution, IUPAC Chemical Data Series No. 23, ed. Serjeant, E. P. and Dempsey, B.; Pergamon Press, Oxford, UK, **1979**; (c) Bordwell, F. G.; Drucker, G. E. and Fried, H. E.; *J. Org. Chem*., **1981**, 46, 632-635.

[7] Pedzisa, L. and Hay, B. P.; *J. Org. Chem*., **2009**, 74, 2554-2560.

[8] Bergamaschi, G.; Boiocchi, M.; Monzani, E. and Amendola, V.; *Org. Biomol. Chem*., **2011**, 9, 8276-8283.

[9] Gans, P.; Sabatini, A. and Vacca, A.; *Talanta*, **1996**, 43, 1739-1753.

[10] Farrugia, L.J.; *J. Appl. Crystallogr*., **1999**, 32, 837-838.

[11] North, A.C.T.; Phillips, D.C. and Mathews, F.S.; *Acta. Crystallogr*., **1968**, A24, 351-359.

[12] Altomare, A.; Burla, M. C.; Camalli, M.; Cascarano, G. L.; Giacovazzo, C.; Guagliardi, A.; Moliterni, A. G.; Polidori, G. and Spagna, R. J.; *J. Appl. Crystallogr*., **1999**, 32, 115-119.

[13] Sheldrick, G. M.; *Acta Crystallogr*., **2008**, A64, 112-122.

[14] Sharma, P. S.; Payagala, T.; Wanigasekara, E.; Wijeratne, A. B.; Huang, J.; Armstrong, D. W.; *Chem. Mater*., **2008**, 20 (13), 4182-4184.

[15] (a) Amendola, V.; Fabbrizzi, L. and Monzani, E.; *Chem. Eur. J*., **2004**, 10, 76-82; (b) Amendola, V.; Boiocchi, M.; Fabbrizzi, L. and Palchetti, A.; *Chem. Eur. J*., **2005**, 11, 5648-5660.

[16] (a) Sate, K.; Aral, S. and Yamagishi, T.; *Tetrahedron Lett*., **1999**, 40, 5219-5222; (b) Ihm, H.; Yun, S.; Kim, H. G.; Kim, J. K. and Kim, K. S.; *Org. Lett.*, **2002**, 4, 2897; (c) Kwon, J. Y.; Singh, N. J.; Kim, H. N.; Kim, S. K.; Kim, K. S. and Yoon, J.; *J. Am. Chem. Soc.*, **2004**, 126, 8892; (d) Yoon, J.; Kim, S. K.; Singh, N. J. and Kim, K. S.; *Chem. Soc. Rev*., **2006**, 35, 355-360; (e) Amendola, V.; Boiocchi, M.; Fabbrizzi, L. and Fusco, N.; *Eur. J. Org. Chem*., **2011**, 6434-6444; (f) Amendola, V.; Boiocchi, M.; Colasson, B.; Fabbrizzi, L.; Rodriguez Douton, M. J. and Ugozzoli, F.; *Angew. Chem., Int. Ed*., **2006**, 45, 6920-6924; (g) Chun, Y.; Singh, N. J.; Hwang, I. C.; Woo

Lee, J.; Yu, S. U. and Kim, K. S.; *Nat. Commun*., **2013**, 4, 1797; (h) Toure, M.; Charles, L.; Chendo, C.; Viel, S.; Chuzel, O. and Parrain, J. L.; *Chem. Eur. J*., **2016**, 22, 8937-8942.

[17] Desiraju, G. R. and Steiner, T.; *The Weak Hydrogen Bond in Structural Chemistry and Biology*, Oxford University Press, New York, NY, **1999**.

[18] Amyes, T. L.; Diver, S. T.; Richard, J. P.; Rivas, F. M. and Toth, K.; *J. Am. Chem. Soc*., **2004**, 126, 4366-4374.

[19] (a) *Anion Receptor Chemistry*, ed. Sessler, J. L.; Gale, P. A. and Cho, W. S.; *RSC Publishing*, **2006**; (b) *Anion Coordination Chemistry*, ed. Bowman-James, K.; Bianchi, A. and Garcı´a-Espana, E.; JohnWiley & Sons, New York, **2012**; (c) Busschaert, N.; Caltagirone, C.; Van Rossom, W. and Gale, P.; *Chem. Rev*., **2015**, 115(15), 8038-8155; (d) Gale, P. and Caltagirone, C.; *Chem. Soc. Rev*., **2015**, 44(13), 4212-4227; (e) Giese, M.; Albrecht, M. and Rissanen, K.; *Chem. Rev*., **2015**, 115(16), 8867-8895; (f) Blazek Bregovic, V.; Basaric, N. and Mlinaric-Majerski, K.; *Coord. Chem. Rev*., **2015**, 295, 80-124; (g) Saha, I.; Lee, J. T. and Lee, C. H.; *Eur. J. Org. Chem*., **2015**, 3859-3885; (h) Elmes, R. B. P. and Jolliffe, K. A.; *Chem. Commun*., **2015**, 51(24), 4951-4968; (i) Chang, K. C.; Sun, S. S.; Odago, M. O. and Lees, A. J.; *Coord. Chem. Rev*., **2015**, 284, 111-123, and references therein.

[20] Hay, B. P. and Bryantsev, V. S.; *Chem. Commun*., **2008**, 2417-2428.

[21] Cai, J. and Sessler, J. L.; *Chem. Soc. Rev*., **2014**, 43, 6198-6213, and references therein.

[22] Frisch, M. J. et al., Gaussian 09, revision D.02, Gaussian, Inc., Wallingford, CT, **2009**.

[23] (a) Foster, J. P.; Weinhold, F.; *J. Am. Chem. Soc.*, **1980**, 102, 7211-7218; (b) Reed, A. E.; Weinstock, R. B.; Weinhold, F.; *J. Chem. Phys.*, **1985**, 83, 735-746.

* The H-6 signal is a multiplet due to coupling with the fluorine nuclei in the ortho and meta positions.

4. Synthesis and study in solution of a dansyl-modified azacryptand

4.1. Introduction

The detection of transition metal ions is a very important field in supramolecular chemistry due to significant role of cations in medicine, biology and chemistry.[1-6] For this reason, many cation sensors have been synthesized and studied; fluorescent chemosensors, in particular, are very fascinating due to the low detection limits of the fluorescence technique.[7-11] Polyamine macrobicycles, such as bistren azacryptands, are known for their binding capabilities towards transition metal ions. Moreover, by introduction of fluorescent signaling units (e.g. anthracene or naphthalene) in their molecular framework, these systems can be converted into efficient chemosensors.[12-22] Bistren cages can encapsulate two transition metal ions (e.g. Cu^{2+} or Zn^{2+}), one of each bound to the four amine nitrogen atoms of a tris(2-aminoethyl)amine (*tren*) subunit. The unsaturated apical position can be occupied by a solvent molecule or an ambidentate anion; in this way the encapsulated metal ion achieves five-coordination, according to an axially compressed trigonal bipyramidal geometry.

In general, azacryptands containing fluorescent units are scarcely emitting at neutral pH; the emission is actually quenched through a photoinduced electron transfer (PET) process, from the secondary amino groups to the fluorophore.[23] Among the best known fluorescent fragments, the dansyl fluorophore (5-dimethylamino-1-naphthalene sulfonate) is characterized by an intense fluorescence emission in the visible spectrum, due to a charge-transfer excited state.[24] Biological compatibility and high emission quantum yield make dansylated chemosensors promising for application under physiological conditions.[25-27] In this chapter, the synthesis and study of a new asymmetric azacryptand (**1**, see Figure 1), characterized by three p-xylyl spacers, one of which is functionalized with a dansyl fragment, is reported.

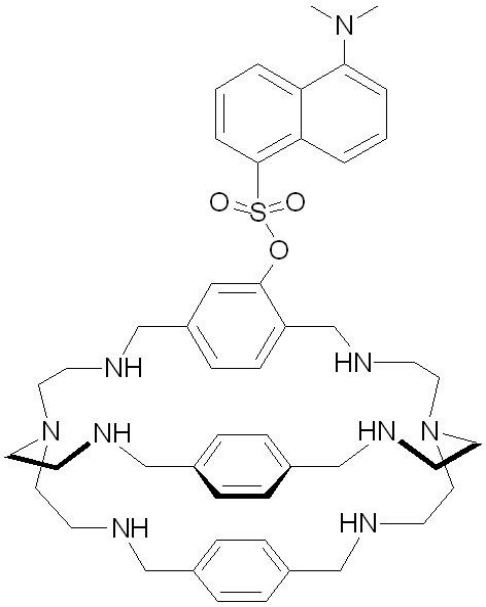

Figure 1. Monodansyl cage **1**.

4.2. Experimental

4.2.1. Chemicals and Methods

All reagents for syntheses were purchased form Aldrich/Fluka or Alfa-Aesar Chemical Co. and used without further purification. All reactions were performed under nitrogen. The solutions used in titrations were prepared from freshly opened solvent bottles. Mass spectra were acquired on a Thermo-Finnigan ion-trap LCQ Advantage Max instrument equipped with an ESI source, and NMR spectra were recorded on a Bruker ADVANCE 400 spectrometer (operating at 9.37 T, 400 MHz). UV−vis spectra were run on a Varian Cary 100 SCAN spectrophotometer with quartz cuvettes of the appropriate path length (0.1−1 cm) at 25.0 ± 0.1 °C under inert conditions. Emission spectra were recorded on a Perkin- Elmer LS 50B instrument.

4.2.2. Potentiometric titrations

All titrations were performed at 25.0 ± 0.1 °C. Protonation constants of ligand **1** were determined in a MeOH/water (3:2) mixture, 0.07 M in $NaNO_3$. In a typical experiment, 10 mL of a 7×10^{-4} M ligand solution were treated with an excess of a 1.0 M HNO_3 standard solution. Titrations were performed by addition of 10 μL aliquots of carbonate-free standard 0.1 M NaOH, recording 80-100 points for each titration. Complexation constants were determined by carrying out a similar potentiometric titration experiment, with the additional presence of 2 eqv. of $Cu^{II}(CF_3SO_3)_2$. Prior to each potentiometric titration, the standard electrochemical potential (E°) of the glass electrode was determined in the MeOH/water mixture, by a titration experiment according to the Gran method.[31] Protonation and complexation titration data (emf vs. mL of NaOH) were processed with the Hyperquad package[32] to determine the equilibrium constants (reported in Table 1). In the pH-spectrophotometric / spectrofluorimetric titration experiments the UV-Vis /emission spectra of the solution were recorded after each addition of standard 0.1 M NaOH.

4.2.3. Spectrophotometric and spectrofluorimetric titrations

UV-Vis spectra of the azacryptand in the presence of metal ions were run on a Varian Cary 100 SCAN spectrophotometer with quartz cuvettes of the appropriate path length (0.1-1 cm) at 25.0 ± 0.1 °C under inert conditions. In any case, the concentration of the ligand and the optical path were adjusted to obtain spectra with AU ~ 1.

Titrations with metal ions were performed at 25.0 ± 0.1 °C in pure water and in MeOH/water (3:2) mixture, buffered at pH 8 (0.07 M HEPES). In a typical experiment, the solution of the receptor was titrated with a 100-fold more concentrated solution of the trifluoromethanesulfonate salt of the envisaged transition metals. In spectrofluorimetric titrations, the sample was excited at a wavelength corresponding to an isosbestic point in the family of UV-vis spectra. Titration data were processed with a non-linear least-squares procedure (Hyperquad® package),[32] in order to determine the equilibrium constants.

4.2.4. Synthesis

4.2.4.1. Synthesis of 2-dansyl-1,4-benzenedicarboxaldehyde

The 2-hydroxy-1,4-benzenedicarboxaldehyde was obtained following the procedures reported in the literature.[28] While, the 2-dansyl-1,4-benzenedicarboxaldehyde was prepared by modifying a described procedure.[29]

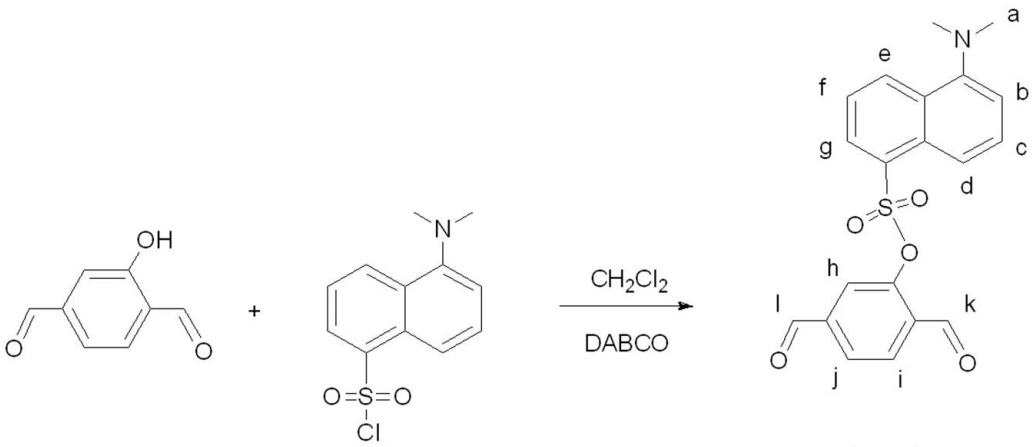

2-hydroxy-1,4-benzenedicarboxaldehyde (0.1 g, 0.68 mmol) and dansyl chloride (0.2 g, 0.68 mmol) were suspended in 2 mL of CH_2Cl_2. 0.1g of 1,4-diazabicyclo octane (0.93 mmol) in 1 mL of CH_2Cl_2 was added and the reaction mixture was stirred at room temperature for 48 hrs under an inert atmosphere. The crude product was purified by column chromatography (SiO_2, hexane, hexane-AcOEt mixture 5%-25% gradient). A yellow solid was obtained. (Yield 52%)

^{1}H -NMR (400 MHz, $CDCl_3$, ppm): δ 3.1 (6H, s, H-a), 7.3 (1H, d, H-b), 7.4 (1H, d, H-h), 7.5 (1H, t, H-f), 7.7 (1H, t, H-c), 7.8 (1H, dd, H-j), 8.0 (1H, d, H-i), 8.1 (1H, dd, H-g), 8.5 (1H, d, H-d), 8.7 (1H, d, H-e), 9.9 (1H, s, H-k), 10.2 (1H, s, H-l).

4.2.4.2. Synthesis of azacryptand 1

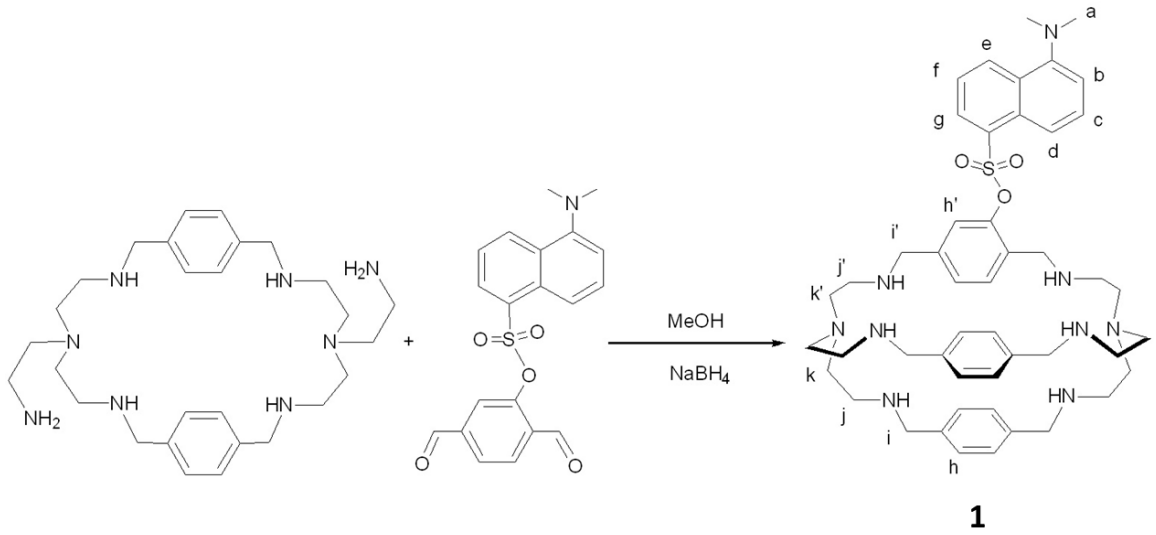

1

A solution of 2-dansyl-1,4-benzenedicarboxaldehyde (0.10 g, 0.26 mmol) in 70 ml of MeOH was added dropwise to a stirred solution of the p-xylyl intermediate macrocycle (0.13 g, 0.26 mmol, prepared following a published procedure[30]) in 120 mL of MeOH over 3 h at room temperature. After 24 h stirring the mixture was heated to 50 °C and the imine bonds were reduced with $NaBH_4$ (0.2 g, 5.2 mmol). When the addition was complete, the stirring was continued at 50 °C overnight. The solvent was eliminated, the residue was dissolved in basic water (20 mL, 3 M NaOH) and extracted with 15 ml of CH_2Cl_2 (x 7). The collected organic phases were dried over Na_2SO_4 and evaporated to dryness. An orange solid was obtained (Yield 54%).

MS-ESI (MeOH): m/z 425.2 $[M + 2H]^{2+}$, 848.6 $[M + H]^{+}$.

^{1}H-NMR (400 MHz, CD_3OD, ppm): δ 2.8 (24H, m, H-k, H-k', H-j, H-j'), 2.9 (6H, s, H-a), 3.5 (4H, d, H-i), 3.7 (8H, d, H-i'), 6.8 (11H, m, H-h, H-h'), 7.2 (1H, d, H-b), 7.4 (1H, t, H-f), 7.6 (1H, t, H-c), 8.1 (1H, d, H-g), 8.4 (1H, d, H-d), 8.6 (1H, d, H-e).

4.2.4.3. Synthesis of 2

In order to clarify the coordination properties of the new fluorescent azacryptand, the model compound **2** was synthesized by modifying a described procedure.[29]

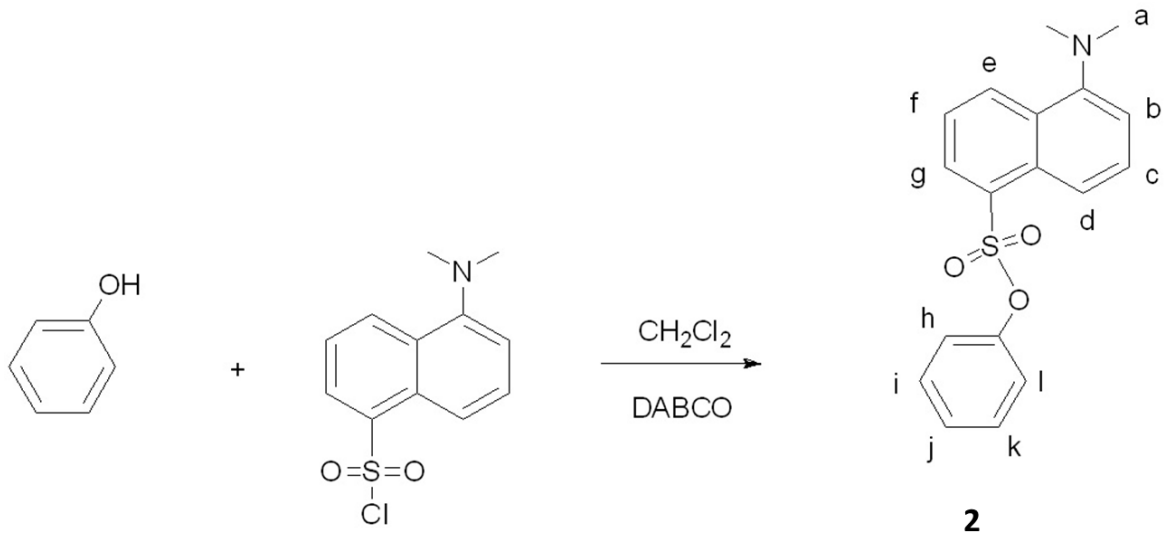

2

Phenol (0.1 g, 1.0 mmol) and dansyl chloride (0.3 g, 1.0 mmol) were dissolved in 2 mL CH_2Cl_2. 0.2g of 1,4-diazabicyclooctane (1.8 mmol) in 1 mL of CH_2Cl_2 was added and the reaction mixture was stirred at room temperature for 24 hrs under an inert atmosphere. The crude product was purified by column chromatography (SiO_2, hexane:AcOEt mixture 1:1). A yellow solid was obtained. (Yield 45%)

^{1}H-NMR (400 MHz, $CDCl_3$, ppm): δ 2.9 (6H, s, H-a), 6.8 (3H, m, H-h, H-i, H-l), 7.1 (2H, m, H-j, H-k), 7.2 (1H, s, H-b), 7.4 (1H, t, H-f), 7.7 (1H, t, H-c), 8.1 (1H, dd, H-g), 8.5 (1H, d, H-d), 8.6 (1H, d, H-e).

4.3. Results and discussion

Bistren symmetric cryptands are usually synthesized through Schiff base condensation of two molecules of tris(2-aminoethyl)amine (*tren*) and three molecules of the desired dialdehyde[33] followed by reduction with $NaBH_4$ of the imine groups. The new asymmetric azacryptand required a multi-step synthesis.[23,28,29] In particular 1 mol of mono-BOC-protected tren was first reacted with 1 mol of the 1,4-p-xylyl dialdehyde, obtaining the intermediate polyimine macrocycle. After reduction with $NaBH_4$ and deprotection of the secondary amine groups, the precursor was reacted with 2-dansyl-1,4-benzenedicarboxaldehyde, in a 1:1 ratio. Reduction of the imine groups yielded azacryptand **1** without further purification. Thanks to this approach, we obtained a new fluorescent receptor with a fluorescent dansyl group covalently linked to one of the three p-xylyl spacers.

The novel fluorescent azacryptand **1** was studied by potentiometric, UV-Vis and emission titrations in MeOH:water 3:2 mixture (0.07M $NaNO_3$), in order to determine the protonation constants and investigate the metal ion complexation equilibria. The obtained results pointed out that the receptor was fluorescent at neutral pH, showing the typical emission band of the dansyl group. Metal addition induced a partial quenching of the dansyl emission; this behavior was more pronounced with Cu(II), which reduced the receptor's emission by 60 %. Also the model compound **2**, due to its florescent properties, was studied by spectrofluorimetric titration. In fact compound **2** show the typical band of the dansyl fluorophore, but the addition of Cu(II) to a solution of **2** had no effect on the emission.

In the case of receptor **1**, quenching was driven by a static mechanism, attributable to the formation of the inclusion dicopper complex $[Cu_2\mathbf{1}]^{4+}$. In order to test the stability of copper complexes under physiological conditions, spectrofluorimetric titrations with Cu(II) were performed in water at pH=8 (HEPES 0.07M) and the values of binding constants, K_{11} and K_{12} ,were determined.

4.3.1. Potentiometric/pH-spectrophotometric studies in aqueous/methanol mixture

In order to study the acid-base behavior of the new receptor, potentiometric titrations were performed on the asymmetric azacryptand (**1**) in H_2O:MeOH 3:2 mixture (0.07 M $NaNO_3$, at 25°C). Experimental results were fitted with HyperQuad package[32] and the obtained protonation constants are reported in Table 1.

	Log β values		**Log β values**
$[H\mathbf{1}]^{+}$	8.63 (1)	$[CuH_3\mathbf{1}]^{5+}$	30.13 (1)
$[H_2\mathbf{1}]^{2+}$	16.75 (1)	$[CuH_2\mathbf{1}]^{4+}$	25.56 (2)
$[H_3\mathbf{1}]^{3+}$	23.89 (1)	$[Cu_2\mathbf{1}]^{4+}$	17.87 (2)
$[H_4\mathbf{1}]^{4+}$	29.95 (2)	$[Cu_2\mathbf{1}(OH)]^{3+}$	10.63 (2)
$[H_5\mathbf{1}]^{5+}$	35.76 (2)		
$[H_6\mathbf{1}]^{6+}$	38.79 (2)		
$[H_7\mathbf{1}]^{7+}$	40.49 (2)		

Table 1. Logarithmic protonation and complex formation constants for **1** (standard deviations in parentheses).

Seven protonation equilibria were determined for **1**, attributable to the protonation of the six secondary amines of the cage and the tertiary amine of the dansyl group. Notably, the protonation constant obtained for the NMe_2 group, i.e. logK = 1.7, is comparable to that reported by Prodi and coworkers for a similar dansylated system.[34] Protonation of the tertiary amino groups on the receptor was not observed in these conditions.

pH-spectrophotometric titrations further confirmed these results; Figure 2 shows the family of spectra taken over the course of the pH-spectrophotometric titration of **1** (0.5mM) in MeOH:H_2O mixture (0.07 M $NaNO_3$).

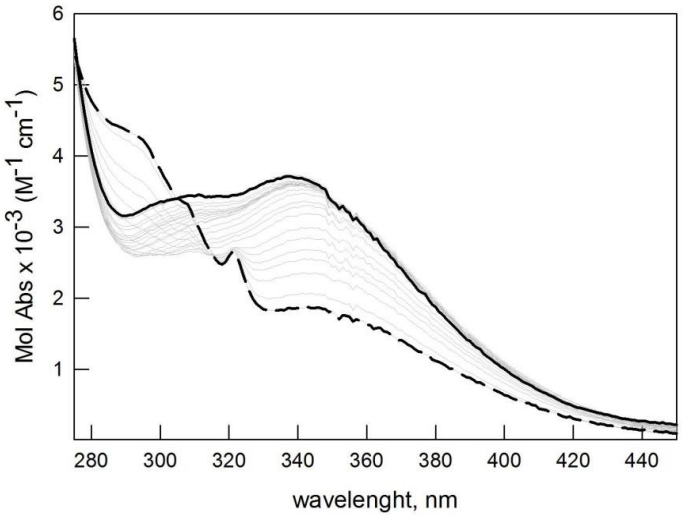

Figure 2. Family of UV-vis. spectra taken over the pH-spectrophotometric titration of **1** (0.5mM, T=25°C, 0.07M $NaNO_3$). Long dash line: initial spectrum at pH=2.5; solid line: spectrum at pH=11.

In the acidic pH interval, the receptor showed the typical UV-Vis spectrum of the naphthyl group[35] characterized by an intense band at λ_{max}=288 nm (black dashed line spectrum). As a consequence of the dansyl group deprotonation, the absorption at 288 nm decreases and a new band appears at 340 nm. This new band is due to the typical charge transfer of the dansyl group (NMe_2→ naphthyl).[24] The titration profiles obtained at 288 and 340 nm very well fit the distribution diagram of the species shown in Figure 3.

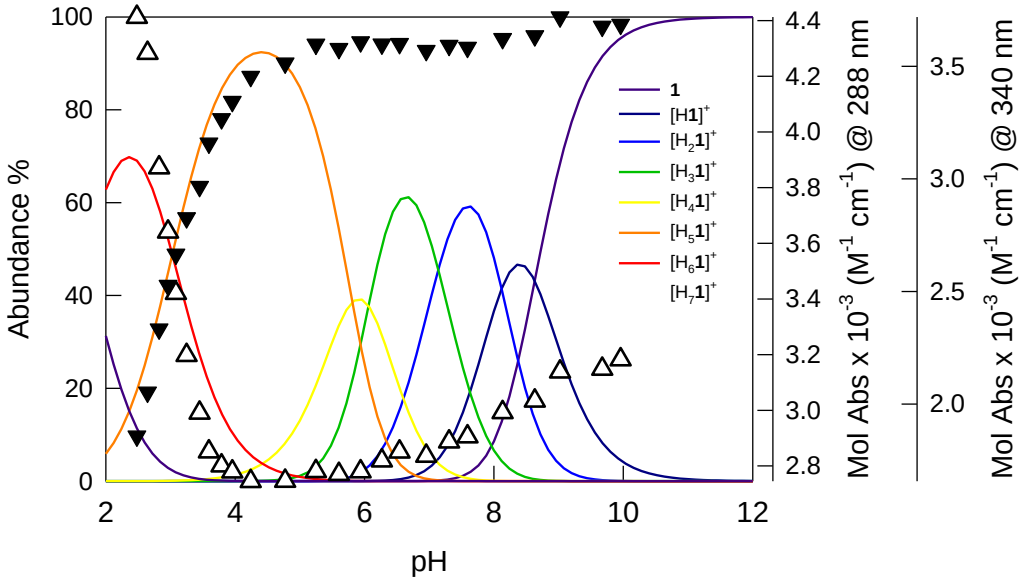

Figure 3. Distribution diagram of the species (% abundance vs. pH) obtained upon potentiometric titration of **1** in H_2O:MeOH 3:2 mixture(0.5 mM, 0.07 M $NaNO_3$, at 25 °C). The corresponding protonation constants are shown in Table 1. Triangles : profiles of Mol Abs ($\times 10^{-3}$, M^{-1} cm^{-1}) at 288 nm (black) and 340 nm (white) respectively, obtained upon pH-spectrophotometric titration.

4.3.2. Potentiometric titrations in the presence of Cu(II) and pH-spectrophotometric studies of receptor 1

To investigate the complexation equilibria with Cu(II), potentiometric titrations were performed on **1** in the presence of 2 equivalents of $Cu^{II}(CF_3SO_3)_2$. The titrations were carried out on samples containing **1** ($5x10^{-4}$ M) and two equivalents of $Cu(CF_3SO_3)_2$ in a H_2O/MeOH (3:2), mixture (0.07M $NaNO_3$) . The solutions were treated with an excess of HNO_3 1 M and titrated with standard NaOH (0.1M). The best fit of experimental data was obtained by assuming the formation of different Cu(II)-containing species on increasing pH: $[CuH_3\mathbf{1}]^{5+}$, $[CuH_2\mathbf{1}]^{4+}$, $[Cu_2\mathbf{1}]^{4+}$, $[Cu_2\mathbf{1}(OH)]^{3+}$.

The corresponding formation constants are reported in Table 1, and the distribution diagram is shown in Figure 4.

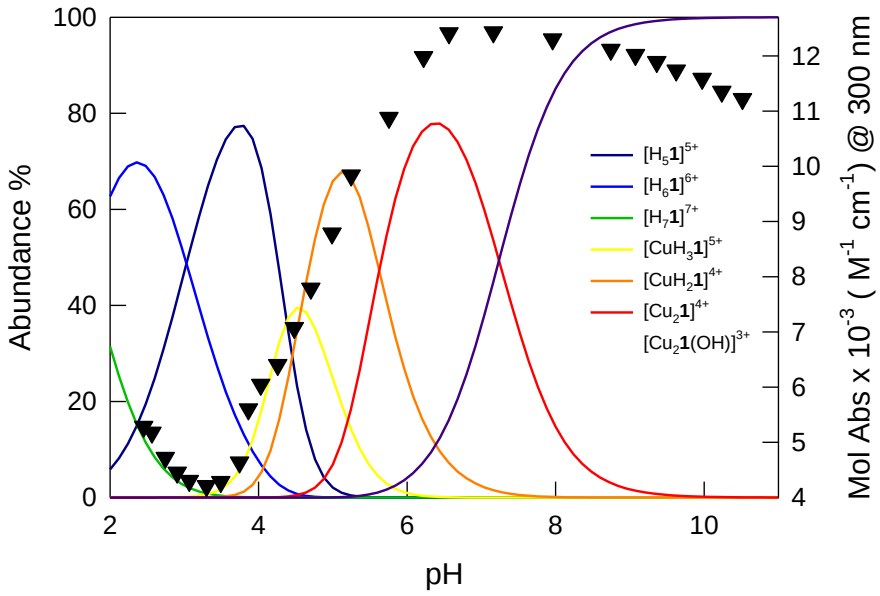

Figure 4. Distribution diagram of the species (% abundance vs. pH) obtained upon potentiometric titration of **1** (0.5 mM), in the presence of 2 equiv. $Cu(CF_3SO_3)_2$ (0.07 M $NaNO_3$, H_2O:MeOH 3:2 at 25 °C). The corresponding constants are shown in Table 1. Black triangles: profile of Mol Abs ($\times10^{-3}$, M^{-1} cm^{-1}) at 300 nm vs. pH, obtained upon pH-spectrophotometric titration of **1** (0.5 mM), in the presence of 2 equiv. $Cu(CF_3SO_3)_2$.

As evidenced by the distribution diagram (Figure 4), between pH 2 and 4, the azacryptand is in the polyprotonated forms (i.e. $H_7\mathbf{1}^{7+}$, $H_6\mathbf{1}^{6+}$ and $H_5\mathbf{1}^{5+}$), in which both the secondary amino groups of the cage and the dansyl tertiary amino group are protonated.

On increasing pH, the formation of copper containing species occurs: $[CuH_3\mathbf{1}]^{5+}$ (39% at pH=4.5) and $[CuH_2\mathbf{1}]^{4+}$ (68% at pH=5.1, see Figure 4). The dicopper complex, $[Cu_2\mathbf{1}]^{4+}$, is the major species in solution at pH 6.4 (78%). In $[Cu_2\mathbf{1}]^{4+}$, each Cu(II) ion occupies one of the *tren* units, adopting the typical trigonal-bipyramidal geometry. The apical positions on the metal ions are occupied by water molecules. Under further addition of NaOH, the deprotonation of the coordinated water molecules occurs, leading to the stable hydroxide complex $[Cu_2\mathbf{1}(OH)]^{3+}$. Due to its high stability, this species predominates in solution (> 90 %) over the pH range of 8.5-11.

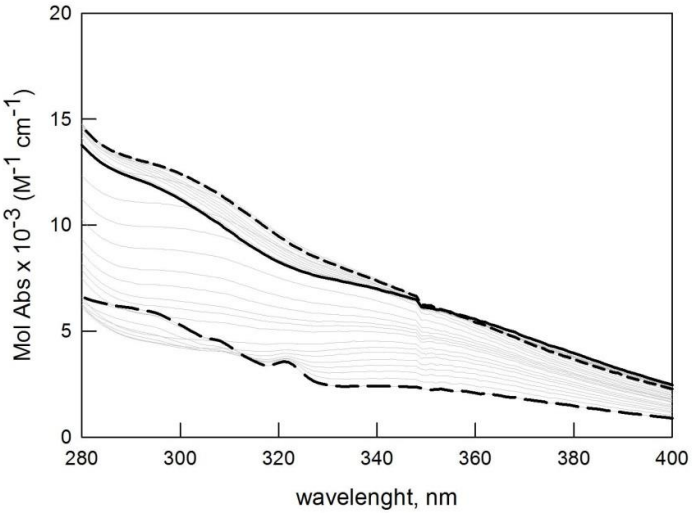

Figure 5. UV-vis. spectra taken upon pH-spectrophotometric titration of **1** (0.5 mM), in the presence of 2 eqv. of $Cu(CF_3SO_3)_2$ (in H_2O:MeOH 3:2, 0.07 M $NaNO_3$, at 25°C). Long dash line: initial spectrum at pH 2.4; short dash line: spectrum at pH 6.4, corresponding to the maximum of the $[Cu_2\mathbf{1}]^{4+}$ species; solid line: pH 11, spectrum corresponding to the hydroxide complex $[Cu_2\mathbf{1}(OH)]^{3+}$.

Figure 5 shows the family of spectra taken during the pH-spectrophotometric titration of **1** (0.5 mM) in the presence of 2 eqv. of $Cu(CF_3SO_3)_2$. The formation of copper containing species is accompanied by the development of a band around 300 nm, attributable to a ligand to metal charge transfer [i.e. N(amine) $\rightarrow$ Cu(II)]. The LMCT band develops at pH = 3.5 with the formation of the complex $[CuH_3\mathbf{1}]^{5+}$ and reaches its maximum intensity at pH = 6.8, in the presence of the dicopper species $[Cu_2\mathbf{1}]^{4+}$. When the deprotonation of the coordinated water molecules occurs, the charge transfer band undergoes a slight blue shift (see Figure 5, black solid line) due to the different coordination sphere around Cu(II). The profile obtained at 300 nm well fits the distribution diagram of the Cu(II) species shown in Figure 4.

4.3.3. pH-spectrofluorimetric studies in aqueous solution

The presence of the dansyl unit, close to the receptor's cavity, allowed us to follow the formation of copper complexes through emission studies. Due to the dependence of the azacryptand emission on pH, we first performed pH-spectrofluorimetric studies on **1** (0.05 mM) in H_2O:MeOH 3:2 mixture (0.07 M $NaNO_3$, at 25°C). The family of emission spectra, recorded after each addition of standard 0.1 M NaOH to the solution of **1**, is reported in Figure 6. The excitation wavelength was chosen at 314 nm, corresponding to an isosbestic point in the corresponding pH-spectrophotometric titration (see Figure 2).

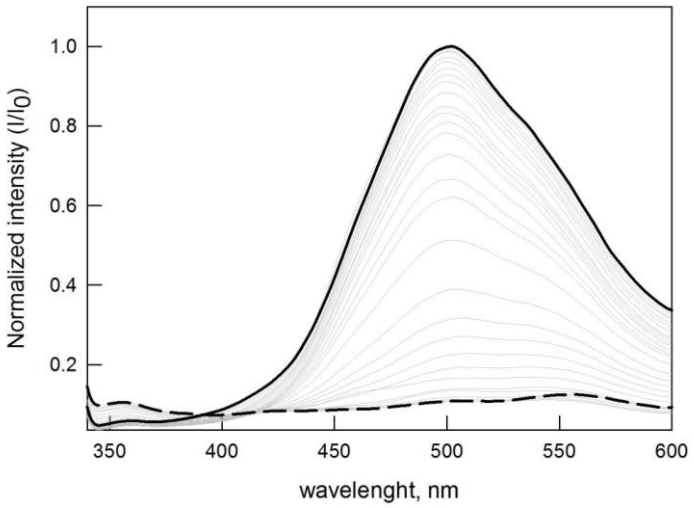

Figure 6. Family of emission spectra recorded during the pH-spectrophotometric titration of **1** (0.05mM, T=25°C, 0.07M $NaNO_3$). Long dash line: initial spectrum at pH=2.5; solid line: spectrum at pH=10.5.

Differently to what was observed for other polyamines cages, e.g. containing anthacenyl spacers[23], the emission of **1** was found to increase with increasing pH, reaching the maximum intensity over pH 7 (see Figure 7). In fact, on increasing pH, the deprotonation of the dansyl tertiary amino group occurred and a new band at 500 nm appeared, corresponding to the typical CT transition of the dansyl fluorophore.[36, 37]

Interestingly, the deprotonation of the azacryptand did not affect the emission intensity. This depends on the distance between the fluorophore and the receptor's amine groups. This separation is actually large enough to prevent the quenching process by photo-induced electron transfer.

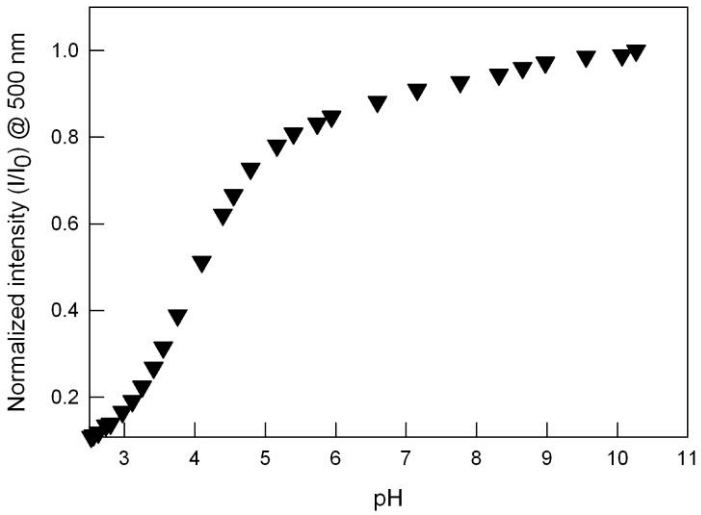

Figure 7. Normalized intensity vs. pH at 500 nm obtained upon pH-spectrofluorimetric titration of **1** (0.05 mM).

4.3.4. Studies on 1 with metal ions in MeOH

In order to evaluate the binding tendencies of cage **1** towards metal ions, spectrofluorimetric titrations were performed with Cu(II) and Zn(II) in MeOH.

The family of spectra, taken over the course of the titration on **1** (0.02 M) with $Cu(CF_3SO_3)_2$ and $Zn(CF_3SO_3)_2$, are shown in Figure 8 (a and b, respectively). The studies were performed in organic solvent, (i.e. MeOH) to compare the results with those obtained for the model system **2**, which is scarcely soluble in water ($<10^{-6}$ M). The emission spectrum of the free receptor **1** shows the intense CT band at 500 nm (λexc= 350 nm) of the dansyl moiety.

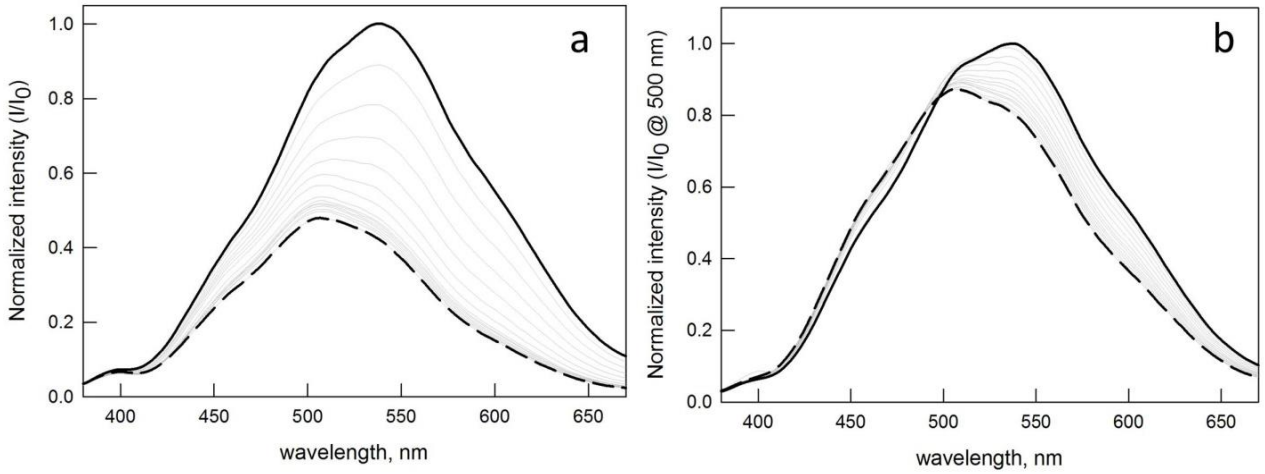

Figure 8. Spectrofluorometric titration of cage **1** (0.02mM) with $Cu^{II}(CF_3SO_3)_2$ (a) and $Zn^{II}(CF_3SO_3)_2$ (b), in MeOH (λexc= 350 nm). Solid black line: initial spectrum of the free ligand **1**; dashed black line: final spectrum.

Metal complexation generally affects the dansyl emission band. Figure 8 shows the changes in the fluorescence of receptor **1**, observed upon addition of copper. This metal ion induced the partial quenching of the dansyl unit (by about 60 % of the initial intensity); the obtained titration profile I/I_0 at 538 nm is shown in Figure 13 (black triangles). Quenching was due to the formation of a dicopper complex with the dansyl cage, in fact the titration profile reached a *plateau* after the addition of 2 eqv. Cu(II). The copper ions (Cu(II), d^9) within the cavity quench the excited state of the fluorophore through a static quenching mechanism, via either electron-transfer or energy transfer process.

Binding studies on receptor **1** were performed also with Zn(II) in the same conditions. Upon addition of zinc, the emission band of **1** underwent a blue-shift and a small decrease in intensity (Figure 11 b). The maximum variation of the emission was obtained after addition of 2 equivalents of Zn(II) due to the formation of the $[Zn^{II}_2\mathbf{1}]^{4+}$ complex (Figure 10, grey triangles)**.**

4.3.5. Studies on 2 with $Cu^{II}(CF_3SO_3)_2$ in MeOH

In order to demonstrate that receptor's quenching was due to the formation of a stable dicopper complex, emission studies were also performed on the model compound **2** (Figure 9). Compound **2** shows the typical band of the dansyl fluorophore.

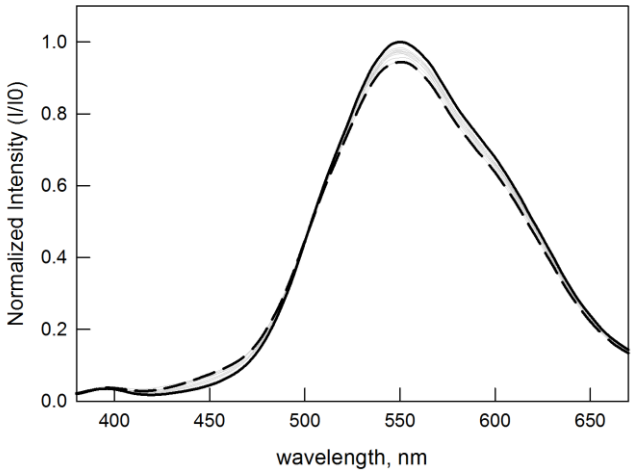

Figure 9. Spectrofluorometric titration **2** (0.02mM) with $Cu^{II}(CF_3SO_3)_2$ in MeOH (λexc= 350 nm). Solid black line: initial spectrum of the free ligand **2**; dashed black line: final spectrum.

Notably, the addition of copper to a solution of **2** did not induce any significant change in the emission (see white triangles in Figure 10). This result confirms that, in the case of cage **1**, the

fluorescence quenching was mainly driven by a static mechanism, associated to the coordination of two copper ions within the receptor's cavity.

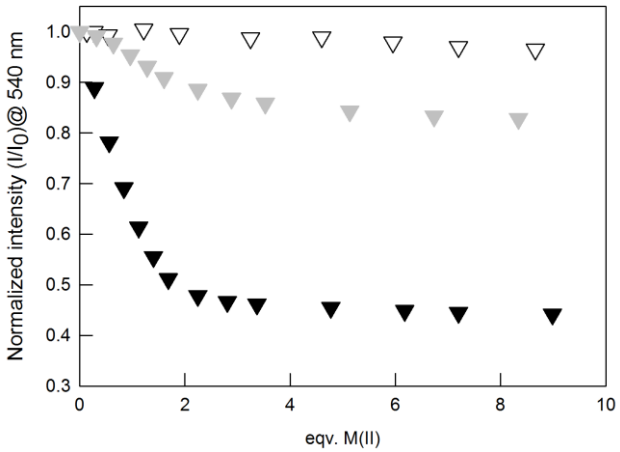

Figure 10. Profiles of the normalized emission intensity (I/I_0) at 540 nm versus number of equivalents of added metal ion. Black triangles: **1** (0.02 mM) with $Cu^{II}(CF_3SO_3)_2$, grey triangles: **1** (0.02 mM) with $Zn^{II}(CF_3SO_3)_2$, and white triangles: **2** (0.025 mM) with $Cu^{II}(CF_3SO_3)_2$.

4.3.6. Studies on 1 with metal ions in H_2O

In order to evaluate the stability of the copper complex in physiological conditions, the formation of the complex was also investigated in water. In particular, spectrofluorimetric titrations were performed on cage **1** (0.015 mM) with aqueous Cu(II) at pH=8 (HEPES), where the $[Cu_2\mathbf{1}(OH)]^{3+}$ complex is the predominant species (85%) in solution.

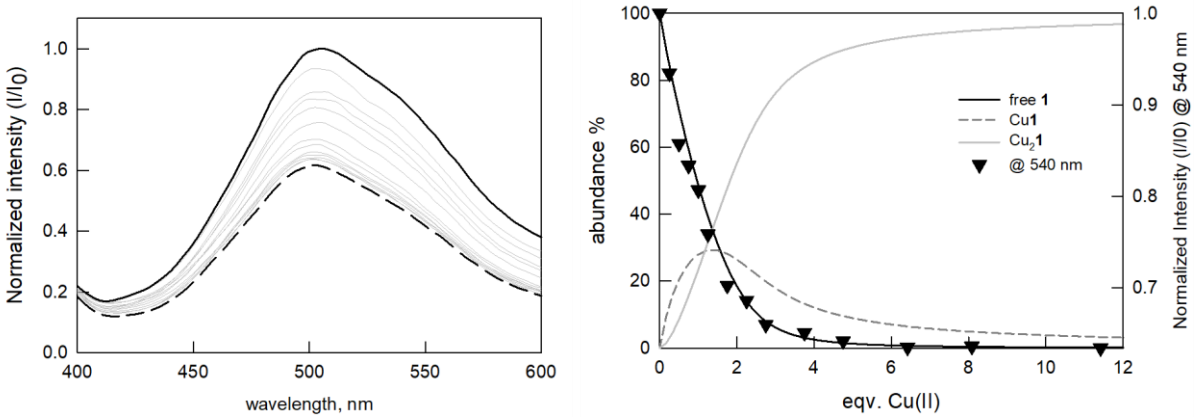

Figure 11. Spectrofluorimetric titration of **1** (0.015mM) with $Cu^{II}(CF_3SO_3)_2$ 2.5 mM (a) in H_2O (0.07 M HEPES pH=8) (λexc= 340 nm). (b) Distribution diagrams of the species present at the equilibrium; black triangles, normalized intensity of the emission at 540 nm, right vertical axis.

Figure 11a shows the family of emission spectra recorded during the titration of receptor **1** (0.015 M), at pH 8 (HEPES buffer, 0.07M), with a solution 2.5 mM of $Cu(CF_3SO_3)_2$. Copper addition promoted the quenching of the receptor's fluorescence (by about 40% of the initial intensity). This confirms the interaction of **1** with Cu(II) in water. The best fitting of the experimental data was obtained by assuming the formation of two species in solution with 1:1 and 2:1 Cu^{II}:L stoichiometry and the corresponding binding constants are reported in Table 2.

Equilibrium	Log K values
1 + Cu^{2+} ⇆ $[Cu\mathbf{1}]^{2+}$	5.34 (1)
$[Cu\mathbf{1}]^{2+}$ + Cu^{2+} ⇆ $[Cu_2\mathbf{1}]^{4+}$	5.25 (1)

Table 2. Log K values for the equilibria in water (HEPES 0.07M pH=8, 25°C), (In parentheses: standard deviations).

The corresponding distribution diagram is shown in Figure 11b. The emission intensity profile versus eqv. of Cu(II) fits very well the profile of the free ligand (solid line). This further confirms that the partial quenching of the receptor emission is due to the formation of the dicopper complex.

4.4. Conclusions

In this chapter, the synthesis of the new asymmetric fluorescent azacryptand **1,** containing a dansyl fragment anchored to one of the p-xylyl spacers, is reported. The system was investigated through potentiometric, UV-Vis and emission titrations in MeOH:water 3:2 mixture (0.07M $NaNO_3$). These studies pointed out that the azacryptand **1** displays its full fluorescence at neutral pH, with the typical dansyl emission. The binding tendencies of **1** towards Cu(II) and Zn(II) were evaluated in MeOH and in aqueous solution. The addition of metal ions induced the decrease of **1**'s emission; this behavior was more pronounced with Cu(II), which quenched the emission intensity by about 60 %. The titration profiles showed the formation of dimetallic complexes with both Cu(II) and Zn(II) with a 2:1 metal:ligand stoichiometry.

Studies on the model fluorophore **2** confirmed that, in the case of **1**, the quenching is driven by the formation of the complex. The affinity towards Cu^{2+} was also evaluated under physiological conditions. Spectrofluorimetric titrations in water at pH = 8 with Cu^{2+} allowed the determination of

two binding constants: $LogK_{11}$ = 5.34(1) and $LogK_{12}$ = 5.25(1) for the formation of $[Cu\mathbf{1}]^{2+}$ and $[Cu_2\mathbf{1}]^{4+}$ species, respectively.

The research described in this chapter was published in International Journal of Inorganic Chemistry, Volume 2016 (2016), Article ID 3415690.

Supplementary Section

1S. NMR spectra

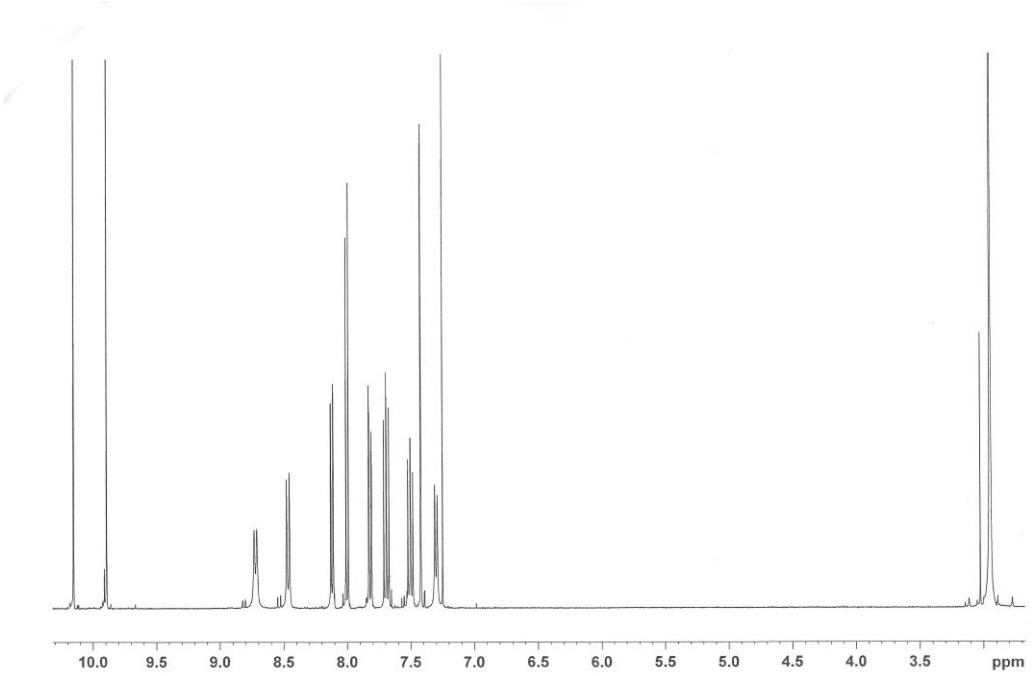

Figure S1. ^{1}H-NMR spectrum of 2-dansyl-1,4-benzenedicarboxaldehyde in $CDCl_3$.

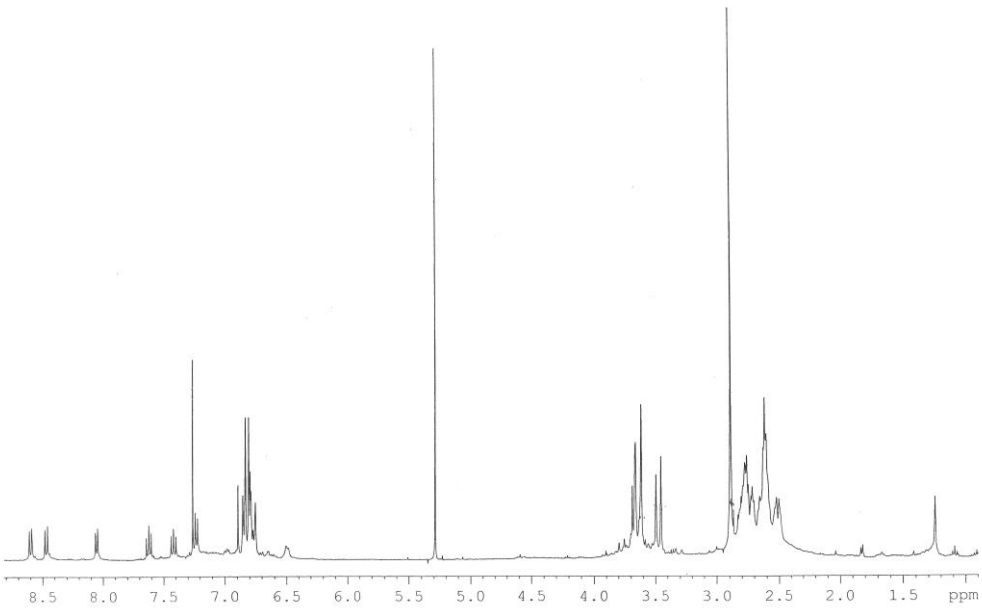

Figure S2. ^{1}H-NMR spectrum of dansyl cage **1** CD_3OD.

References

[1] Berggren, G.; Adamsaka, A.; Lambertz, C.; Simmons, TR.; Esselborn, J.; Atta, M.; Gambarelli, S.; Mouesca, JM.; Reijerse, E.; Lubitz, W.; Happe, T.; Artero, V.; Fontecave, M.; *Nature*.; **2013**, 499, 66-69.

[2] Qiu, J. and Burns, P. C.; *Chem. Rev*., **2013**, 113, 1097-1120.

[3] Zhao, Q.A.; Li, F.Y.; Huang, C.H.; *Chem. Soc. Rev.*, **2010**, 39, 3007-3030.

[4] Varol, M.; *J.App. Pharm*., **2016**, 8, no.1, 1-2.

[5] Que, E.L.; Domaille, D.W.; Chang, C.J.; *Chem. Rev.*, **2008**, 108, no.5, 1517-1549.

[6] Lan, A. P.; Chen, J.; Chai, Z. F.; Hu, Y.; *Biometals*, **2016**, 29, no. 134, 1-14.

[7] Yeung, M. C. L. and Yam, V. W. W.; *Chem. Soc. Rev.*, **2015**, 44, 4192-4202.

[8] Kim, H.N.; Ren, W.X.; Kim, J.S.; Yoon, J.; *Chem. Soc. Rev.*, **2013**, 41, 3210-3244.

[9] Jung, J.Y.; Kang, M.; Chun, J.; Lee, J.; Kim, J.; Kim, J.; Kim, Y.; Kim, S.J.; Lee, C.; Yoon, J.; *Chem. Comm.*, **2013,** 49, 176-178.

[10] Chen, J.; Li, Y.; Zhong, W.; Wang, H.; Zhang, P. and Jiang, J.; *Anal. Methods*, **2016**, 8, 1964-1967.

[11] Ruan, Y.B.; Li, C.; Tang, J.; Xie, J.; *Chem. Comm.*, **2010**, 46, 9220-9222.

[12] Hao, H. G.; Zheng, X. D. and Lu, T. B.; *Angew. Chem. Int. Ed.*, **2010**, 49, 8148-8151.

[13] Xie, G.Y.; Jiang, L. and Lu, T. B.; *Dalton Trans.*, **2013**, 42, 14092-14099.

[14] Siters, K. E.; Sander, S. A.; Devlina, J. R. and Morrow, J. R.; *Dalton Trans.*, **2015**, 44, 3708-3716.

[15] Fabbrizzi, L.; Faravelli, I.; Francese, G.; Licchelli, M.; Perotti, A. and Taglietti, A.; *Chem. Comm.*, **1998**, 9, 971-972.

[16] Wild, A. A. C.; Fennell, K.; Morgan, G. G.; Hewagea, C. M. and Malthouse, J. P. G.; *Dalton Trans.*, **2014**, 43, 13557-13562.

[17] Caballero-Jiménez, J.; Habib, F.; Ramírez-Rosales, D.; Grande-Aztatzi, R.; Merino, G.; Korobkov, I.; Singh, M. K.; Rajaraman, G.; Reyes-Ortega, Y. and Murugesu, M.; *Dalton Trans.*, **2015**, 44, 8649-8659.

[18] (a) McKee, V.; Nelson, J. and Town, R. M.; *Chem. Soc. Rev*., **2003**, 32, 309-325. (b) Bond, A. D.; Derossi, S.; Jensen, F.; Larsen, F. B.; McKenzie, C. J. and Nelson, J.; *Inorg. Chem*., **2005**, 44, no. 17 5987-5989.

[19] Mateus, P.; Delgado, R.; André, V. and Duarte, M. T.; *Inorg. Chem.*, **2015**, 54, 229-240.

[20] Saeed, M. A.; Fronczek, F. R.; Huanga, M. J. and Hossain, Md. A.; *Chem. Comm.*, **2010**, 46, 404-406.

[21] Amendola, V.; Bergamaschi, G.; Buttafava, A.; Fabbrizzi, L. and Monzani, E.; *J. Am. Chem. Soc.*, **2010**, 132, no. 1, 147-156.

[22] Alibrandi, G.; Amendola, V.; Bergamaschi, G.; Fabbrizzi, L.; Licchelli, M.; "Bistren cryptands and cryptates: versatile receptors for anion inclusion and recognition in water", *Org. Biomol. Chem.*, **2015**, 13, 3510-3524.

[23] Amendola, V.; Bergamaschi, G.; Boiocchi, M.; Alberto, R. and Braband, H.; *Chem. Sci.*, **2014**, 5, 1820-1826.

[24] Li, Y. H.; Chan, L. M.; Tyer, L.; Moody, R.T.; Hirnel, C.M.; Hercules, D.M.; *J. Am. Chem. Soc.*, **1975**, 97, no. 11, 3118-3126.

[25] Li, D. P.; Wang, Z. Y.; Cao, X. J.; Cui, J.; Wang, X.; Cui, H. Z.; Miao, J. Y. and Zhao, B. X.; *Chem. Comm.*, **2016**, 52, 2760-2763.

[26] Bhoi, A. K.; Sahu, P. K.; Jha, G. and Sarkar**,** M.; *RSC Adv.*, **2015**, 5, 61258-61269.

[27] Parola, A. J.; Lima, J. C.; Pina, F.; Pina, J.; De Melo, J. S.; Soriano, C.; Garcia-Espana, E.; Aucejo, R.; Alarcon, J.; *Inorganica Chimica Acta*, **2007**, 360, 1200-1208.

[28] Pallavicini, P.; Amendola, V.; Bergamaschi, G.; Cabrini, E.; Dacarro, G.; Rossi, N.; Taglietti, A.; *New J. Chem.*, **2016**, 40, 5722-57302016.

[29] Miller, S. C.; *J. Org. Chem.*, **2010**, 75, 4632-4635.

[30] Bergamaschi, G.; Boiocchi, M.; Perrone, M. L.; Poggi, A.; Viviani, I. and Amendola, V.; *Dalton Trans.*, **2014**, 43, 11352-11360.

[31] (a) Gran, G.; *Analyst.*, **1952**, 77, 661-771. (b) Gans, P. and O'Sullivan, B.; *Talanta*, **2000**, 51, 33-37.

[32] Gans, P.; Sabatini, A. and Vacca, A.; *Talanta*, **1996**, 43, 1739-1753. http://www.hyperquad.co.uk/index.htm, accessed on 20 February 2013.

[33] (a) McDowell, D.; Nelson, J.; *Tetrahedron Lett*., **1988**, 29, 385-386. (b) Chen, D.; Martell, A. E.; *Tetrahedron,* **1991**, 47. no.34. 6895-6902.

[34] Prodi, L.; Montalti, M.; Zaccheroni, N.; Dallavalle, F.; Folesani, G.; Lanfranchi, M.; Corradini, R.; Pagliari, S. and Marchelli, R.; *Helv. Chim. Acta*, **2001**, 84, no. 3, 690-706.

[35] Berlman, I.B.; *Handbook of Fluorescence Spectra of Aromatic Molecules, 2nd ed*., *Academic Press*, London, **1971**.

[36] Nelissen, H. F. M.; Venema, F.; Uittenbogaard, R. M.; Feiters, M. C. and Nolte, R. J. M.; *J. Chem. Soc., Perkin Trans. 2*, **1997**, 2045-2053.

[37] Passaniti, P.; Ceroni, P.; Balzani, V.; Lukin, O.; Yoneva, A. and Vögtle, F.; *Chem.- Eur. J.*, **2006**, 12, no. 22, 5685-5690.

5. A triphenylic azacryptand

5.1. Introduction

The development of sensors for the real-time determination of anions with non-invasive methods is one of the topics of current interest.[1] The selective recognition of aliphatic and aromatic (di)carboxylate anions in water, in particular, is considered a very interesting field due to the biological and environmental role of these substrates. To achieve this goal, molecular cages seem to be more suitable than open chain receptors, allowing the selective binding of dicarboxylate species even in water. Among cage receptors, the bistren cryptands are of particular interest due to the easy synthetic procedure and the possibility of tuning both cavity size and selectivity using different spacers between the *tren* units.[2]

Dicopper complexes of azacryptands have the advantage of being active as anion receptors in aqueous solution even at neutral pH (e.g. in physiological condition).[3] In the case of bidentate anions, such as dicarboxylates, selectivity is connected to the fitting of the anion bite length[4-6] with the distance between the apical positions of the two copper ions within the cage's cavity.

In order to develop a selective receptor for dicarboxylates with long bites, we synthesized a new azacryptand containing triphenyl spacers (**L**).

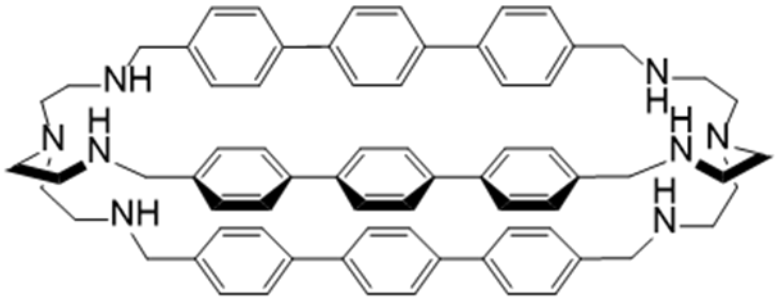

L

The binding properties of the dicopper complex were investigated towards the anionic substrates shown in Figure 1, e.g. biphenyl-4,4′-dicarboxylate, dfc^{2-}; 4,4'-sulfonyldibenzoate, $sdbz^{2-}$; terephthalate, tph^{2-}; benzoate, bz^{-}, through both UV-vis. titrations and competition experiments. In the latter case, the indicator displacement paradigm[7] was applied.

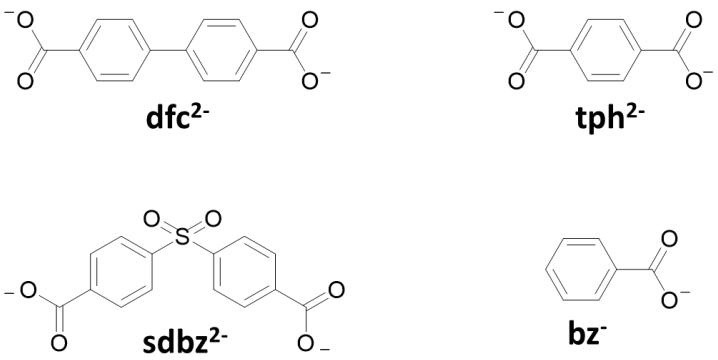

Figure 1. Anionic substrates study in this work.

5.2. Experimental section

5.2.1. Chemicals and Methods

All reagents and solvents were purchased from Sigma-Aldrich, and used without further purification. [1,1':4',1"-Terphenyl]-4,4"-dicarboxaldehyde was synthesized according to a known procedure.[8] In the synthesis of **L**, $NaBH_3CN$ was employed a reducing agent for imine bonds.[9] The solutions used in titrations were prepared from freshly opened solvent bottles. Mass spectra were acquired on a Thermo-Finnigan ion-trap LCQ Advantage Max instrument equipped with an ESI source, and NMR spectra were recorded on a Bruker ADVANCE 400 spectrometer (operating at 9.37 T, 400 MHz). UV-vis spectra were run on a Varian Cary 100 SCAN spectrophotometer with quartz cuvettes of the appropriate path length at 25.0 ± 0.1 °C under inert conditions. Emission spectra were recorded on a Perkin- Elmer LS 50B instrument. Titration data were processed with the Hyperquad package[10] to determine the equilibrium constants. All the computational studies were carried out using the GAUSSIAN09 program package.[11] The structures were optimized in the gas phase at the B3LYP/6-31 G level of theory. EPR spectra were recorded on a Bruker EMX X-band continuous wave spectrometer equipped with a EPR cavity Bruker ER4119HS and a temperature control unit. Solutions for EPR studies were obtained, by mixing the $[Cu_2(\mathbf{L})](CF_3SO_3)_4$ complex with 1 eqv. of the anion in 4:1 (v:v) $MeCN:H_2O$ mixture (pH 7).

5.2.2 Synthesis of L

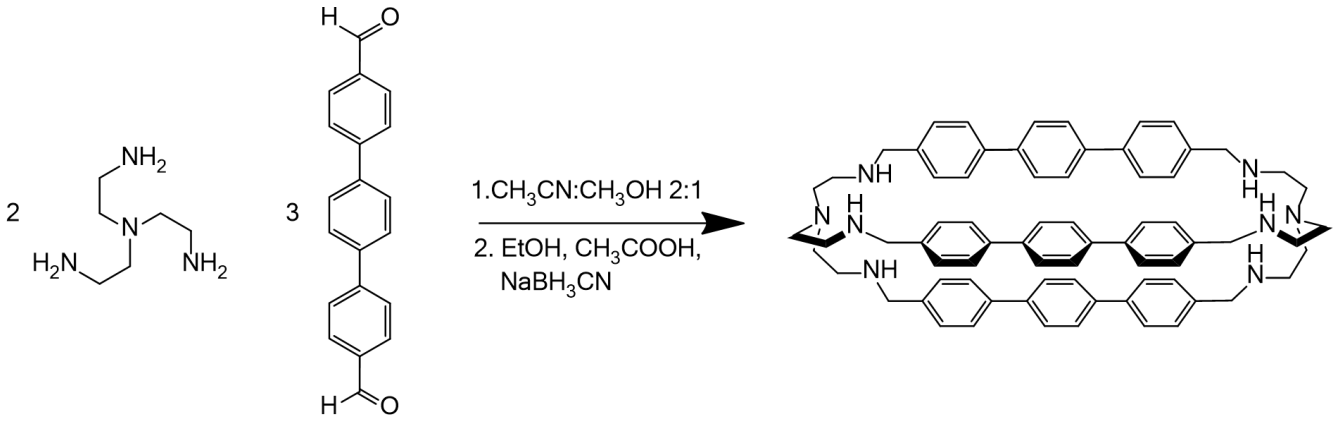

100 mg of [1,1':4',1''-Terphenyl]-4,4''-dicarboxaldehyde (100 mg, 0.35 mmol) in 60 mL of 2:1 $CHCl_3$:MeOH were added to a solution of *tren* (36 µl, 0.35 mmol) in 120 mL of the same medium. The reaction mixture was stirred for 24 hrs. at RT, before taking to dryness. The solid residue was suspended in EtOH (100 mL), and dissolved by addition of CH_3COOH. The imine bonds was reduced by addition of $NaBH_3CN$ (3 eqv. per C=N) to the mixture at RT. The solution was then stirred at 50°C overnight. After basification with excess NaOH(aq), EtOH was evaporated and the aqueous layer was extracted with $CHCl_3$ (10 × 25 mL). The reunited organic phases was dried over anhydrous Na_2SO_4. After evaporation, a white solid was obtained. Yield: 70%

ESI-MS (MeOH): m/z 528.7 $[\mathbf{L}+2H]^{2+}$

^{1}H-NMR (d_6-DMSO + 1M CF_3SO_3H in D_2O, 400 MHz), δ (ppm): 7.61 (d, 12H, H-a), 7.49 (s, 12H, H-c), 7.34 (d, 12H, H-b), 4.20 (s, 12H, H-3), 3.12 (s, 12H, H-2), 2.76 (s, 12H, H-1).

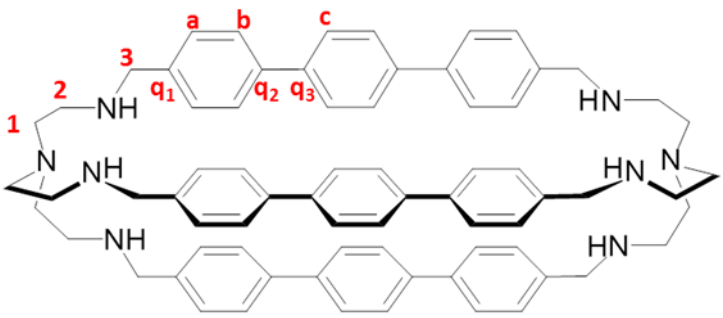

^{13}C-NMR (d_6-DMSO + 1M CF_3SO_3H in D_2O, 400 MHz), δ (ppm): 139.04 (C-q2), 137.44 (C-q3), 130.04 (C-q1), 129.69 (C-b), 126.37-126-14 (C-a, C-c), 48.99 (C-3), 48.62 (C-1), 42.70 (C-2).

5.2.3. Synthesis of $[Cu_2L](CF_3SO_3)_4$

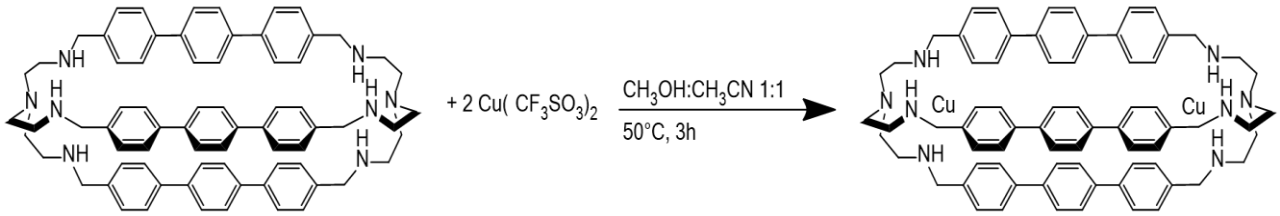

55.1 mg (0.052 mmol) of **L** was suspended in 40 mL of MeOH:MeCN 1:1 (v/v) mixture. 38.3 mg $Cu(CF_3SO_3)$ (0.107 mmol) in 5 mL MeOH was then added, and the obtained solution was refluxed for 3 hrs. After filtering, the solvent was evaporated and the solid residue was treated with Et_2O. A light green powder was obtained. Yield: 67%

ESI-MS (MeOH): m/z 590.22 $[Cu^{II}_2(\mathbf{L}\text{-}2H^+)]^{2+}$, m/z 665.16 $[Cu^{II}_2(\mathbf{L}\text{-}H+CF_3SO_3)]^{2+}$ and m/z 740.04 $[Cu^{II}_2\mathbf{L}(CF_3SO_3)_2]^{2+}$.

5.3. Results and discussion

Receptor **L** was synthesized from the *tren* polyamine and [1,1':4',1''-Terphenyl]-4,4''-dicarboxaldehyde[8] using a known procedure.[12] Ligand **L** was then complexed with 2 eqv. Cu(II), as the triflate salt, and the compound $[Cu_2\mathbf{L}](CF_3SO_3)_4$ was isolated and characterized. The free ligand **L** was found to be poorly soluble at neutral pH in both aqueous solution and organic:water mixtures, due to the presence of bulky spacers.[4] As a consequence, potentiometric studies could not be performed, and the distribution diagram of the ligand at varying pH values is not available. Studies in solution were carried out directly on the dicopper complex, $[Cu_2\mathbf{L}](CF_3SO_3)_4$, in 1:4 (v:v) H_2O:MeCN solution. Anion binding was followed through UV-vis. titrations on the dicopper cryptate and by the "indicator displacement" approach.[7] In this case, a fluorescent indicator (**I**) was

chosen, containing a suitable binding group for the dicopper complex, C, such as a dicarboxylate unit. In the chemosensing ensemble solution, C binds and quenches the emission of **I**. Upon addition of a competing anionic guest, **I** is displaced from the azacryptand's cavity and its fluorescence is restored.

5.3.1. pH-spectrophotometric titration studies

To evaluate the formation of dicopper complex of azacryptand **L**, a pH-spectrophotometric titration was performed. This study was done at 25 °C in CH_3CN:H_2O 4:1 mixture ($NaCF_3SO_3$ 0.05 M). In a typical experiment, the solution of the complex ($[Cu_2\mathbf{L}](CF_3SO_3)_4$, 0.2 mM) was titrated with a 100-fold more concentrated solution of sodium hydroxyde .

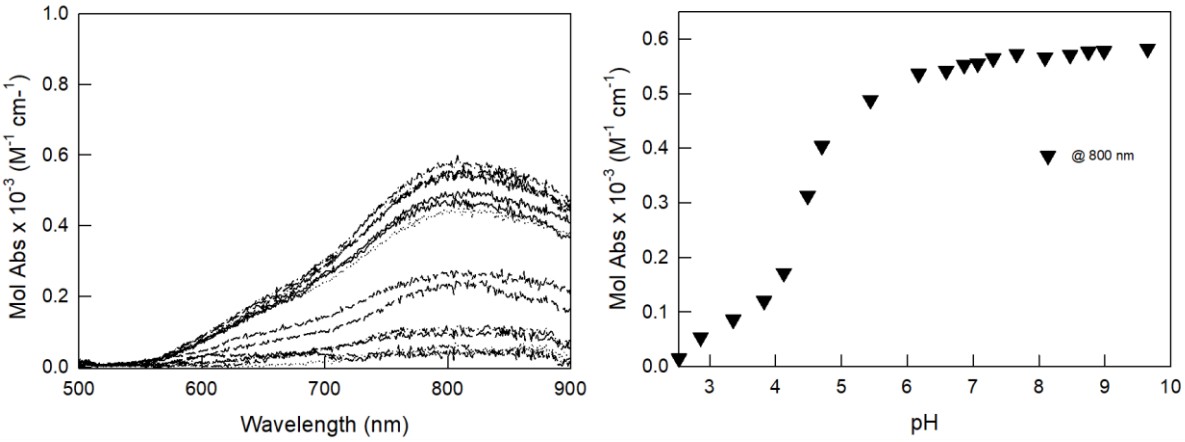

Figure 2. pH-spectrophotometric titration (left) and profile at 800 nm (right) of $[Cu_2\mathbf{L}](CF_3SO_3)_4$.

The results confirmed that Cu(II) complexation begins around pH 4 with the development of large d-d bands between 650 and 850 nm, typical of the trigonal-bipyramidal CuN_5 chromophore (e.g. Cu(II) complexes with tripodal bistren-type receptors).[13] Maximum absorbance was observed over pH 6, where the ligand is fully complexed as $[Cu_2\mathbf{L}]^{4+}$. Probably, the apical position of each copper ion is occupied by a water molecule as found in other bistren complexes.[4,14] Unfortunately, crystals suitable for X ray diffraction studies were not obtained so it was not possible to verify this hypothesis.

5.3.2. Spectrophotometic titrations studies of $[Cu_2L](CF_3SO_3)_4$

The affinity of the dicopper complex towards dicarboxylate anions (as the TBA salts) was investigated through UV-vis. titrations at pH 7 in 1:4 (v:v) H_2O:MeCN solution (0.02M HEPES, T = 25°C). In this case, to a solution of $[Cu_2\mathbf{L}](CF_3SO_3)_4$ (50 µM, 25 ml, path length = 10 cm) incremental amounts of anion were added, and the corresponding UV-vis. spectra were recorded. The coordination of (di)carboxylates to the copper ions within the cage was accompanied by a change in the intensity of the d-d bands. In particular, the band at 810 nm decreased in intensity and shifted towards higher energies; while the absorbance between 670 and 700 nm increased.

The family of UV-vis spectra, as well as the titration profiles with the superimposed distribution diagrams, are reported in Figures below:

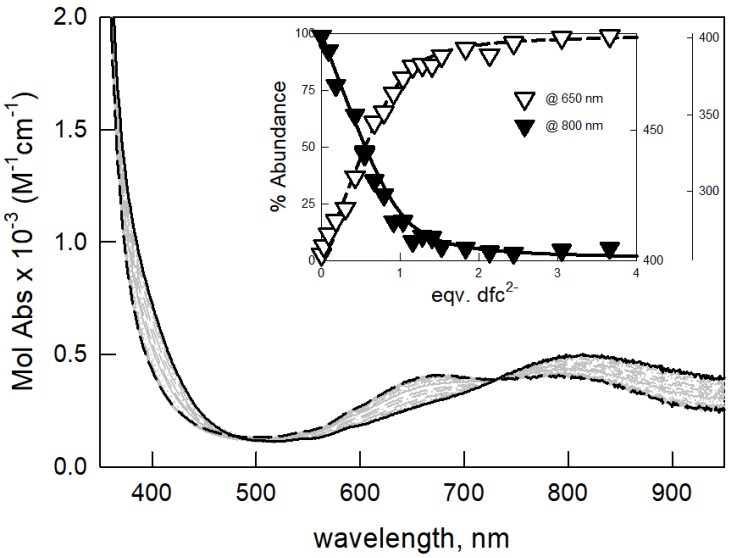

Figure 3. UV-vis. spectra taken upon titration of $[Cu_2\mathbf{L}](CF_3SO_3)_4$ (50µM) with dfc^{2-} (as the TBA salt) in H_2O:MeCN 1:4 at pH 7 (0.02M HEPES; path length = 10 cm). The inset shows the titration profiles at 650 and 800 nm, with the superimposed distribution diagram of the dicopper complex containing species: dotted line, $[Cu_2\mathbf{L}(dfc)]^{2+}$; solid line, $[Cu_2\mathbf{L}]^{4+}$; $LogK_{11}$ = 5.46(2).

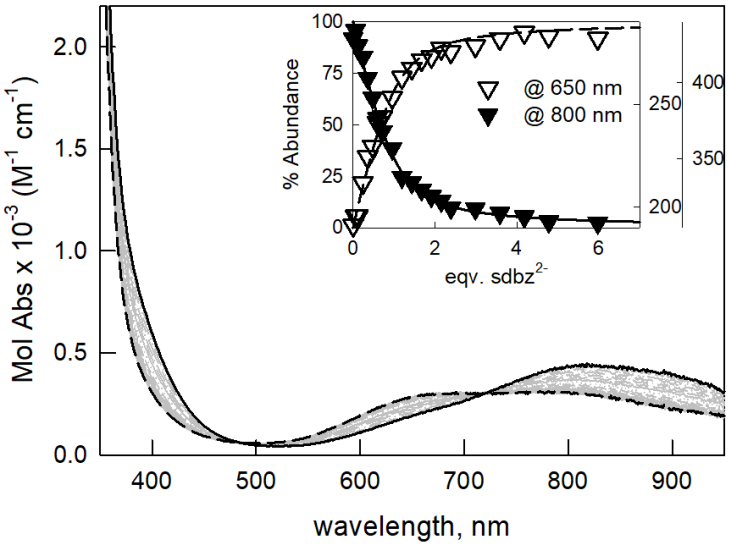

Figure 4. UV-vis. spectra taken upon titration of $[Cu_2\mathbf{L}](CF_3SO_3)_4$ (50µM) with $sdbz^{2-}$ (as the TBA salt) in H_2O:MeCN 1:4 at pH 7 (0.02M HEPES; path length = 10 cm). The inset shows the titration profiles at 650 and 800 nm, with the superimposed distribution diagram of the dicopper complex containing species: dotted line, $[Cu_2\mathbf{L}(sdbz)]^{2+}$; solid line, $[Cu_2\mathbf{L}]^{4+}$; $LogK_{11}$ = 5.08 (1).

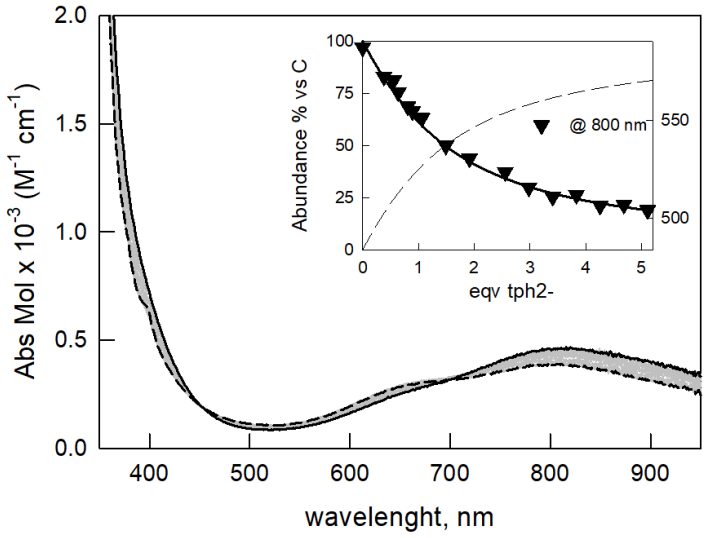

Figure 5. UV-vis. spectra taken upon titration of $[Cu_2\mathbf{L}](CF_3SO_3)_4$ (50µM) with tph^{2-} (as the TBA salt) in H_2O:MeCN 1:4 at pH 7 (0.02M HEPES; path length = 10 cm). The inset shows the titration profiles at 800 nm, with the superimposed distribution diagram of the dicopper complex containing species: dotted line, $[Cu_2\mathbf{L}(tph)]^{2+}$; solid line, $[Cu_2\mathbf{L}]^{4+}$; $LogK_{11}$ = 4.43 (4).

The maximum wavelength of the d-d bands, in the final spectrum, slightly changed according to the added anion. However, from the fitting of the titration profiles, the binding constants for the formation of a 1:1 adduct were obtained with the investigated dicarboxylate species (see Table 1).

	$LogK_{11}^{UV\text{-}vis}$ / $\lambda_{fin}^{UV\text{-}vis}$ (nm)	
dfc^{2-}	5.46(3)	670, ≅ 780
sdbz^{2-}	5.08(1)	686, ≅ 780
tph^{2-}	4.43(4)	690(sh.), 800
bz^{-}	n.a.	n.a.

Table 1. Binding constants obtained by UV-vis titrations. n.a.: not available.

As shown in Table 1, among the investigated dicarboxylate anions, equilibrium constants decreased along the series dfc^{2-} > sdbz^{2-} > tph^{2-}. As expected, the highest affinity is for dfc^{2-}, whose bite better matches the distance between Cu(II) ions within the cavity (see computational study).
For the benzoate anion (bz^{-}), only small changes were observed in the UV-vis. spectrum. These changes were attributed to a weak interaction between bz^{-} and the compex; however, no binding constants were obtained from data treatment.

5.3.3. Spectrofluorimetric titration studies

Anion binding studies were also performed using the indicator displacement (ID) paradigm.[7] We chose 6-TAMRA (i.e. 6-Carboxytetramethylrhodamine, see Figure 6) as a fluorescent indicator for the presence of a 1,4-phenyldicarboxylate unit, on the dye's core, that could bind to copper ions within the cage's cavity.

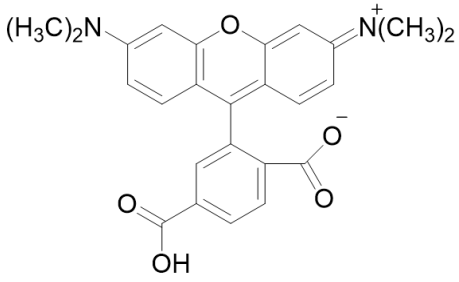

Figure 6. 6-Carboxytetramethylrhodamine (6-TAMRA).

Even if the 6-TAMRA's bite is not optimal for our receptor, the interaction of the indicator with the dicopper complex in aqueous solution is expected to be favoured by hydrophobic effects and by π-π interactions between the rhodamine core and the tri-phenyl spacers.[3,15] Moreover, 6-TAMRA is

commercially available and it was successfully employed by Fabbrizzi for the fluorescent detection of dicarboxylates in water, using the dicopper cage with diphenyl spacers as the receptor.[4]

5.3.4. Titration of 6-TAMRA (I) with $[Cu_2L](CF_3SO_3)_4$ in H_2O:MeCN 1:4 mixture

The binding of 6-TAMRA to $[Cu_2\mathbf{L}](CF_3SO_3)_4$ was studied by UV-vis. and fluorimetric titrations in 1:4 H_2O:MeCN solution, buffered at pH 7 (0.02M HEPES). In these conditions, the indicator was fully fluorescent (λem = 570 nm) and showed an absorption band in the visible region with a maximum at 554 nm.

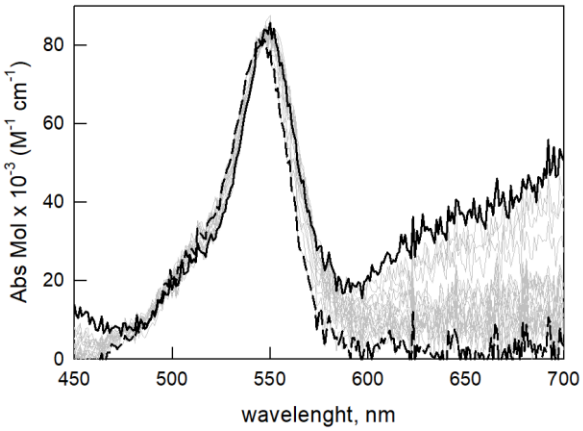

Figure 7. Family of UV-vis. spectra recorded during the titration of 6-TAMRA (0.25 μM, path length = 1 cm) with $[Cu_2\mathbf{L}](CF_3SO_3)_4$ in H_2O:MeCN 1:4 at pH 7 (0.02M HEPES).

Figure 7 shows the family of UV-vis. spectra recorded during the titration of 6-TAMRA (0.25 μM, path length = 1 cm) with $[Cu_2\mathbf{L}](CF_3SO_3)_4$ in H_2O:MeCN 1:4 at pH 7 (0.02M HEPES). Upon dicopper complex addition, only little changes were observed in the absorption spectrum around 554 nm.

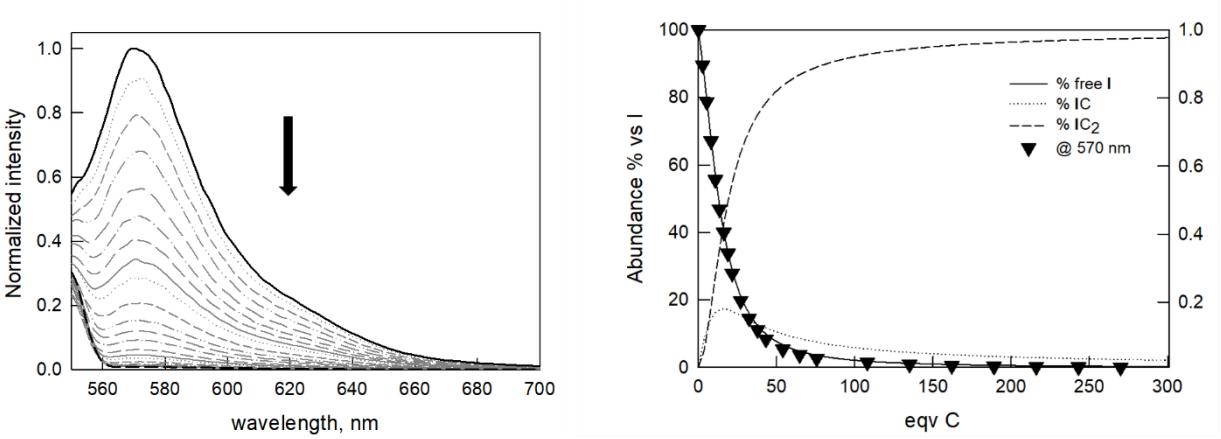

Figure 8. Normalized emission spectra taken upon titration of 6-TAMRA, **I** (0.25 μM, λexc = 548 nm) with $[Cu_2\mathbf{L}](CF_3SO_3)_4$ (C) in H_2O:MeCN 1:4 at pH 7 (0.02M HEPES) (left). The titration profile as the normalised intensity at 570 nm vs. eqv. of the added complex, with the superimposed distribution diagram of the indicator containing species (**I** = 6-TAMRA; C = $[Cu_2\mathbf{L}]^{4+}$; **I**C and **I**C_2 = 1:1 and 1:2 **I**:C adducts, respectively) (right).

In the case of spectrofluorimetric titration, the addition of the dicopper complex led to a significant quenching of 6-TAMRA's fluorescence (see Figure 8). Treatment of the emission data allowed us to calculate two equilibrium constants, corresponding to the formation of 1:1 and 1:2 adducts between 6-TAMRA and $[Cu_2\mathbf{L}]^{4+}$.

The corresponding equilibria are:

$$\mathbf{I} + C \rightleftarrows \mathbf{I}C, \qquad \text{Log}K_{11} = 5.06(2)$$

$$\mathbf{I} + 2C \rightleftarrows \mathbf{I}C_2, \qquad \text{Log}K_{12} = 5.82(5)$$

The formation of adducts with 1:2 **I**:C stoichiometry had been already observed in the binding studies of dicopper azacryptate with indicator in methanol:water mixture.[16] As shown in Figure 8, the indicator emission is completely quenched above 100 eqv. of the added complex, i.e. where the indicator is in the **I**C_2 form (> 90%).

5.3.5. Titrations of chemosensing ensemble solution with dicarboxylate anions in H_2O:MeCN 1:4 mixture

For competition assays with dicarboxylates species, a chemosensing ensemble solution was prepared by mixing C (50 µM) and **I** (0.25 µM) in 1:4 H_2O:MeCN at pH 7 (0.02M HEPES). In these conditions, the indicator is bound to the receptor (as the **I**C_2 species), thus the emission is quenched.

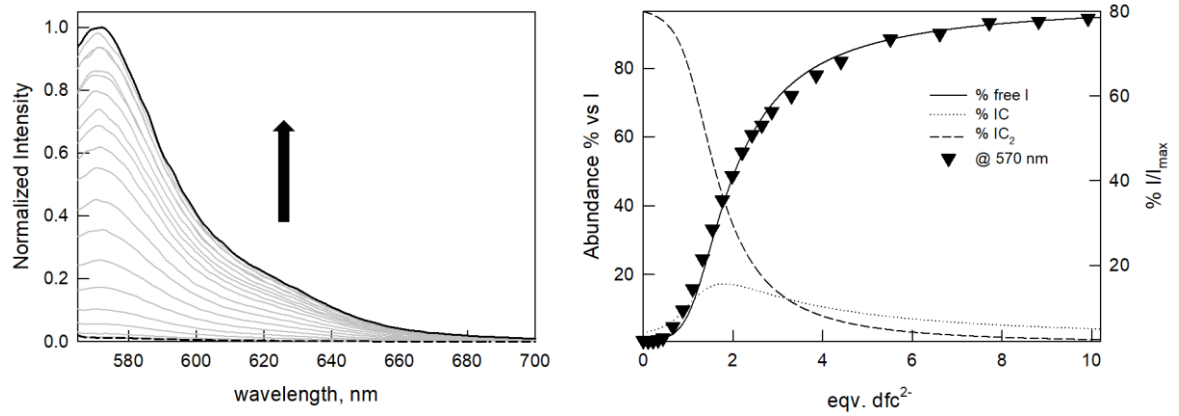

Figure 9. Normalized emission spectra (right) taken upon titration of the chemosensing ensemble solution (0.25 µM **I**; 50 µM C, λexc = 548 nm) with dfc^{2-} (as the TBA salt) in H_2O:MeCN 1:4 at pH 7 (0.02M HEPES). The titration profile (left), as % I/I_{max} (I_{max}= emission intensity of **I** in the absence of C) vs. eqv. of the dicarboxylate anion, with the superimposed distribution diagram of the indicator containing species (**I** = 6-TAMRA; C = $[Cu_2\mathbf{L}]^{4+}$; **I**C and **I**C_2 = 1:1 and 1:2 **I**:C adducts, respectively).

Upon titration with dfc^{2-}, the indicator is displaced and the emission intensity is restored up to 80% (see Figure 9). In particular, a full restoration of fluorescence is not obtained with a large excess of the competing dfc^{2-} anion, reasonably due to collisional quenching effects of the dicopper complex on free 6-TAMRA.

A similar trend was observed with $sdbz^{2-}$ (see Figure 10). These results are consistent with a formation of stable anion:receptor complexes for both dfc^{2-} and $sdbz^{2-}$.

In particular, the fitting of the experimental curves for a 1:1 anion:cage equilibrium led to binding constants, which resulted very close to those determined by UV-vis titrations (see Table 1 and 2).

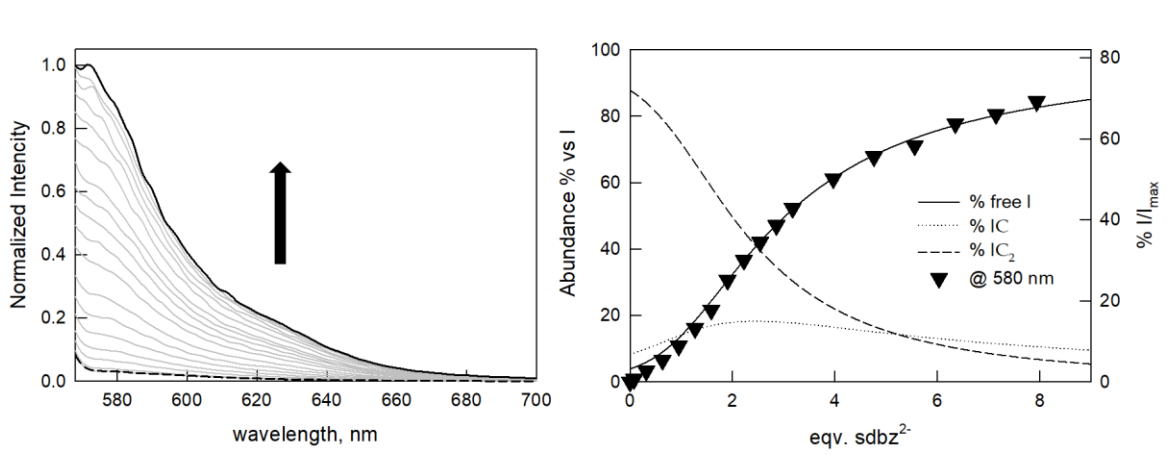

Figure 10. Normalized emission spectra (right) taken upon titration of the chemosensing ensemble solution (0.25 μM **I**; 50 μM C, λexc = 548 nm) with $sdbz^{2-}$ (as the TBA salt) in H_2O:MeCN 1:4 at pH 7 (0.02M HEPES). The titration profile (left), as % I/I_{max} (I_{max}= emission intensity of **I** in the absence of C) vs. eqv. of the dicarboxylate anion, with the superimposed distribution diagram of the indicator containing species (**I** = 6-TAMRA; C = $[Cu_2\mathbf{L}]^{4+}$; **I**C and **I**C_2 = 1:1 and 1:2 **I**:C adducts, respectively).

Competition experiments were also done with tph^{2-}, bz^- and aliphatic dicarboxylates –OOC-(CH_2)n-COO–(as the TBA salts; n= 3, 5, ..., 8, 10), however a minor recovery of the indicator emission was obtained (see Figure 13 and Table 2).

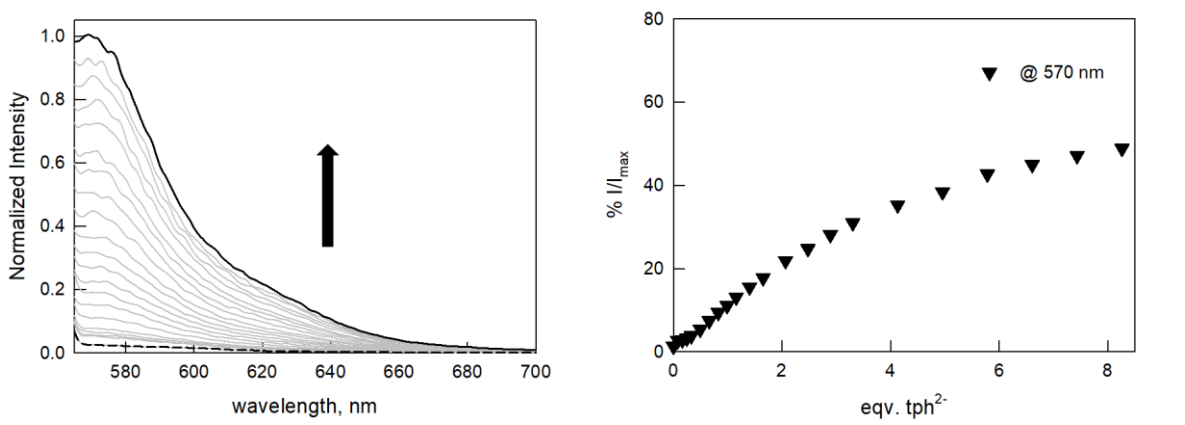

Figure 11. Normalized emission spectra (right) taken upon titration of the chemosensing ensemble solution (0.25 μM **I**; 50 μM C, λexc = 548 nm) with tph^{2-} (as the TBA salt) in H_2O:MeCN 1:4 at pH 7 (0.02M HEPES). The titration profile (left), as % I/I_{max} (I_{max}= emission intensity of **I** in the absence of C) vs. eqv. of the dicarboxylate anion.

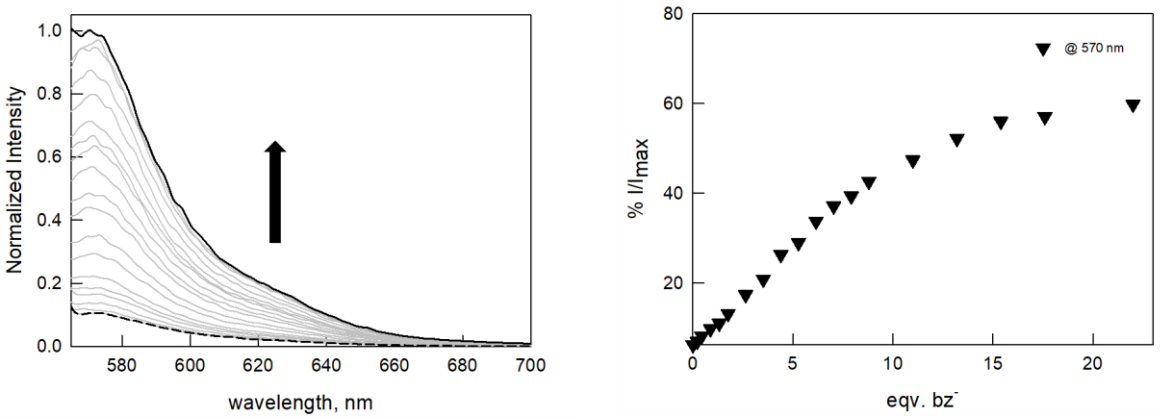

Figure 12. Normalized emission spectra (right) taken upon titration of the chemosensing ensemble solution (0.25 μM **I**; 50 μM C, λexc = 548 nm) with bz^- (as the TBA salt) in H_2O:MeCN 1:4 at pH 7 (0.02M HEPES). The titration profile (left), as % I/I_{max} (I_{max}= emission intensity of **I** in the absence of C) vs. eqv. of the dicarboxylate anion.

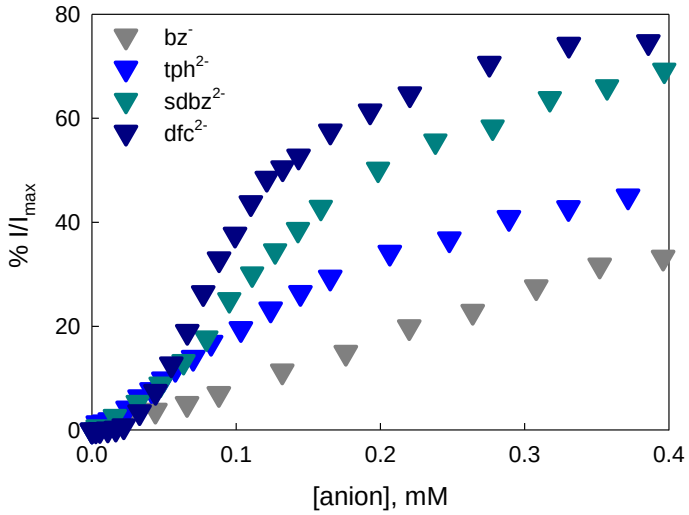

Figure 13. Spectrofluorimetric titration profiles obtained for different dicarboxylates (as the TBA salts) using chemosensing ensemble solutions of C (50 μM) and **I** (0.25 μM) in 1:4 H_2O:MeCN at pH 7 (0.02M HEPES).

	$LogK_{11}^{ID}$ / % I/I_{max}	
dfc^{2-}	5.46(4)	75%
$sdbz^{2-}$	5.01(1)	70%
tph^{2-}	n.a.	46%
bz^-	n.a.	36%

Table 2. Binding constants obtained by fluorimetric (indicator displacement, ID) titrations. %I/I_{max} = % recovery of the emission intensity at 570 nm (taken at 8 eqv. of the added anion). n.a.: not available

The lower affinity of both aliphatic dicarboxylates and tph^{2-} for the cage, compared to **I**, is likely connected to the smaller hydrophobic and π-π interactions between these anionic guests and the cavity.[5]

5.3.6. ESI-MS studies of the adducts

Direct evidence of the formation of stable 1:1 complexes between the receptor and the anions (i.e. dfc^{2-} and $sdbz^{2-}$) was provided by the ESI mass spectrometry studies performed on equimolar solutions of the dicarboxylate anion and $[Cu_2(\mathbf{L})]^{4+}$ (30 μM in MeCN:H_2O 4:1).

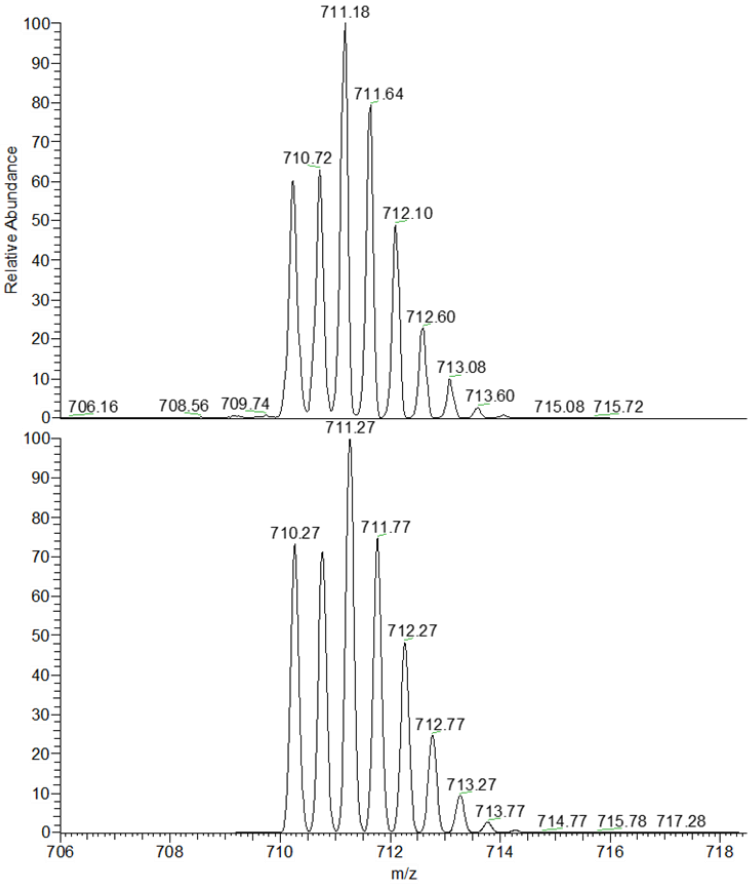

Figure 14. Top: zoom scan of the peak at 711 m/z, obtained from the experimental mass spectrum of an equimolar solution of $[Cu_2\mathbf{L}]^{4+}$ and dfc^{2-} in MeCN:H_2O 4:1. Bottom: simulated peak, calculated for the double charged adduct $[Cu_2C_{86}H_{86}N_8O_4]^{2+}$.

In Figure 14 is reported the experimental, double positively charged peak at 711 m/z corresponding to the adduct $[Cu_2\mathbf{L}\text{-dfc}]^{2+}$. The comparison with the simulated zoom scan (shown below) confirmed the attribution of the signal to the species of formula $[Cu_2C_{86}H_{86}N_8O_4]^{2+}$ (i.e. $[Cu_2\mathbf{L}\text{-dfc}]^{2+}$).

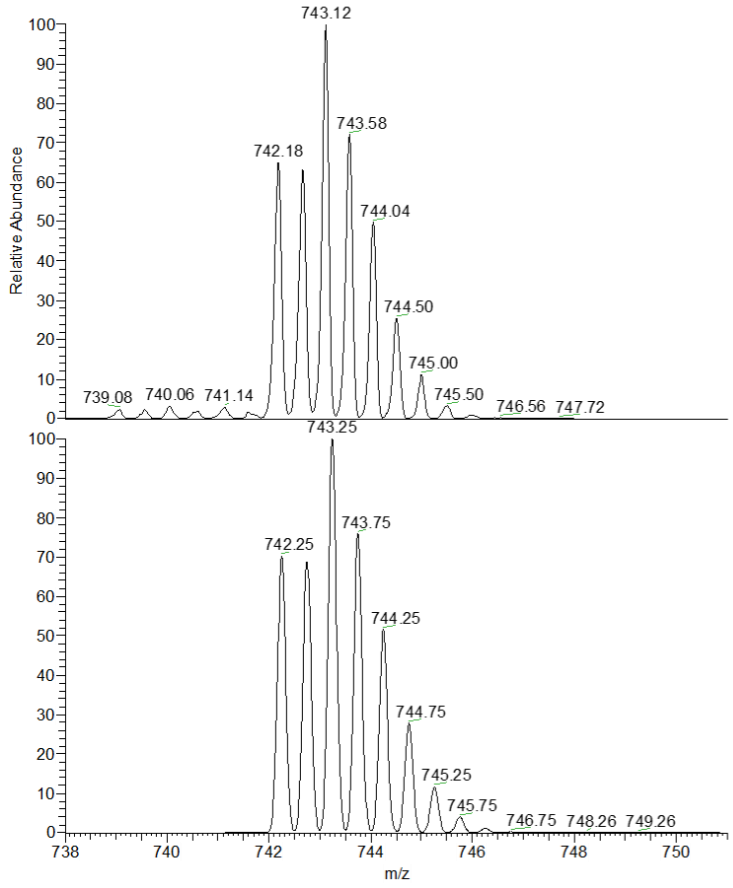

Figure 15. Top: zoom scan of the peak at 743 m/z, obtained from the experimental mass spectrum of an equimolar solution of $[Cu_2\mathbf{L}]^{4+}$ and $sdbz^{2-}$ in MeCN:H_2O 4:1. Bottom: simulated peak, calculated for the double charged adduct $[Cu_2C_{86}H_{86}N_8O_6S]^{2+}$.

Figure 15 shows the experimental, double positively charged peak at 743 m/z corresponding to the adduct $[Cu_2\mathbf{L}\text{-sdbz}]^{2+}$. The comparison with the simulated zoom scan (shown below) confirmed the attribution of the signal to the species of formula $[Cu_2C_{86}H_{86}N_8O_6S]^{2+}$ (i.e. $[Cu_2\mathbf{L}\text{-sdbz}]^{2+}$).

In the case of other anions, no corresponding peaks were observed in ESI-MS, probably due to the weak receptor:anion interaction.

5.3.7. Computational studies

Unfortunately, crystals suitable for X ray diffraction studies were not obtained. Therefore, the structure of the anion inclusion complexes was investigated by a preliminary computational study in the gas phase, starting from the known crystal structure of the Cu_2(p-xylyl cage)·$2H_2O$[17], that was optimized at the B3LYP/6-31G level of theory (Gaussian09 program package)[11].

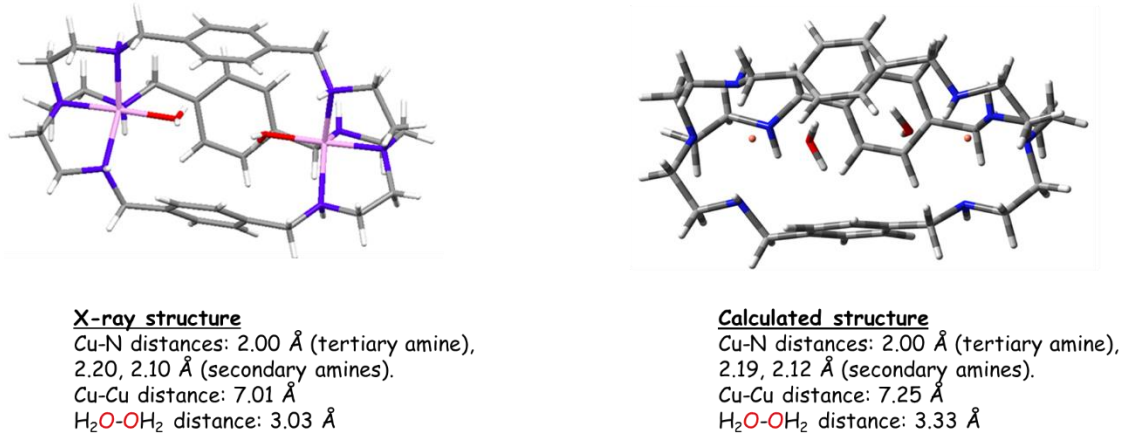

Figure 16. Comparison between crystal and calculated structures.

The x-ray structure of the Cu_2(p-xylyl cage)·$2H_2O$ and the corresponding calculated one are very similar, as shown by the values of the bond distances, reported in Figure 16, that are comparable in the two cases. On the basis of this result, the study was extended to the dicopper complex of the triphenylic cage [Cu_2**L**]. The starting geometry was prepared through GaussView 5.0 and optimized at the same level of calculation.

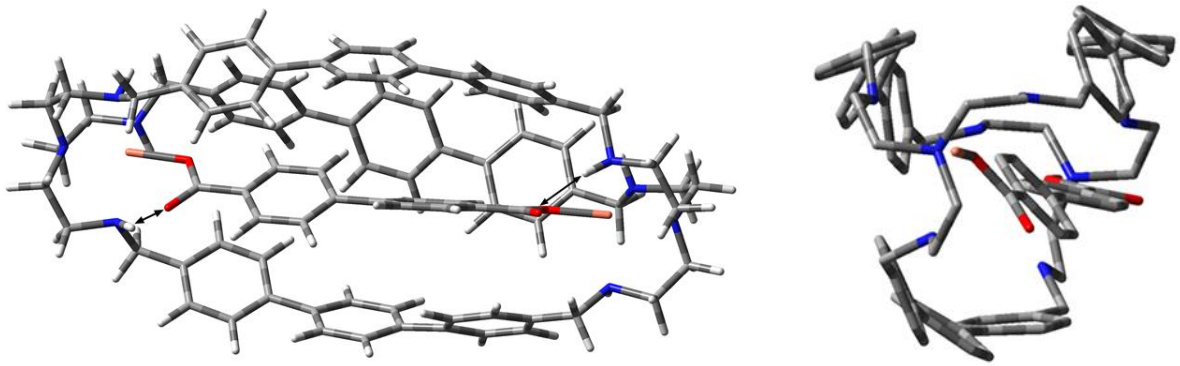

Figure 17. Lateral and side view of Cu_2**L**-dfc^{2-} adduct.

In the most stable conformation of the dicopper complex (see Figures 17 and 18), the Cu(II) ions have a distorted trigonal bipyramidal geometry with Cu-N distances: 2.02 Å (tertiary amine), 2.16, 2.19, 2.38 Å (secondary amines) and the Cu-Cu distance is 14.96 Å. Otherwise, the anion bite (COO-OOC distance) is slightly different in the case of dfc^{2-} and $sdbz^{2-}$, being 11.17 Å and 11.14 Å, respectively.

In the preferred conformer the anions do not lie in the center of the cavity but slightly outside. However, there is symmetry in coordination, because the Cu-carboxylate distance is the same on both sides (1.89 Å for dfc^{2-} and 1.91 Å for $sdbz^{2-}$, respectively).

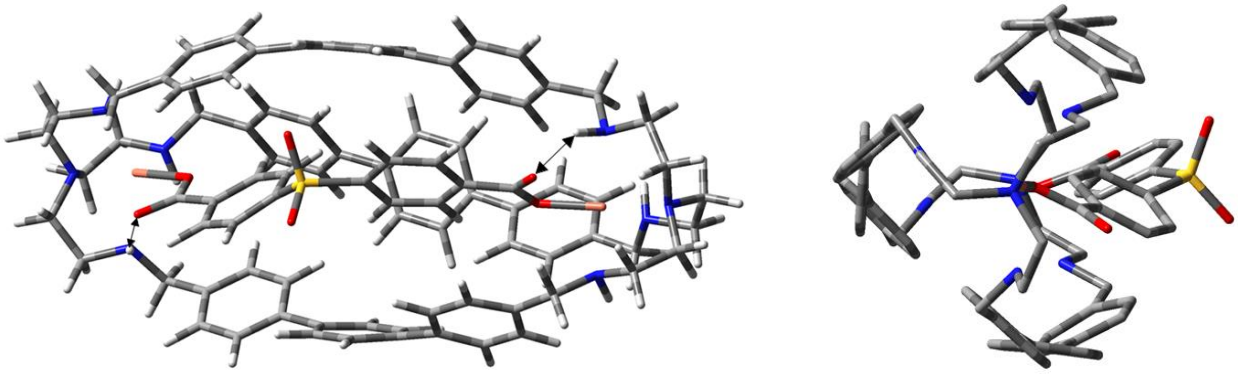

Figure 18. Lateral and side view of Cu_2**L**-$sdbz^{2-}$ adduct.

In both cases, each copper ion is coordinated by the carboxylate unit, which acts as a monodentate ligand, using only one oxygen in the metal coordination. Furthermore, the other oxygen atom of the carboxylate unit, in both structures, forms a hydrogen bond (indicated with the arrow in the figures) with the N-H group of the cage (O···H distance is 1.88 Å for dfc^{2-} and 1.92 Å for $sdbz^{2-}$, respectively). Finally, we performed calculations under the same conditions for the Cu_2**L**-terephtalate adduct (see Figure 19) to justify the minor interaction between receptor and anion, as observed in solution (see Tables 1 and 2).

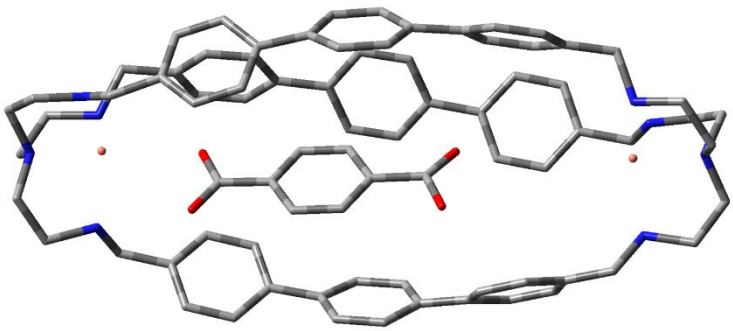

Figure 19. Lateral view of Cu_2**L**-tph^{2-} adduct.

For the terephthalate anion, the coordination is asymmetric (Cu-carboxylate distance: 2.87Å and 4.99Å), i.e. the anion is very closed to one of the two Cu(II) ions. This is reasonable considering the small size of this substrate compared to the other two examined. In fact, the anion bite is 7.39 Å[18], so it is too small to coordinate both metal centres, due to large distance between the copper ions (i.e. 14.96 Å).

These results open the way to future studies, much more focused on the conformational preferences of both host and guest.

5.3.8. EPR studies

Further information about our systems were obtained through EPR studies in MeCN:H_2O 4:1, pH = 7 (at 120 K). Samples were prepared using dicopper complex $[Cu_2\mathbf{L}]^{4+}$, at 0.3 mM concentration. The EPR spectrum of the dicopper complex displayed two different sets of not perfectly overlapped four-line signals (see a in Figure 20). This indicates that the two Cu^{II} centres are not identical and experience a different environment.

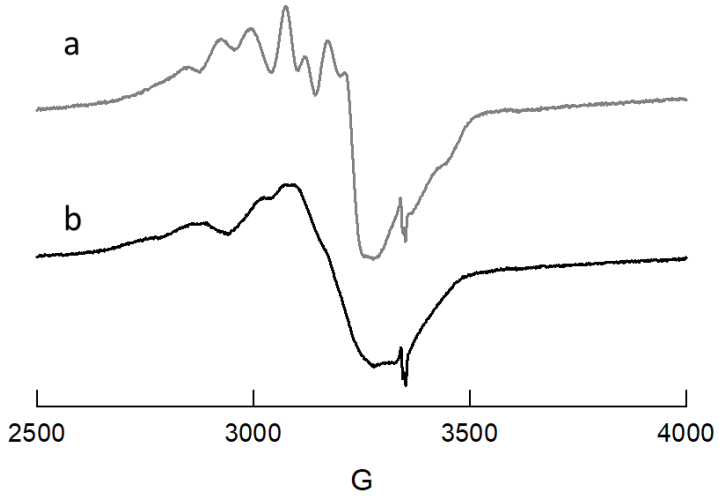

Figure 20. EPR spectra of $[Cu_2\mathbf{L}]^{4+}$ (a) and of its adduct with dfc^{2-} (b). The samples were prepared at 0.3 mM for $[Cu_2(\mathbf{L})]^{4+}$ and the anion in MeCN:H_2O 4:1 (v:v), pH =7. The EPR spectra were recorded at 31.81 mW, frequency (ν) of 9.40 GHz, and T = 120 K.

The experimental spectrum is better explained considering the presence of two not equivalent copper ions, i.e. their coordination spheres are different. In fact, two different sets of g and a values could be determined (g-tensor values: g1 = 2.355, g2 = 2.170, g3 = 2.085 and g1 = 2.355, g2 =

2.205, g3 = 2.065, respectively; hyperfine tensor values, in mT: a1 = 7.5, a2 = 4.5, a3 = 6.7 and a1 = 7.5, a2 = 4.5, a3 = 5.0, respectively; see Figure S7).

Interestingly, by addition of 1 eqv. of dfc^{2-} to the solution containing dicopper azacryptate, the EPR spectrum changed significantly (see b in Figure 20). This is probably due to the ferromagnetic interaction between the two copper(II) centers, promoted by the bridging anion dfc^{2-}, in the inclusion complex $[Cu_2\mathbf{L}\text{-}dfc]^{2+}$. This interaction was too weak to completely turn off magnetism but leads to the enlargement of the signal and consequently, the EPR spectra did not allow us to determine the set of parameters.

5.4. Conclusions

In this chapter, I reported the synthesis and characterization of a new azacryptand containing triphenyl spacers (**L**) suitable for the recognition of dicarboxylate anions with long bites. The cage **L** was synthesized from tren and [1,1':4',1''-Terphenyl]-4,4''-dicarboxaldehyde using a known procedure.[12] This new symmetrical cage has a longer and more lipophilic cavity than similar azacryptands (e.g. biphenyl or p-xylyl cage).[4,17] The low solubility of this cage in aqueous solution prohibits potentiometric investigations, so anion binding was followed using the dicopper complex. The binding properties of the dicopper complex were investigated towards lipophilic dicarboxylate anions, such as biphenyl-4,4′-dicarboxylate, dfc^{2-}; 4,4'-sulfonyldibenzoate, $sdbz^{2-}$; terephthalate, tph^{2-}; benzoate, bz^{-}, through both UV-vis. titrations and indicator displacement experiments. In the latter case, 6-TAMRA was chosen as a fluorescent indicator (**I**), due to the presence of a suitable binding group for the dicopper complex, i.e. the dicarboxylate unit. In the chemosensing ensemble solution, the dicopper complex binds and quenches the emission of 6-TAMRA. Upon addition of a competing anionic guest, the indicator was displaced from the azacryptand's cavity and fluorescence was restored. The dimetallic cryptate $[Cu_2\mathbf{L}]^{4+}$ interact very well with dfc^{2-} and $sdbz^{2-}$ anions with respect to the other investigated anions. This is due to capability of these two anions to match the distance between the two Cu(II) ions within the cryptate's cavity, as demonstrated through computational studies.

Supplementary Section

1S. NMR spectra

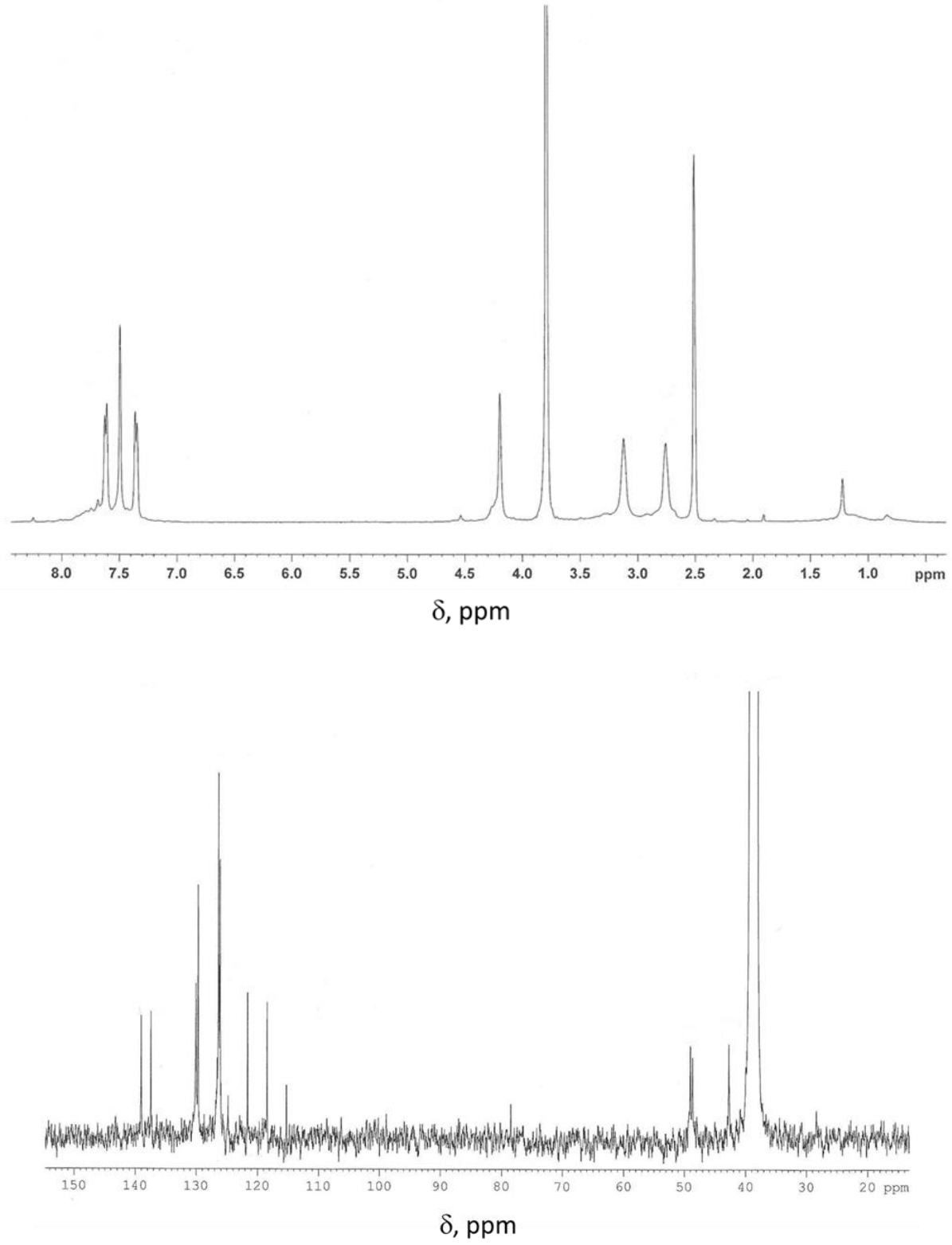

Figure S1. ^{1}H- and ^{13}C-NMR spectra of **L** in d_6-DMSO + 1M CF_3SO_3H in D_2O.

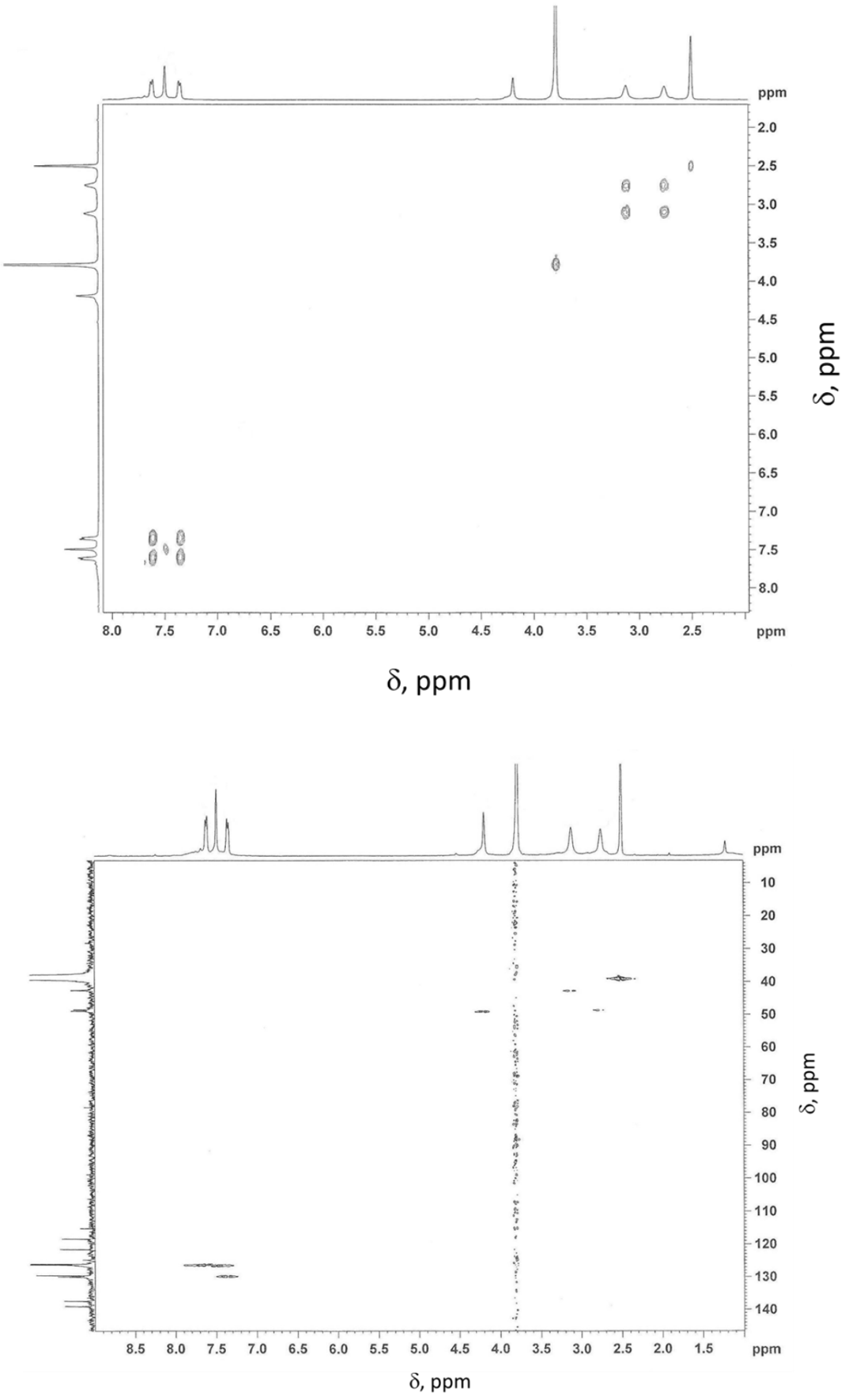

Figure S2. COSY and ^{1}H, ^{13}C-HSQC spectrum of **L** in d_6-DMSO + 1M CF_3SO_3H in D_2O.

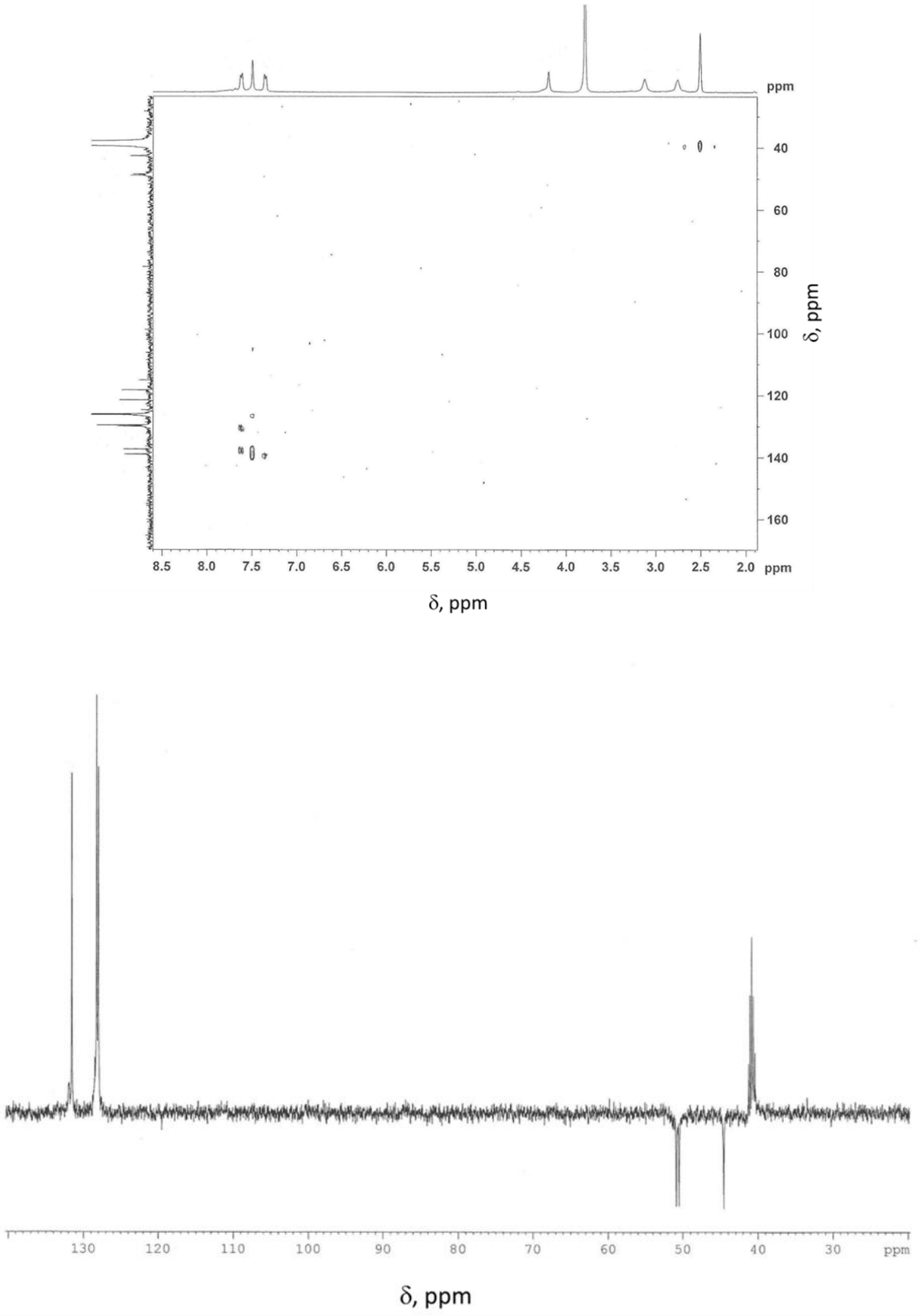

Figure S3. ^{1}H, ^{13}C-HMBC spectrum and DEPT135 of **L** in d_6-DMSO + 1M CF_3SO_3H in D_2O.

2S. ESI-MS spectra

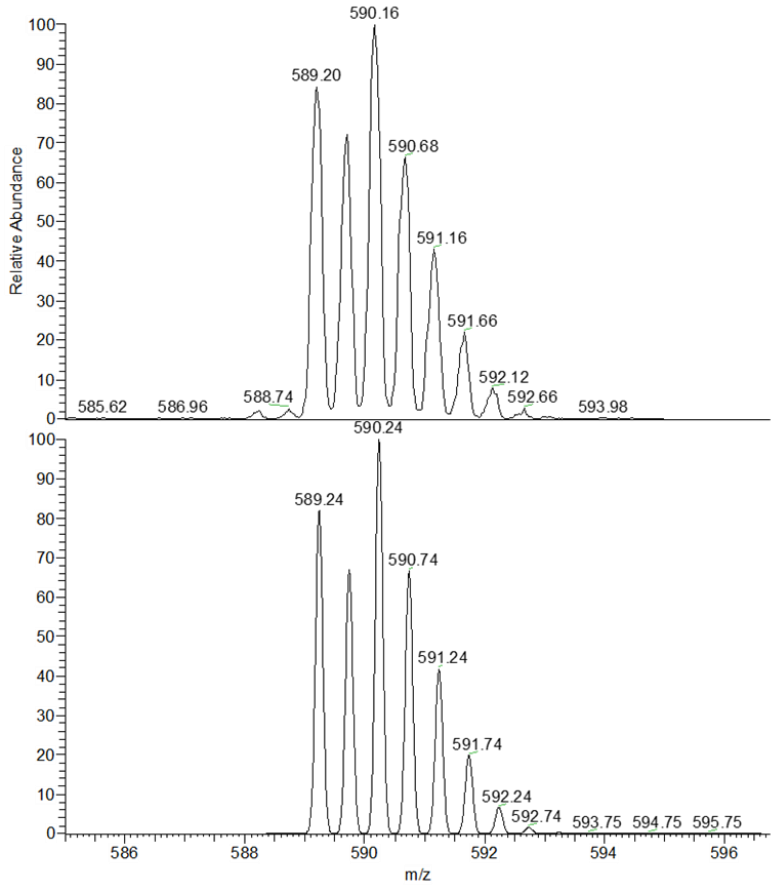

Figure S4. Top: zoom scan of the peak at 590 m/z, obtained from the experimental ESI-MS spectrum of a solution of $[Cu_2\mathbf{L}(CF_3SO_3)_4]$ in MeCN:H_2O 4:1. Bottom: simulated peak, calculated for the species $[Cu_2C_{72}H_{76}N_8]^{2+}$ (i.e. $[Cu^{II}_2(\mathbf{L}\text{-}2H^+)]^{2+}$).

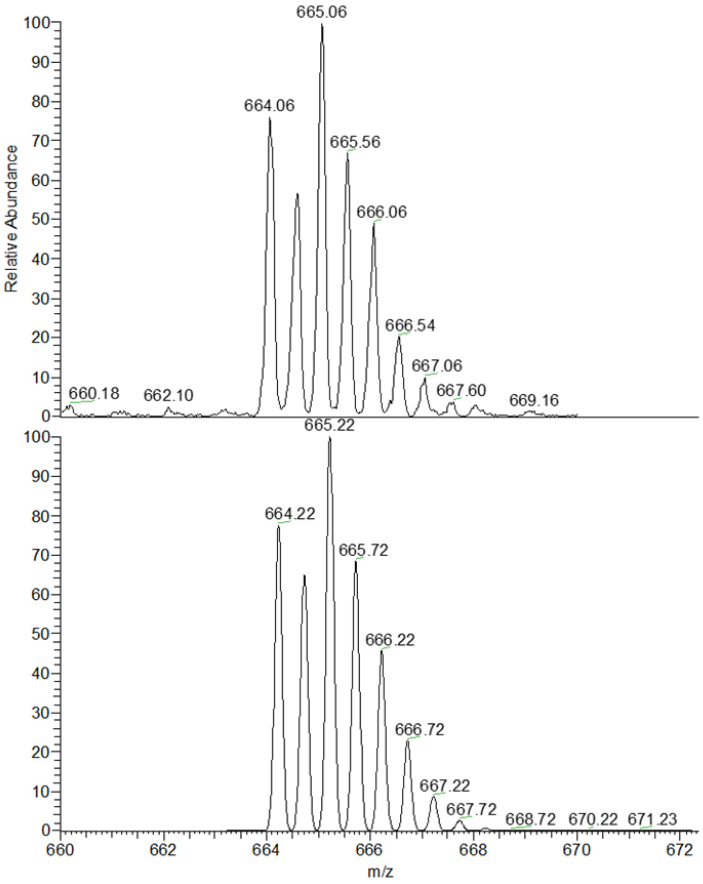

Figure S5. Top: zoom scan of the peak at 665 m/z, obtained from the experimental ESI-MS spectrum of a solution of $[Cu_2\mathbf{L}(CF_3SO_3)_4]$ in MeCN:H_2O 4:1. Bottom: simulated peak, calculated for the species $[Cu_2C_{73}H_{77}N_8O_3F_3S]^{2+}$ (i.e. $[Cu^{II}_2(\mathbf{L}\text{-}H{+}CF_3SO_3)]^{2+}$).

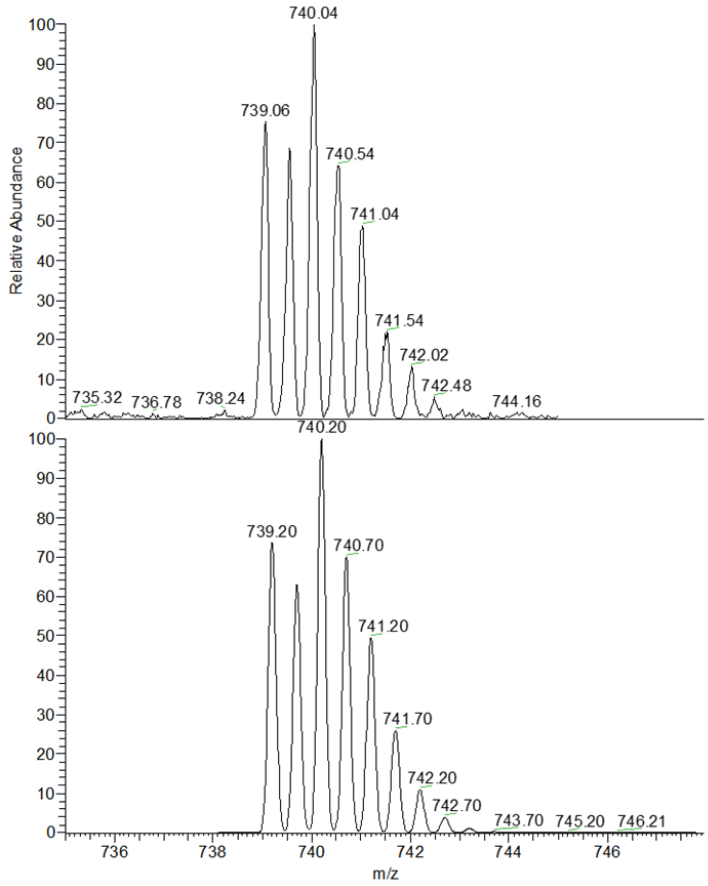

Figure S6. Top: zoom scan of the peak at 740 m/z, obtained from the experimental ESI-MS spectrum of a solution of $[Cu_2\mathbf{L}(CF_3SO_3)_4]$ in MeCN:H_2O 4:1. Bottom: simulated peak, calculated for the species $[Cu_2C_{74}H_{78}N_8O_6F_6S_2]^{2+}$ (i.e. $[Cu^{II}_2\mathbf{L}(CF_3SO_3)_2]^{2+}$).

In the case of dicopper complex, the ESI-MS studies revealed the presence of three double-charged species, in which either the copper centers are in the +2 oxidaton state, but in the first case (pick 590 m/z) ligand is doubly deprotonated ($[Cu^{II}_2(\mathbf{L}\text{-}2H^+)]^{2+}$), while in the second case (665 m/z) is once deprotonated ($[Cu^{II}_2(\mathbf{L}\text{-}H+CF_3SO_3)]^{2+}$). Notably, this processes (i.e. ligand deprotonation) is common in the ESI-MS spectra of copper complexes with polyamine ligands, especially using MeOH as solvent.[18]

3S. EPR studies

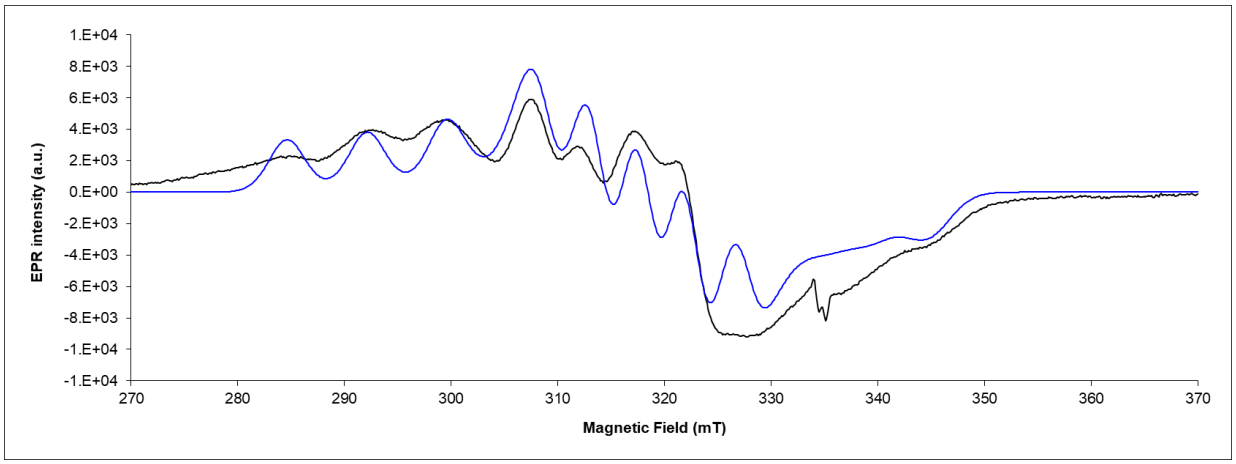

Figure S7. EPR spectrum of $[Cu_2(\mathbf{L})]^{4+}$ (0.3 mM in MeCN:H_2O 4:1 (v:v), pH = 7). The black one is the experimental spectrum, the blue one is simulated. The EPR parameters obtained from the simulation of experimental spectrum are: values of g-tensor g1 = 2.355, g2 = 2.170, g3 = 2.085 and g1 = 2.355, g2 = 2.205, g3 = 2.065; and values of the hyperfine tensor a1 = 7.5, a2 = 4.5, a3 = 6.7 and a1 = 7.5, a2 = 4.5, a3 = 5.0 (in mT).

References

[1] Sessler, J. L.; Gale, P. A.; Cho, W. S.; Anion Receptor Chemistry, (Monographs in Supramolecular Chemistry, ed. J. F. Stoddart), *Royal Society of Chemistry:* Cambridge, **2006**.

[2] Amendola, V.; Bergamaschi, G.; Miljkovic, A. *Supramol. Chem.*, **2017**, DOI:10.1080/10610278.2017.1339885 and references therein.

[3] Marcotte, N. and Taglietti, A.; *Supramolecular Chemistry*, **2003**, Vol. 15 (7-8), 617-625.

[4] Boiocchi, M.; Bonizzoni, M.; Fabbrizzi, L.; Piovani, G.; Taglietti, A.; *Angew. Chem. Int. Ed.*, **2004**, 43, 3847-3852.

[5] Mateus, P.; Delgado, R.; André, V.; Duarte, M.T.; *Inorg. Chem.*, **2015**, 54, 229-240.

[6] Mateus, P.; Lima, L. M. P.; Delgado, R. *Polyhedron*, **2013**, 52, 25-42.

[7] Wiskur, S. L.; Ait-Haddou, H.; Lavigne, J. J.; Anslyn, E. V.; *Acc. Chem. Res.*, **2001**, 34, 963.

[8] Bounos, G.; Ghosh, S.; Lee, A. K.; Plunkett, K. N.; DuBay, K. H.; Bolinger, J. C.; Zhang, R.; Friesner, R. A.; Nuckolls, C.; Reichman, D. R. and Barbara, P. F.; *J. Am. Chem. Soc*., **2011**, 133, 10155-10160.

[9] Borch, R. F.; Bernstein, M. D.; Dupont Durst, H.; *J. Am. Chem. Soc.*, **1971**, 93 (12), 2897-2904.

[10] Gans, P.; Sabatini, A.; Vacca, A.; *Talanta*, **1996**, 43, 1739-1753.

[11] Frisch, M. J. et al., Gaussian 09, revision B.01, Gaussian, Inc., Wallingford, CT, **2010**.

[12] Jazwinski, J.; Lehn, J. M.; Lilienbaum, D.; Ziessel, R.; Guilhem, J. and Pascard, C.; *J. Chem. Soc., Chem. Commun.*, **1987**, 1691.

[13] (a) Duggan, M.; Ray, N.; Hathaway, B.; Tomlinson, G.; Brint, P.; Pelin, K. *J. Chem. Soc., Dalton. Trans.* **1980**, 1342-1199. (b) Mateus, P.; Delgado, R.; Brandão, P.; Félix, V. *Chem. Eur. J.* **2011**, 17, 7020-7031. (c) Thaler, F.; Hubbard, C. D.; Heinemann, F. W.; van Eldik, R.; Schindler, S.; Fábián, I.; Dittler-Klingemann, A. M.; Hahn, F. E.; Orvig, C. *Inorg. Chem.* **1998**, 37, 4022-4029. (d) B. J. Hathaway and D. E. Billing, *Coord. Chem. Rev*., **1970**,5, 143; (e) R. J. Dudley, B. J. Hathaway, P. G. Hodgson, P. C. Power and D. J. Loose, *J. Chem. Soc., Dulron Trans*., **1974**, 1005.

[14] G. Alibrandi, V. Amendola, G. Bergamaschi, L. Fabbrizzi and M. Licchelli *Org. Biomol. Chem*., **2015**, 13, 3510-3524.

[15] McCleskey, S. C.; Metzger, A.; Simmons, C. S.; Anslyn, E. V.; *Tetrahedron*, **2002**, 58, 621.

[16] Amendola, V.; Bergamaschi, G.; Buttafava, A.; Fabbrizzi, L. and Monzani, E.; *J. Am. Chem. Soc.* **2010**, 132, 147-156.

[17] Yang, L. Z.; Li, Y.; Zhuang, X. M.; Jiang, L.; Chen, J. M.; Luck, R.L.; Lu, T. B.; *Chem.-Eur.J.* **2009**, 15, 12399

[18] Gianelli, L.; Amendola, V.; Fabbrizzi, L.; Pallavicini, P.; Mellerio, G. G.; *Rapid Commun. Mass Spectrom*. **2001**, 15, 2347-2353.

6. Pseudorotaxane structures from a dicopper(II) cryptate and dicarboxylate axles*

6.1. Introduction

As already mentioned, molecular cages are commonly applied by supramolecular researchers for achieving selective recognition of molecular guests in competing media.[1] In this work, we explored the possibility of using azacages to obtain novel supramolecular architectures, like (pseudo)rotaxane structures. [2]

The importance of this type of supramolecules is especially due to their application in the design of molecular machines, [3] as reported in the works by Beer,[4] Leigh,[5] Sauvage,[6] Stoddart[7] and other Authors. [8–9] The first work on rotaxanes was reported by Harrison et al. in 1967. [10] However, only recently, systems containing crown ether-based cryptands [11-15] and metal cages [16] have been applied in rotaxane preparation.

The aim of this work was to evaluate the application of dimetallic cages in the construction of (pseudo)rotaxane structures in aqueous solution. To achieve this goal we used the dicopper complex of the cage (**L**), reported by Fabbrizzi[17] as possible wheel and appropriately substituted terephthalate anions as the pseudo-thread ($\mathbf{2}^{2-}$-$\mathbf{4}^{2-}$).

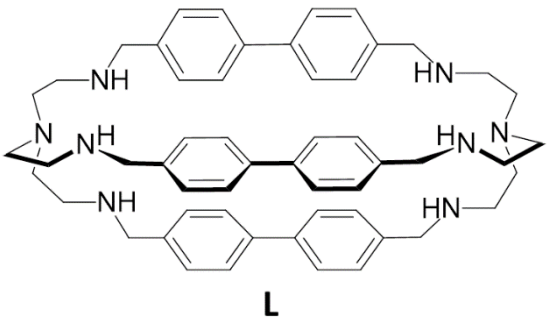

L

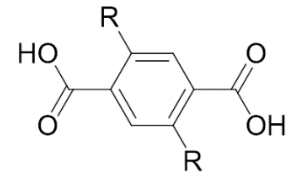

R: H H_2**1**

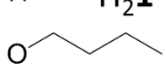

H_2**2**

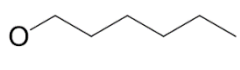

H_2**3**

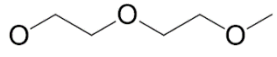

H_2**4**

* Text and figures reproduced in part with permission from "Self-Assembly of Pseudorotaxane Structures from a Dicopper(II) Molecular Cage and Dicarboxylate Axles" by V. Amendola, A. Miljkovic, L. Legnani, L. Toma, D. Dondi and S. Lazzaroni, ***Inorganic Chemistry***, Forum Article, http://pubs.acs.org/articlesonrequest/AOR-kTaPbRHIPU5sRNivVrtm **(DOI:** 10.1021/acs.inorgchem.7b02534) - copyright **2018** American Chemical Society.

In fact, this dicopper azacryptate, having rigid diphenyl spacers, was found to have a higher affinity for the terephthalate anion than for the other isomeric dicarboxylates. This result was due to the correspondence of terephthalate's bite (7.39 Å)[18] with the distance between the apical positions of copper ions in the cryptate, i.e. 7.355(4) Å. [17]

6.2. Experimental Section

All reagents and solvents were purchased from Sigma-Aldrich and Alfa-Aesar. Syntheses of azacryptand **L**[17] and of the dicarboxylic acids H_2**1**–H_2**4** [19-20] have been reported elsewhere. Mass spectra were acquired on a Thermo-Finnigan ion trap LCQ Advantage Max instrument equipped with an ESI source, NMR spectra on a Bruker AVANCE 400 spectrometer (operating at 9.37 T, 400 MHz). UV-Vis spectra were run on Varian Cary 50 and 100 SCAN spectrophotometers. EPR spectra were recorded on a Bruker EMX X-band continuous wave spectrometer equipped with a EPR cavity Bruker ER4119HS and a temperature control unit. All UV-vis. titrations were performed at 25°C on solutions of the dicopper complex $[Cu_2(\mathbf{L})](CF_3SO_3)_4$, obtained *in-situ* by adding 2 eqv. of $Cu(CF_3SO_3)_2$ to the solution of **L**. [17] For the determination of binding constants, solutions of the dicopper cryptate were titrated with 1000-fold more concentrated solutions of Na_2**1**–Na_2**4**. After each addition of the titrant solution, UV-Vis spectra were recorded (path length: 10 cm). Titration data were processed with the Hyperquad package [21] to determine the equilibrium constants. Solutions of the pseudo-rotaxanes for EPR and ESI-MS studies were obtained, by mixing the *in-situ* prepared $[Cu_2(\mathbf{L})](CF_3SO_3)_4$ complex with 1 eqv. of the thread in 9:1 (v:v) MeOH:H_2O mixture (0.005M HEPES, pH 7).

All the calculations were carried out using the GAUSSIAN09 program package.[22] The structures were optimized at the UB3LYP/6-31G(d) level [23] for all atoms, except Cu for which the effective core potential LanL2DZ was used. All the optimization were performed in water as solvent, using the classical polarizable continuum model (PCM).[24] Optimizations on both the singlet and triplet spin states were performed on the complexes.

6.2.1. Syntheses

6.2.1.1. Preparation of $Na_2$2

100 mg (0.32 mmol) of H_2**2** were dissolved in 15 mL of EtOH, 2.5 eqv of EtONa were then added and the mixture was stirred for 3 hours at room temperature.
Afterwards, the solution was concentrated, the white precipitate was filtered and dried under vacuum. Yield: 70%

HRMS (MeOH): m/z 311.1224 [H_2**2**+H]$^+$, 333.1302 [H_2**2**+Na]$^+$, 355.1121 [H**2**+2Na]$^+$, 377.0941 [**2**+3Na]$^+$, 643.2716 [2(H_2**2**)+Na]$^+$.

UV-vis. (MeOH:H_2O 9:1, pH 7 HEPES buffer): λ_{max} = 313 nm, ε_{max} = 2412 M^{-1} cm^{-1}

^{1}H-NMR (CD_3OD, 400 MHz), δ (ppm): 7.06 (s, 2H, H-a), 4.00 (t, 4H, H-b), 1.76 (m, 4H, H-c), 1.52 (m, 4H, H-d), 0.99 (t, 6H, H-e).

^{13}C-NMR (CD_3OD, 400 MHz), δ (ppm): 150.17, 131.86, 114.53, 69.66, 31.96, 19.38, 13.28.

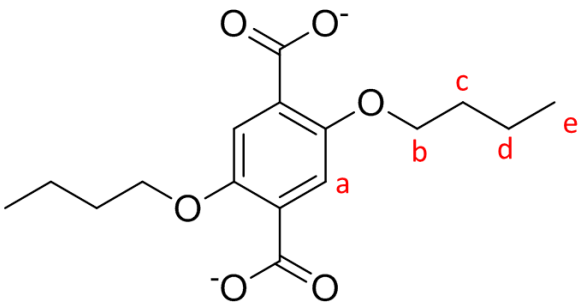

6.2.1.2. Preparation of $Na_2$3

100 mg (0.27 mmol) of H_2**3** were dissolved in 15 mL of EtOH, 2.5 eqv of EtONa were added and the reaction mixture was stirred for 3 hours at room temperature.
The solution was then concentrated, the white precipitate was filtered and dried under vacuum. Yield: 80%

UV-vis. (MeOH:H_2O 9:1, pH 7 HEPES buffer): λ_{max} = 313 nm, ε_{max} = 3679 M^{-1} cm^{-1}

HRMS (MeOH): m/z 367.1849 [H_2**3**+H]$^+$, 389.1927 [H_2**3**+Na]$^+$, 411.1746 [H**3**+2Na]$^+$, 755.3963 [2(H_2**3**)+Na]$^+$

^{1}H-NMR (CD_3OD, 400 MHz), δ (ppm): 7.12 (s, 2H, H-a), 4.02 (t, 4H, H-b), 1.79 (m, 4H, H-c), 1.49 (m, 4H, H-d), 1.37 (m, 8H, H-e H-f), 0.94 (t, 6H, H-g).

^{13}C-NMR (CD_3OD, 400 MHz), δ (ppm): 150.30, 114.96, 70.10, 32.13, 29.59, 25.88, 22.63, 13.29.

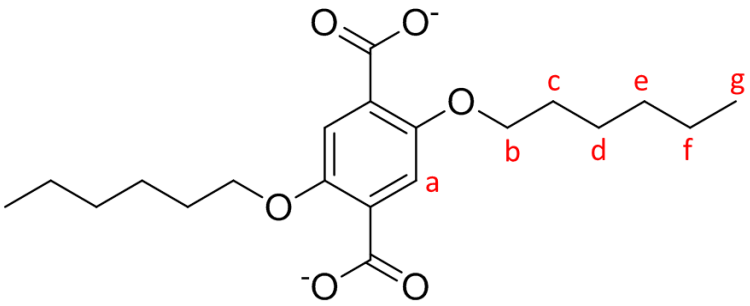

*6.2.1.3. Preparation of Na_2**4***

100 mg (0.25 mmol) of H_2**4** were dissolved in 15 mL of EtOH, 2.5 eqv of EtONa were added and the reaction mixture was stirred for 3 hours at room temperature.
The solution was then concentrated, the white precipitate was filtered and dried under vacuum. Yield: 75%

UV-vis. (MeOH:H_2O 9:1, pH 7 HEPES buffer): λ_{max} = 310 nm, ε_{max} = 3310 M^{-1} cm^{-1}

HRMS (MeOH): m/z 425.1413 $[H_2\mathbf{4}+Na]^+$, 447.1233 $[H\mathbf{4}+2Na]^+$

^{1}H-NMR (CD_3OD, 400 MHz), δ (ppm): 7.28 (s, 2H, H-a), 4.21 (t, 4H, H-b), 3.86 (t, 4H, H-c), 3.74 (t, 4H, H-d), 3.59 (t, 8H, H-e), 3.38 (s, 6H, H-f).

^{13}C-NMR (CD_3OD, 400 MHz), δ (ppm): 152.14, 116.91, 73.33, 71.90, 70.98, 70.81, 59.42.

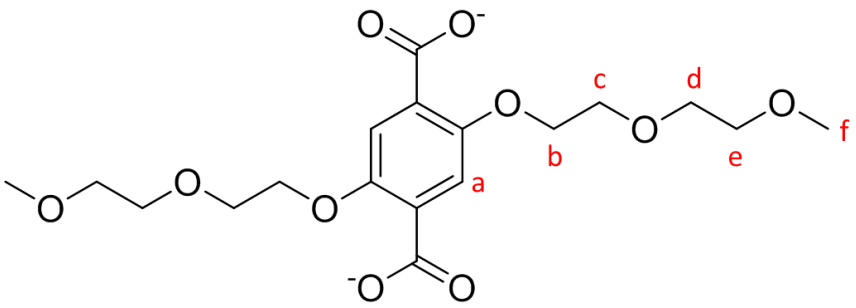

6.3. Results and Discussion

The dicopper(II) complex of cage **L** was synthesized and studied by Fabbrizzi et al. as a receptor for dicarboxylate anions in water.[17] These studies demonstrated the very high affinity of $[Cu_2(\mathbf{L})]^{4+}$ for the terephthalate anion.

In this chapter, we exploited the affinity of $[Cu_2(\mathbf{L})]^{4+}$ for the appropriately substituted terephthalate anions to obtain the spontaneous assembling of pseudorotaxane structures in aqueous solution. The first step was the functionalization of the terephthalic acid, to obtain a family of novel molecular threads. As the reagent, we used diethyl 2,5-dihydroxyterephthalate, following a procedure reported in the literature to obtain compounds H_2**2**-H_2**4.** Then acids were treated with EtONa and precipitated as the sodium salts Na_2**2**-Na_2**4**. All the molecular threads had a terephthalate unit, potentially capable of bridging the azacryptate's copper centers, and two arms [**2** = *n*-butoxy-; **3** = *n*-hexyloxy-; **4** = 2-(2-methoxyethoxy)ethoxy-], pending on both sides of the terephthalate group. Due to the poor solubility of Na_2**2**, Na_2**3** and the dicopper complex in pure water, experimental studies were done in MeOH:H_2O 9:1 (v:v) at pH 7 (HEPES buffer).

6.3.1. Spectrophotometric studies

The interaction between the anionic guests, i.e. Na_2**2–**Na_2**4**, and the dicopper complex $[Cu_2\mathbf{L}]^{4+}$ was studied by UV-vis spectroscopy following two different strategies (see Figure 1).

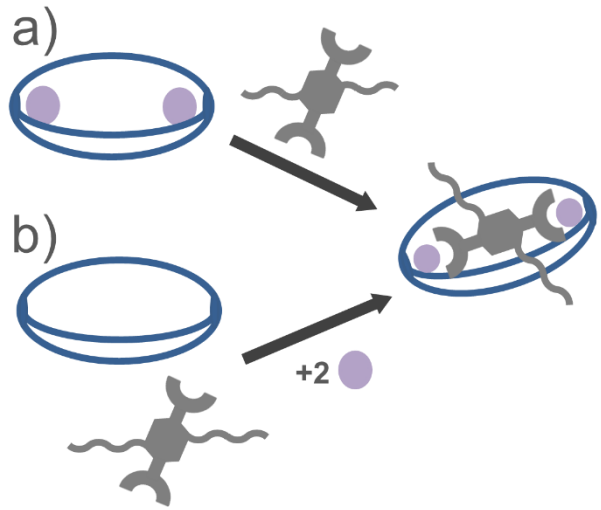

Figure 1. Strategies followed for self-assembling studies.

Strategy a) is the "classical" approach, that consists in the titration of the dicopper complex with solutions of Na_2**2**-Na_2**4** in MeOH:H_2O 9:1 (v:v, 0.005 M HEPES pH 7, T=25°C). Solutions of $[Cu_2(\mathbf{L})](CF_3SO_3)_4$ (70 μM) were prepared, by mixing the azacryptand with 2 eqv. of $Cu(CF_3SO_3)_2$ in water/methanol mixture. These solutions were than characterized by ESI-MS spectrometry, which showed the presence of the dicopper complex, as the dominant species (see Figure S10). The UV-vis. spectra of $[Cu_2(\mathbf{L})]^{4+}$ solutions showed the typical d-d bands of dicopper cryptates, with a maximum around 800 nm and a weak shoulder at 680 nm (path length: 10 cm, see the black dotted line in Figures below). These results indicate that the Cu(II) ions have a trigonal bipyramidal geometry.[17]

Titrations with solutions of threads (i.e. Na_2**2–** Na_2**4)** showed that the d-d bands of the dicopper complex change (see Figures 2-4) due to a variation in the coordination sphere of the Cu(II) ions. For all the investigated guests, the titration profiles showed a slope variation around 1 eqv. of the added anion, indicating the formation of a 1:1 adduct.

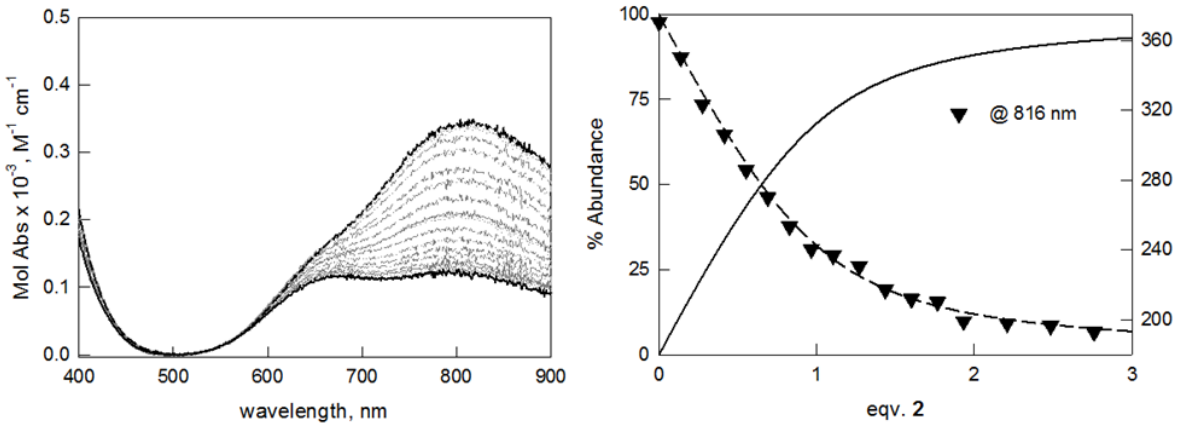

Figure 2. On the left: family of UV-vis. spectra taken upon titration of $[Cu_2(\mathbf{L})]^{4+}$ (70μM) with Na_2**2** (dashed black line: initial spectrum; solid black line: final spectrum) in MeOH:H_2O 9:1 (0.005M HEPES, pH 7). On the right: profile of Molar Absorbance (at 816 nm) *vs.* eqv. of the added axle, with the superimposed diagram of the species in solution, calculated for $Log K_{11}$ = 4.98(2). Reproduced with permission from ref. 28.

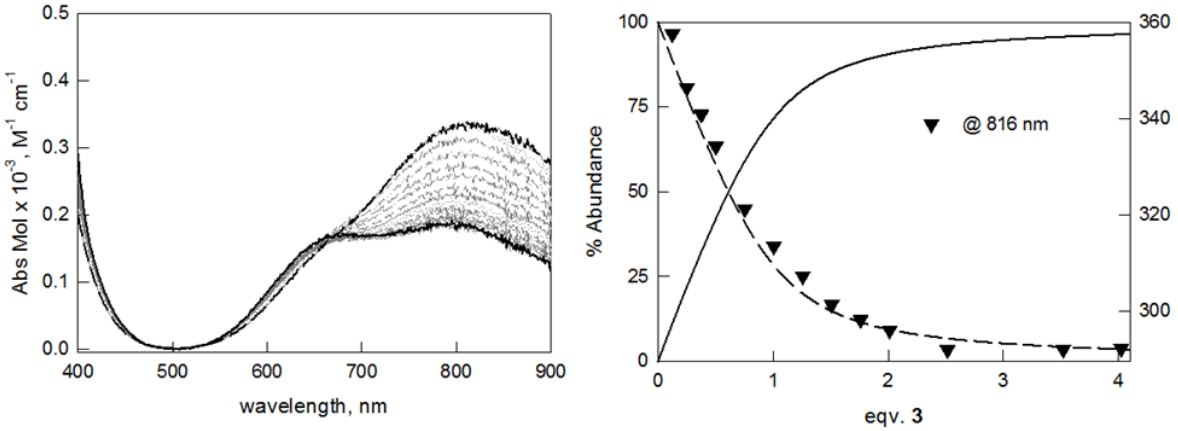

Figure 3. On the left: family of UV-vis. spectra taken upon titration of $[Cu_2(\mathbf{L})]^{4+}$ (70μM) with Na_2**3** (dashed black line: initial spectrum; solid black line: final spectrum) in MeOH:H_2O 9:1 (0.005M HEPES, pH 7). On the right: profile of Molar Absorbance (at 816 nm) *vs.* eqv. of the added axle, with the superimposed diagram of the species in solution, calculated for *Log*K_{11} = 5.10(3). Reproduced with permission from ref. 28.

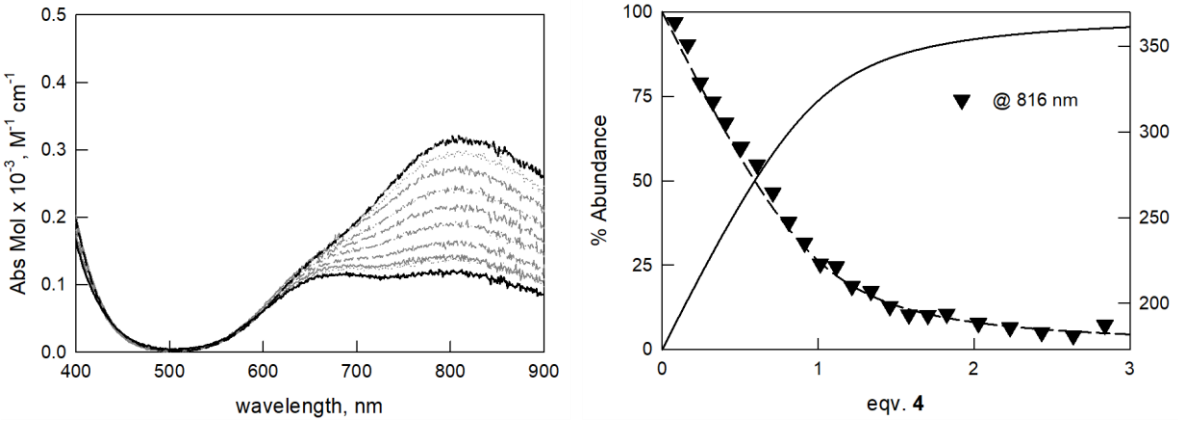

Figure 4. Left: family of UV-vis. spectra taken upon titration of $[Cu_2(\mathbf{L})]^{4+}$ with a solution of Na_2**4** (dashed black line: initial spectrum; solid black line: final spectrum) in MeOH:H_2O 9:1 (0.005M HEPES, pH 7). Right: profile of Molar Absorbance (at 816 nm) *vs.* eqv. of the added axle, with the superimposed diagram of the species in solution, calculated for *Log*K_{11} = 5.18(1). Reproduced with permission from ref. 28.

We also performed the spectrophotometric titration with the sodium salt of terephthalate, Na_2**1**, to evaluate the interaction between the guest and the host in our conditions (i.e. MeOH:H_2O 9:1 v:v, 0.005 M HEPES pH 7, T=25°C). In this case (Figure 5), the titration profile was very steep (*Log*K_{11} > 6), confirming the high affinity of complex $[Cu_2(\mathbf{L})]^{4+}$ for this dicarboxylate guest, as found by Fabbrizzi in pure water.[17]

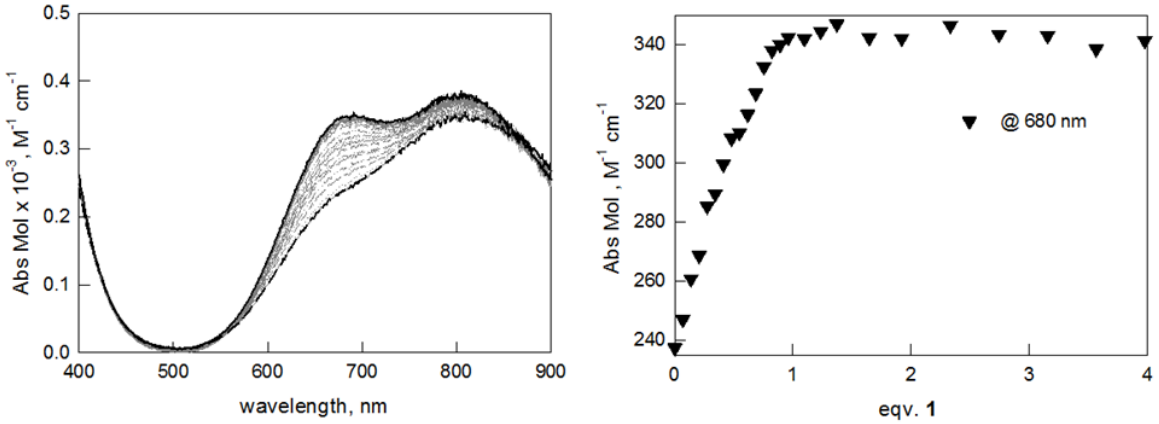

Figure 5. On the left: family of UV-vis. spectra taken upon titration of $[Cu_2(\mathbf{L})]^{4+}$ (70μM) with $Na_2\mathbf{1}$ (dashed black line: initial spectrum; solid black line: final spectrum) in MeOH:H_2O 9:1 (0.005M HEPES, pH 7). On the right: profile of Molar Absorbance (at 680 nm) *vs.* eqv. of the added axle. Reproduced with permission from ref. 28.

The fitting of the titration data allowed us to determine the binding constants for $\mathbf{2}^{2-}$–$\mathbf{4}^{2-}$ (see Table 1). For the investigated guests, the binding constants are similar to each other, but the affinity is significantly lower than that for the terephthalate anion. This implies that the presence of lateral chains reduces the affinity of the anions for $[Cu_2(\mathbf{L})]^{4+}$.

Anion	***LogK$_{11}$***
$\mathbf{2}^{2-}$	4.98(2)
$\mathbf{3}^{2-}$	5.10(3)
$\mathbf{4}^{2-}$	5.18(1)

Table 1. Affinity constants determined by UV-vis titrations with threads (as Na salts) in MeOH:H_2O 9:1 (0.005M HEPES, pH 7) . In parenthesis, the standard deviations are reported.

Strategy b) consists in spectrophotometric titration of solution containing equimolar amounts of threads (i.e. $\mathbf{3}^{2-}$and $\mathbf{4}^{2-}$**)** and **L** (70μM), with standard $Cu(CF_3SO_3)_2$ in MeOH:H_2O 9:1 (0.005M HEPES, pH 7). This strategy was chosen to confirm the role of Cu(II). In fact, the interaction of the threads with the azacryptand is mostly driven by the binding of the terephthalate unit to the two Cu(II) ions within the cage's cavity. In the Figures 7 and 8, the spectra recorded during the titrations with Cu^{II} are reported.

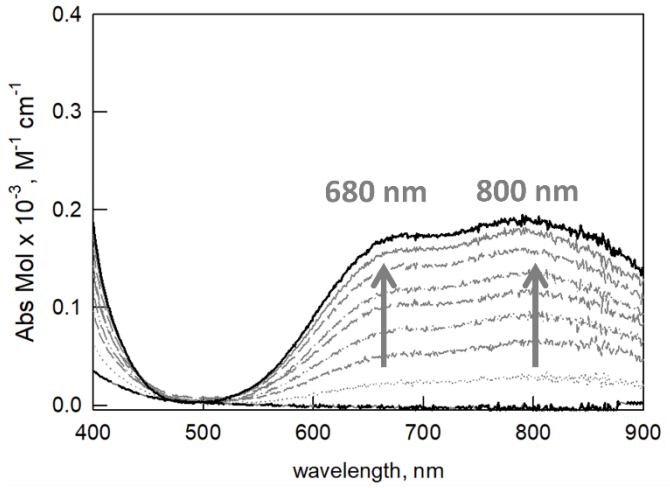

Figure 6. UV-vis. spectra taken upon the addition of sub-stoichiometric amounts of $Cu(CF_3SO_3)_2$ to an equimolar solution of **L** and $\mathbf{3}^{2-}$ in MeOH:H_2O 9:1 ([**L**] = [$\mathbf{3}^{2-}$]= 70μM; 0.005M HEPES, pH 7). Reproduced with permission from ref. 28.

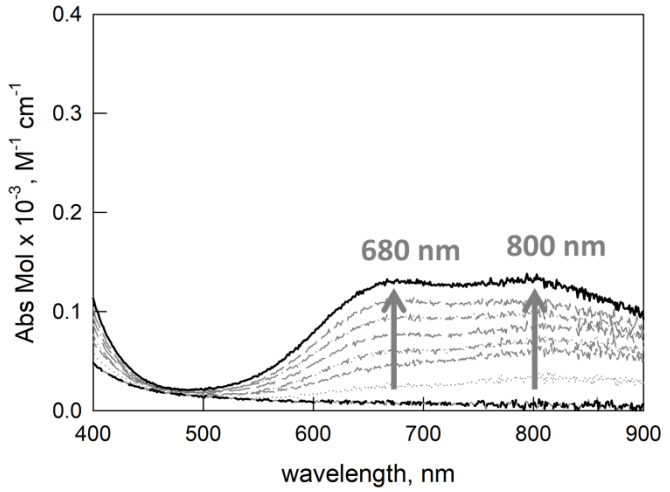

Figure 7. UV-vis. spectra taken upon the addition of sub-stoichiometric amounts of $Cu(CF_3SO_3)_2$ to an equimolar solution of **L** and $\mathbf{4}^{2-}$ in MeOH:H_2O 9:1 ([**L**] = [$\mathbf{4}^{2-}$]= 70 μM; 0.005M HEPES, pH 7). Reproduced with permission from ref. 28.

Upon Cu(II) addition, the development of d-d bands (at ~ 680 and ~ 800 nm) showed the formation of the inclusion complexes (see Figures 7 and 8 for $[Cu_2(\mathbf{L})\text{-}\mathbf{3}]^{2+}$ and $[Cu_2(\mathbf{L})\text{-}\mathbf{4}]^{2+}$, respectively). As expected, the maximum absorbance of the two bands was achieved around 2 eqv. of Cu(II). The final spectrum corresponded to that obtained with Strategy a), after the addition of 1eqv. of the thread to the $[Cu_2(\mathbf{L})]^{4+}$ complex. This result confirms that both approaches [a) and b) in Figure 1] lead to the same result, i.e. the spontaneous assembling of the $[Cu_2(\mathbf{L})\text{-thread}]^{2+}$ adduct.

Unfortunately, due to precipitation of $Cu(OH)_2$ after the equivalence, the binding constants were not determined.

6.3.2. ESI-MS studies of the adducts

We also performed ESI mass spectrometry studies on equimolar solutions of the threads and $[Cu_2(\mathbf{L})]^{4+}$ (70 μM, 0.005M HEPES in MeOH:H_2O 9:1, pH 7) to confirm the formation of stable 1:1 complexes between the receptor and the anions (i.e. $\mathbf{3}^{2-}$ and $\mathbf{4}^{2-}$).

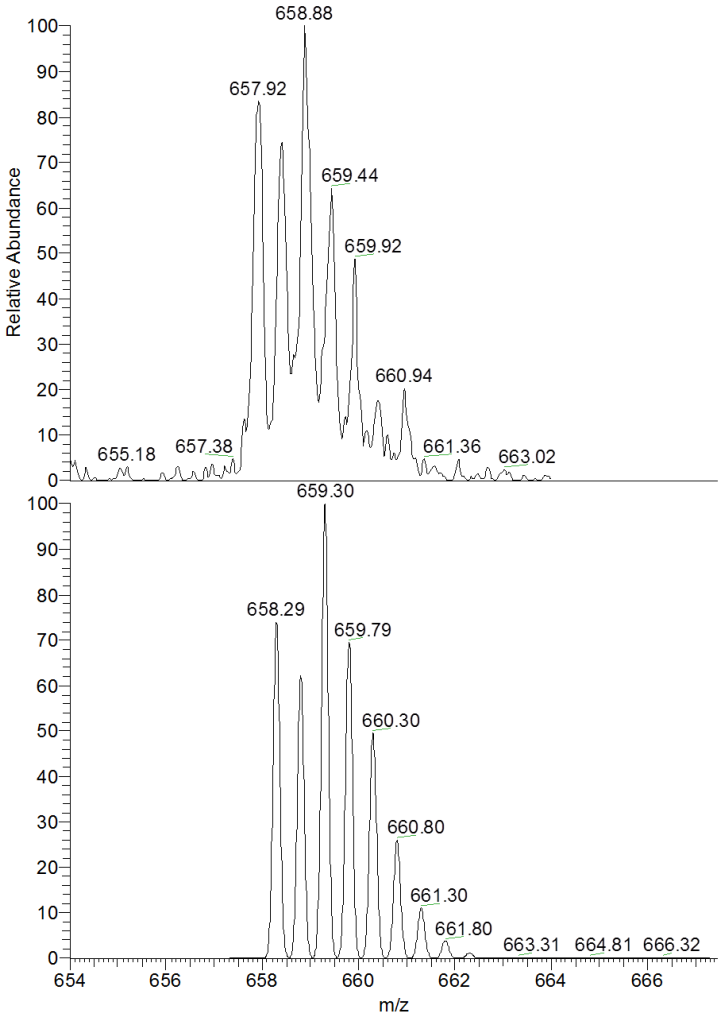

Figure 8. Top: zoom scan of the peak at 659 m/z, obtained from the experimental mass spectrum of an equimolar solution of $[Cu_2(\mathbf{L})]^{4+}$ and $\mathbf{3}^{2-}$ in MeOH:H_2O 9:1 (0.005M HEPES, pH 7). Bottom: simulated peak, calculated for the species $[Cu_2C_{74}H_{94}N_8O_6]^{2+}$ (i.e. $[Cu_2(\mathbf{L})\text{-}\mathbf{3}]^{2+}$). Reproduced with permission from ref. 28.

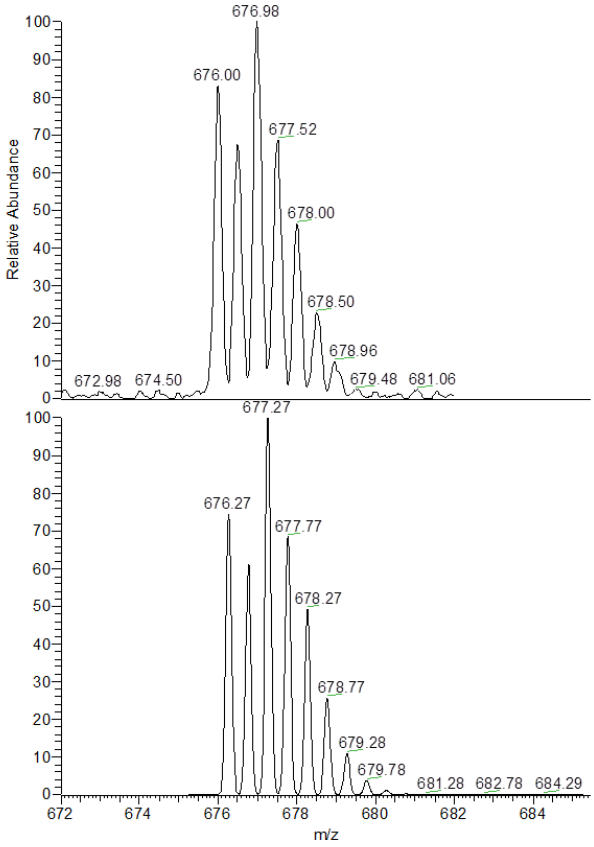

Figure 9. Top: zoom scan of the peak at 677 m/z, obtained from the experimental mass spectrum of an equimolar solution of $[Cu_2(\mathbf{L})]^{4+}$ and $\mathbf{4}^{2-}$ in MeOH:H_2O 9:1 (0.005M HEPES, pH 7). Bottom: simulated peak, calculated for the double charged assembly $[Cu_2C_{72}H_{90}N_8O_{10}]^{2+}$ (i.e. $[Cu_2(\mathbf{L})\text{-}\mathbf{4}]^{2+}$). Reproduced with permission from ref. 28.

Figure 8 and 9 show the experimental peaks corresponding to the complexes $[Cu_2(\mathbf{L})\text{-}\mathbf{3}]^{2+}$ and $[Cu_2(\mathbf{L})\text{-}\mathbf{4}]^{2+}$, respectively (see Figures S11 for $[Cu_2(\mathbf{L})\text{-}\mathbf{1}]^{2+}$). The comparison with the simulated zoom scan (shown below) confirmed the attribution of the signals to the species of formula $[Cu_2C_{74}H_{94}N_8O_6]^{2+}$ and $[Cu_2C_{72}H_{90}N_8O_{10}]^{2+}$ in the case of $[Cu_2(\mathbf{L})\text{-}\mathbf{3}]^{2+}$ and $[Cu_2(\mathbf{L})\text{-}\mathbf{4}]^{2+}$, respectively.

6.3.3. EPR Studies

Further information about our systems were obtained through EPR studies in MeOH:H_2O 9:1 (HEPES buffer, pH 7 at 120 K). Samples were prepared by mixing azacryptand **L** 0.5mM with 2 eqv. of $Cu(CF_3SO_3)_2$.

The EPR spectrum of the dicopper complex displayed the typical four-line hyperfine pattern of Cu(II) (I = 3/2) complexes, indicating that the two metal centers are identical and independent [see a) in Figure 10]. In fact, a single set of g and A values could be determined (g-tensor values: g1 =

2.29, g2 = 2.20, g3 = 2.08; hyperfine tensor values, in mT: a1 = 10.0, a2 = 3.0, a3 = 5.6, see Figure S12). This is due to the large separation between the copper ions, corresponding to 11.305(6) Å.[17]

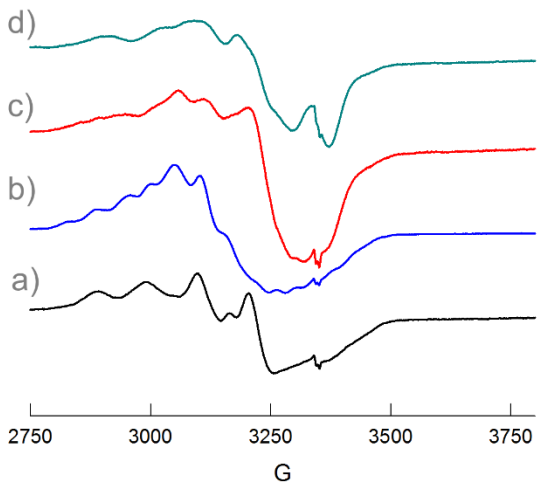

Figure 10. EPR spectra of a) $[Cu_2(\mathbf{L})]^{4+}$ and of its adducts with b) $\mathbf{1}^{2-}$, c) $\mathbf{2}^{2-}$ and d) $\mathbf{4}^{2-}$ dicarboxylates. The samples were prepared at 0.5 mM for $[Cu_2(\mathbf{L})]^{4+}$ and the guests in MeOH:H_2O 9:1 (v:v), pH = 7. The EPR spectra were recorded at 31.81 mW, frequency (ν) of 9.395 GHz, and T = 120 K. Reproduced with permission from ref. 28.

By addition of $Na_2\mathbf{1}$ (1 eqv.) to the azacryptate, the EPR spectrum changed significantly. In fact, two four-line not perfectly overlapped signals appeared. This is due to the different coordination sphere of the two Cu(II) ions, promoted by the bridging anion $\mathbf{1}^{2-}$ in the inclusion complex $[Cu_2(\mathbf{L})\text{-}\mathbf{1}]^{2+}$ [see b) in Figure 10].

Also the EPR spectra of solutions containing equimolar amounts of $[Cu_2(\mathbf{L})]^{4+}$ and the threads [see c) and d) for $\mathbf{2}^{2-}$ and $\mathbf{4}^{2-}$, respectively and Figure S13 for $\mathbf{3}^{2-}$] indicate that the two Cu(II) centers are not identical i.e. their coordination spheres are different.

Unfortunately, in this case the quality of the EPR spectra did not allow us to determine the set of parameters. This is probably due to the presence of different conformations at the equilibrium for the pseudo-rotaxane structures in solution. This hypothesis was verified by computational studies.

6.3.4. Computational studies

In the absence of crystals suitable for diffraction studies, insights into the structure of our assemblies were provided by computational investigations in solvent, through DFT calculations. Starting from the crystal structure of the compound $[Cu^{II}_2(\mathbf{L})(H_2O)_2](NO_3)_4\cdot 2H_2O$ [17], we used the crystallographic coordinates of the complex $[Cu^{II}_2(\mathbf{L})(H_2O)_2]^{4+}$ for a first optimization setting the

spin multiplicity at the triplet state. The optimized structure (Figure 11) maintained unchanged all the structural features of the starting geometry, *i.e.* the trigonal-bipyramidal geometry at each copper center, a Cu···Cu distance of 11.19 Å (11.31 Å in the crystal structure), the same chirality at the *tren* subunits [all the three dihedral angle τ_{tren} (N_{tert}-C-C-N_{sec}) of both *trens* are positive with values of ≈ 50-55°], the *S* configuration of the three diphenyl moieties.

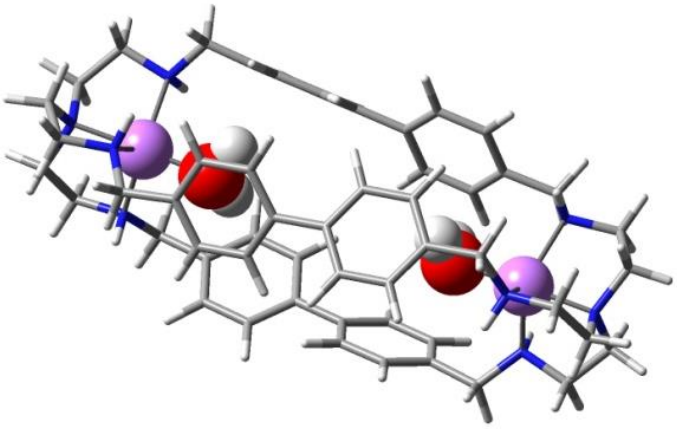

Figure 11. Optimized structure of the complex $[Cu^{II}_2(\mathbf{L})(H_2O)_2]^{4+}$. Reproduced with permission from ref. 28.

Then, we started the investigation of the three-dimensional properties of the inclusion complex $[Cu_2(\mathbf{L})\text{-}\mathbf{1}]^{2+}$ by building a series of different starting geometries, obtained by replacement of the coordinated water molecules with a terephthalate anion, and taking into account the conformational freedom of both the host and the guest. Each terephthalate's carboxylate group should coordinate with copper in a monodentate η^1 fashion but, in principle, the bidentate η^2 fashion cannot be excluded. Moreover, also in the case of η^1 coordination on both metal centers, the coordinating oxygen atoms may be on the same side of terephthalate (i.e. "*cis*") or on opposite sides ("*trans*") with, respectively, a shorter or longer bite length. As far as the host is concerned, we explored the possibility of alternative geometries in which the complex shows the *tren* units with opposite chirality ($\tau_{tren} \approx 50°$ at one subunit and $\tau_{tren} \approx -50°$ at the other one). Taking into consideration also the configuration of the diphenyl moieties, we named this situation as *meso-SSS*-host opposed to *homo-SSS*-host, the case in which the *tren* units have the same chirality. This means that geometries with the *meso-RRR*-host and *homo-RRR*-host arrangements have to be built and optimized as well as intermediate situations with co-existing *R* and *S* diphenyl configurations.

Actually, after optimization of all the conceivable starting geometries of the complex, a group of conformers very close in energy, **1A**-**H** (Figure 12), were found to be largely preferred; all of them

show a η^1 coordinated terephthalate anion with a "*cis*" carboxylate arrangement. Compared to the C_2 symmetrical global minimum **1A** (*homo-SSS*-host), the other conformers differ either in the diphenyl or in the *tren* chirality. Conformer **1B**, for example, differs only in the configuration of one diphenyl group (*homo-RSS*-host) and is only 1.90 kcal/mol higher in energy. Conformer **1D** is even more stable (E_{rel} = 0.62 kcal/mol), though it has all the three diphenyls in the *R* configuration (*homo-RRR*-host). The most stable *meso*-host conformer, **1E**, which differs from **1A** only in the chirality of a *tren* subunit, has a relative energy of 1.47 kcal/mol. Notably, the coordination mode in **1A** is very similar to that found by Delgado et al. in the crystal structure of the terephthalate inclusion complex of the dicopper azacryptate with biphenylmethane spacers. [25] In fact, a bowl conformation is adopted in **1A** by the receptor, which binds the terephthalate anion through hydrogen bonds, C-H$\cdots\pi$ and $\pi\cdots\pi$ interactions, in addition to the carboxylate coordination to copper. One side of the terephthalate benzo group point towards the cage's cavity and the other one outside, thus differentiating the unsubstituteted aromatic positions. The coordinated carboxylate oxygen atoms and the Cu$\cdots$Cu distances are, respectively, 6.85 and 10.67 Å with Cu-O distances of 1.91 Å. Notably, in the crystal structure of the complex coordinating two water molecules, [17] the separation between the water oxygen atoms was slightly longer, 7.355(4) Å, but the value of 6.85 Å for **1A** is in full agreement with the value of 6.946(11) Å found in the Delgado's inclusion complex. Each Cu(II) center located in the *tren* subunits features a trigonal-bipyramidal geometry distorted towards a square-pyramidal geometry, as indicated by the value (τ = 0.79) of the corresponding index structural parameter [26] and by the elongation of one of the Cu-N_{sec} bonds that assumes the value of 2.33 Å compared to 2.23 and 2.28 Å for the two other non-apical Cu-N_{sec} bonds.

The "*trans*" terephthalate arrangement was found to originate much less stable complexes, the two most significant being reported in Figure 12. When combined with η^1 coordination a "*trans*" terephthalate gives rise to a conformer, **1I**, less stable by 14.62 kcal/mol, whereas with η^2 coordination an even less stable complex **1J** (16.10 kcal/mol) could be located. In these cases, it should be noted the longer distance of the coordinated carboxylate oxygen atoms (bite length), 7.09 and 7.35 Å for **1I** and **1J**, respectively, though the Cu$\cdots$Cu distance is almost unchanged (10.76 and 10.69 Å, respectively).

To verify that the triplet state was preferred over the other possible spin states, optimizations of the $[Cu_2(\mathbf{L})\text{-}\mathbf{1}]^{2+}$ adduct in the **1A** geometry were performed in the singlet state both in the closed and open-shell mode. As expected, the closed-shell singlet state was found to be considerably disfavored, being 39.51 kcal/mol less stable than the triplet. Conversely, the energy of the open-

shell singlet was identical with that of the triplet. No significant differences in the geometry of the complex was found among the three different spin states.

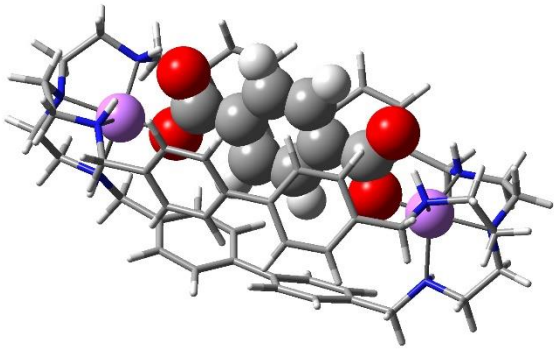

1A (*homo-SSS*, 0.00)

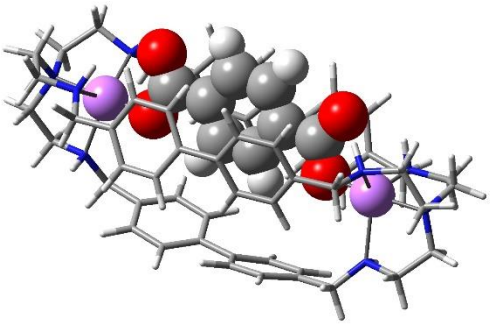

1B (*homo-RSS*, 1.90)

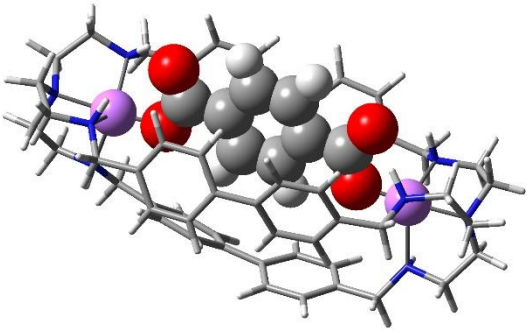

1C (*homo-RRS*, 1.37)

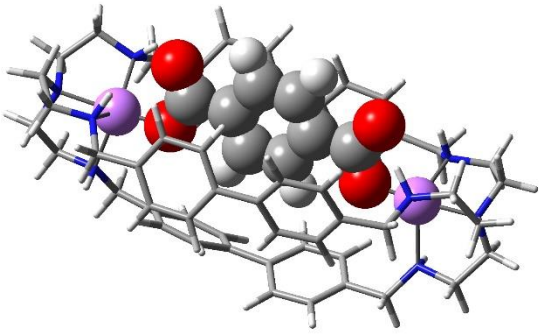

1D (*homo-RRR*, 0.62)

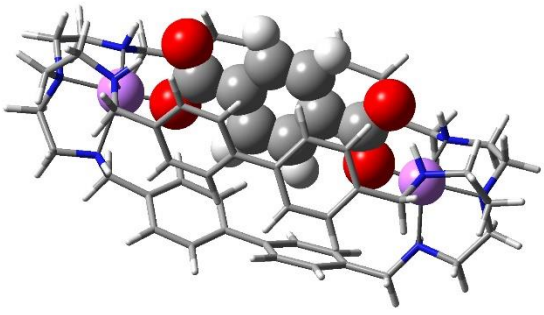

1E (*meso-SSS*, 1.47)

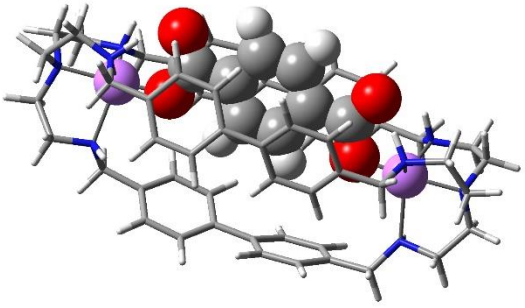

1F (*meso-RSS*, 1.96)

Figure 12. (Continued on next page)

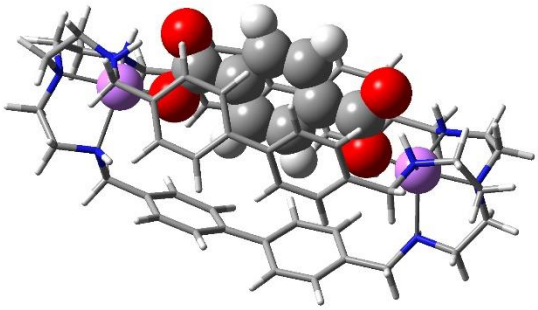

1G (*meso-RRS*, 2.48)

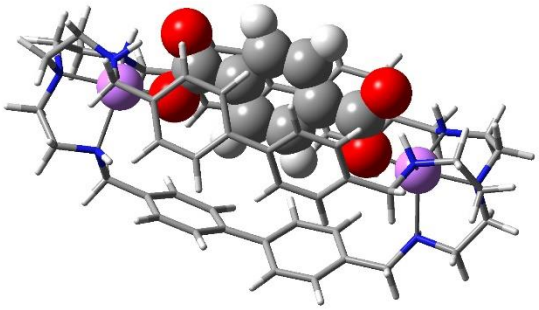

1H (*meso-RRR*, 2.07)

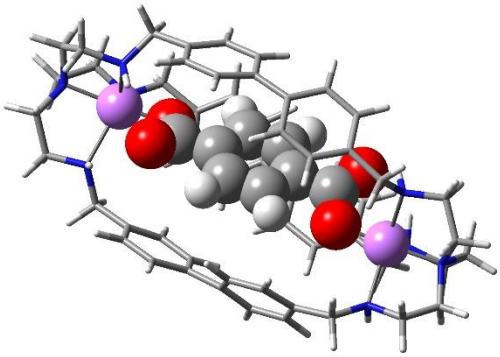

1I (*homo-RSS*, 14.62)

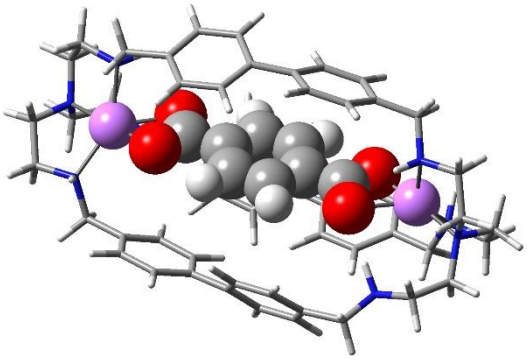

1J (*homo-SSS*, 16.10)

Figure 12. Three-dimensional plot of the most significant conformers of the inclusion complex $[Cu_2(\mathbf{L})\text{-}\mathbf{1}]^{2+}$(in parentheses, the *tren* units geometry, the diphenyl configuration, and the relative energy in kcal/mol). Reproduced with permission from ref. 28.

Then, the pseudorotaxane structures were built, starting from the optimized conformers of $[Cu_2(\mathbf{L})\text{-}\mathbf{1}]^{2+}$, by addition of the proper side chains to terephthalate. Anion $\mathbf{2}^{2-}$ was modeled as such, whereas the chains of $\mathbf{4}^{2-}$ were shortened to 2-methoxyethoxy, since it is expected that only the portions of the chains closer to the aromatic ring influence the binding mode. For the same reason, we found unnecessary to model $\mathbf{3}^{2-}$, being $\mathbf{2}^{2-}$ representative also of its behavior. Actually, the conformational behavior of the complexes of $\mathbf{2}^{2-}$ and $\mathbf{4}^{2-}$ was shown to be almost superimposable, so that the following discussion is referred only to the latter.

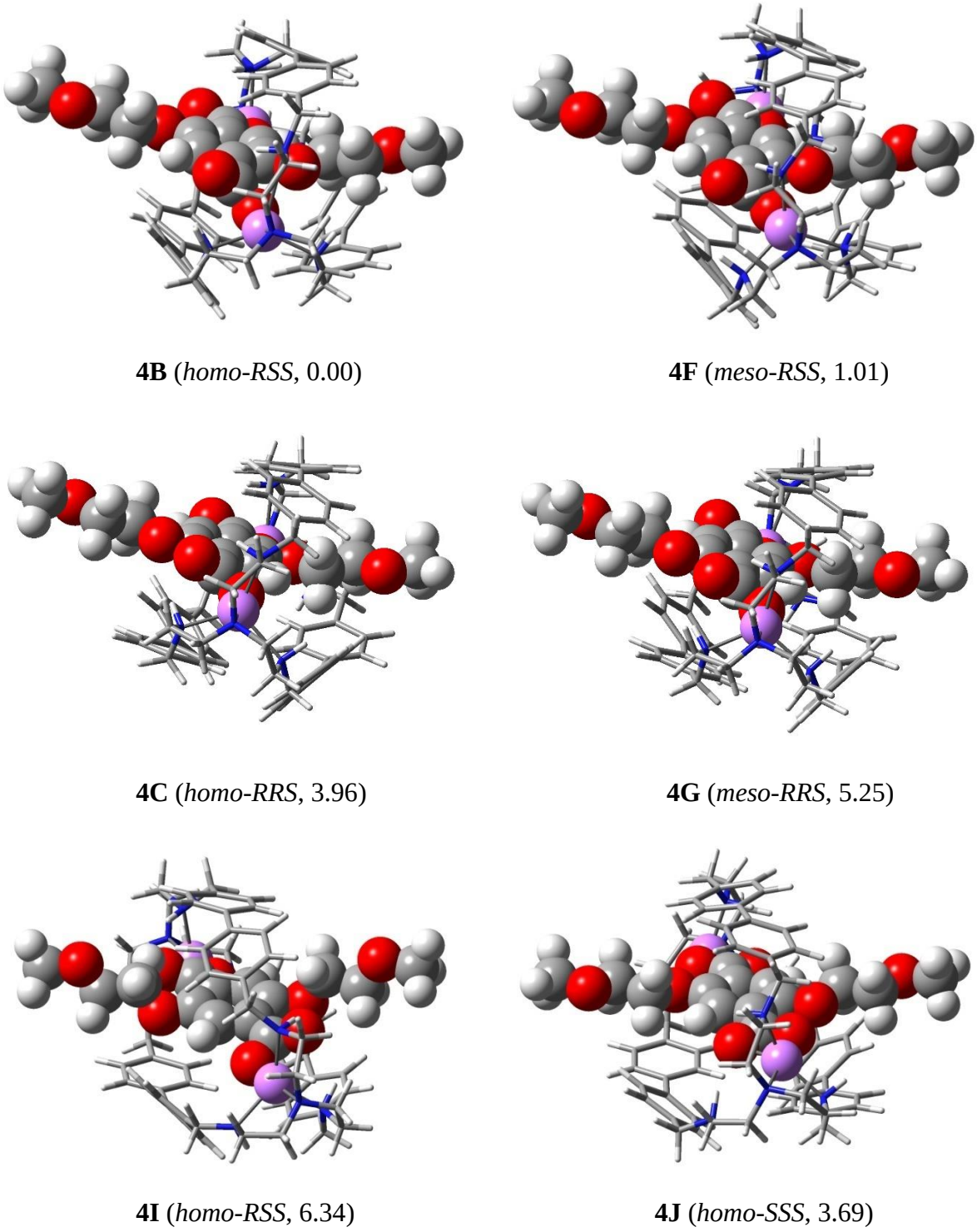

Figure 13. Three-dimensional plot of the most significant conformers of the inclusion complex $[Cu_2(\mathbf{L})\text{-}\mathbf{4}]^{2+}$ (in parentheses, the *tren* units geometry the diphenyl configuration, and the relative energy in kcal/mol). Reproduced with permission from ref. 28.

After optimizations of the starting geometries in the triplet state, conformer **4B**, derived from **1B**, was preferred over the other conformers with the same η^1 coordination and "*cis*" carboxylate

arrangement (Figure 13). Optimizations of **4B** using alternative spin states indicated that, once again, the triplet and open-shell singlet states are largely preferred over the closed-shell singlet state, disfavored by 35.38 kcal/mol. The starting geometry built from **1A** converged to **4B**, too, thus indicating in this case a neat preference for the *homo-RSS*-host over the *homo-SSS*-host arrangement. Conformer **4F** (*meso-RSS*-host), is less stable than **4B** only by 1.01 kcal/mol, thus indicating a possible co-existence in solution of both the conformers. It is also worthy pointing out a significant peculiarity of the $\mathbf{4}^{2-}$ complexes *vs.* the $\mathbf{1}^{2-}$ ones, *i.e.* the great relative stabilization of the "*trans*" terephthalate arrangement. In fact, the "*trans*" geometries **4I-J** (Figure 13) were much closer in energy to their global minimum **4B** than **1I-J** to **1A**. In particular, **4J**, which presents the unusual η^2 coordination of carboxylate groups to copper, is only 3.69 kcal/mol less stable than **4B** compared to the corresponding value of 16.10 kcal/mol for **1J**. Though the relative order of stability between the "*cis*" and the "*trans*" geometries is not reverted, this means that the presence of the terephthalate side chains introduces a severe strain in the "*cis*" complexes differently from the "*trans*" ones. This strain is not enough to make preferred the "*trans*" complexes but clearly explains the much lower affinity for the host of anion $\mathbf{4}^{2-}$ as compared to $\mathbf{1}^{2-}$.

Nevertheless, the "*cis*" global minimum **4B** and the next minimum **4F** are the only ones populated at room temperature and a close inspection of their geometrical features can give account of the experimental evidences. A comparison of **4B** with **1B** shows that the main changes in the host structure are caused by one of the 2-methoxyethoxy side chains, the one linked to the side of the terephthalate benzo group that points towards the cage's cavity (*inner* chain), whereas the other chain (*outer* chain) doesn't disturb the geometry at all. In order to find room for itself, the *inner* chain moves two diphenyl groups away and causes a severe distortion in the coordination sphere of the closer copper ion. In fact, though the two Cu(II) centers are both characterized by a geometry intermediate between the trigonal bipyramidal and the square-pyramidal geometry, the Cu center nearest to the *outer* chain is closer to the former geometry (τ = 0.73), almost conserving the geometry found in **1B** (τ = 0.78), whereas the center nearest to the *inner* chain can be better described as square-pyramidal (τ = 0.37), as also confirmed by the severe elongation of one of the Cu-N_{sec} linkages to 3.28 Å. A comparison of **4F** with **1F** shows less pronounced differences in the coordination sphere of the copper ions (Figure 13). In fact, the geometry of the coordination center nearest to the *inner* chain is characterized by τ = 0.80. This significant difference with respect to **4B** can be explained by the opposite chirality of the surrounding *tren* unit ($\tau_{tren} \approx$ -50°). Actually, also in **4F**, as well as in **4B**, the two copper ions are non-equivalent as they experiment a different chemical environment.

All the above considerations apply also for the complexes of $\mathbf{2}^{2-}$ and the corresponding located conformers are reported in the Supplementary Section (Figure S14).

6.4. Conclusions

In this work, we applied different dicarboxylate anions $\mathbf{2}^{2-}$-$\mathbf{4}^{2-}$, as possible guests for the dicopper(II) complex $[Cu_2(\mathbf{L})]^{4+}$. This complex can recognize terephthalate, at pH 7, both in water and in methanol/water mixture. The strong binding is due to the fit of the anion bite length with the separation between the copper(II) ions inside the cavity. Our computational studies on the adduct $[Cu_2(\mathbf{L})\text{-}\mathbf{1}]^{2+}$ showed that terephthalate adopts a "cis" configuration of the carboxylate units. Hydrogen bonds, C-H$\cdots\pi$ and $\pi\cdots\pi$ interactions with the azacryptand cooperate with coordinative interactions in the stabilization of the inclusion complex.

The affinity of $[Cu_2(\mathbf{L})]^{4+}$ for the terephthalate guest is reduced in the presence of alkyl or polyoxoethylene chains on both sides of the aryl core. However, spectroscopic and ESI-MS investigations on equimolar solutions of $[Cu_2(\mathbf{L})]^{4+}$ and $\mathbf{2}^{2-}$-$\mathbf{4}^{2-}$ showed the formation of 1:1 complexes with all the investigated anions, with binding constants ranging between 4.98 and 5.18 Log units. The formation of the host:guest complexes involves the threading of the guests through the macrobicyclic cavity of the dicopper cage. The driving force behind the formation of these pseudo-rotaxane structures is the coordination of the terephthalate unit to the copper ions within the cage's cavity. Theoretical calculations showed that the conformation of the pseudo-rotaxane complex, $[Cu_2(\mathbf{L})\text{-}\mathbf{4}]^{2+}$, corresponding to the global minimum in water, is similar to that of $[Cu_2(\mathbf{L})\text{-}\mathbf{1}]^{2+}$, with the included terephthalate group adopting a "cis" arrangement around the copper centers. However, one of the two 2-methoxyethoxy chains points towards the cage's cavity, while the other chain aims to the outside. The inner chain exerts a steric effect inside the cavity, moving away two diphenyl spacers and causing the distortion of the coordination geometry around the nearby Cu(II) ion. These findings are in agreement with the experimental results of our EPR and UV-vis. studies. Furthermore, the steric effect may explain the lower affinity constants obtained with $\mathbf{2}^{2-}$-$\mathbf{4}^{2-}$ compared to that of the bare terephthalate species (LogK > 6) in methanol/water mixture.

Supplementary Section

1S. NMR Spectra

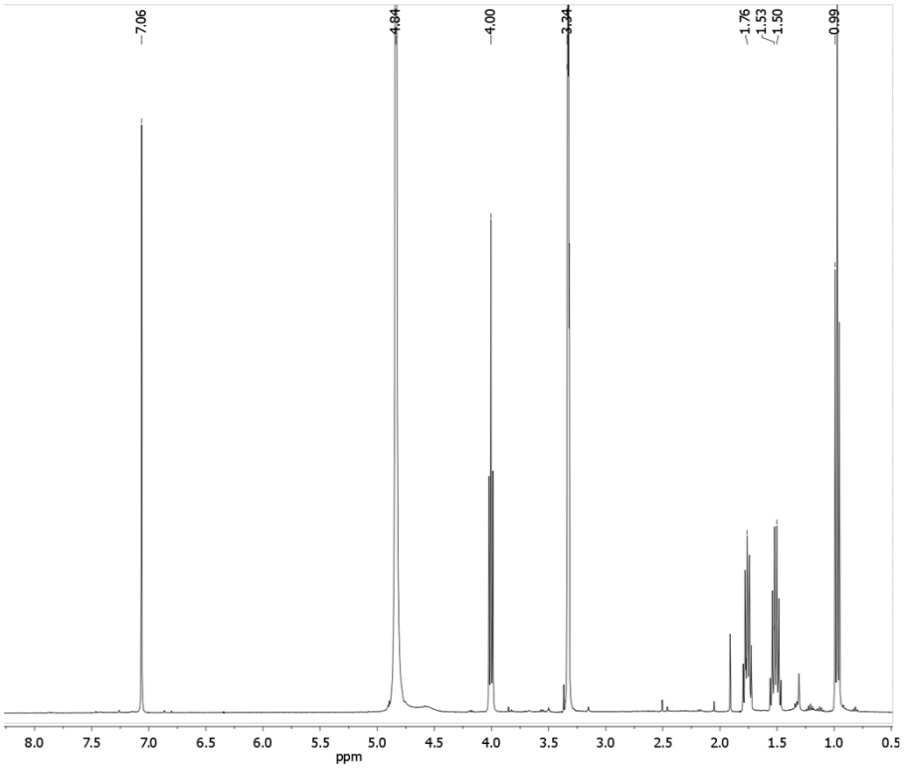

Figure S1. ^{1}H-NMR spectra of Na_2**2** in CD_3OD. Reproduced with permission from ref. 28.

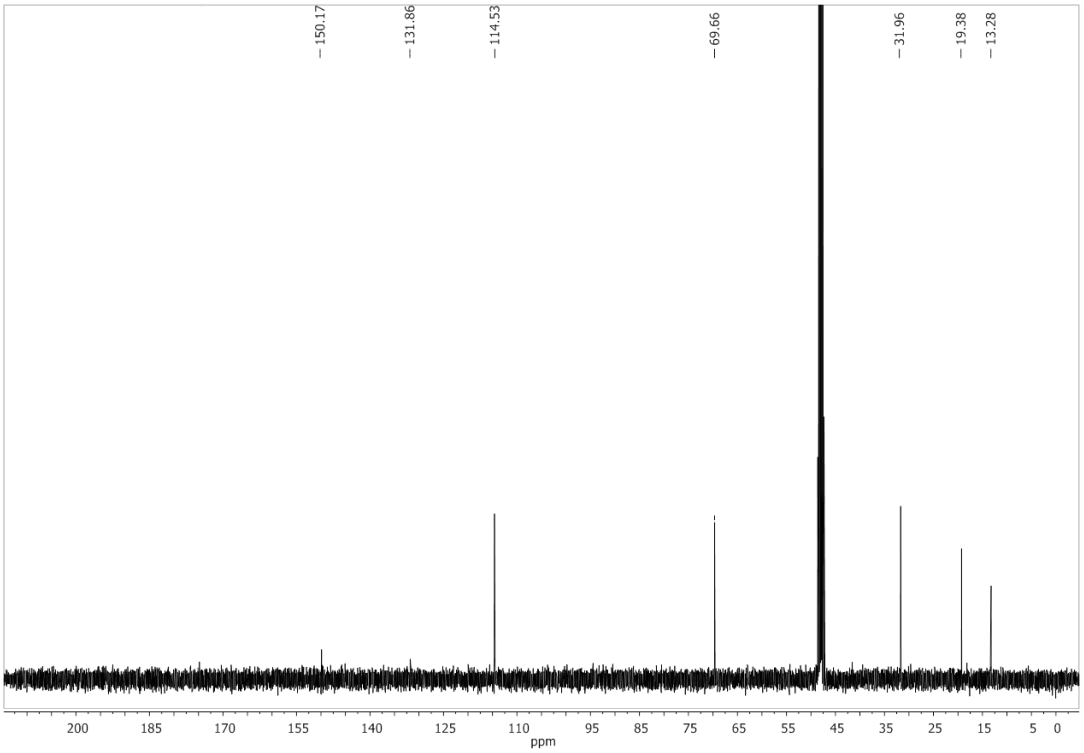

Figure S2. ^{13}C-NMR spectra of Na_2**2** in CD_3OD. Reproduced with permission from ref. 28.

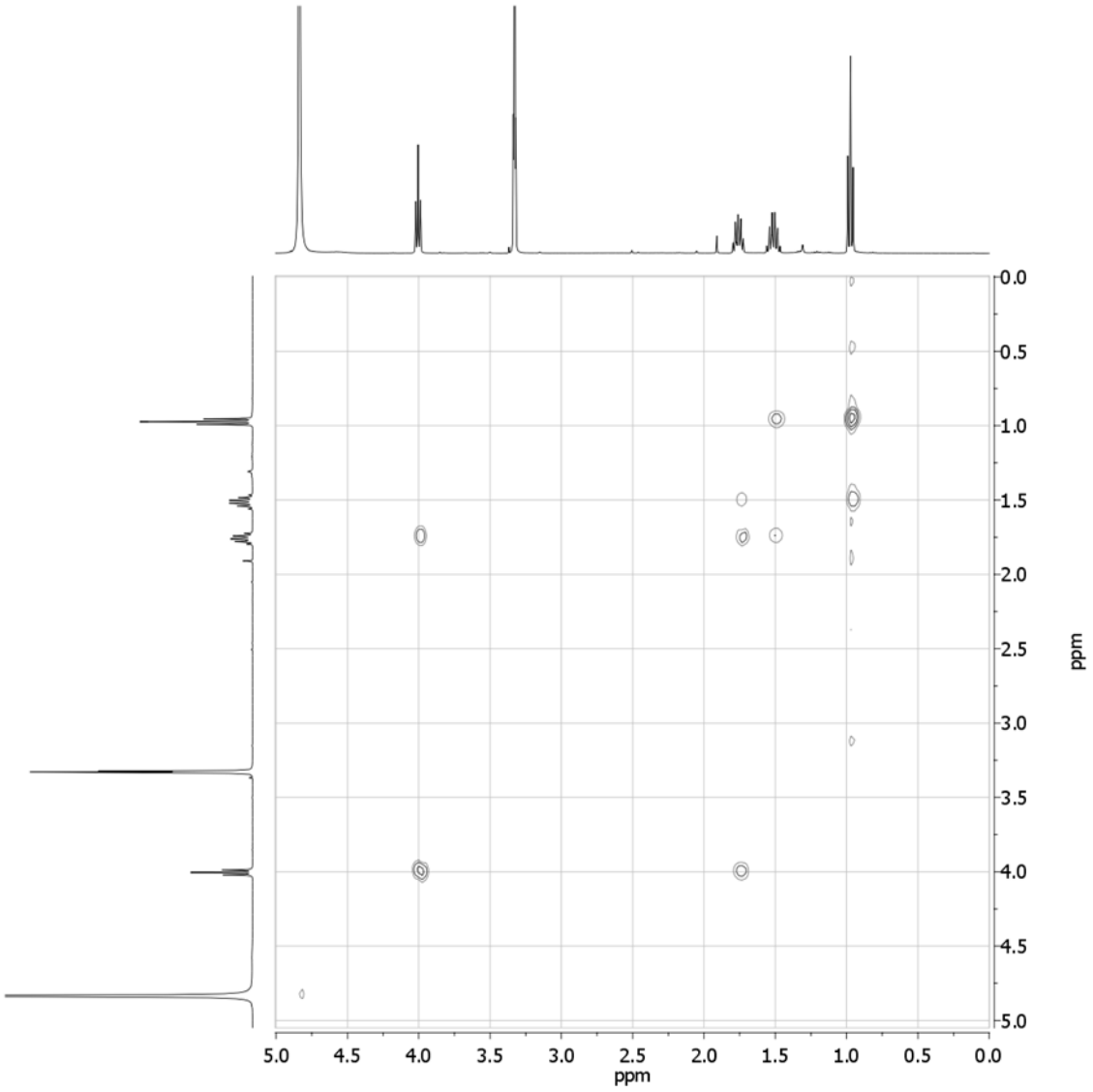

Figure S3. COSY spectrum of Na_2**2** in CD_3OD. Reproduced with permission from ref. 28.

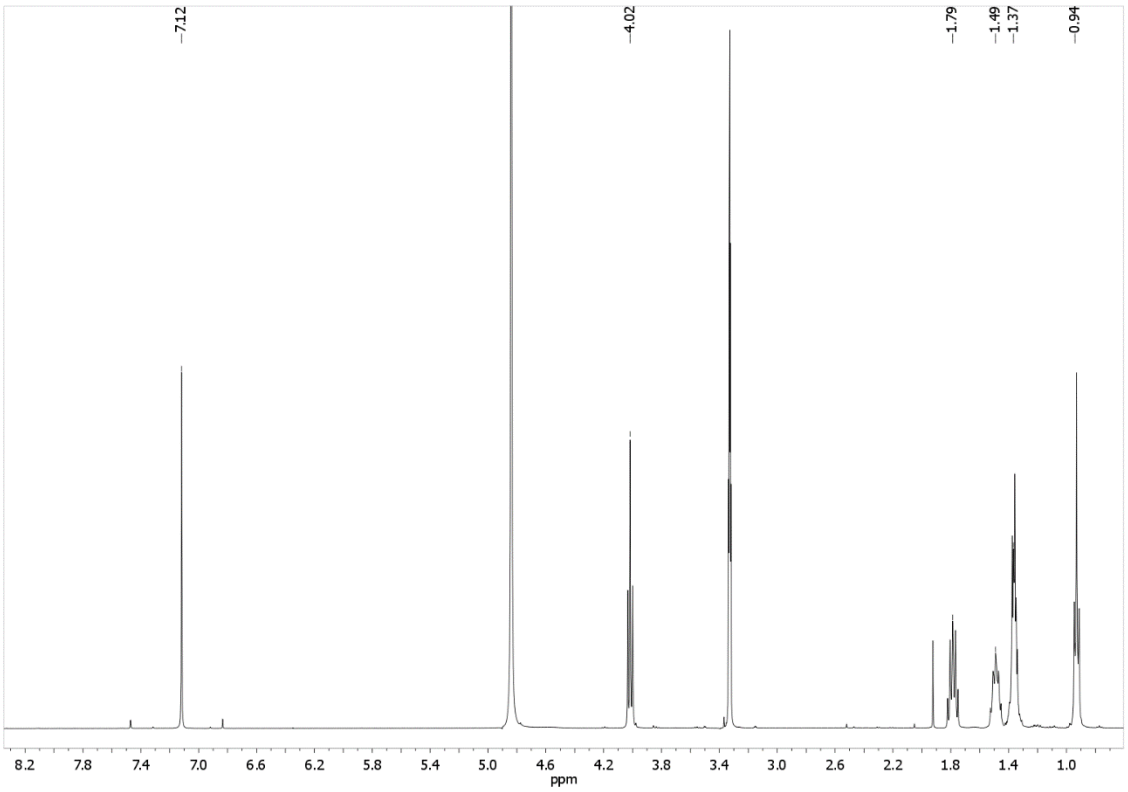

Figure S4. ^{1}H-NMR spectra of Na_2**3** in CD_3OD. Reproduced with permission from ref. 28.

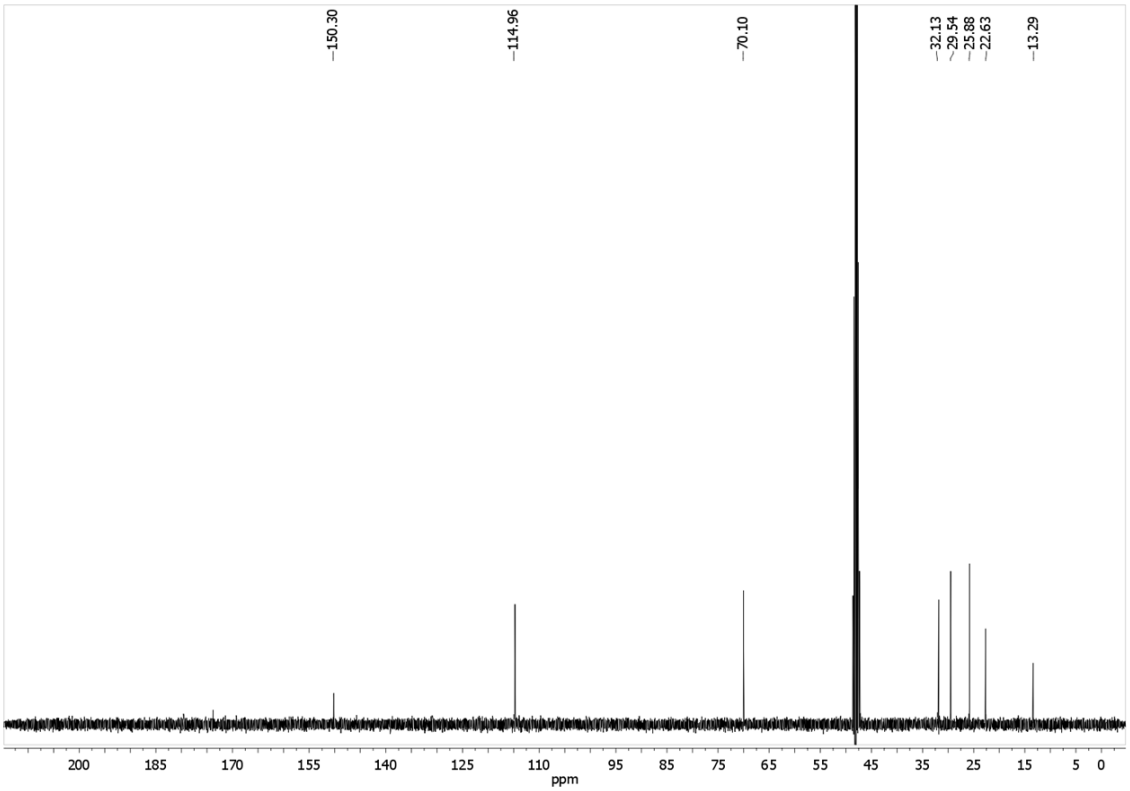

Figure S5. ^{13}C-NMR spectra of Na_2**3** in CD_3OD. Reproduced with permission from ref. 28.

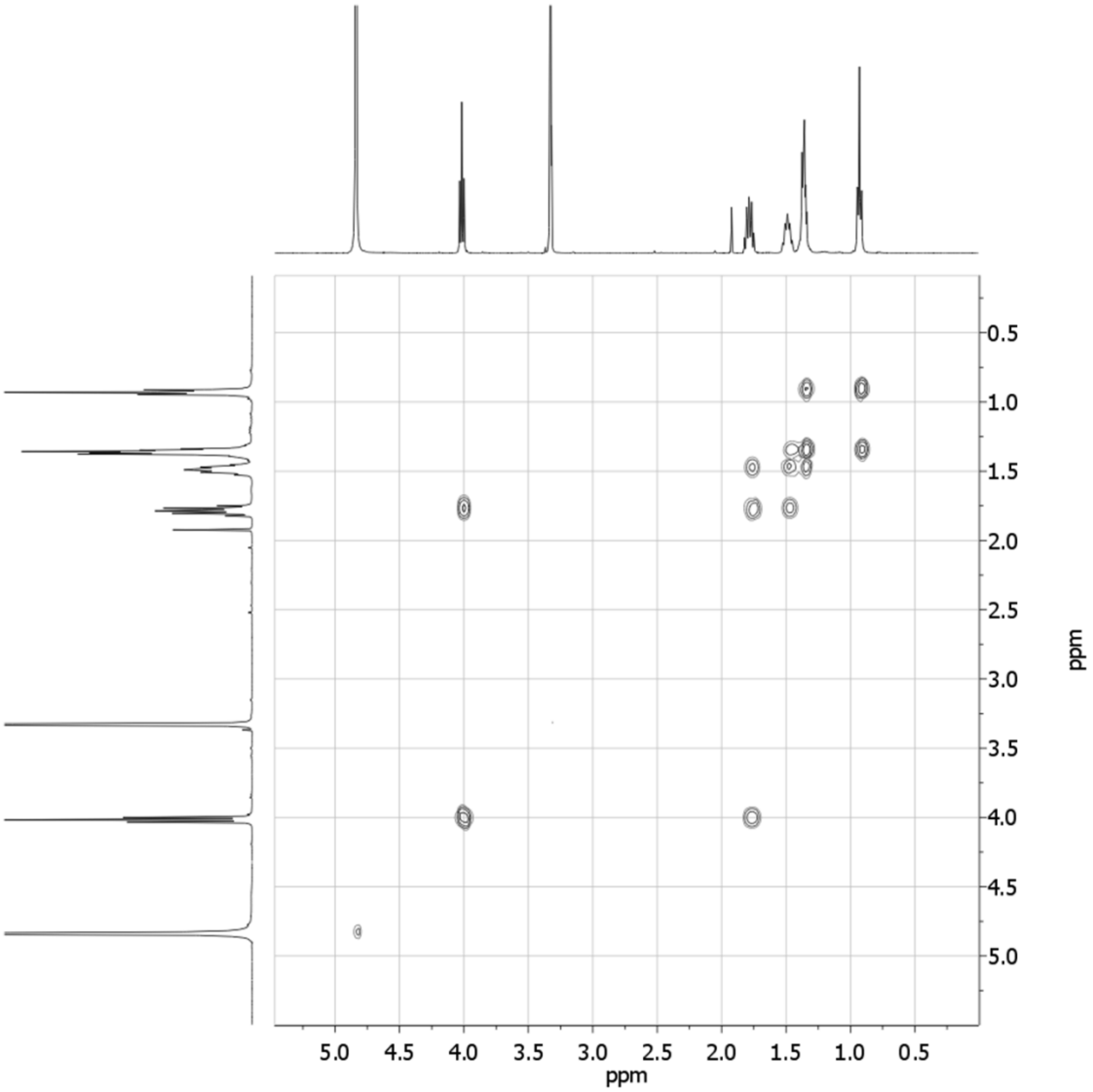

Figure S6. COSY spectrum of Na_2**3** in CD_3OD. Reproduced with permission from ref. 28.

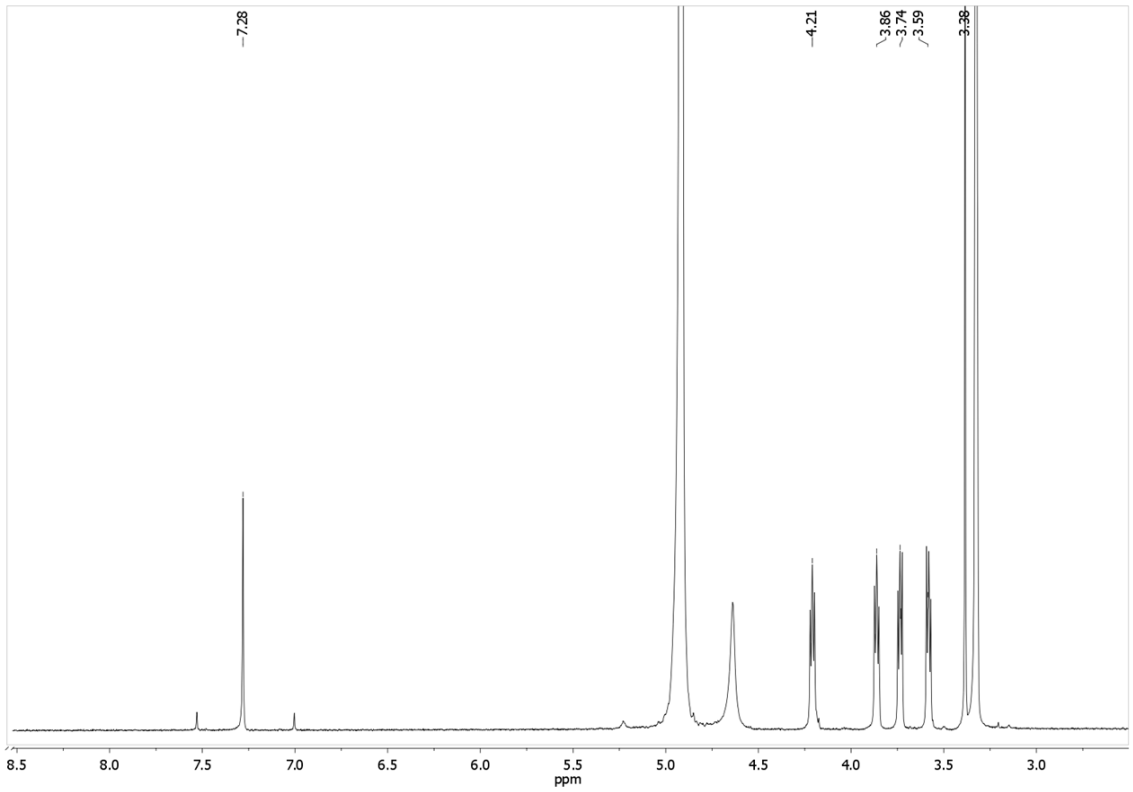

Figure S7. ^{1}H-NMR spectra of Na_2**4** in CD_3OD. Reproduced with permission from ref. 28.

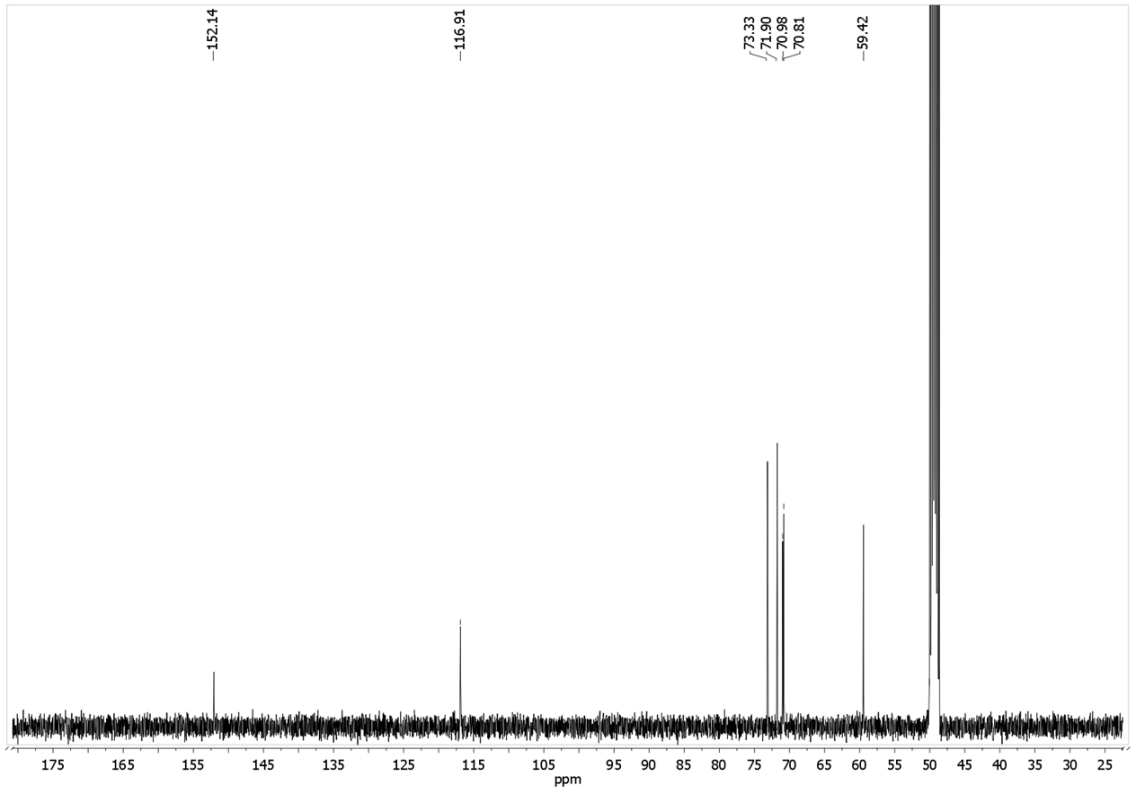

Figure S8. ^{13}C-NMR spectra of Na_2**4** in CD_3OD. Reproduced with permission from ref. 28.

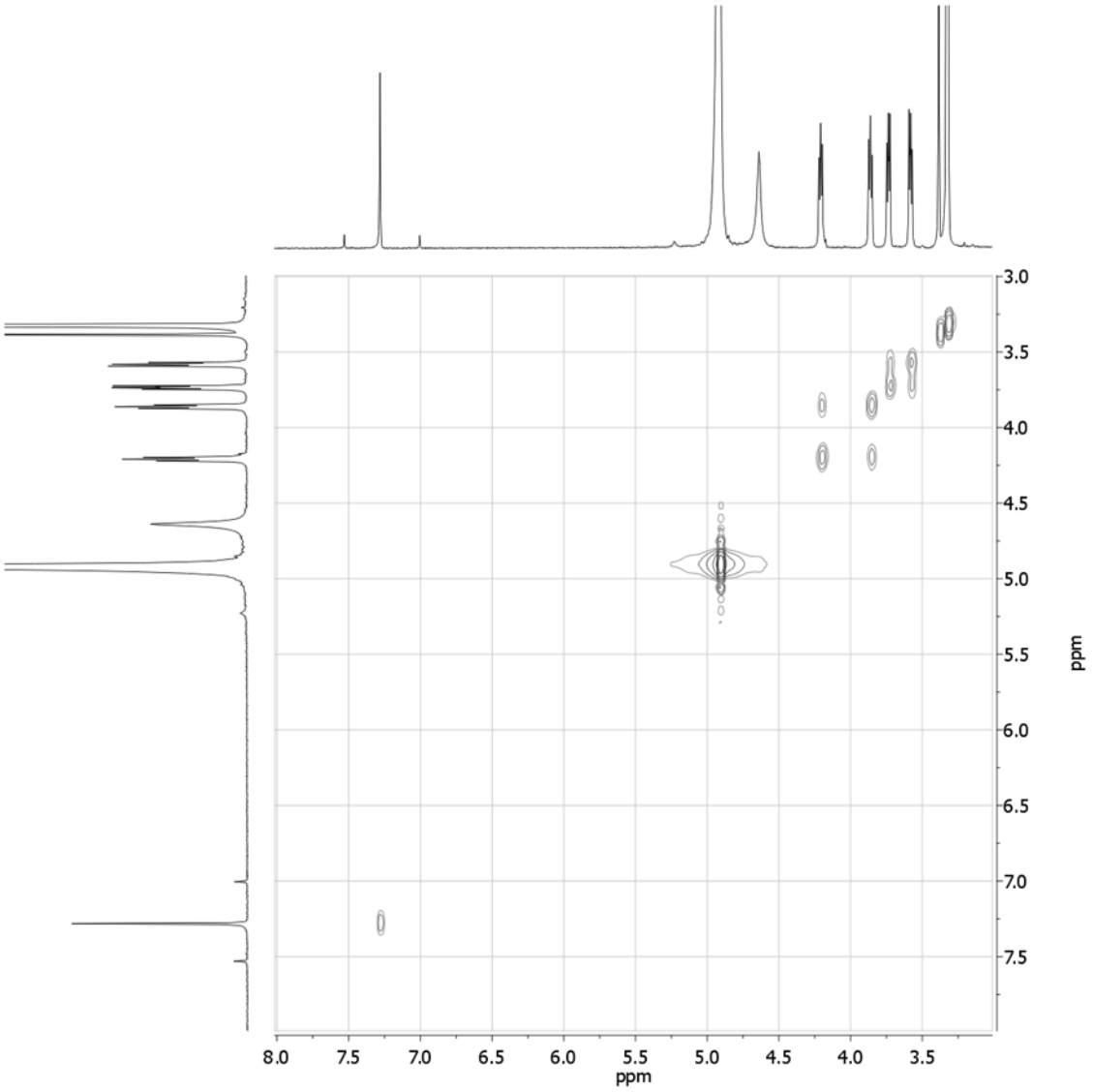

Figure S9. COSY spectrum of Na_2**4** in CD_3OD. Reproduced with permission from ref. 28.

2S. *ESI-MS spectra*

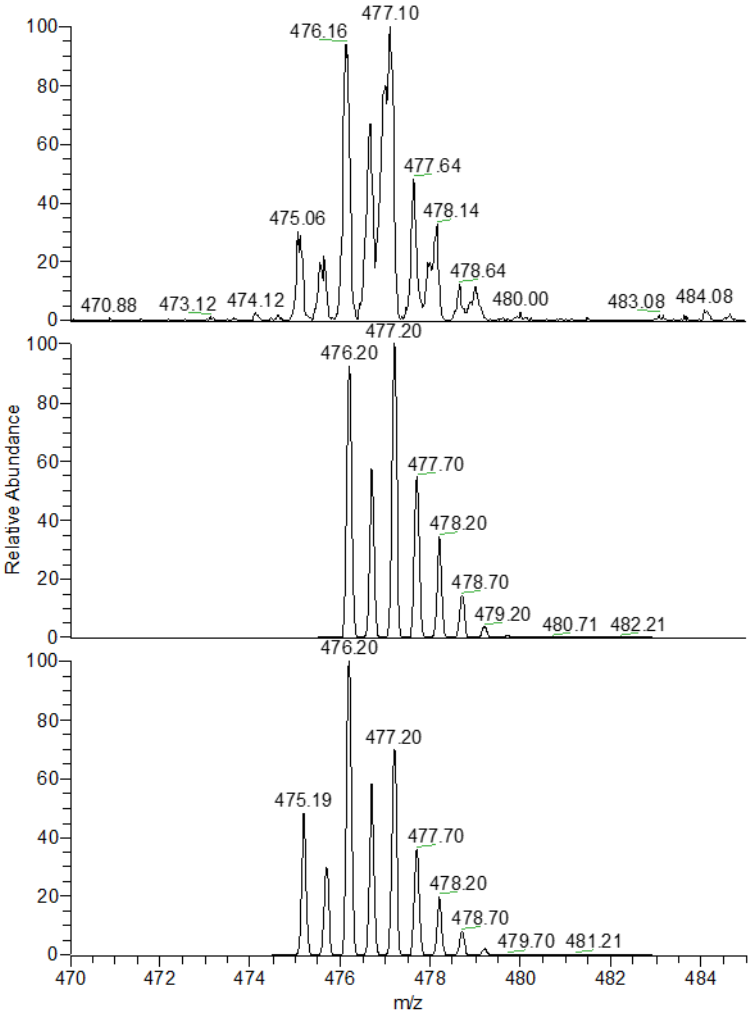

Figure S10. Top: zoom scan of the peak at 477 m/z, obtained from the experimental mass spectrum of the solution of $[Cu_2(\mathbf{L})]^{4+}$ in MeOH:H_2O 9:1 (0.005M HEPES, pH 7) prepared for UV-vis. titrations. Middle: simulated peak, calculated for the species $[Cu^{I}_2C_{54}H_{66}N_8]^{2+}$ (i.e. $[Cu^{I}_2(\mathbf{L})]^{2+}$). Bottom: simulated peak, calculated for $[Cu^{II}_2C_{54}H_{64}N_8]^{2+}$ (i.e. $[Cu^{II}_2(\mathbf{L}\text{-}2H^+)]^{2+}$). Reproduced with permission from ref. 28.

The experimental peak results from the contribution of two double-charged species (~50%), in which either the copper centers are in the +1 oxidaton state ($[Cu^{I}_2(\mathbf{L})]^{2+}$) or the ligand is doubly deprotonated ($[Cu^{II}_2(\mathbf{L}\text{-}2H^+)]^{2+}$). Both processes (i.e. ligand deprotonation and Cu(II) reduction) are common in the ESI-MS spectra of copper complexes with polyamine ligands, especially using MeOH as solvent.[27]

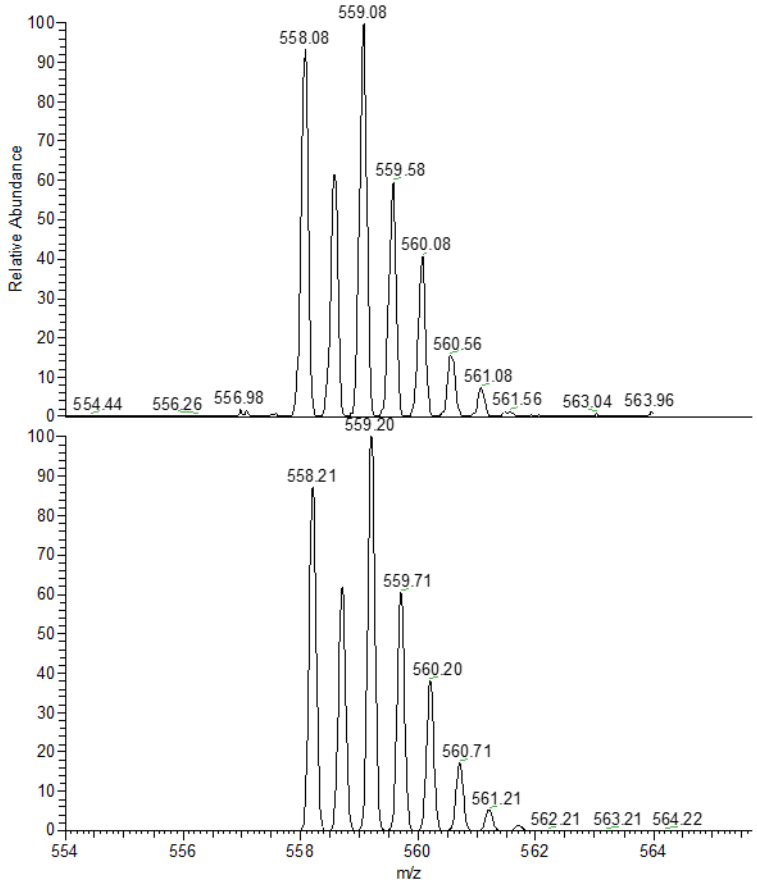

Figure S11. Top: zoom scan of the peak at 559 m/z, obtained from the experimental mass spectrum of an equimolar solution of $[Cu_2(\mathbf{L})]^{4+}$ and $\mathbf{1}^{2-}$ in MeOH:H_2O 9:1 (0.005M HEPES, pH 7). Bottom: simulated peak, calculated for the species $[Cu_2C_{62}H_{70}N_8O_4]^{2+}$ (i.e. $[Cu_2(\mathbf{L})\text{-}\mathbf{1}]^{2+}$). Reproduced with permission from ref. 28.

3S. EPR studies

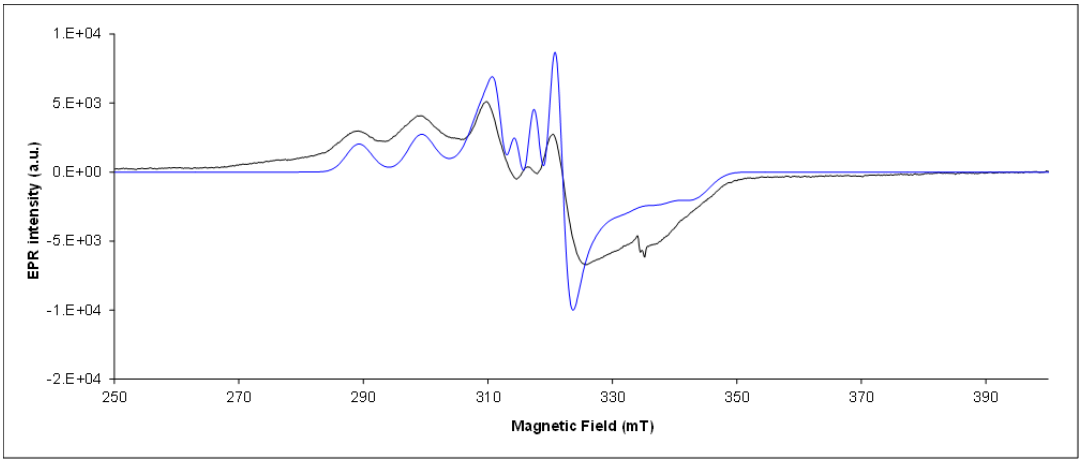

Figure S12. EPR spectrum of $[Cu_2(\mathbf{L})]^{4+}$ (0.5 mM in MeOH:H_2O 9:1 (v:v), pH = 7). The black one is the experimental spectrum, the blue one is simulated. The EPR parameters obtained from the simulation of experimental spectrum are: Values of g-tensor g1 = 2.29, g2 = 2.20, g3 = 2.08; and values of the hyperfine tensor a1 = 10.0, a2 = 3.0, a3 = 5.6 (in mT). Reproduced with permission from ref. 28.

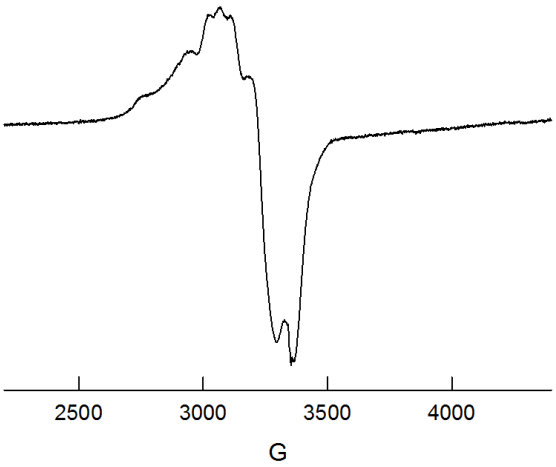

Figure S13. EPR spectrum of the adduct $[Cu_2(\mathbf{L})\text{-}\mathbf{3}]^{2+}$. The sample was prepared at 0.5 mM for $[Cu_2(\mathbf{L})]^{4+}$ and the guest in MeOH:H_2O 9:1 (v:v), pH = 7. The EPR spectra were recorded at 31.81 mW, frequency (v) of 9.395 GHz, and T = 120 K. Reproduced with permission from ref. 28.

4S. Computational Studies

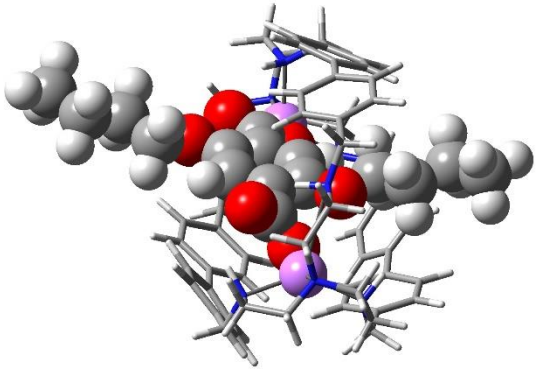

2B (*homo-RSS*, 0.00)

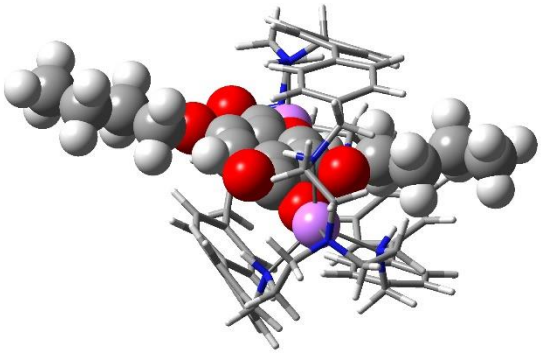

2F (*meso-RSS*, 1.19)

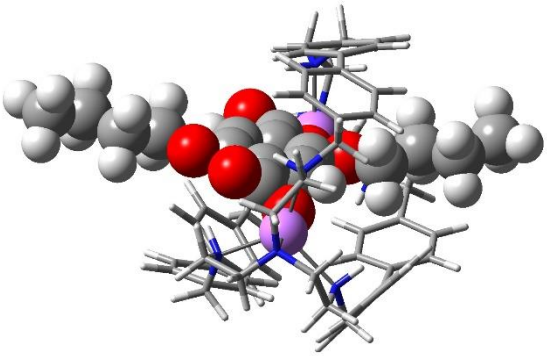

2C (*homo-RRS*, 4.00)

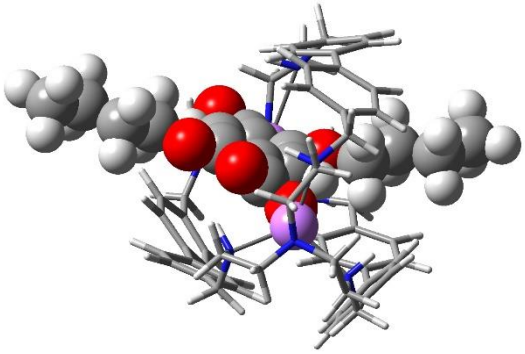

2G (*meso-RRS*, 5.15)

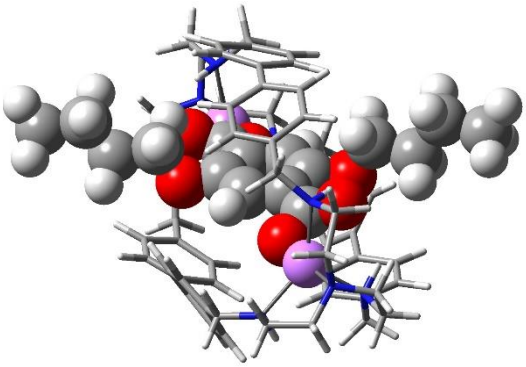

2I (*homo-RSS*, 5.49)

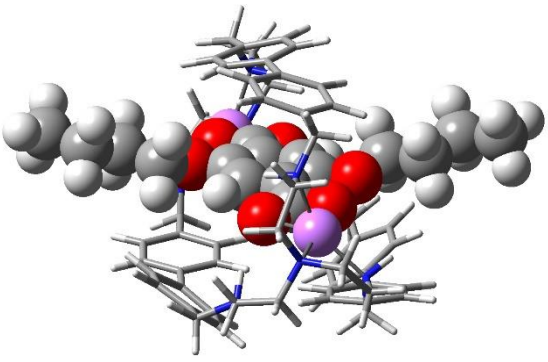

2J (*homo-SSS*, 1.91)

Figure S14. Three-dimensional plot of the most significant conformers of the inclusion complex $[Cu_2(\mathbf{L})\text{-}\mathbf{2}]^{2+}$ (in parentheses, the *tren* units geometry the diphenyl configuration, and the relative energy in kcal/mol). Reproduced with permission from ref. 28.

References

[1] Cram, D. J. in *The Design of Molecular Hosts, Guests, and their Complexes*; Nobel Lecture, 8th December **1987**.

[2] Lawrence, D.S.; Jiang, T.; Levitt, M.; *Chem. Rev.* **1995**, 95, 2229-2260.

[3] (a) Balzani, V.; Gomez-Lopez, M.; Stoddart, J. F.; *Acc. Chem. Res.* **1998**, 31, 405-414; (b) Sauvage, J. P.; *Acc. Chem. Res*. **1998**, 31, 611-619; (c) Collin, J. P.; Dietrich-Buchecker, C.; Gavina, P.; Jimenez-Molero, M.C.; Sauvage, J. P.; *Acc. Chem. Res.* **2001**, 34, 477-487; (d) Kay, E. R.; Leigh, D. A.; Zerbetto, F.; *Angew. Chem. Int. Ed.* **2007**, 46, 72-191; (e) Abendroth, J.M.; Bushuyev, O.S.; Weiss, P.S.; Barrett, C.J.; *ACS Nano,* **2015**, 9(8), 7746-7768 and references therein.

[4] Lewis, J.E.M.; Beer, P.D.; Loeb S.J.; Goldup, S.M.; *Chem. Soc. Rev*. **2017**, 46, 2577-2591 and references therein.

[5] Goldup, S.M.; Leigh, D.A.; Lusby, P.J.; McBurney, R.T.; Slawin, A.M.Z.; *Angew. Chem. Int. Ed.,* **2008**, 47, 3381-3384.

[6] (a) Sauvage, J. P.; Dietrich-Buchecker, C. Eds. *Molecular Catenanes, Rotaxanes and Knots: A Journey Through the World of Molecular Topology*; Wiley-VCH Verlag GmbH: Weinheim, Germany, **1999**; (b) Sauvage, J. P. in *Chemical Topology to Molecular Machines*; Nobel Lecture, 8th December **2016**.

[7] (a) Raymo, F.M.; Stoddart, J.F.; *Chem. Rev.* **1999**, 99(7), 1643-1664; (b) Li, D.; Paxton, W. F.; Baughman, R. H.; Huang, T. J.; Stoddart, J. F.; Weiss, P. S.; *MRS Bull.* **2009**, 34, 671-681; (c) Stoddart, J.F. in *Design and Synthesis of Molecular Machines based on the Mechanical Bond*; Nobel Lecture, 8th December **2016**.

[8] Schalley, C.A.; Beizai, K.; Vogtle, F.; *Acc. Chem. Res.* **2001**, 34, 465-476.

[9] Han, X.; Liu, G.; Liu, S. H. and Yin, J.; *Org. Biomol. Chem*. **2016**, 14, 10331-10351.

[10] Harrison, I. T.; Harrison, S.; *J. Am. Chem. Soc.* **1967**, 89(22), 5723–5724.

[11] (a) Lin, C. F.; Liu, Y. H.; Lai, C. C.; Peng, S.-M.; Chiu S. H.; *Angew. Chem. Int. Ed.* **2006**, 45, 3176-3181; (b) Hsueh, S. Y.; Lai, C. C.; Liu, Y. H.; Peng, S. M.; Chiu S. H.; *Angew. Chem. Int. Ed.* **2007**, 46, 2013-2017; (c) Lin, C. F.; Lai, C. C.; Liu, Y. H.; Peng, S. M.; Chiu S. H.; *Chem. Eur. J.*

2007, 13, 4350-4355; (d) Chuang, C. J.; Lai, C. C.; Liu, Y. H.; Peng, S. M.; Chiu S. H.; *Chem. Eur. J.* **2012**, 18, 16698-16707; (e) Chuang, C. J.; Yen, M. L.; Lai, C. C.; Liu, Y. H.; Peng, S. M.; Chiu S. H.; *Chem. Commun*. **2013**, 49, 4199-4201.

[12] Li, S.; Liu, M.; Zheng, B.; Zhu, K.; Wang, F.; Li, N.; Zhao, X. L.; Huang, F.; *Org. Lett.* **2009**, 11(15), 3350-3353.

[13] Klivansky, L.M.; Koshkakaryan, G.; Cao, D.; Liu Y.; *Angew. Chem. Int. Ed*. **2009**, 48, 4185-4189.

[14] Li, J.; Wei, P.; Wu, X.; Xue, M; Yan, X.; Zhou, Q.; *RSC Adv.* **2013**, 3, 21289-21293.

[15] Ye, Y.; Wang, S.-P.; Zhu, B.; Cook, T.R.; Wu, J.; Li, S.; Stang, P.J.; *Org. Lett.* **2015**, 17, 2804-2807.

[16] Clever; G.H.; Shionoya, M.; *Chem. Eur. J.* **2010**, 16, 11792-11796.

[17] Boiocchi, M.; Bonizzoni, M.; Fabbrizzi, L.; Piovani, G.; Taglietti, A.; *Angew. Chem. Int. Ed.* **2004**, 43, 3847-3852.

[18] Yang, L. Z.; Li, Y.; Zhuang, X. M.; Jiang, L.; Chen, J. M.; Luck, R.L.; Lu, T. B.; *Chem.-Eur.J.* **2009**, 15, 12399.

[19] Choi, E. Y.; Gao, C.; Lee, S. H. and Kwon, O. P.; *Bull. Korean Chem. Soc.* **2012**, 33, No. 4, 1264-1268.

[20] Henke, S.; Schneemann, A.; Kapoor, S.; Winter, R. and Fischer, R. A.; *J. Mater. Chem*., **2012**, 22, 909-918.

[21] Gans, P.; Sabatini, A.; Vacca, A.; *Talanta*, **1996**, 43, 1739-1753.

[22] Frisch, M. J.; Trucks, G. W.; Schlegel, H. B.; Scuseria, G. E.; Robb, M. A.; Cheeseman, J. R.; Scalmani, G.; Barone, V.; Mennucci, B.; Petersson, G. A.; Nakatsuji, H.; Caricato, M.; Li, X.; Hratchian, H. P.; Izmaylov, A. F.; Bloino, J.; Zheng, G.; Sonnenberg, J. L.; Hada, M.; Ehara, M.; Toyota, K.; Fukuda, R.; Hasegawa, J.; Ishida, M.; Nakajima, T.; Honda, Y.; Kitao, O.; Nakai, H.; Vreven, T.; Montgomery, J. A. Jr.; Peralta, J. E.; Ogliaro, F.; Bearpark, M.; Heyd, J. J.; Brothers, E.; Kudin, K. N.; Staroverov, V. N.; Keith, T.; Kobayashi, R.; Normand, J.; Raghavachari, K.; Rendell, A.; Burant, J. C.; Iyengar, S. S.; Tomasi, J.; Cossi, M.; Rega, N.; Millam, J. M.; Klene, M.; Knox, J. E.; Cross, J. B.; Bakken, V.; Adamo, C.; Jaramillo, J.; Gomperts, R.; Stratmann, R. E.; Yazyev, O.; Austin, A. J.; Cammi, R.; Pomelli, C.; Ochterski, J. W.; Martin, R. L.; Morokuma, K.;

Zakrzewski, V. G.; Voth, G. A.; Salvador, P.; Dannenberg, J. J.; Dapprich, S.; Daniels, A. D.; Farkas, O.; Foresman, J. B.; Ortiz, J. V.; Cioslowski, J.; Fox, D. *J. Gaussian 09, Revision B.01*; Gaussian, Inc.: Wallingford, CT, 2010.

[23] (a) Becke, A. D.; *J. Chem. Phys.* **1993**, 98, 5648-5652; (b) Lee, C.; Yang, W.; Parr, R. G.; *Phys. Rev. B,* **1988**, 37, 785-789.

[24] (a) Cancés, E.; Mennucci, B.; Tomasi, J.; *J. Chem. Phys.*, **1997**, 107, 3032-3042; (b) Cossi, M.; Barone, V.; Cammi, R.; Tomasi, J.; *Chem. Phys. Lett.*, **1996**, *255*, 327-335; (c) Barone, V.; Cossi, M.; Tomasi, J.; *J. Comput. Chem.*, **1998**, 19, 404-417.

[25] Mateus, P.; Delgado, R.; André, V.; Duarte, M.T.; *Inorg. Chem.*, **2015**, 54, 229-240.

[26] Addison, A. W.; Rao, T. N.; Reedijk, J.; van Rijn, J.; Verschoor, G. C.; *J. Chem. Soc., Dalton Trans.*, **1984**, 1349-1356.

[27] Gianelli, L.; Amendola, V.; Fabbrizzi, L.; Pallavicini, P.; Mellerio, G. G. *Rapid Commun. Mass Spectrom.* **2001**, 15, 2347-2353.

[28] Amendola, V.; Miljkovic, A.; Legnani, L.; Toma, L.; Dondi, D.; and Lazzaroni, S.; *Inorganic Chemistry - Forum Article* submitted (Manuscript ID ic-2017-02534v). Unpublished work copyright **2017**, American Chemical Society.